REACTOR MATERIALS

A Quarterly Technical Progress Review

Prepared for DIVISION OF TECHNICAL INFORMATION, USAEC, by
R. W. DAYTON, E. M. SIMONS, and ASSOCIATES, BATTELLE MEMORIAL INSTITUTE

November 1962

FEATURE ARTICLE:

Radiation Effects in Reactor Ceramics

● VOLUME 5

● NUMBER 4

TECHNICAL PROGRESS REVIEWS

To meet the needs of industry for concise summaries of current atomic developments, the Atomic Energy Commission is publishing this series, Technical Progress Reviews. Issued quarterly, each of the reviews digests and evaluates the latest findings in a specific area of nuclear technology and science.

The four journals published in this series are:

Nuclear Safety, Wm. B. Cottrell, W. H. Jordan, and associates, Oak Ridge National Laboratory

Power Reactor Technology, W. H. Zinn and J. R. Dietrich, General Nuclear Engineering Corporation

Reactor Materials, R. W. Dayton, E. M. Simons, and associates, Battelle Memorial Institute

Reactor Fuel Processing, Stephen Lawroski and associates, Chemical Engineering Division, Argonne National Laboratory

Each journal may be purchased ($2.00 per year for subscription and individual issues $0.55) from the Superintendent of Documents, U. S. Government Printing Office, Washington 25, D. C. See back cover for remittance instructions and foreign postage requirements.

The views expressed in this publication do not necessarily represent those of the United States Atomic Energy Commission, its divisions or offices, or of any Commission advisory committee or contractor.

Availability of Reports Cited in This Review

Unclassified AEC reports are available for inspection at AEC depository libraries and are sold by the Office of Technical Services, Department of Commerce, Washington 25, D. C. Some of the reports cited are not available owing to their preliminary nature; however, the information contained in them will eventually be made available in formal progress or topical reports.

Unclassified reports issued by other Government agencies or private organizations should be requested from the originator.

Unclassified British and Canadian reports may be inspected at AEC depository libraries. British reports are sold by the British Information Service, 45 Rockefeller Plaza, New York, N. Y.; Canadian reports (AECL series) are sold by the Scientific Document Distribution Office, Atomic Energy of Canada, Ltd., Chalk River, Ontario, Canada.

Classified U. S. and foreign reports identified in this journal as Classified may be purchased by properly cleared Access Permit Holders from the Division of Technical Information Extension, U. S. Atomic Energy Commission, P. O. Box 1001, Oak Ridge, Tenn. Such reports may be inspected at classified AEC depository libraries.

REACTOR MATERIALS

A REVIEW OF RECENT DEVELOPMENTS

Prepared for DIVISION OF TECHNICAL INFORMATION, USAEC,
by R. W. DAYTON, E. M. SIMONS, and ASSOCIATES,
BATTELLE MEMORIAL INSTITUTE

● NOV. 1962

● VOLUME 5

● NUMBER 4

Foreword

Reactor Materials is one of a series of quarterly technical progress reviews broadly covering the field of nuclear science and technology. Under the auspices of the USAEC Division of Technical Information, *Reactor Materials* is prepared by Battelle personnel from worldwide literature. It covers properties, behavior, and fabrication processes of materials applicable to nuclear reactor components and associated equipment.

The reader will recognize that the scope of this Review is too broad to permit detailed coverage of every topic. Rather, the authors and editors attempt to combine the highlights of significant new developments into an informative summary of current research for both management and the technical specialist. As a rule, enough of the results are presented to define the research and summarize the findings. For readers desiring more information on any particular topic, a complete set of references is provided at the end of each section.

Each quarter, a number of bibliographies, monographs, and books appear on subjects within the scope of *Reactor Materials*. Although the main purpose of this Review is to call attention to findings that are new and significant, such publications are noted in the text because they often represent excellent compilations of available information on important materials topics.

R. W. DAYTON
E. M. SIMONS
R. W. ENDEBROCK
Battelle Memorial Institute

Contents

FEATURE ARTICLE

Radiation Effects in Reactor Ceramics 1

by T. S. Elleman and T. G. Knorr, Battelle Memorial Institute

Foreword

I FUEL AND FERTILE MATERIALS . . . 16

Uranium Metal and Alloys 16
Plutonium 22
Thorium 25
Dispersion Fuels 26
Coated-Particle Fuel Materials 27
Refractory Fuel and Fertile Materials . . . 34
Basic Studies of Radiation Effects on Fuel Materials 38
References 39

II MODERATOR MATERIALS 43

Graphite 43
Beryllium Metal and Alloys 44
Beryllium Oxide 50
Beryllides 51
Solid Hydrides 52
References 53

III NUCLEAR POISONS 55

Metallic Poison Materials 55
Dispersion Control and Shielding Materials 55
References 56

IV CLADDING AND STRUCTURAL MATERIALS 57

Corrosion 57
Radiation Effects in Nonfuel Materials . . . 63
Selected Mechanical Properties of Cladding and Structural Materials . . . 71
Selected Metallurgical Aspects of Cladding and Structural Materials . . . 72
Diffusion Studies 74
Ceramic Technology 74
References 75

V SPECIAL FABRICATION TECHNIQUES 79

Melting, Hot and Cold Working 79
Cladding 80
Welding and Brazing 85
Explosive Forming 87
Nondestructive Testing 88
References 88

INDEX, VOLUME 5 91

Issued quarterly by the U. S. Atomic Energy Commission. Funds for printing this publication approved by the Director of the Bureau of the Budget on November 1, 1960.

FEATURE ARTICLE

Radiation Effects in Reactor Ceramics

By T. S. Elleman* and T. G. Knorr†

(Editor's Note: Since its inception, Reactor Materials *has dealt exclusively with recent literature on reactor-materials technology.*

With this issue the editorial staff of Reactor Materials *inaugurates, on an experimental basis, the inclusion of a review or state-of-the-art article each quarter. Topics are selected on the basis of potential reader interest, timeliness, and appropriateness to the reactor-materials field. The articles will be directed toward providing background information to readers who are not specialists in the field covered.*

Information about the behavior of ceramic reactor materials exposed to pile radiations is summarized briefly in the article below. The reams of literature on the subject have been sorted and condensed, and the major theoretical and experimental findings to date are presented. Readers who are not working in this field may be impressed by how much work is being done in this complex area. However, as is pointed out in the review, there is more reason to be impressed with how little is known in this important area.)

Introduction

In the following review, certain mechanisms of radiation damage in ceramics are summarized briefly, and a number of the property changes that occur in the radiation field of a reactor are discussed. Since the discussion is oriented toward reactor applications, emphasis has been placed on changes of physical properties of interest in reactor design. Some of these changes are density, strength, and thermal conductivity. The properties discussed are those affected by structural changes and not those affected by electronic or magnetic changes.

Most irradiation studies in ceramics have been performed with Al_2O_3, BeO, SiO_2, and various forms of carbon, and some information is available for SiC and ZrO_2. Because of the difficulty associated with standardizing experimental conditions and because of the relatively long irradiation times required to simulate reactor exposures, rather large gaps exist in our understanding of radiation behavior of ceramics, and examples of apparent contradiction in results are readily found.

Background

Cause of Damage

The properties of ceramic materials change under the influence of radiation because atoms are displaced from their initial positions and possibly because of thermal effects. As with metals, atom displacements occur as a consequence of collisions between the bombarding radiation and atoms of the material being irradiated. In order for such collisions to result in displacements, a minimum energy must be transmitted[1] which, for most materials, is in the range of 25 to 100 ev. In compounds different displacement energies might be required for the

*Assistant Chief, Radioisotopes and Radiation Division.

†Senior Physicist, Physics of Solids Division.

different atoms of the compound. For example, in alpha Al_2O_3, 50 ev is required for aluminum-ion displacements and 90 ev for oxygen-ion displacements.[2] Crystal structure of the material also influences the displacement energy. In graphite 30 ev is required to displace a carbon atom,[3] whereas 80 ev is required to displace a carbon atom from its position in the diamond structure.[4]

Atom displacements can also be produced by ionization, and in ceramics, unlike metals, this can occur with relatively low incident energies. Thus X radiation produces optical centers in alkali halides and other ionic crystals, which shows that, in some way not yet completely understood, the ionizing radiation is able to displace an atom from its lattice position. Since such radiations as fission recoils dissipate much of their energy by ionization effects, damage from such radiations can be far more severe in nonmetals than in metals.

Nature of Defected Region

The type of damage produced depends on the type of radiation. For example, if atom displacements are caused by gamma irradiation or neutrons, defects or defect clusters will be produced more or less randomly throughout the material. Defects produced in sufficient number may agglomerate to form dislocation loops. Such loops have been observed with the electron microscope in graphite and other layer type materials.[5–10]

If defects are produced by energetic heavy ions, the damage is confined in a dense trail corresponding to the path of the bombarding ion. Such dense trails are referred to as spikes and are generated by the incident ion and displaced atoms that are themselves energetic enough to produce additional displacements. Only recently have theoretical studies of spike phenomena progressed past the conceptual stage. Most of this work has been concerned with displacement spikes that are produced as a result of hard sphere type collisions (Refs. 11–13, 14*a*, and 15–26). Certain experiments suggest that a thermal process is also operating, and a recent report[27] contains an excellent discussion of most of these experiments (see also Refs. 28–30). The much more extensive damage resulting from the ionizing effects of fission recoils produces individual fission spikes that have been directly observed with the electron microscope.[31–40] Material migration has been used to explain some of the effects observed in these experiments, whereas ion bombardment of quartz and vitreous silica produces surface effects that have been explained in terms of displacement mechanisms only.[41] Fission-recoil tracks have also been directly observed in graphite,[42] several types of mica,[43,44] and in various nonreactor materials.[45–47] Conclusions of these studies indicate that, particularly for the mica studies, thermal processes are more important for the production of the observed effects than are ionization processes. Other experiments with fission tracks in mica indicate positive evidence to support the fact that a stable high-temperature phase has been formed by the fission damage.[48] Detailed explanations for the formation of the various damage effects in ceramics are not yet available. However, some idea of the relative importance of the various mechanisms appears to be evolving.

Other theoretical studies have been concerned with ranges of various atoms or ions in different materials,[49–54] the effects of structure[55–59] and impurities,[60–63] and the effects produced in a layered structure such as graphite.[64–67] A number of general references,[68–71] recent conferences,[72–75] and survey articles[76–98] are also of general interest.

Radiation Exposure

Some of the data on observed property changes in ceramic oxides are presented in the following sections.

Most of the data were obtained from specimens irradiated in reactors at ambient temperatures. The amount of damage is, of course, related to the exposure of the specimens to damage-producing radiations. For unfueled ceramic materials, fast-neutron irradiation is the primary source of damage, since this is the only type of radiation capable of producing large numbers of displaced atoms. Thus, in this case, exposure to fast neutrons is the significant measure of exposure and should be given in the reference. However, since this quantity is less readily determined than the exposure to thermal neutrons, the latter number is often the only one given, and therefore this quantity will be found from place to place in this report. Estimates of fast-neutron exposure can be deduced from such data only from detailed information about the particular reactor

and reactor position in which the radiation was made. The fast-neutron flux may be from 10 to 100% of the thermal flux, depending upon the reactor and location.

Another common unit of exposure to fast neutrons is megawatt-days per ton (Mwd/ton) of uranium, which is the irradiation exposure received by the sample during the period required for the ton (2000 lb) of uranium in the immediate vicinity of the sample to generate 1 Mwd of fission heat. Computations are made for other locations, from the detailed neutron spectrum of the reactor and a theory of the number of displacements produced by neutrons of various energies. As normally used for giving graphite irradiation exposure, this is one of the more meaningful numbers.

For fueled samples most of the radiation damage is caused by fission recoils. In this case the thermal-neutron flux and the concentration of fissionable material determine the amount of damage.

Irradiation-Induced Property Changes

Dimensional Changes

Changes in density and dimensions are probably the most commonly observed consequences of materials irradiation. Point defects produced during the irradiation result in a decrease in density and an increase in one or more of the specimen dimensions. When an atom recoils into an interstitial position, a lattice stress is induced which is usually relieved by expansion. The displaced atom leaves a vacancy. If the bonding is ionic, atoms of like charge will be adjacent to this vacancy, and an expansion will also occur here because of the electrostatic repulsion of adjacent atoms. The stress introduced in a lattice with unsymmetric bonding is relieved by preferred expansion in particular directions, which results in dimensional changes that are anisotropic.

Dimensional changes resulting from neutron irradiations have been measured for single-crystal Al_2O_3 (Refs. 14*b* and 99–102) and MgO (Refs. 101 and 103–105), sintered Al_2O_3 (Refs. 14*b*, 101, and 102) and BeO (Refs. 14*c*, 14*d*, and 106–118), graphite (Refs. 14*b*, 14*e*, 14*f*, 119*a*–*c*, and 120–129), cubic SiC (Refs. 130 and 131), and ZrO_2 (Ref. 132), hexagonal SiC, monoclinic ZrO_2 (Ref. 132), tetragonal ZrO_2 (Ref. 133), and various forms of SiO_2, including quartz,[134–141] tridymite,[135] low cristobalite,[135,142] coesite,[136] and vitreous[134,141,143] silica. Most of the fast-neutron irradiations were carried out at temperatures under 200°C and at fast-neutron exposures ranging up to 2×10^{21} nvt. Measurements were usually taken at ambient temperatures with the specimens removed from the neutron flux. Changes in density, specimen dimensions, or lattice parameters were determined as indications of the radiation effects. The complexity of the data prevents a tabular presentation of results, but the general trends observed are described in the following paragraphs.

Although differences in technique and specimen structure have contributed to differences in behavior for some compounds, it appears that the ceramics least subject to neutron-radiation-induced expansion are Al_2O_3, MgO, cubic and tetragonal ZrO_2, and coesite (a high-density synthetic form of silica formed at high pressures). These materials generally exhibited dimensional and density changes of much less than 1% and usually less than $^1/_{10}$% for neutron exposures in the range 1 to 5×10^{20} nvt (thermal). Densities of these materials tend to decrease during irradiation. However, occasional increases in density have been observed in some of the sintered materials.[14b] Preferred expansion along a particular crystal axis was observed in Al_2O_3, but the maximum expansion was only about twice the expansion in any other direction.[100] Although these materials did not exhibit pronounced dimensional changes, the number of studies is quite limited, and the maximum indicated neutron exposure is not high. A more thorough study of radiation effects in these materials is needed.

BeO and cubic and hexagonal SiC generally exhibited larger density and dimensional changes during irradiation than the materials just discussed. However, monoclinic ZrO_2, graphite, and various forms of silica exhibited even more pronounced dimensional changes.

Early studies[14c,14d,107] of dimensional changes in BeO during irradiation revealed increases of only a few tenths of a percent at exposures up to 5×10^{20} nvt. However, recent studies (Refs. 111, 116, 117, and 144) at exposures up to 3×10^{21} nvt have revealed expansions of 4 to 6%. The expansion increased with increasing exposure and with decrease in irradiation tem-

perature. In a number of cases the expansion was sufficient to cause specimen powdering. This powdering[111] was most pronounced in specimens irradiated below 400°C.

The initial density has been observed to have a decided effect on the density changes produced by irradiation. For example, the expansion under neutron irradiation of a BeO specimen having a density of 3.0 g/cm^3 was about double that of a specimen with a density of 2.7 g/cm^3 after a similar exposure.[108]

The irradiation[131] of SiC resulted in a 2.5% decrease in density after a neutron exposure of 1.3×10^{20} nvt.

Graphite is of particular interest, since its expansion during irradiation is large and anisotropic. Growth occurs perpendicular to the *c* axis, which is the axis of weakest atomic bonding, whereas only slight expansion or even contraction occurs along the other axes.[129] Expansion perpendicular to the *c* axis is observed only at ambient irradiation temperatures, and high-temperature irradiation produces contraction, as discussed later. At 10^{21} nvt and ambient irradiation temperatures, the lattice expansion[145] along the *c* axis may be as much as 16%, but the gross sample expansion is generally much less than this since voids in the graphite absorb most of the crystalline expansion. In one set of experiments,[146] the radiation-produced-expansion rate of CSF graphite was observed to be constant (0.26% per 1000 Mwd/ton) up to an exposure of 5000 Mwd/ton. In the range from 5000 to 11,000 Mwd/ton, the expansion rate was also relatively constant but was only about one-third of the above rate. Chemical impurities in graphite have also been observed to affect the radiation-induced expansion. For example, the addition of 1 wt.% iron oxide to Texas coke-base graphite resulted in a greater expansion after irradiation than was observed in pure material.

Irradiation of graphite[147] at 150°C resulted in damage an order of magnitude less than that produced by an equivalent irradiation at 30°C, apparently because of the greater defect mobility at the higher temperature.[14e,123] Irradiation of graphite at even higher temperatures produced a contraction rather than an expansion,[124,125] tentatively attributed to a more efficient ordering of the graphite crystallites. Contraction has been observed at irradiation temperatures as high as 1200°C. Figure 1 illustrates the effect of irradiation temperatures on the dimensional changes produced in a CSF graphite. At low irradiation temperatures, a 4% expansion occurred which was perpendicular to the extrusion direction (10^{21} nvt), whereas a 1% contraction occurred in the parallel direction. Increasing the irradiation temperature reduced the effect and, in the temperature range 300 to 400°C, a contraction in both directions was observed. Higher temperatures produced essentially no change in dimensions. Studies to find the most radiation-resistant graphite for exposures at temperatures of 500°C indicated that the best moderator material should be fabricated from a fine-grained needle coke that is graphitized at 3000°C or above without a pitch impregnation.[128]

Silica, although not normally regarded as a reactor material, is worthy of brief discussion because of the complexity of its irradiation behavior. Irradiation of quartz produces an anisotropic expansion along the *a* crystallographic axis which is 10 times the expansion in the other directions. The decrease in density[135] reaches a saturation of about 15% after 1.5×10^{20} nvt. The density drops slowly up to 5×10^{19} nvt and then changes more rapidly until saturation is reached, in direct contrast to observations in other oxides. The unexpected expansion behavior can be explained[137] by assuming that vitreous zones are initially formed in the structure by the irradiation and are prevented from expanding by the rigid surrounding structure. As the irradiation continues, these struc-

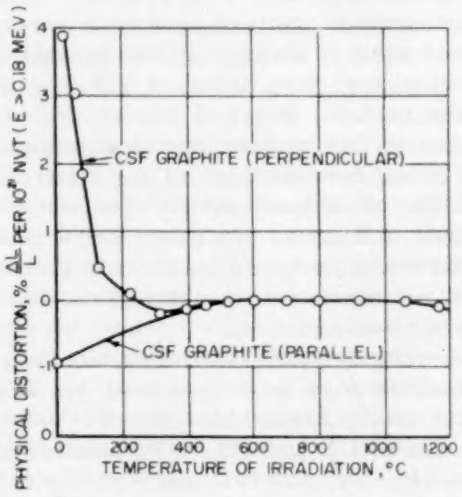

Fig. 1 Effect of irradiation temperature on graphite physical distortion.[125]

tures become plastic, and the stresses produced by lattice disorder are relieved by expansion. This explanation is supported by annealing data that indicate that irradiated quartz will revert to normal quartz during heating unless there has been appreciable radiation-produced expansion. If appreciable expansion has occurred, then heating will produce a polycrystalline form of quartz that contains large numbers of voids. Tridymite[135] and cristobalite[135] behave like quartz during neutron irradiation, but vitreous silica[148] increases in density to yield a form equivalent in density to that attained by irradiated quartz, tridymite, or cristobalite.

The irradiation of ceramics by charged particles heavier than neutrons can produce significant dimensional changes. In one investigation[101] the recoil alpha particles and tritium atoms from the $Li^6(n,\alpha)H^3$ reaction in lithium-impregnated Al_2O_3 did not produce any greater effect than that obtained by neutron irradiation of Al_2O_3 alone; however, the irradiation of Al_2O_3 with recoil fragments from uranium fissions at 290°C did result in pronounced dimensional changes. In another study,[149] specimens of Al_2O_3 that contained dispersed UO_2 showed complete destruction of the Al_2O_3 crystal structure after doses of 2×10^{18} fissions/cm^3 and a 30% volume increase after 9×10^{19} fissions/cm^3. Metallographic examination and X-ray diffraction indicated no significant changes in the UO_2; therefore the expansion was attributed to damage in the Al_2O_3. Calculations showed that the fission fragments caused about 100 times more damage than would be expected by theory. This is in contrast to comparisons for neutron irradiations, where the observed damage is 40 to 50 times less than that predicted.

Dispersions[33] of 70 wt.% ZrO_2, 13 wt.% CaO, and 17 wt.% UO_2 showed no significant dimensional changes at 9×10^{19} fissions/cm^3, and compacts[14c,150] of BeO and UO_2 generally showed linear expansions of less than 1% for exposures up to 10^{19} fissions/cm^3. However, at exposures of 10^{21} fissions/cm^3, solid solutions of ZrO_2-UO_2 exhibited expansions as large as 25%, and BeO-UO_2 compacts showed a 10% density decrease.[151] This fission-fragment exposure is large, and specimen deterioration is to be expected.

Although the importance of composition, specimen density, and behavior of the fissionable material represent large uncertainties in the interpretation of these results, it does appear that relatively large dimensional changes are produced by recoil fission fragments.

Alteration of Mechanical Properties

Changes in mechanical properties are often observed following neutron irradiation of a ceramic specimen. Properties that have been observed to change include tensile strength, hardness, crushing strength, creep, and elastic modulus. Such changes are usually explained in terms of dislocation mechanisms. Radiation-produced defects are considered to inhibit dislocation motion, which results in enhanced mechanical strength. However, the blocking of dislocations, if it occurs on a few planes, also increases the probability of crack formation, which results in a more brittle material or one that might tend to shatter by powdering. In a few cases the data have been sufficiently consistent to permit a comparison of a mechanical-property change with other radiation-produced changes, thus providing a basis for better understanding of radiation-damage mechanisms. However, in many cases the limited amount of data or lack of reliability in the observed property changes has tended to obscure the radiation-induced changes in the mechanical properties. Difficulties in reproducing measurements often result in a reluctance to acknowledge radiation effects unless the observed change is quite large.

Experiments designed to measure changes in mechanical properties following neutron irradiation have been carried out for single-crystal and sintered Al_2O_3 (Ref. 14*b*), pressed BeO (Refs. 14*c*, 106–108, 111, 113, and 152), graphite (Refs. 119*a*, 119*b*, and 153), ZrO_2 (Ref. 14*b*), SiO_2 (Refs. 154–156), and a number of natural minerals such as spinel ($MgO \cdot Al_2O_3$), forsterite ($MgO \cdot SiO_2$), and mica.[14b] The information available for Al_2O_3, ZrO_2, and the minerals containing MgO is quite limited but tends to indicate similarities in behavior. These compounds[14b] exhibited Young's modulus changes of less than 10% after exposures up to 1.6×10^{20} nvt. Irradiation of BeO from 3×10^{19} to 1×10^{20} nvt produced no significant changes in either Young's modulus or crushing strength.[14c,106,107] However, workers[14d] who used hot-pressed beryllia cylinders of slightly higher density observed a factor of 2 to 5 decrease in compression strength, and a factor of 2 decrease in

elastic modulus after 5×10^{20} nvt (thermal). Other investigators[152] observed crushing-strength decreases of 60 to 80% in a wide selection of beryllia ceramics at neutron exposures of 2×10^{21} nvt. Powdering of BeO specimens at exposures of 2×10^{20} to 3×10^{21} nvt has also been observed (Refs. 108, 111, 113, and 157). High specimen density and low irradiation temperature appear to be factors that favor powdering, but specimen-preparation techniques are also important. Powdering occurs at neutron exposures below those which will be encountered in a reactor core; therefore a solution to this problem appears necessary if BeO is to find extensive use as a reactor component.

Compacts of 2 wt.% UO_2 in BeO and 10 wt.% UO_2 in BeO exhibited changes in mechanical properties after exposures of 3×10^{19} to 1×10^{20} nvt (thermal), whereas comparison specimens of pure BeO remained unchanged.[14c] The fueled specimens showed decreases of 20 to 30% in crushing strength and similar decreases in elastic modulus. The effects appeared to saturate by 3×10^{19} nvt (thermal), since no significant increases were observed at higher exposures. The 10 wt.% UO_2 specimens did not show greater damage than the 2 wt.% UO_2 specimens, in spite of the higher fission-fragment exposures. A tentative explanation advanced for the lack of dependence on fission exposure is that annealing effects occurred in the 10 wt.% UO_2 specimens because of the higher irradiation temperature resulting from the increased fission rate. Nevertheless, the results appear to show significantly greater damage in the fueled specimens than in the unfueled samples, thus supporting other data that indicate that fission fragments produce more damage than fast neutrons.

Irradiation of graphite produces a stronger and harder material. Cross-breaking strength and compression strength appear to increase linearly with neutron exposure,[119a] reaching values three to four times the preirradiation strength at doses of about 5×10^{19} nvt. At higher exposures the strength decreases until apparent stabilization is obtained at about twice the preirradiation strength. Figure 2 shows a plot of specimen strength vs. neutron exposure which illustrates the strength maximum that occurs at about 10^{20} nvt. Difference in the change of cross-breaking strength and compression strength is indicated. Young's modulus increases[119a,119b] also show saturation at a value three times the preirradiation modulus after about 10^{20} nvt. This saturation is followed by a slight decrease in modulus at still higher neutron exposures.

Irradiation hardening produces a graphite that is more difficult to machine, as evidenced by penetration of a carbide-tipped drill in a standardized machining test.[119a] The hardness increase in graphite is in contrast to a hardness decrease (about a factor of 5) that has been observed in diamond after 8×10^{20} nvt.

Phase Transformations

Two types of radiation-induced phase transformations may be distinguished. In one type the radiation accelerates a transition from a metastable to a stable configuration, whereas in the other type the transition is apparently from a stable to a metastable configuration. The first process is merely an acceleration of a transition that is occurring naturally, whereas the second process involves the introduction of a new mechanism that permits the metastable phase to form. Such mechanisms have been explained in terms of thermal effects that are produced in the various spikes, or in terms of enhanced diffusion that occurs because of defects produced by the irradiations.

Examples of accelerated rates are readily found; typical are the low-temperature conversion of white to gray tin,[158] the ordering of

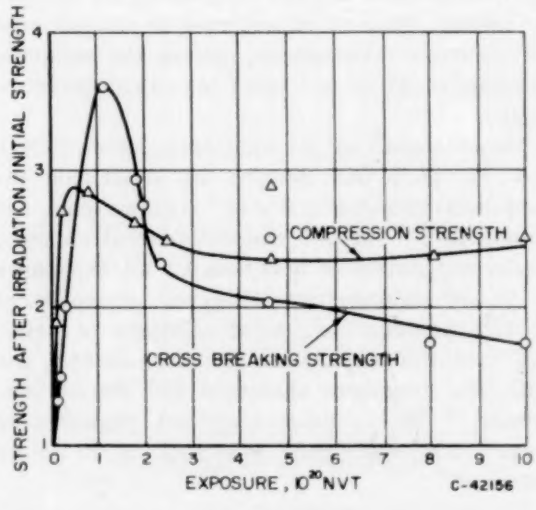

Fig. 2 Changes in mechanical strength as function of neutron exposure for parallel-cut KC graphite.[119a]

disordered superlattice alloys,[159] and the precipitation of a second phase in a supersaturated alloy.[160] Examples of apparent transition from a stable to a metastable phase have been observed in the radiation-induced change of monoclinic ZrO_2 to a cubic structure[161] and the low-temperature transition from a tetragonal $BaTiO_3$ to a cubic structure.[162] It was originally postulated that the ZrO_2 cubic phase formed so as to reduce the lattice strain introduced by the recoil interstitial atoms. However, subsequent studies showed that pure ZrO_2 would not transform,[163] whereas ZrO_2 containing trace impurities of uranium would transform when irradiated.[163,164] This led to the speculation that regions of the high-temperature cubic phase formed in thermal spikes produced by the fission fragments and were frozen in because of the rapid dissipation of the heat. It was calculated that about 3.4×10^{16} fissions/cm^3 were required to produce complete conversion to the cubic phase. However, when a thin film of absorbing material was interposed between the ZrO_2 and uranium during irradiation,[165] the monoclinic-to-cubic transformation did not occur even though the required fission-fragment energy was deposited in the ZrO_2. It was suggested that the uranium that sputtered into the ZrO_2 during the normal irradiation was necessary for initiation of the transformation, possibly producing nucleating sites for the formation of the cubic phase. However, a more recent study has shown that, in the transformation of ZrO_2 containing 0.5 wt.% uranium, the uranium atoms themselves did not act as nucleating sites for the transformation.[166]

The radiation-produced phase transformation in ZrO_2 is the most extensively studied example of this effect, but phase transformation studies have been carried out for other materials of interest. Quartz, tridymite, and crystobalite each exhibit low-temperature (alpha) and high-temperature (beta) modifications that occur at temperatures ranging from 120 to 570°C. The difference in the α and β forms is one of slight rotation between adjacent SiO_4 tetrahedra. Therefore the process is easily reversible. After neutron irradiation to 5×10^{19} nvt, it was observed that the $\alpha \rightarrow \beta$ transition no longer occurred in quartz, a fact that the authors attributed to stress generated by interstitial atoms produced from neutron irradiation.[135,136] However, other workers showed that, after 1.3×10^{19} nvt exposure, the $\alpha \rightarrow \beta$ transition temperature was markedly lowered for crystobalite.[142] These results appear to show radiation-produced restriction and enhancement of phase transformation in only slightly different materials.

Changes in Thermal Conductivity

Thermal-conductivity changes in a radiation field warrant close attention both because thermal conductivity is a critical parameter in reactor operation and because the changes produced in this property by neutron irradiation often seem to be particularly large. Although irradiation-produced density and dimensional changes are generally in the range of a few percent, the thermal resistivity may change by as much as a factor of 20 or 30. Changes in thermal properties occur because of the modified phonon scattering which results from the defects produced during irradiation. High-temperature annealing removes most of the damage, but some residual radiation effects generally remain.

Irradiation of single-crystal Al_2O_3 and sintered Al_2O_3 specimens to 3×10^{19} nvt and 3×10^{20} nvt reduced the thermal conductivity about one-half and one-fourth the preirradiation value, respectively.[14b] Sintered and single-crystal specimens behaved about the same. There was no indication of saturation effects. Crystals of $MgO \cdot SiO_2$ and $MgO \cdot Al_2O_3$ exhibited about the same behavior,[14b] and they supply a crude estimate of what might be expected from MgO.

Irradiation of vitreous silica at temperatures of 2 to 15°K and maximum exposures of 4.1×10^{19} nvt resulted in an increase in thermal conductivity, the magnitude of which is in agreement with that predicted by theory.[167]

Hot-pressed BeO specimens were irradiated at exposures ranging from 3×10^{19} nvt to about 2×10^{21} nvt, and considerable variation was obtained for the thermal conductivities (Refs. 14*b*–*d*, 114, 152, and 168). Depending on the investigator, the postirradiation conductivities ranged from around 0.9 of the preirradiation value down to a low of about 0.2 of the preirradiation value. Typical data that illustrate the range of thermal conductivities encountered are presented in Table 1. The specimen densities and measurement temperatures employed in the determination are also included. The data in the table indicate that specimen densities and measurement techniques could

explain some of the differences in values, but the information presented in the various papers was not sufficiently detailed to permit comparisons on this basis.

The irradiation of uranium-fueled BeO at 3 to 7×10^{19} nvt (thermal) produced a decrease by a factor of 4 to 6 in thermal conductivity, whereas a comparable irradiation of pure BeO produced a decrease by only a factor of 2. Again, this demonstrates the greater damaging effect of fission fragments.

Table 1 RADIATION-PRODUCED THERMAL-CONDUCTIVITY CHANGES IN BeO (SUMMARY OF RESULTS)

Total fast-neutron exposure, neutrons/(cm²)(sec)	Temp. during measurement, °C	Original specimen density, g/cm³	(Postirradiation thermal conductivity)/(initial condition)	Ref.
3.6×10^{19}	90		0.60	2
7×10^{19}	140	2.99	0.19	5
7×10^{19}	140	2.74	0.31	5
7×10^{19}	30	2.8	0.66	1
5×10^{20}	80	2.60	0.90	11
2×10^{21}	550	2.8	0.30	146
	130	3.0	0.80	12

Thermal conductivity of graphite changes rapidly during irradiation. Thermal resistivities 40 to 50 times the preirradiation value have been observed[119a,119b] after fast-neutron exposures of 1.3×10^{20} nvt. As shown in Fig. 3, thermal resistivity appeared to change in proportion to the neutron exposure up to about 3×10^{20} nvt, where approaching saturation caused a gradual decrease in the rate of change. Slight differences were obtained in measurements taken in the parallel and transverse directions, but the saturation exposures were about the same. The thermal conductivity changes less during irradiation at higher temperatures; thus thermal conductivity decreased by a factor of only 2 during irradiation at 150°C.

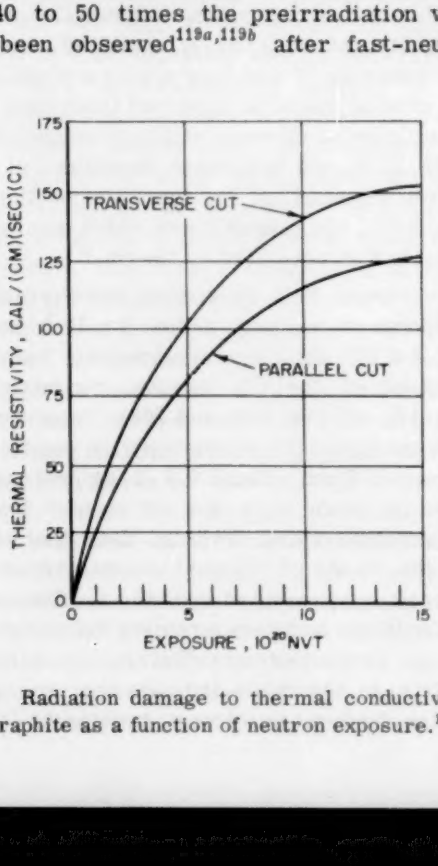

Fig. 3 Radiation damage to thermal conductivity of CSF graphite as a function of neutron exposure.[119a]

A similar effect was noted in postirradiation annealing of irradiated graphite, where annealing temperatures of about 400°C caused a decrease by a factor of 2 in the change in thermal resistivity.[119b] It is interesting to note that BeO, which exhibited much smaller radiation changes than graphite, also was much more resistant to annealing. Heat-treatment of BeO specimens between 500 and 600°C produced only a slight annealing of the thermal resistivity, and heating to a temperature in the range of 1000 to 1400°C was required to remove most of the damage.[14c,14d]

Chemical-Reactivity Changes

Increases in chemical reaction rates are often observed when the reacting species are subjected to a radiation field. The increased rate is usually attributed to the formation of more reactive free-radical species by the irradiation or to changes in the surface properties of one of the reacting solids. Most of the reported work on in-pile chemical reactivity of ceramics describes the reactions of graphite with CO_2 (Refs. 169–172) or oxygen.[173–175]

These systems are of interest in gas-cooled-reactor programs, since excessive reaction of graphite with the gas coolant could result in eventual destruction of the reactor core.

In most studies of the in-pile reaction of graphite with CO_2 or oxygen, approximately an order of magnitude increase in reaction rate was observed over the out-of-pile reaction rate. Occasional cases of decrease in reaction rate during irradiation were also found.[174] Most results were consistent with the explanation that the rate increases were due to the production of active species in the CO_2 or oxygen during the irradiation, which attacked the graphite. In cases where the graphite was removed from the high reactor flux but the CO_2 was still passed through the reactor, the rate of graphite oxidation could be varied by changing the time lag between exposure of the gas to the radiation field and contact of the gas with the graphite.

Increased reaction rates were also observed in out-of-pile studies of graphite.[175] Pits produced in the graphite by irradiation were believed to facilitate chemical attack of the previously continuous graphite layers and result in increased reaction rates.

A similar process may also explain the increased oxidation rates observed for SiC during irradiation with 37-Mev alpha particles.[176] When weight gain was used as an indication of oxidation rate, the irradiated specimens increased in weight three to five times faster than control specimens. Since it has been suggested that SiC may be stabilized by a thin oxide layer on the surface, pitting of the surface layer would be expected to produce an increase in reaction rate.

Although relatively few studies on reactivity changes of reactor ceramics following irradiation have been performed, enough work has been done with other materials to support the existence of an effect. Observations have been made of increased rates of NiO reduction and Fe_2O_3 dissolution following proton irradiation,[177,178] increased catalytic activity of alumina, silica gel, and quartz following gamma irradiation,[179–181] and increased gas absorption on alumina following neutron irradiation.[182] A recent conference entitled "Reactivity of Solids" included a session on reactivity induced by irradiation, and a number of interesting papers on the subject were presented.[183]

Changes in Diffusion Rate

It is generally accepted that diffusion in solids takes place via defects in the crystal, which are often vacancies or interstitials. Since neutrons and fission fragments produce such defects, a close connection between diffusion and irradiation is to be expected. Several investigators[184,185] have developed theories relating diffusion to radiation intensity, and in-pile experiments on self-diffusion in metals have been carried out, the results of which are in agreement with the theoretical predictions. The magnitude of the radiation-enhanced diffusion is dependent both upon the production rate and upon the annihilation rate of the generated defects, and different materials thus exhibit different behavior. However, the diffusion coefficient produced by radiation is small, and the effect is observable only at low temperatures where thermal diffusion is negligible.[186] For this reason radiation-enhanced diffusion is not expected to be important in reactor ceramics that are maintained at moderately high operating temperatures, and there have been few investigations of this effect in ceramics.

Figure 4 shows an example of radiation-enhanced diffusion observed in alpha brass with the aid of resistivity measurements. No apparent radiation effect is observed at temperatures above 200°C. The dashed line shows the diffusion behavior predicted by theory, whereas the experimental points show the close agreement with theory.

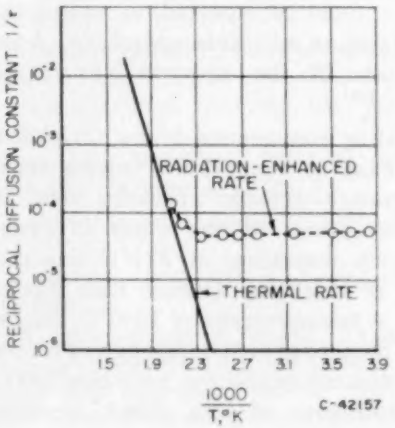

Fig. 4 Radiation-enhanced diffusion in alpha brass.[186] Dashed curve is the theoretical rate, and circles are the data points.

Experiments[187] have been performed to investigate the effect of irradiation on gas diffusion in Al_2O_3. Specimens of hydrated Al_2O_3 and alpha Al_2O_3 were irradiated to a fuel burnup of 1440 Mwd/ton, and the emanation method was used to measure thoron diffusion in the Al_2O_3 during postirradiation heating. The effect of irradiation on gas release was insignificant, and the only observed change in release behavior was a slight decrease in gas release rate at low temperatures.

A similar absence of irradiation effects was observed in the release of the fission product Xe^{133} from alpha Al_2O_3 during heating.[188] No significant differences in the fractional release of Xe^{133} were observed over the concentration range used.

Annealing of Defects

An important factor in limiting radiation damage in material is the annealing of defects that occur during heating. Often a temperature increase of several hundred degrees is sufficient to anneal out most radiation-produced property changes. This is particularly true in graphite, where the low-temperature irradiation damage is quite high.[119b] In many ceramics measurable annealing is first observed in the temperature range 250 to 400°C, whereas temperatures of 600 to 1000°C produce considerable annealing of the changes in physical properties. Finally, heating to 1200 to 1500°C results in recovery that is nearly complete, with only slight color changes persisting beyond 1800°C (Refs. 14*c*, 14*d*, 99, 100, 107, 109, and 189–196). As might be expected, annealing is a function of time as well as temperature. A quantitative study of the process becomes quite complex.[197]

Annealing also occurs *during* irradiation, and an increase in temperature during irradiation may produce greater recovery than thermal annealing alone. In one study of graphite,[123] irradiation annealing at 335°C was more effective in removing damage than thermal annealing at temperatures of 1300°C. Since only a limited number of high-temperature irradiations to high neutron exposures have been performed, the significance of this effect is difficult to estimate.

In one annealing study[198] of graphite that contracted during irradiation, the specimen did not recover its original dimensions. This behavior tended to support the theory that the irradiation-induced contraction resulted from relief of stresses frozen in during fabrication.[198] This explanation was supported by an additional study in which it was observed that annealing of the graphite prior to irradiation reduced the amount of contraction obtained during the irradiation.[199]

In most of the described experiments, the irradiations were carried out at ambient temperatures not exceeding 200°C, and the materials were not subjected to the annealing that would occur during actual high-temperature reactor operation. For this reason many investigators chose to regard the quoted effects as upper limits that may bear only a slight relation to the actual behavior of the material as a reactor component.

Conclusions

Several ceramic materials such as Al_2O_3 and BeO appear to exhibit satisfactory stability under many irradiation conditions, although possible complications are suggested by the fission-fragment-induced swelling of Al_2O_3 and the disintegration of BeO compacts at high neutron exposures. Graphite exhibits relatively pronounced radiation-produced changes, but annealing may reduce these to manageable limits in actual reactor operation. Materials such as ZrO_2, MgO, SiO_2, and SiC have not been studied extensively, and a discussion of their properties is limited to a rather narrow range of experimental conditions. The fact that fission fragments have greater damaging effects compared with neutrons warrants further study of ceramics if they are to be exposed to fission recoils during reactor utilization.

The number and scope of radiation-damage studies in ceramics appear to be increasing each year, and much useful information, particularly in the areas of fission-fragment effects, high-temperature irradiations, and irradiations to exposures greater than 10^{21} nvt, will soon be forthcoming. Many of these experiments will be reviewed in future issues of *Reactor Materials*.

References

1. P. G. Lucasson and R. M. Walker, Research Directed Toward the Study of the Radiation

Damage Thresholds of the Elements, Report 61-GC-166, General Electric Co., April 1961.
2. G. W. Arnold and W. D. Compton, *Phys. Rev. Letters*, 4: 66–68 (1960).
3. I. T. Myers, H. V. Larson, and J. S. Loomis, Resistivity Changes in Electron Irradiated Graphite, USAEC Report HW-SA-2207, Hanford Atomic Products Operation, 1960.
4. C. D. Clark et al., *Proceedings of the International Conference on Semiconductor Physics*, pp. 316–319, Academic Press, New York, and Prague Publishing House of the Czechoslovak Academy of Sciences, 1961.
5. W. Bollmann, *Phil. Mag.*, 5(8): 621 (1960).
6. G. K. Williamson and C. Baker, *Phil. Mag.*, 6(8): 312 (1961).
7. W. T. Eeles, *Nature*, 188: 287–289 (1960).
8. W. Bollmann, *J. Appl. Phys.*, 32: 869–876 (1961).
9. L. C. F. Blackman, *Research (London)*, 13: 492–502 (1960).
10. K. Izui and F. E. Fujita, *J. Phys. Soc. Japan*, 16: 1032 (1961); 16: 1829 (1961).
11. E. M. Baroody, *Phys. Rev.*, 116: 1418–1424 (1959).
12. K. Weiser, *Phys. Rev.*, 126: 1427 (1962).
13. M. A. Mokul'skii, Processus Cinetiques Dans Une Substance Irradiee, French Report CEA-tr-R-1400, 1960.
14. *Proceedings of the Second United Nations International Conference on the Peaceful Uses of Atomic Energy, Geneva, 1958*, United Nations, New York, 1958:
   a. A. K. Seeger, On the Theory of Radiation Damage and Radiation Hardening, Vol. 6, p. 250.
   b. J. H. Crawford, Jr., and M. C. Wittels, Radiation Stability of Nonmetals and Ceramics, Vol. 5, p. 300.
   c. J. R. Gilbreath and O. C. Simpson, The Effect of Reactor Irradiation on the Physical Properties of Beryllium Oxide, Vol. 5, p. 367.
   d. J. Elston and R. Caillat, Physical and Mechanical Properties of Sintered Beryllia Under Irradiation, Vol. 5, p. 345.
   e. R. E. Nightingale, Damage to Graphite Irradiated Up to 1000°C, Vol. 7, p. 295.
   f. H. W. Davidson and H. W. Losty, The Effect of Neutron Irradiation on the Mechanical Properties of Graphite, Vol. 7, p. 307.
15. W. D. Compton and G. W. Arnold, *J. Appl. Phys.*, 31: 621–625 (1960).
16. G. Nemeth, *Nuovo Cimento*, 21: 764–772 (1961).
17. K. Tharmalingam and A. B. Lidiard, *Phil. Mag.*, 6: 1157–1162 (1961).
18. A. C. Damask and G. J. Dienes, *Phys. Rev.*, 125: 444–446, 447–450 (1962).
19. R. O. Hatcher and G. J. Dienes, *Phys. Rev.*, 124: 726–735 (1961).
20. J. R. Beeler, Jr., and D. G. Besco, Knock-on Cascades and Point Defect Configurations in Binary Materials, USAEC Report ORO-547, General Electric Co., Flight Propulsion Laboratory Dept.; also presented at the International Symposium on Radiation Damage to Solids and Reactor Materials, Venice, Italy, May 7–11, 1962 (proceedings to be published).
21. C. Lehmann, Zur Bildung Von Defekt-Kaskaden in Kristallen Beim Beschuss Mit Energiereichen Korpuskularstrahlen, Report NP-9141, 1959.
22. Oak Ridge National Laboratory, Solid State Division Annual Report for the Period Ending August 31, 1960, USAEC Report ORNL-3017, Dec. 6, 1960.
23. J. B. Gibson et al., *Phys. Rev.*, 120: 1229 (1960).
24. M. Yoshida, *J. Phys. Soc. Japan*, 16: 44–50 (1961).
25. E. Brown and G. H. Goedecke, *J. Appl. Phys.*, 31: 932–934 (1960).
26. G. J. Dienes and A. C. Damask, Radiation Effects in Inorganic Solids, *Discussions of the Faraday Soc.*, 31: 29–37 (1961); also see Theory of Annealing of Vacancies and Divacancies in Pure Metals, USAEC Report BNL-5214, Brookhaven National Laboratory, 1961.
27. G. R. Piercy, *J. Phys. Chem. Solids*, 23: 463–477 (1962).
28. K. A. Muller, *Phys. Rev.*, 123: 1550 (1961).
29. A. Corciovei and D. Greco, *Compt. rend.*, 252: 3964 (1961).
30. A. M. Kosevich and L. V. Tanatarov, *Soviet Phys.-Solid State*, 2: 2676 (1961).
31. T. S. Noggle and J. O. Stiegler, *J. Appl. Phys.*, 33: 1726–1730 (1962).
32. J. O. Stiegler and T. S. Noggle, *J. Appl. Phys.*, 33: 1894–1895 (1962).
33. J. J. Kelsch et al., *J. Appl. Phys.*, 33: 1475–1482 (1962).
34. T. S. Noggle and J. O. Stiegler, Symposium on Radiation Effects in Refractory Fuel Compounds, *ASTM Special Tech. Publ. No. 306*, pp. 47–63 (1962).
35. *Reactor Core Materials*, 3(4): 39 (November 1960); 4(1): 55 (February 1961).
36. T. K. Bierlein and B. Mastel, *J. Appl. Phys.*, 31: 2314 (1960).
37. T. K. Bierlein and B. Mastel, *J. Appl. Phys.*, 31: 2315 (1960).
38. T. K. Bierlein and B. Mastel, Experimental Evidence of Fission Fragment Damage in Some Metals and Nonmetals, USAEC Report HW-68919, Hanford Atomic Products Operation, Mar. 1, 1961.
39. T. G. Knorr and C. M. Schwartz, in Progress Relating to Civilian Applications During April 1962, USAEC Report BMI-1577 (Del.), Battelle Memorial Institute, May 1, 1962.

40. J. A. Brinkman, Fission Damage in Metals, USAEC Report NAA-SR-6642, Atomics International, Mar. 1, 1962.
41. R. L. Hines and R. Arndt, *Phys. Rev.*, 119: 623 (1960).
42. K. Izui and F. E. Fujita, *J. Phys. Soc. Japan*, 16: 1032 (1961).
43. E. C. H. Silk and R. S. Barnes, *Phil. Mag.*, 4(8): 970–972 (1959).
44. G. Bonfiglioli, A. Ferro, and A. Mojoni, Electron Microscope Investigation on the Nature of Tracks of Fission Products in Mica, Report AFOSR-981, May 1961.
45. F. P. Bowden and L. T. Chadderton, *Nature*, 192: 31–34 (1961).
46. F. P. Bowden and H. M. Montaqu-Pollock, *Nature*, 191: 556–559 (1961).
47. K. Izui and F. E. Fujita, *J. Phys. Soc. Japan*, 16: 1779 (1961).
48. P. B. Price and R. M. Walker, *Phys. Rev. Letters*, 8: 217 (March 1962); also see General Electric Research Laboratory Reports 62-RL-(2969M) and 62-RL-(2970M).
49. G. Leibfried, *J. Appl. Phys.*, 33: 1933–1943 (1962).
50. D. K. Holmes and G. Leibfried, *J. Appl. Phys.*, 31: 1046 (1960).
51. N. A. Protopopov et al., *At. Energ. (USSR)*, 10: 166–168 (1961).
52. D. Powers and W. Whaling, *Phys. Rev.*, 126: 61–69 (1962).
53. P. Armbruster, *Z. Physik*, 166: 341–354 (1962).
54. M. T. Robinson et al., paper presented at International Colloquium on Ion Bombardment, Bellevue, France, Dec. 4–8, 1961.
55. G. Leibfried, *J. Appl. Phys.*, 31: 117–121 (1960).
56. A. H. Cottrell, *Nucl. Power*, 5: 130–131 (1960).
57. C. Lehmann and G. Leibfried, *Z. Physik*, 162: 203–214 (1961); also in Report NP-9814.
58. E. M. Baroody, *Phys. Rev.*, 124: 745–747 (1961).
59. M. W. Thompson, *Nucleonics*, 18: 135 (1960).
60. A. N. Goland, Report MRL-116, March 1962.
61. A. Sosin, *Phys. Rev.*, 122: 1112–1116 (1961).
62. R. R. Hasiguti, *J. Phys. Soc. Japan*, 15: 1807–1814 (1960).
63. A. C. Damask and G. J. Dienes, *Phys. Rev.*, 120: 99 (1960).
64. I. Isuzuka, *J. Phys. Soc. Japan*, 16: 407–413 (1961).
65. Vm. Agranovich and L. P. Semenov, *At. Energ. (USSR)*, 10: 572–576 (1961).
66. G. R. Hennig, *Nucl. Sci. Eng.*, 3: 514–528 (1958).
67. T. Iwata, *J. Phys. Soc. Japan*, 16: 197–205 (1961).
68. D. S. Billington and J. H. Crawford, Jr., *Radiation Damage in Solids*, Princeton University Press, Princeton, N. J., 1961.
69. F. Seitz and J. S. Koehler, Displacement of Atoms During Irradiation, *Solid State Phys.*, Vol. II, pp. 307–448, Academic Press Inc., New York, 1956.
70. G. J. Dienes and G. H. Vineyard, *Radiation Effects in Solids*, Interscience Publishers, Inc., New York, 1957.
71. G. H. Kinchin and R. S. Pease, The Displacement of Atoms in Solids by Radiation, *Repts. Progr. Phys.*, 18: 1 (1955).
72. IAEA Symposium on Radiation Damage to Solids and Reactor Materials, Venice, Italy, May 7–11, 1962 (proceedings to be published).
73. Fifth International Congress for Electron Microscopy, Philadelphia, Aug. 29–Sept. 5, 1962 (proceedings to be published by the Academic Press Inc.).
74. American Physical Society Meeting, Seattle, Aug. 27–29, 1962 (to be published as a Bulletin of the American Physical Society).
75. International Conference on Crystal Lattice Defects, Kyoto, Japan, Sept. 7–12, 1962.
76. C. R. Tipton, Jr. (Ed.), *Reactor Handbook, Volume 1, Materials* (2nd ed.), Interscience Publishers, New York, 1960.
77. F. A. Levi, Mechanical Properties of Irradiated Solids, *Nuovo Cimento, Suppl. 12*, 2: 124–294 (1959).
78. A. H. Cottrell, Effect of Nuclear Radiation on Engineering Materials, *J. Brit. Nucl. Energy Conf.*, 5: 64 (1960).
79. D. S. Billington and J. H. Crawford, Jr., Solid State Division Annual Report for Period Ending August 31, 1961, USAEC Report ORNL-3213, Oak Ridge National Laboratory, Dec. 29, 1961.
80. W. L. Kosiba, Part I. Survey of Data on the Irradiation Effects of Al_2O_3 and Inconel-X, USAEC Report GAMD-2363, General Atomic Div., General Dynamics Corp., June 29, 1961.
81. R. S. Barnes, Radiation Effects in Cladding Materials, *Nucl. Power*, 5: 122 (1960).
82. I. B. Cadoff, A Literature Survey on the Relationship Between Dimensional Changes Produced by Radiation and Crystal Structure, USAEC Report WADC-TR-58-325, New York University, June 1958.
83. E. M. Doss, Radiation Damage to Non-Metallic Materials, USAEC Report NAA-SR-Memo-1890, Atomics International, May 8, 1957.
84. H. Goldstein, *Fundamental Aspects of Reactor Shielding*, Addison-Wesley Publishing Company, Inc., Reading, Mass., 1959.
85. C. G. Collins, W. J. Stapp, and V. P. Calkins, Survey and Evaluation Report on Radiation Damage to Ceramic Material, USAEC Report DC-55-6-101, General Electric Co., Aircraft Nuclear Propulsion Dept., June 16, 1955.
86. R. G. Gex (Comp.), Effects of Nuclear Radiation on the Optical, Electrical, and Thermophysical Properties of Solids: An Annotated Bibliography, Report NP-10969, Lockheed Aircraft Corp., August 1961.

87. M. C. Wittels and F. A. Sherrill, Some Irradiation Effects in Non-Metallic Crystals, *Advan. in X-Ray Anal.*, 3: 269–288 (1960).
88. J. Zombik, The Effects of Radioactive Rays on Ceramics, *Energia Atomtech.*, 11: 644–647 (1958).
89. Radiation Effects in Inorganic Solids, *Discussions of the Faraday Soc.*, 31: (1961).
90. V. J. Linnenbom, The Effects of Radiation Materials, Part 3, Radiation Damage Mechanisms; Insulating Materials, *Insulation*, 6: 11–15 (1960).
91. G. H. Vineyard, *Discussions of the Faraday Soc.*, 31: 7–23 (1961); also USAEC Report BNL-5453, April 1961.
92. S. Amelinckx, Radiation Effects in Ionic Crystals, Report NP-9483, Centre d'Étude de l'Énergie Nucléaire, 1960.
93. J. Howie, Radiation Damage in Ceramics, *Nucl. Eng.*, 6: 299 (1961).
94. Refractory Material. A Literature Search, USAEC Report TID-3560, American Society for Metals, November 1961.
95. W. N. Reynolds and J. N. W. Simmons, The Effects of High Flux Neutron Irradiation on the Physical Properties of Graphite, British Report AERE-R-3871, November 1961.
96. H. Bridge, B. J. Kelley, and B. S. Gray, Stored Energy and Dimensional Changes in Reactor Graphite, British Report TRG-Report-119, Aug. 29, 1961.
97. A. Sosin, Atomistic Interpretation of Radiation Effects in Metals, USAEC Report NAA-SR-4301, Atomics International, Dec. 1, 1959.
98. R. Sizemann, Fundamentals of the Physical Radiation Effects on Solid Bodies, *Nukleonik*, 1: 357 (1959).
99. J. J. Antal, *Phys. Rev.*, 112: 103–111 (1958).
100. D. G. Martin, *Phys. Chem. Solids*, 10: 64 (1959).
101. D. S. Billington, Solid State Diffusion, Annual Progress Report, USAEC Report ORNL-2829, Oak Ridge National Laboratory, Dec. 11, 1959.
102. Oak Ridge National Laboratory, Solid State Division Semiannual Progress Report for Period Ending August 30, 1955, USAEC Report ORNL-1945, Jan. 30, 1956.
103. F. J. P. Clarke, *Phil. Mag.*, 2(8): 607–615 (May 1957).
104. F. J. P. Clarke, Irradiation Damage in Single Crystals of Magnesium Oxide, British Report AERE-M/R-1863, Feb. 1, 1956; Some Further Experiments on Radiation Damage in Magnesium Oxide, British Report AERE-M/R-1863A, May 1957.
105. O. Liskowsky, Radiation Effects on Al_2O_3-Al_2O_3MgO-MgO, German Report NP-10397, April 1961.
106. F. J. P. Clarke and G. Tappin, Physical Property Changes in Beryllium Oxide Due to Reactor Irradiation, British Report AERE-R-3164, January 1960.
107. F. J. P. Clarke and J. Williams, The Stability of BeO Under Reactor Conditions, British Report AERE-M/M-229, April 1959.
108. J. Elston, C. Gewiss, and C. Labbe, The Effect of Thermal Treatment on the Properties of Sintered Beryllium Oxide of Various Densities, Irradiated by Neutrons, Translation DEG-Inf.-Ser.-104, 1960.
109. G. E. Bacon and S. A. Wilson, *Acta Cryst.*, 8: 844 (1955).
110. Frisby, Bisson, and Caillat, *J. Nucl. Mater.*, 1: 106 (1959).
111. R. P. Shields, J. E. Lee, Jr., and W. E. Browning, Jr., Effects of Fast-Neutron Irradiation and High Temperature in Beryllium Oxide, USAEC Report ORNL-3164, Oak Ridge National Laboratory, Apr. 2, 1962.
112. F. J. P. Clarke, Irradiation Damage in Beryllium Oxide, British Report AERE-R-3971, February 1962.
113. J. Elston and C. Labbe, *J. Nucl. Mater.*, 4: 143 (1961).
114. R. C. McGill and J. A. G. Smith, The Thermal Conductivity of Irradiated and Unirradiated Beryllia, British Report AERE-R-3019, July 1959.
115. J. B. Rich, G. B. Redding, and R. S. Barnes, The Effects on Heating Neutron Irradiated Beryllium, British Report AERE-M/R-2685, September 1958.
116. General Electric Co., Flight Propulsion Laboratory Dept., High-Temperature Materials and Reactor Component Development Programs. Volume I. Materials. First Annual Report, USAEC Report GEMP-106A, Feb. 28, 1962.
117. C. G. Collins, paper presented at IAEA Symposium on Radiation Damage to Solids, Venice, Italy, May 7–11, 1962 (proceedings to be published).
118. F. J. P. Clarke et al., *J. Nucl. Mater.*, 4: 121–124 (1961); 4: 125–132 (1961).
119. *Proceedings of the International Conference on the Peaceful Uses of Atomic Energy, Geneva, 1955*, United Nations, New York, 1956:
    a. W. K. Woods, L. P. Bupp, and J. F. Fletcher, Irradiation Damage to Artificial Graphite, Vol. 7, p. 455.
    b. G. H. Kinchin, The Effects of Irradiation on Graphite, Vol. 7, p. 472.
    c. G. R. Hennig and J. E. Hove, Interpretation of Radiation Damage to Graphite, Vol. 7, p. 666.
120. W. L. Kosiba, Quarterly Progress Report for April 1–June 30, 1955, USAEC Report BNL-355, Brookhaven National Laboratory, September 1955.
121. L. D. Loch, A. E. Austin, R. J. Harrison, and W. J. Duckworth, Effect of Constitution of Graphites on Their Stability Under Low-Temperature Irradiation, USAEC Report BMI-1042

(Del.), Battelle Memorial Institute, Sept. 30, 1955.
122. A. W. Smith, *Phys. Rev.*, 94(5): 1417 (June 1954).
123. R. E. Nightingale, Irradiation Annealing in Graphite. I. An Experimental Study, USAEC Report TID-7565 (Pt. 1) (p. 21–32), Hanford Atomic Products Operation, Mar. 16, 1959.
124. J. M. Davidson, E. M. Woodruff, and H. H. Yoshikawa, High Temperature Radiation Induced Graphite Contraction, USAEC Report HW-57900 (Rev.), Hanford Atomic Products Operation, Feb. 2, 1959.
125. J. M. Davidson and J. W. Helm, Effect of Temperature on Radiation-Induced Contraction of Reactor Graphite, USAEC Report HW-SA-2201, Hanford Atomic Products Operation, May 31, 1961.
126. *Reactor Core Materials*, 3(3): 28 (August 1960) (taken from classified USAEC Report HW-64108A).
127. *Reactor Core Materials*, 3(3): 28 (August 1960) (taken from classified USAEC Report HW-63303A).
128. *Reactor Core Materials*, 4(2): 18 (May 1961).
129. A. E. Austin and R. J. Harrison, *Proceedings of the Third Conference on Carbon*, Pergamon Press, Ltd., London, 1959.
130. W. Primak et al., *Phys. Rev.*, 103(5): 1184–1191 (1956).
131. J. T. Howe (Ed.), Solid State Division Semiannual Progress Report for Period Ending August 31, 1953, USAEC Report ORNL-1606, Oak Ridge National Laboratory, Dec. 10, 1953.
132. Oak Ridge National Laboratory, Solid State Division Semiannual Progress Report for Period Ending Feb. 29, 1956, USAEC Report ORNL-2051, June 22, 1956.
133. W. Yeniscavich and M. L. Bleiberg, The Effect of Irradiation on BeO + UO_2, ThO_2 + UO_2, and ZrO_2 + CaO + UO_2, USAEC Report WAPD-BT-20, Westinghouse Electric Corp., Bettis Atomic Power Laboratory, Dec. 7, 1960.
134. W. Primak, *Phys. Rev.*, 110(6): 1240–1254 (1958).
135. M. Wittels and F. A. Sherrill, *Phys. Rev.*, 93(5): 1117–1118 (1954).
136. M. Wittels, *Phil. Mag.*, 2: 1445–1461 (1957).
137. P. G. Klemens, *Phil. Mag.*, 8(1): 938–941 (1956).
138. Johnson and Pease, *Phil. Mag.*, 45(1): 651 (1954).
139. W. Primak, *Phys. Chem. Solids*, 13: 279–286 (1960).
140. W. Primak et al., *J. Am. Ceram. Soc.*, 38: 135–139 (1955).
141. J. H. Crawford, Jr., *Progr. Nucl. Energy, Ser. V: Metallurgy and Fuels*, Vol. 2, pp. 531–550, Pergamon Press, New York, 1960.
142. O. Krisement and G. Trömel, *Z. Naturforsch.*, 15a: 634–640 (July 1960).
143. J. S. Lukesh, *Phys. Rev.*, 97(2): 15, 345–346 (1955).
144. General Electric Co., Flight Propulsion Laboratory Dept., High-Temperature Materials Program Progress Report No. 10A, Part A, USAEC Report GEMP-10A, Apr. 16, 1962.
145. G. E. Bacon, Radiation Damage in Graphite, *J. Chim. Phys.*, 57: 828–836 (October 1960).
146. *Reactor Core Materials*, 3(2): 12 (May 1960) (taken from classified USAEC Report HW-62587A).
147. *Reactor Materials*, 5(1): 25 (February 1962).
148. G. Mayer and M. Lecomte, *J. Phys. Radium*, 21: 846–852 (1960).
149. R. M. Berman, M. L. Bleiberg, and W. Yeniscavich, Fission Fragment Damage to Crystal Structures, USAEC Report WAPD-T-1125, Westinghouse Electric Corp., Bettis Atomic Power Laboratory, Feb. 2, 1960; also *J. Nucl. Mater.*, 2: 129–140 (June 1960).
150. D. E. Johnson, J. Koretzky, and A. K. Smalley, Irradiation of BeO-UO_2 Ceramics, USAEC Report GA-2268, General Atomic Div., General Dynamics Corp., 1961.
151. Westinghouse Electric Corp., Bettis Atomic Power Laboratory, Pressurized Water Reactor (PWR) Project Technical Progress Report for the Period October 24, 1960 to December 23, 1960, USAEC Report WAPD-MRP-89, Feb. 3, 1961.
152. J. M. Tobin, Some Effects of Neutron Irradiation on Selected Beryllia Materials, USAEC Report GA-2648, General Atomic Div., General Dynamics Corp., Apr. 30, 1962.
153. J. W. Brightwell, The Irradiation Creep of Graphite and Carbon—An Interim Summary Report, Report IGC-NPCC-MWP(G)/P-52, General Electric Co., Ltd., July 22, 1959.
154. M. W. Thompson, The Strength of Silica Glass After Pile Irradiation at +100°C and −196°C, British Report AERE-M/R-2305, June 1957.
155. J. Wright and D. W. Brook, Experiments on the Strength of Glass After Fast Neutron Irradiation, British Report AERE-C/R-345, May 1949.
156. G. S. Zhdanov et al., *Kristallografiya*, 3: 720 (1958); English translation in *Soviet Phys.-Cryst.*, 3: 728 (1960).
157. *Reactor Materials*, 5(2): 35 (May 1962).
158. J. Fleeman and G. J. Dienes, *J. Appl. Phys.*, 26: 652 (1955).
159. F. H. Blewitt and R. R. Coltman, *Phys. Rev.*, 85: 384 (1952).
160. G. F. Murray and W. E. Taylor, *Acta Met.*, 2: 52 (1954).
161. M. C. Wittels and F. A. Sherrill, *J. Appl. Phys.*, 27: 643–644 (1956).
162. M. C. Wittels and F. A. Sherrill, *J. Appl. Phys.*, 28: 606 (1957).
163. M. C. Wittels, *Phys. Rev. Letters*, 3: 176–177 (1959).
164. J. Adam and B. Cox, *J. Nucl. Energy: Pt. A: Reactor Sci.*, 11: 31–33 (November 1959).

165. J. Adam and B. Cox, *Phys. Rev. Letters*, 3(12): 543–554 (1959).
166. *Reactor Materials*, 5(2): 49 (May 1962).
167. A. P. Cohen, *J. Appl. Phys.*, 29: 591–593 (1958).
168. R. W. Powell, *Trans. Brit. Ceram. Soc.*, 53: 389 (1954).
169. H. B. F. Gow and W. R. Marsh, The Effect of Temperature on the Carbon Dioxide–Graphite Reaction Under Pile Irradiation, British Report AERE-C/M-36, November 1958; Temperature Effects on the Radiation Induced Reaction of Carbon Dioxide with Graphite, British Report AERE-R-3194, May 1960.
170. P. C. Davidge and W. R. Marsh, The Effect of Pile Radiation on the Carbon Dioxide–Graphite Reaction, British Report AERE-R-3706, January 1956.
171. T. B. Copestake and N. S. Corney, The Reaction Between Carbon and Carbon Dioxide Under Irradiation, USAEC Report TID-7597 (pp. 76–123), Mar. 3, 1961.
172. R. S. Sach, The Stoichiometry of the Radiation Induced Reaction Between CO_2 and Graphite, British Report AERE-R-3721, August 1961.
173. P. C. Davidge, M. Tomlinson, and J. Wright, The Oxidation of Graphite During Irradiation in Oxygen, British Report AERE-C/R-1450, April 1959.
174. W. J. Kosiba and G. J. Dienes, *Advan. Catalysis*, 9: 398–405 (1957).
175. G. R. Hennig, Effect of Radiation on the Oxidation of Graphite Single Crystals, in US/UK Graphite Conference Held at St. Giles Court, London, Dec. 16–18, 1957, USAEC Report TID-7565, pp. 133–140.
176. L. B. Ballweg, W. E. Browning, J. G. Henry, and H. T. King, The Chemical Effects of Alpha Radiation on Beryllium Carbide and Silicon Carbon in Air at High Temperatures, Report NEPA-1865, Fairchild Engine and Airplane Corp., Apr. 15, 1951. (Classified)
177. M. T. Simnad et al., *J. Appl. Phys.*, 29: 1630 (1958).
178. M. T. Simnad and R. Smoluchowski, *J. Chem. Phys.*, 23: 1961 (1955).
179. E. H. Taylor and H. W. Kohn, *J. Am. Chem. Soc.*, 79: 252 (1957).
180. H. W. Kohn and E. H. Taylor, *J. Phys. Chem.*, 63: 500 (1959).
181. H. W. Kohn and E. H. Taylor, *J. Phys. Chem.*, 63: 966 (1959).
182. D. A. Young, *Phys. Chem. Solids*, 5: 119 (1960).
183. J. H. DeBoer, *Reactivity of Solids*, pp. 416–488, Elsevier Publishing Company Ltd., London, 1961.
184. W. M. Lomer, Diffusion Coefficients in Copper Under Fast Neutron Irradiation, British Report AERE-T/R-1540, December 1954.
185. G. J. Dienes and A. C. Damask, *J. Appl. Phys.*, 29: 1713–1721 (1958).
186. A. C. Damask, *Nucleonics*, 20(7): 43–46 (1962).
187. J. N. Gregory and S. Moorbath, The Effect of Pile Irradiation on the Emanating Power of Alumina, British Report AERE-C/M-129.
188. D. L. Morrison et al., in Progress Relating to Civilian Applications During February 1962, USAEC Report BMI-1569, Mar. 1, 1962 (Classified); also Progress Relating to Civilian Applications During May 1962, USAEC Report BMI-1581, June 1, 1962 (Classified), Battelle Memorial Institute.
189. J. J. Antal, *Bull. Am. Phys. Soc.*, 2(7): 356 (1957).
190. D. G. Martin, Dimensional Changes in Single Crystals of Synthetic Sapphire after Irradiation, British Report AERE-M/M-212, November 1958.
191. W. Primak and R. A. Uphaus, *J. Chem. Phys.*, 29: 972–973 (1958).
192. W. N. Reynolds, *Nature*, 189: 824–826 (Mar. 11, 1961).
193. P. W. Levy, *Discussions of the Faraday Soc.*, 31: 118–129 (1961); also see USAEC Report BNL-5218, 1961.
194. H. U. Astroem, *Arkiv. Fysik*, 20: 161 (1961).
195. General Electric Co., Flight Propulsion Laboratory Dept., High Temperature Materials Program. Progress Report No. 6A, Part A, Sept. 15–Nov. 15, 1961, USAEC Report GEMP-6A, Dec. 15, 1961.
196. J. E. Hove, *Progr. Nucl. Energy, Ser. V: Metallurgy and Fuels*, Vol. 2, pp. 551–569, Pergamon Press, New York, 1960.
197. W. Primak and H. Szymanski, *Phys. Rev.*, 101(4): 1268–1271 (1956).
198. *Reactor Core Materials*, 2(4): 14 (November 1959).
199. *Reactor Core Materials*, 3(2): 12 (May 1960) (taken from classified USAEC Report HW-62012A).

Section

I

Reactor Materials

Fuel and Fertile Materials

Uranium Metal and Alloys

Unalloyed Uranium

Investigators at General Telephone[1] have measured the self-diffusion coefficient of alpha uranium as a function of crystallographic direction at 640°C. The averages of two measurements made in each direction are $D_{(100)} = 1.8 \times 10^{-14}$ cm^2/sec, $D_{(010)} = 0.72 \times 10^{-14}$ cm^2/sec, and $D_{(001)} = 0.66 \times 10^{-14}$ cm^2/sec.

The Israeli Atomic Energy Commission has issued a survey report[2] on the grain refinement of uranium. Topics covered include methods of grain refinement, substructures in uranium, and grain-size measurement. The English[3] have examined thin films of uranium by electron diffraction. Films formed by condensation in a vacuum of 10^{-6} torr show a surface structure that appears to be predominantly alpha UH_3. The hydride is probably formed by reaction of uranium with the residual water vapor in the vacuum system. When the films are heated by an intense electron beam in the poor vacuum of the electron microscope, oxidation to UO_2 occurs.

Investigators at Iowa State University[4] have determined the fatigue properties, yield strength (0.2% offset), tensile strength, and modulus of elasticity for normal uranium dingot at elevated temperatures. These properties are summarized in Figs. I-1 and I-2. All the properties decreased in value with increasing temperature. However, at about 350°C they showed some irregularities. These irregularities can possibly be explained by the fact that, at lower temperatures, deformation by twinning predominates, whereas slipping predominates above 350°C.

Workers at Argonne[5] made X-ray diffraction measurements of rolled uranium sheet that had been reduced 76% in thickness at room temperature and annealed at various temperatures. Contrary to previously reported observations, they noted that as-rolled and recrystallized materials have different preferred orientations. The preferred orientations of samples annealed at 380 and 400°C were very similar, but different from those found in samples annealed at 450°C. However, samples which had been annealed at 380°C and which were reannealed at 450°C had essentially no change in the preferred orientation. Dilatometric measurements parallel and normal to the rolling direction did not conclusively substantiate the X-ray diffraction measurements. Recrystallization at temperatures from 360 to 450°C of the homogeneously deformed as-rolled structure was characterized by the formation of extremely fine grains in the early stage, which later were absorbed by

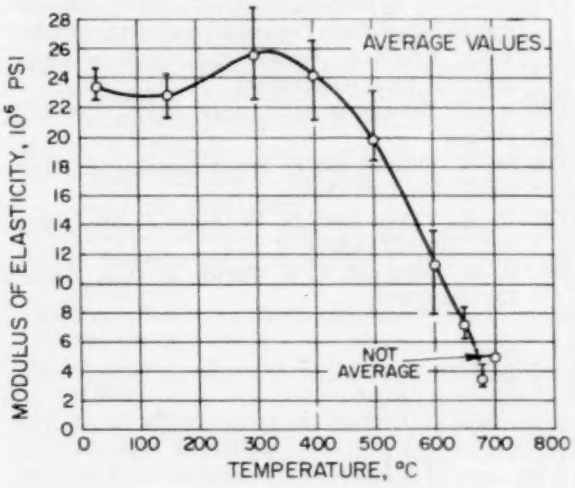

Fig. I-1 Modulus of elasticity as a function of temperature for uranium dingot.[4]

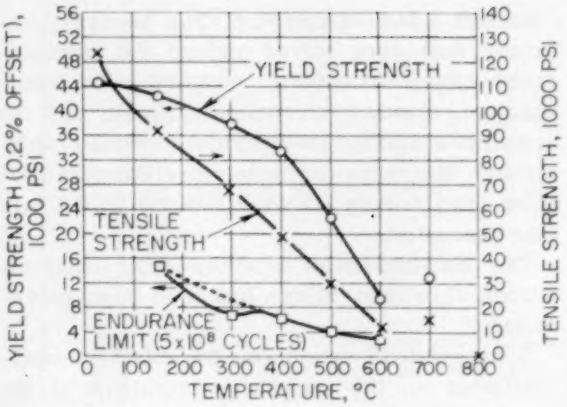
YIELD STRENGTH
TENSILE STRENGTH
ENDURANCE LIMIT (5 x 10⁸ CYCLES)
YIELD STRENGTH (0.2% OFFSET), 1000 PSI
TENSILE STRENGTH, 1000 PSI
TEMPERATURE, °C
0 100 200 300 400 500 600 700 800
0 4 8 12 16 20 24 28 32 36 40 44 48 52 56
0 10 20 30 40 50 60 70 80 90 100 110 120 130 140

Fig. I-2 Yield strength, tensile strength, and endurance limit as functions of temperature for uranium dingot.[4]

growth of somewhat larger grains. Evidence of ordinary secondary recrystallization was observed in specimens annealed at 600°C.

Table I-1 shows the results of high-temperature irradiations of unalloyed uranium, performed by Atomics International.[6] Swelling was significant in all specimens except the one irradiated at an average temperature of 635°F (335°C).

Experimenters at Hanford[7] have made a comparison between the in-reactor swelling of uranium clad with Zircaloy-2 and the swelling of irradiated (at low temperature) unclad uranium after ex-reactor annealing. The following conclusions were drawn:

1. The volume of uranium increases with increasing irradiation temperature or post-irradiation annealing temperature.
2. The Zircaloy-2 cladding offers very little restraint to in-reactor swelling with the rod geometry employed.
3. For a given burnup and equivalent in-reactor or ex-reactor temperatures, final estimates of unrestrained swelling are the same.
4. Postirradiation annealing experiments may provide reasonably accurate predictions of swelling under particular conditions of temperature and low restraint.

Recent articles of interest appearing in the *Journal of Nuclear Materials* and *Nuclear Science and Engineering* include "A Study of the Melting of Irradiated Uranium,"[8] "The Release of Krypton 85 from Irradiated Uranium on Thermal Cycling Through the Phase Changes,"[9] and "Kinetics of Structural Changes During Beta Transformation of Uranium."[10]

(M. S. Farkas)

Alpha-Phase Uranium Alloys

The English[11] have studied transformation temperatures and grain sizes as a function of cooling rate for uranium–0.15, 0.3, and 0.5 at.% chromium alloys. The possibility that grain refinement of large bars can be achieved by cooling from the beta phase in air or under a controlled flow of gas is suggested. The transformation mechanism involved in grain refinement would not be orientation dependent, and

Table I-1 UNALLOYED-URANIUM IRRADIATION DATA[6]

Specimen description	Average irradiation temp.,* °F	Average central temp., °F	Burnup, at.%	Diameter increase, %	Length increase, %	Volume increase (from density), %	Volume increase (calculated from dimensions), %	0.1 at.% burnup		
								% ΔV	% ΔD	% ΔL
†	635	710	0.13	4.0	5.0	0.9	13.0	0.72	3.1	3.8
‡	750	840	0.15	5.0	4.9	5.0	14.9	3.3	3.3	3.3
†	845	950	0.18	5.9	2.7	6.0	14.5	3.4	3.3	1.5
‡	950	1070	0.20	8.5	4.9	14.0	21.9	7.0	4.2	2.4
†	1025	1150	0.22	6.7	2.3	8.8	15.7	4.1	3.0	1.0
‡	1070	1220	0.23	6.4	4.1	12.2	16.9	5.4	2.8	1.8
§	1130	1270	0.24	3.8	5.1	10.1	12.7	4.2	1.6	2.1
†	1140	1280	0.24	7.6	4.8	13.1	20.0	5.4	3.2	2.0
‡	1105	1240	0.23	9.3	5.1	13.5	23.7	5.8	4.0	2.2
†	1050	1180	0.22	7.8	2.2	11.3	17.8	5.1	3.5	1.0
‡	995	1120	0.21	9.3	3.9	15.1	22.5	7.2	4.4	1.9
§	950	1070	0.20	3.7	7.2	11.1	14.6	5.5	1.8	3.6

* Sum of average fuel surface and average fuel central temperatures (during period in higher flux position) divided by 2.
† Cast and beta quenched.
‡ Alpha rolled and beta quenched.
§ Same as ‡, but with 5-mil stainless-steel restraining jacket.

the grain size achieved by continuous cooling would be finer than that achieved by isothermal transformation.

The uranium-rhenium phase diagram, determined by Iowa State University,[12] is shown in Fig. I-3. The uranium-URe_2 eutectic composition is at 10.5 wt.% rhenium. The maximum solubility of rhenium in beta uranium is about 1.9 wt.% rhenium, and it occurs at 680°C. The maximum solubility of rhenium in alpha uranium is slightly less than 0.5 wt.%, and it occurs at 643°C. The solubility at room temperature is small but detectable, i.e., less than 0.5 wt.%. The solubility of uranium in rhenium near room temperature is 0.7 wt.%.

The Russians[13] have published the results of extensive phase-equilibria studies. The binary diagrams produced were uranium-molybdenum, -niobium, and -zirconium. The ternary diagrams that were solved include the uranium-molybdenum-zirconium, uranium-zirconium-titanium, uranium-zirconium-niobium, and the uranium-molybdenum-chromium systems. Quaternary diagrams for uranium-zirconium-niobium-molybdenum alloys at 800 and 1000°C are also presented.

The constitution of uranium-rich, uranium-silicon-aluminum alloys has also been determined.[14]

A program to determine the effect of heat-treatment on the irradiation stability of the uranium–2 wt.% zirconium alloy was performed by Argonne.[15] This alloy, as quenched from 800°C, had a martensitic alpha structure that was supersaturated with zirconium. Reheating to 550°C and holding for 24 hr resulted in coarsening of the martensitic needles and the formation of some spheroids of delta phase in the martensitic matrix. Slow cooling from 800°C resulted in a coarse martensitic structure and the beginning of delta spheroid formation. Quenching from 800°C into a lead bath at 550°C and holding for 1 hr produced a structure very similar to the previous two. The chill-cast alloy had a fine martensitic structure. Coarsening of the martensitic structure occurred in chill-cast specimens that were annealed for 1 hr and vacuum cooled.

A series of various heat-treated, enriched uranium–2 wt.% zirconium alloys were irradiated to burnups of 0.08 to 0.189 at.% at temperatures from 307 to 383°C. The results are given in Table I-2. Conclusions arrived at are as follows:

1. Cast uranium–2 wt.% zirconium fuel slugs showed the least tendency to change in length (average +0.12%) when irradiated. Of the four groups of wrought slugs, the as-quenched changed length the least (average +0.48%). The three groups of wrought specimens in which some annealing occurred had about the same tendency to elongate (average +2.08%).

2. The ratio of length change to burnup was smallest for the chill-cast slugs [average was +0.8 μin./(in.)(ppm burnup)], and was +1.4 μin./(in.)(ppm burnup) for the chill-cast and annealed slugs. The average ratio for the as-quenched wrought slugs was +2.2 μin./(in.)(ppm burnup). The other wrought slugs had an average ratio of about +13 μin./(in.)(ppm burnup).

3. Five slugs (each 0.385 in. in diameter) that were slow cooled from 800°C provided

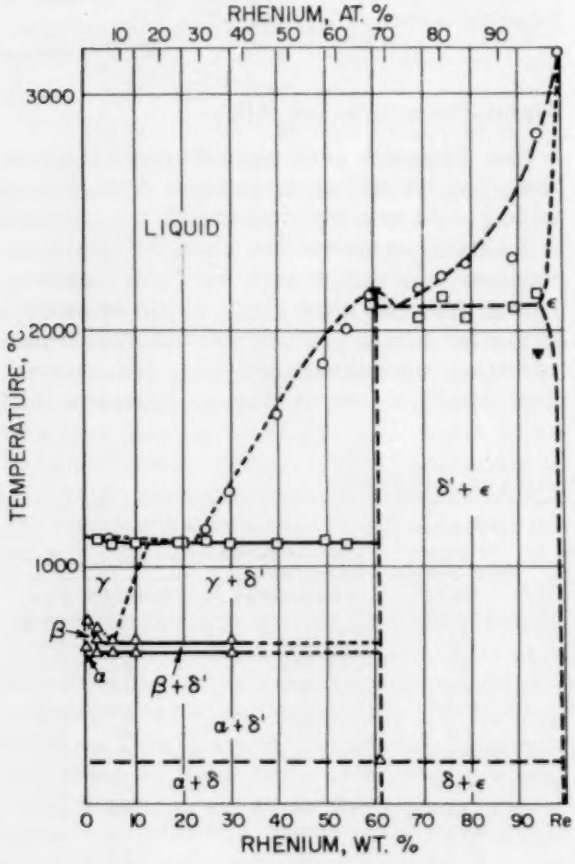

Fig. I-3 Uranium-rhenium phase diagram.[12] □, melting points (solidus). ○, melting points (liquidus). △, differential thermal arrests. ×, temperature-resistance inflection points. ▼, quenched sample (two-phase).

Table I-2 MEASUREMENTS DATA FOR IRRADIATED URANIUM–2 WT.% ZIRCONIUM FUEL SLUGS

Table 1-2 MEASUREMENTS DATA FOR IRRADIATED URANIUM–2 WT.% ZIRCONIUM FUEL SLUGS[15]

Preirradiation history*	Nominal slug dia., in.	Burnup per slug, at.%	Average temp., °C	Length change, %	Length change (ΔL)/burnup, (μin./in.)/ppm burnup	Dia. change, %	Dia. change/ burnup, (μin./in.)/ ppm burnup	Dia. change (%)/ length change (%)	Density decrease, %	Volume increase (%)/ burnup (at.%)	Hardness, R_A
1	0.385	0.118	309	−0.39	−3.3	+1.04	+8.8	−2.67	0.25	2.1	69
	0.385	0.132	307	0.00	0.0	+1.30	+9.8		0.31	2.4	72
	0.365	0.187	338	+1.31	+7.0	+0.82	+4.4	+0.62	0.75	4.1	75
	0.365	0.189	339	+0.99	+5.2	+0.54	+2.9	+0.55	0.71	3.8	70
2	0.385	0.152	354	+1.05	+6.9	−0.26	−1.7	−0.25	1.00	6.6	67
	0.385	0.171	353	+2.65	+15.5	−0.78	−4.6	−0.29	0.74	4.4	71
	0.365	0.187	382	+2.96	+15.8	0.00	0.0	0.00	1.71	9.3	66
	0.365	0.189	383	+2.55	+13.5	+0.54	+2.9	+0.21	2.80	15.3	64
3	0.385	0.118	309	+3.01	+25.5	−1.04	−8.8	−0.34	0.46	3.9	71
	0.385	0.123	374	+1.26	+10.3	−0.26	−2.1	−0.21	0.59	4.2	67
	0.385	0.123	374	+1.29	+10.5	+1.04	+8.5	+0.81	0.76	6.2	65
	0.385	0.138	374	+1.18	+8.5	0.00	0.0	0.00	0.76	5.6	67
	0.385	0.152	354	+2.58	+16.5	−0.52	−3.4	−0.20	0.75	5.0	68
	0.365	0.189	339	+2.59	+13.7	0.00	0.0	0.00	1.28	6.9	70
	0.365	0.189	339	+2.53	+13.4	−0.27	−1.4	−0.11	1.10	5.9	68
4	0.385	0.080	309	+1.35	+16.8	0.00	0.0	0.00	0.34	4.3	68
	0.385	0.129	309	+2.09	+16.2	0.00	0.0	0.00	0.60	4.7	70
	0.365	0.189	383	+2.12	+11.2	+0.55	+2.9	+0.26	2.16	11.7	65
	0.365	0.189	383	+2.05	+10.8	+0.82	+4.3	+0.40	1.70	9.2	64
5	0.385	0.103	354	−0.03	−0.3	+0.78	+7.6	−26.00	0.39	3.8	69
	0.365	0.113	339	0.00	0.0	+0.27	+2.4		0.53	4.8	70
	0.385	0.167	354	−0.12	−0.7	+0.78	+4.7	−6.50	1.10	6.7	69
	0.365	0.189	339	+0.30	+1.6	+1.64	+8.7	+5.46	1.53	8.2	68
6	0.385	0.084	374	+0.09	+1.1	+0.26	+3.1	+2.88	0.47	5.6	66
	0.365	0.113	383	+0.16	+1.4	+1.09	+9.6	+6.81	0.82	7.4	67
	0.385	0.136	374	0.00	0.0	+0.78	+5.7		0.78	5.7	68
	0.365	0.189	383	+0.59	+3.1	+1.64	+8.7	+2.78	2.85	15.5	65

* Heat-treatments:
1. Wrought; heated 1 hr at 800°C, water quenched.
2. Wrought; heated 1 hr at 800°C, water quenched, 24 hr at 550°C.
3. Wrought; heated 1 hr at 800°C, air cooled in bomb.
4. Wrought; heated 1 hr at 800°C, quenched in 550°C lead bath for 1 hr, air cooled in bomb.
5. Chill cast slugs.
6. Chill cast slugs; annealed 1 hr at 550°C, vacuum cooled in cold chamber.

data which indicated that the ratio of length change to burnup decreases with increasing temperature in the range from 309 to 374°C. If burnup is excluded as a factor, the colder the slug is in this group of specimens, the greater the length increase.

4. Slugs that were farther removed from the condition of phase equilibrium because of their preirradiation treatment had the greater dimensional stability when irradiated.

5. Density measurements indicated slight decreases in density with increasing burnup and were comparable to unalloyed uranium below 0.180 at.% burnup. Specimens with burnups of 0.187 to 0.189 at.% showed a tendency to swell. Swelling occurred in the specimens at the hottest calculated temperatures, 380 to 385°C. Unalloyed uranium with up to 0.3 at.% burnup did not swell at these temperatures in Experimental Breeder Reactor No. 1. (M. S. Farkas)

Gamma-Phase Uranium Alloys

The Russians have issued a series of papers concerned with transformation of the gamma phase in uranium alloys of molybdenum and niobium.

The transformation of uranium–20, 30, and 40 at.% molybdenum alloys was studied by quenching the alloys from 1000°C and then heating at gradually increasing temperatures for 50-hr periods. Hardness measurements and X-ray analyses were performed after each heating period. Hardness values, phase identification, and lattice-dimension changes are reported.[13a] The transformation from gamma to delta is postulated as proceeding by the formation of small ordered regions of delta within the gamma phase, with the two phases being coherent across their (0 0 1) planes. Transformation continues by the growth of the ordered delta regions.

Studies of gamma-phase transformations in uranium–10, 20, 30, 40, and 60 at.% niobium and in ternary alloys of uranium-niobium-molybdenum in which the niobium-molybdenum ratios were 3:1, 1:1, and 1:3 have been performed.[13b] Hardness changes, gamma stability, and phase agglomeration were investigated. It was found that the gamma-phase decomposition in alloys containing 40, 60, 70, and 80 at.% uranium was slowest when the niobium:molybdenum ratio was approximately 1:3.

The decomposition of the gamma phase in the uranium-molybdenum-zirconium system has also been investigated.[13c] On the basis of results obtained by annealing samples at 1000°C and then reheating to 500°C for 100 and 1000 hr, it is concluded that the gamma phase is decomposed fairly rapidly in this system. The gamma phase was found to decompose either into a single different phase or into a mixture of four phases, the latter being clearly a nonequilibrium condition.

Gamma-phase stability was the subject of a study of uranium-zirconium-niobium-molybdenum alloys.[13d] Alloy additions to uranium of 20, 30, 40, and 50 at.% were investigated. It was generally observed that gamma stability increased with increased alloy content. Hardness, however, decreased with increasing alloy content, the hardness probably being related to the amount of alpha-uranium decomposition product present. (A. A. Bauer)

Aluminum-Uranium Alloys

The thermal conductivity of aluminum-uranium alloys with varying amounts of uranium, in both the cast condition and the 620°C heat-treated condition, has been studied in some detail by Chalk River.[16] The heat-treatment improved conductivity for alloys containing up to 30 wt.% uranium, but it had an apparent detrimental effect on alloys containing more uranium. The higher uranium alloys contained UAl_3 and UAl_4, and the heat-treatment converted the UAl_3 to UAl_4, causing a decrease in compound density (UAl_3 has a density of 6.7 g/cm^3, and UAl_4 has a density of 5.7 g/cm^3). The resulting increase in volume could account for the reduced thermal conductivity.

In the case of a 0.15 wt.% uranium alloy heat-treated to 5°C above the eutectic temperature (646°C), a grain-boundary network of UAl_4 was produced which reduced the conductivity of the alloy from 0.502 to 0.586 cal/(cm)(sec)(°C).

As a part of the same study, the solubility of uranium in aluminum was determined to be 0.08 ± 0.02 wt.% uranium at the eutectic temperature of 646°C. Fabrication studies indicate that the rate of work hardening of an aluminum–21 wt.% uranium alloy is about three times that of unalloyed aluminum.

Radioactivity in the Low-Intensity Test Reactor water coolant was traced to uranium

contamination from surfaces of the aluminum-clad aluminum-uranium plate type fuel elements. Oak Ridge[17] performed uranium analyses that were based on neutron-activation studies of machined layers from fuel-plate surfaces. These analyses showed that rolling-mill equipment contaminated with enriched uranium transferred as much as 180 ppm U^{235} to plate surfaces. By careful practice the contamination of the cladding can be reduced to 0.6 ppm U^{235}. Diffusion from the core accounts for this. These studies indicate that a good estimate of the diffusion coefficient of uranium into aluminum at 600°C is 2.5×10^{-8} cm^2/sec. Heat-treatments at 600°C prior to irradiation should be limited to 2.5 hr to minimize diffusion.

The results of this investigation also suggested that the solubility limit of uranium in aluminum at 600°C is approximately 60 ppm. (This can be compared with the Chalk River data in a preceding paragraph, which lists the solubility at 646°C as 800 ppm.)

Phillips Petroleum has performed irradiation tests on a number of aluminum-uranium alloys clad with a variety of aluminum alloys.[18] The uranium compositions (using fully enriched uranium) were 18 to 23 wt.%, 35 wt.%, and 45 wt.%. Another series of specimens were all aluminum–35 wt.% normal uranium. These specimens were clad with 1100 aluminum; 6061 aluminum; APM-M257; X-8001 aluminum; X-8003 aluminum; and 5052 aluminum. The data reported to date cover only the alloys containing 18 to 23 wt.% uranium. These were irradiated to burnups of between 13 and 83% of the U^{235} atoms at surface temperatures of 200°C. The specimens swelled only 2 to 3% as a result of this irradiation.

Metallography of specimens having burnups of 51 and 69% of the U^{235} atoms showed little or no effect of fission gas in the UAl_4 particles. There was some evidence of fission-product damage in the matrix immediately surrounding the UAl_4 particles with the higher burnups.

Brookhaven[19] has irradiated several aluminum-uranium fuel elements that were clad with X-8001 aluminum. Type II contained an alloy of aluminum–35 wt.% uranium, and type III contained an aluminum–40 wt.% uranium alloy. Type II was irradiated to a burnup of 39.2% of uranium atoms, and type III was irradiated to a burnup of 15.8% of uranium atoms. The surface temperatures were about 200°C. All plates on each element exhibited warpage and subsequent channel restrictions. Although the method of assembly was thought responsible for the warpage in that it might have induced stresses that were released by thermal cycling, tests with normal elements outside a reactor indicated that this was not the case.

(R. F. Dickerson)

Miscellaneous Dilute Uranium Alloys

An interesting facet of alloy-development work at Ames has been the investigation[20] concerned with developing a container material for molten aluminum–18 wt.% thorium–6 wt.% uranium, which has a melting point of 630°C. Niobium was studied initially as a container, and it held the molten alloy at 700°C for up to 2100 hr without failure. The alloy has also been held for 1200 hr at 800°C in niobium and tantalum. Analyses of the niobium from the first series of tests indicate very little attack or reaction.

(R. F. Dickerson)

Fuel-Water Reactions

Additional studies of the reaction of solid uranium with steam are reported by Argonne.[21] In this study the course of the reaction to produce uranium dioxide and hydrogen is being followed by the volumetric method. Results indicate that the reaction rate is parabolic over the range 500 to 1200°C. A tentative value of 15.4 kcal/mole has been obtained for the activation energy. The reaction is a two-stage linear process at 400°C. It is now apparent that the reactions of uranium with steam and with oxygen both undergo a marked change from a linear or accelerating rate to a slower protective reaction between 400 and 500°C.

Other results from Argonne concern four metal-water experiments conducted in the Transient Reactor Test Facility. In three of these experiments, 89 wt.% zirconium–11 wt.% uranium (93% enriched) alloy plate was melted in water by reactor bursts of 251, 372, and 452 Mw-sec total energy. These plates reacted with the water to the extent of 4, 7.7, and 8.5%, respectively. In the fourth experiment a cylindrical pin of aluminum–10 wt.% U_3O_8 (93% enriched) was subjected to a 940-Mw-sec transient in water. A gas leak made the measurement of the extent of reaction unreliable. However, it is estimated from the hydrogen-

to-helium ratio found in the autoclave following the run that there was greater than 8% reaction.

(A. W. Lemmon, Jr.)

Plutonium

Plutonium Alloys

Los Alamos[22] continues to investigate plutonium-containing fuels for possible use in their molten-plutonium reactor LAMPRE. The effects of plutonium concentration in plutonium-cerium-cobalt alloys on corrosion of unannealed tantalum container materials have been studied. In one series of tests, plutonium concentrations were 4, 5.7, 7.6, 9.5, 11, 13, and 15 g of plutonium per cubic centimeter. After testing at 750°C for 200 hr, all the fuels more concentrated than 9.5 g/cm^3 had penetrated their containers. After 400 hr the 7.6 g/cm^3 fuel showed some penetration, whereas the more dilute fuels showed no failures. In a second series of tests, fuels containing 1, 2, 3, 4, and 5 g of plutonium per cubic centimeter were tested for

Table I-3 SCREENING TESTS OF CONTAINERS FOR ALLOYS BASED ON URANIUM-MANGANESE EUTECTIC[22]

Corrosion specimen	Fuel	Temp., °C	Observations
Unannealed Ta	76.7 at.% U + 18.6 at.% Mn + 4.70 at.% Pu + 500 ppm Si = TiPu 164	800, 850, and 950	Leakage only after the last exposure, i.e., at 950°C
Al_2O_3 container	TiPu 164	900	Unwetted; no visible attack; 170 ppm Al produced in fuel
Container of 94 wt.% ZrO_2 + 6 wt.% CaO	TiPu 164	900	No visible attack; darkened container; less than 5 ppm Zr in fuel
CeO_2 container	TiPu 164	900	No visible attack; darkened container; less than 25 ppm Ce in fuel
Al_2O_3 container	74.1 at.% U + 21.0 at.% Mn + 4.92 at.% Pu + ~70 ppm Si = TiPu 175	900	No visible attack
Container of 94 wt.% ZrO_2 + 6 wt.% CaO	TiPu 175	900	No visible attack; darkened container
CeO_2 container	TiPu 175	900	No visible attack; darkened container
Unannealed Ta	TiPu 164	900	Wetted; fairly strong IGP at the liquid-gas interface
Unannealed Ta	TiPu 175	900	Wetted; fairly strong IGP at the liquid-gas interface
"Cerium sulfide"	TiPu 175	900	Wetted; no visible attack
Y container	78.3 at.% U + 21.7 at.% Mn	900	Wetted; 15-mil penetration near a liquid-gas interface
Y container	78.3 at.% U + 21.7 at.% Mn	950	Wetted; fluidization of Y at spots of fuel in gas phase
BeO container (density = 2.90 g/cm^3)	78.0 at.% U + 22.0 at.% Mn	1000	Wetted near bottom; metallography showed no attack; 84 ppm Be produced in fuel means $\frac{1}{10}$ to $\frac{1}{4}$ mil av. penetration
Container of 98 wt.% Al_2O_3 + 2 wt.% Y_2O_3	TiPu 184 = U + Mn + Pu like TiPu 164 and 175	900	Reaction layer between fuel and container; possibly some volatilized Al
Vitreous MgO container	TiPu 184	900	Very slight reaction layer
BeO container	TiPu 184	900	Unwetted; slight, if any, reaction layer
Vitreous CaO container	TiPu 184	900	Slight dark reaction layer; bulk CaO discolored but not penetrated
Vitreous Y_2O_3 container	TiPu 184	900	Slight, if any, reaction layer; less than 5 ppm Y produced in fuel; best appearance of S-1 to S-5
Single-crystal W in W-coated Al_2O_3 container	TiPu 184	900	Flat meniscus; no obvious attack
Sc container	TiPu 184	900	Wetted; no obvious attack
Single crystal W in container of stock W	TiPu 184	900	Wetted; no obvious attack
Y container	TiPu 184	900	Wetted; no obvious attack

1000 hr at 750°C, followed by 2000 hr at 850°C and 200 hr at 900°C, with no failures. In connection with this study, the crystal structure of Pu_3Co was found to be orthorhombic, spare group *Cmcm* with $a = 3.475 \pm 0.004$ A, $b = 10.976 \pm 0.010$ A, and $c = 9.220 \pm 0.008$ A; $Z = 4$. Calculated density is 14.65 g/cm^3.

The results of corrosion tests of a number of ceramic container materials for molten uranium-plutonium-manganese fuels are summarized in Table I-3.

alloys containing 5 wt.% plutonium are summarized in Table I-5. Alloys containing nickel, copper, uranium, and silicon have given encouraging results.

Los Alamos[24] reports that the maximum solubility of aluminum in delta plutonium is 14.5 ± 0.2 at.% aluminum at the peritectoid temperature. The solubility decreases to 13.6 at.% aluminum at 560°C and to 11.3 at.% aluminum at 350°C. Changes in aged alloys containing the delta phase indicate that the delta phase is stable at room temperature. The intermediate phase PuAl was found to have decomposed into Pu_3Al and $PuAl_2$ after being aged at room temperature for 10 years. The equilibrium decomposition temperature has been fixed at 193 ± 3°C.

Table I-4 RESULTS OF IRRADIATION OF ALUMINUM–10 WT.% PLUTONIUM ALLOYS[23]

Pu^{239}, wt.%	9.87	9.87	6.82	1.90	2.97	2.97	1.90
Burnup of Pu, at.%	4.4	5.2	5.9	5.9	6.0	4.4	2.4
Temperature, °C, at core center (measured)	490	530	510	480	480	450	400
Temperature, °C, at core/sheath interface (estimated)	430	440	440	420	420	410	380
Material adjacent stainless-steel sheath	Al	Al	Al–7.1 wt.% Pu	Al–2.1 wt.% Pu	Al	Al	Al–2.1 wt.% Pu
Change in length of fuel-element assembly, in.	−0.004	−0.001	+0.010	+0.011	+0.010	+0.018	+0.001
Change in volume of fuel	0	0	0	0	0	0	0
Extent of sheath/core reaction	Very slight	Very slight	Slight	Very slight	Very slight	None	None

Chalk River[23] had irradiated seven aluminum alloys containing 2 to 10 wt.% plutonium sheathed in 0.01-in.-thick stainless steel to burnups of up to 6% of the plutonium atoms at center-core temperatures up to 570°C. No changes in volume of the core materials were detected. However, slight changes in overall length of four of the 8.5-in.-long fuel elements were detected. No sheath/core interaction occurred at interfacial temperatures below 420°C. An insignificant interaction occurred between 420 and 440°C. Irradiation data are tabulated in Table I-4.

Thermal and X-ray diffraction analyses have indicated[16] that there may be several polymorphic transformations in $PuAl_3$ between the peritectic temperature of approximately 925°C and the reported decomposition temperature of 1220 to 1270°C. There is also some evidence that $PuAl_4$ passes through several polymorphic transformations between room temperature and its decomposition temperature of approximately 925°C.

Results of high-temperature aqueous-corrosion tests of as-cast aluminum-base ternary

Studies at Battelle[25] indicate that iron-base alloys containing 30 vol.% $PuFe_2$ as a dispersed phase could withstand reductions in thickness of around 25% by rolling at 900 to 950°C. Room-temperature ductility of the iron-base alloy was essentially nil.

After a heat-treatment of 10 hr at 900°C, and following an oil quench, structures of uranium–10 wt.% niobium–5, 10, and 15 wt.% plutonium alloys were observed to be single-phase gamma-uranium solid solution. Hardness of the alloys increased with increasing plutonium content. (V. W. Storhok)

Plutonium Compounds

Los Alamos has initiated cursory studies on the viscous flow properties of PuO_2-UO_2 paste fuels slurried with sodium to determine the

suitability of this mixture for use in LAMPRE. To date, no success is reported[22,26] with a limited particle-size range. Other properties of various PuO_2 and PuO_2-UO_2 fuels are continually being investigated at various laboratories. Battelle has published a summary[27] of an investigation of the reactivity of PuO_2 with various solids and the common reduction phenomenon. Workers at NUMEC (Ref. 28) report again a eutectoid reaction between $PuO_{1.62}$ and $PuO_{2.00}$ at approximately 650°C.

exposures from 1.4×10^{19} to 3.6×10^{19} fissions/cm^3, grain growth was noted in one rod of high initial density. Void formation occurred rather consistently in low-density specimens.[31] After continued irradiation to 16.0×10^{19} fissions/cm^3, microhardness measurements showed that density had increased to nearly 100% of theoretical.[30]

Hanford[32] has accomplished the fabrication of high-density homogeneous $(Pu\text{-}U)O_2$ mixtures by hot rolling or hot pressing the premixed

Table I-5 TWENTY-HOUR AQUEOUS CORROSION TESTS* ON AS-CAST TERNARY ALUMINUM ALLOYS[16]

Alloy composition, wt.%	Depth of corrosion, 10^{-3} in., at various temperatures, °C						
	250	280	300	320	340	360	380
5 Pu, 15 U				0.2	0.3	0.5	0.8
5 Pu, 15 Si				0.4	0.5	0.6	0.8
5 Pu, 1 Ni					0.3	0.4	0.4
5 Pu, 4 Cu				0.2	0.5	0.8	2.3
5 Pu, 2 Zr	G	P	P	>125			
5 Pu, 0.5 Ca		P	>125	>125			
5 Pu, 5 Mg	P	P		>125			

* Tests were carried out on 0.25-in.-diameter specimens. A corrosion depth of $>125 \times 10^{-3}$ in. signifies complete failure. G and P signify good and poor corrosion resistance. Owing to the low temperatures at which these latter tests were carried out, it was not considered worthwhile making accurate measurements. All other measurements, accurate to 0.1×10^{-3} in., were made from microspecimens with a filar micrometer eyepiece attached to the Vickers microscope.

Hanford[29] has published a comprehensive explanation of the effect of oxygen partial pressures on the sintering and reduction of PuO_2. The same laboratory reports a continuous series of solid solutions from 30 to 90 wt.% Pu_2O_3 in the Pu_2O_3-UO_2 system. In the range 30 to 60 wt.%, the structure is face-centered cubic and from 60 to 90 wt.%, it is hexagonal.

The lattice expansion of PuO_2 as a function of temperature is presented in Table I-6 and agrees well with dilatometer measurements.

Irradiation testing of UO_2–3 at.% PuO_2 solid solutions has been reported by Hanford. After

Table I-6 LATTICE EXPANSION[30] OF PuO_2

Temp., °C	a_θ, A	Δ_a/a_θ ($\times 10^3$)
23	5.3958 ± 0.0002	
280	5.4080 ± 0.0002	2.224
500	5.4186 ± 0.0005	4.225
604	5.4227 ± 0.0004	4.948
812	5.434 ± 0.001	7.134
902	5.439 ± 0.002	7.969

powders at 800 to 900°C. Other research on $(Pu\text{-}U)O_2$ solid solutions by Chikalla[33] shows that tungsten-electrode arc-melted PuO_2 is oxygen deficient or contains suboxides, depending on atmosphere employed. Tungsten contamination of the oxide was noted, but it was maintained that no reaction occurred. The condensed vapor after melting was oxygen rich.

Plutonium carbide (PuC) remains of great interest, and a major effort is concentrated on this compound. Figure I-4 shows the phase relations in arc-melted PuC alloys,[34] showing that carbon-deficient PuC exists in the range 39.7 to 49 at.% carbon. The lines designated *A*, *B*, and *C* were obtained from large samples presumably cooled slowly enough to allow a change in carbon solubility. Although X-ray examination showed PuC to exist below 41 at.% carbon, metallographic examination revealed the presence of metallic plutonium and the zeta plutonium-carbon alloy in this range of compositions.[35] Above 48 at.% carbon, a mixture of PuC and Pu_2C_3 exists. Hardness data on plu-

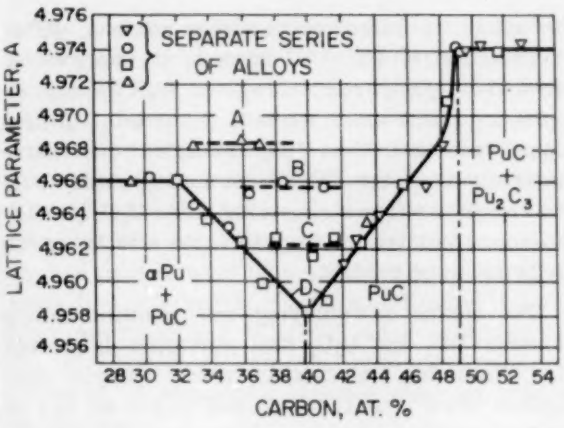

Fig. I-4 Lattice parameters and phase relations of arc-melted PuC alloys.[34]

tonium-carbon alloys[35,36] show a slow increase to a diamond pyramid hardness number (DPHN) of 360 at 39.7 at.% carbon, followed by a large jump to 860 DPHN at 40 at.%. All data indicate a crystallographic change at 39.7 at.% carbon.

Recently published data[37] on the thermal expansion of PuC and Pu_2C_3 are presented in Fig. I-5. The calculated coefficients of linear expansion for PuC and Pu_2C_3 are 10.8×10^{-6}/°C and 14.8×10^{-6}/°C, respectively.

Argonne has successfully fabricated PuC by arc casting[38] into a tantalum-coated graphite mold without fracturing. The same laboratory reports that sintering of (Pu-U)C solid solutions is retarded by both oxygen and free carbon.[39] Hanford has investigated the attack of dry hydrogen on hypostoichiometric PuC and has demonstrated the mechanism to be one of

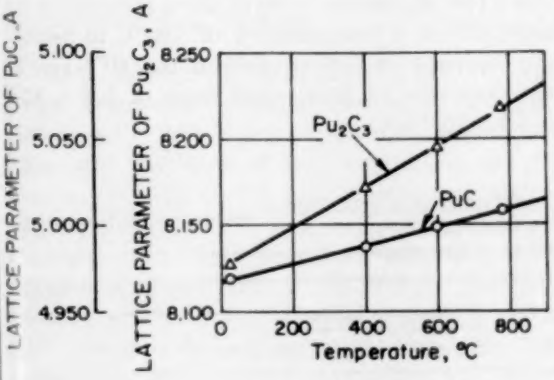

Fig. I-5 Lattice thermal expansion of plutonium carbides.[37]

hydriding of the free plutonium located intergranularly.[30]

Compounds other than the oxides and carbides are receiving a more concentrated study. $PuSi_2$ has been prepared by heating mixtures of PuO_2 and silicon in vacuum at 1385°C. The melting point of the compound is 1795°C in vacuum, and density is reported[34] as 8.47 g/cm³. Russell[40] has obtained a patent on methods of preparing compounds of the general formula $MPuO_3$ or $PuMO_3$ which are potential reactor fuels.

Attempts to prepare plutonium mononitride (PuN) by arc melting have resulted in mixtures of PuN, PuO_2, and uncombined plutonium metal.[37] This impure material vaporized at 2650°C in helium with no melting. It is hypothesized that the compound dissociates prior to melting.

(W. M. Pardue)

Thorium

The Russians have reported the results of investigations of phase relations in several thorium alloy systems. The thorium-cerium[13e] and thorium-zirconium[13f] alloy systems are in general agreement with previously published phase diagrams. A eutectic reaction was found[13g] to occur at 1325°C on the thorium-rich side of the thorium-tin system. Solubility of tin in thorium is approximately 0.2 at.% at 1300 to 1320°C. In the thorium-lead system, a eutectic reaction was determined at 1400°C on the thorium-rich side of the system. Solubility of lead in thorium is about 0.7 at.%. A peritectic reaction occurs at 0.03 at.% thorium and 1330°C in the thorium-beryllium system. Solubility of beryllium in thorium at 1150°C is less than 1 at.% and at room temperature is practically nil. Solubility[13h] of thorium in beryllium is less than 0.01 at.% at temperatures lower than 1250°C. The thorium-beryllium alloys are discussed further in Sec. II under Beryllides. At high temperatures a wide region of body-centered cubic solid solutions exists in the thorium-uranium-zirconium system. Lowering the temperature narrows this region considerably. It was observed that this solid solution decomposes into two ternary solid solutions of equal body-centered cubic lattice and different compositions. Solid solubility of uranium in zirconium-rich solid solutions was greater than in thorium-rich solid solutions.[13i]

The Polish[41] studied mutual solubility of rhenium in thorium and thorium in rhenium. One intermetallic compound corresponding to Re_2Th was identified in the system.

The Bureau of Mines[42] found that additions of holmium to thorium decrease the melting point to 1700°C in a 90 wt.% thorium alloy and to 1650°C in a 60 wt.% thorium alloy. Holmium raises the alpha-to-beta transformation temperature from 1365°C for pure thorium to 1430°C for a 60 wt.% thorium alloy. A 50% addition of neodymium lowers the melting point to 1200°C and the alpha-to-beta transformation temperature to 1160°C. Praseodymium reduced the melting point to 1562°C for a 90 wt.% thorium alloy and to 1215°C for a 50 wt.% thorium alloy. The alpha-to-beta transformation occurs at 1080°C in a thorium–50 wt.% praseodymium alloy.

Studies at Battelle[43] indicate that some surface protection is required to provide complete protection against corrosion of stored thorium. Nickel coatings gave excellent protection, and results with organic coatings were encouraging.

(V. W. Storhok)

Dispersion Fuels

The irradiation and postirradiation heat-treatment of aluminum-UO_2 and aluminum-U_3O_8 fuel specimens was carried out by workers at Phillips Petroleum.[18] Irradiation-induced changes in aluminum-UO_2 cermets, averaged over many specimens, are shown in Table I-7.

Twenty percent-enriched, 54 wt.% UO_2 dispersed in aluminum suffered nearly complete reaction of the UO_2 with the aluminum after 56 at.% U^{235} burnup. Little evidence of porosity was noted, and the plate exhibited good stability.

Sample fuel plates containing U_3O_8 dispersed in aluminum were fabricated, and small quantities of B^N or B_4^NC were added to several plates to study the effect of burnable poisons. After irradiation to 25% U^{235} burnup, it was evident that the U_3O_8 particles reacted with the aluminum as much as or more than the UO_2. It also appeared that the U_3O_8 samples had more porosity than the UO_2 dispersions, which could be due to the fine stringering of the U_3O_8 powder in these particular samples. No effects of the poisons were evident.

To assist in studying the reaction zones around UO_2 and U_3O_8 fuel particles dispersed in aluminum, specimens from sample fuel plates were heat-treated (600°C for 40 hr) to obtain reaction of fuel particles with the aluminum matrix. Not all the specimens reacted, and in several cases only a portion of the particles within a specimen reacted. One completely reacted specimen was found by X-ray diffraction to contain aluminum and UAl_4, but no UO_2, whereas another sample exhibiting little reaction showed aluminum, UO_2, and UAl_3 in detectable amounts. Another sample from the completely reacted specimen was selectively dissolved to remove the aluminum, leaving intermetallic compounds and possibly UO_2. A powder-diffraction pattern on this sample indicated all UAl_4 and no UO_2.

Making use of a relatively new and interesting fuel concept involving glass fibers containing a fissionable material, the Clevite Corp. has developed a potentially useful reactor fuel material. Dispersions of these fueled glass fibers have been incorporated in an aluminum matrix, thus strengthening the aluminum. Nine clad and unclad composite specimens which were prepared by Clevite and which consisted of glass fibers containing 50 wt.% U_3O_8 dispersed in a type 1100 aluminum matrix were irradiated by Battelle[44] at a temperature of 100°C to depletion burnups of 17 to 24% of the U^{235} and to fast-neutron (>1 Mev) exposures of 1.8×10^{20} to 2.6×10^{20} nvt.

Table I-7 AVERAGE WEIGHT, SIZE, AND HARDNESS CHANGES IN IRRADIATED FUEL PLATES WITH CORES OF 6 TO 65 WT.% UO_2 DISPERSED IN ALUMINUM[18]

Range in burnup, % of U^{235} atoms	Change in weight, %	Change in thickness, %	Change in hardness, %		
			Cladding	Matrix	Particle
15 to 30	0.19	2.55	+33	+133	−7
30 to 50	0.31	1.70	+57	+199	4
50 to 77	0.29	2.62	+36	+272	−39

The results of this investigation indicate that a composite fuel material of glass fibers which contained U_3O_8 and which was dispersed in an aluminum matrix possessed good stability during irradiation. The changes in thickness and density experienced by the clad specimens were 1 to 2% and about 1 to 4%, respectively, which is about the same magnitude as the degree of change experienced by uranium-aluminum alloy fuels under similar conditions. Neither localized swelling nor blisters were observed on the irradiated specimens, and there was no evidence of structural damage such as cracks or checks.

The amount of fission gas released by three unclad specimens irradiated to burnups of near 24% could be accounted for by the recoil release mechanism, and therefore the integrity of the material during irradiation is confirmed. This integrity was further confirmed by the results of metallographic examinations, which showed no evidence of fission-fragment recoil damage to the aluminum matrix.

The ultimate strength of the specimens was increased to a degree comparable with the increase in strength of the individual matrix and cladding materials observed in other studies. The ductility of the glass-aluminum material did not change, and a tendency was observed for the elastic modulus to increase.

(D. L. Keller)

Coated-Particle Fuel Materials

Preparation and Testing

Oxide-Base Fuel. Oak Ridge[45] has reported some exploratory studies on coating UO_2 particles with BeO using solution techniques. Spherical particles of BeO containing and enclosing 0- to 10-μ UO_2 particles were prepared by dispersing the UO_2 in a concentrated viscous solution of a basic beryllium salt in a liquid organic medium, drying, and firing. The coatings or products were porous and would therefore require densification to make the BeO protective. Attempts to precipitate $Be(OH)_2$ or $BeCO_3$ on UO_2 particles suspended in solutions of beryllium salts under various conditions were unsuccessful.

Only limited studies[46] on Al_2O_3-coated UO_2 particles were reported by Battelle during the past three months. This work consisted of impaction of coated particles against a steel plate by a high-velocity gas jet in order to separate particles with weaker coatings. However, considerable attention was given to BeO coatings.[25,46,47] A sample of UO_2 coated with 57 μ of BeO at a temperature of 1400°C by the indirect hydrolysis of $BeCl_2$ showed a loss of only 20 ppm UO_2 in the standard acid-leach test. These coated particles had crushing strengths of about 1000 g, and the coating hardness was 1275 to 1425 KHN, which is slightly higher than the 1150 to 1325 KHN for single-crystal BeO. Alpha emission was found to be 13 ppm, and Xe^{133} release at a temperature of 1300°C after neutron activation was 17 ppm. The BeO coating contained about 2 wt.% Al_2O_3 as an impurity picked up from the Mullite reactor. Coating studies at temperatures of 1000 to 1300°C are also under way.

Magnesia coatings have been deposited at Battelle[25,46,47] by use of essentially the same apparatus and techniques previously developed for depositing Al_2O_3, except that the halide was introduced into the fluidized bed as a solid instead of a vapor. Coatings of magnesia up to 60 μ thick were translucent and appeared to be dense and void free with a hardness slightly less than that of fused MgO. In general, all the MgO coatings on a dense UO_2 substrate were found on examination to be cracked when cooled to room temperature. However, MgO coatings on a porous UO_2 substrate revealed a lower incidence of visible cracks. The incidence of cracking was further reduced, but not eliminated, by heat-treating the porous UO_2 substrate before cooling the coated particles. It was concluded that cracking of the MgO coatings resulted from the large difference (4×10^{-6}/°C) in the thermal-expansion coefficient of UO_2 and MgO. The development of MgO coatings was continued, using a pyrolytic carbon (PyC)-coated MgO substrate to temporarily bypass the differential-contraction problem experienced with a UO_2 substrate. Preliminary results indicated that MgO coatings prepared at temperatures of 800, 1100, and 1400°C on a PyC-coated substrate did not protect the carbon from oxidation.

Pelletizing procedures have been further developed[25,46,47] to obtain preferred grain ori-

entation of the graphite matrix supporting Al_2O_3-coated UO_2 particles, as well as to achieve improved dispersion and to permit the use of more severe subsequent fabrication conditions. Fuel-element specimens have been molded at pressures up to 40,000 psi without fuel-particle damage, as shown by neutron-activation tests. The preferred grain orientation was obtained by an intermediate isostatic compaction before the final layers of graphite and binder were applied to the fuel.

Cost estimates for the fluidized-bed vapor-deposition process for coating fuel particles with ceramic films were presented at an American Nuclear Society Symposium on Fluidization, which was held in New York during March.[48] Coating costs for carbon, Al_2O_3, and BeO films on 127-μ slightly enriched fuel particles are summarized in Tables I-8 and I-9. The coating costs for orders of 600 to 6000 kg of fuel per year at present rates of deposition should be between $28 and $413 per kg of fuel for 40-μ coatings, the exact price depending on the coating. At very large production levels, between 68,000 and 680,000 kg/yr, the prices are expected to drop to between $1 and $71 per kg of fuel, again depending upon the type of coating. The more optimistic coating prices are approximately equivalent to a 0.02 mil/kw-hr charge for carbon coatings, 0.1 mil/kw-hr for Al_2O_3, and 1 mil/kw-hr for BeO coatings at 10,000 Mwd/ton burnup, on the basis of previous estimates for reactors having thermal efficiencies of 28%.

Table I-8 COATING COSTS FOR PILOT QUANTITIES OF COATED FUEL AT PRESENT RATES OF DEPOSITION[48]

(Reactor Diameter, 5 In.)

Process description:			
Coating material	Carbon	Alumina	Beryllia
Rate, lb coating/hr/sq ft	6.0	2.0	1.5
Capacity, lb coating/year	6050	2020	1510
Price of coating:			
Yearly operating expenses	$169,000	$172,000	$172,000
Materials expenses (45% yield)	320	5,116	79,310
Total yearly expenses (approximate)	$169,000	$177,000	$251,000
Price/lb coating	$27.90	$87.60	$166.10
Added price for 40-μ coatings on 127-μ fuel:			
Fuel material	UC_2	UO_2	UO_2
Weight coating/weight fuel	0.45	1.50	1.13
Plant capacity, kg fuel/year	6090	611	608
Added price/kg fuel	$28	$289	$413

Table I-9 COATING COSTS FOR COMMERCIAL QUANTITIES OF COATED FUEL AT INCREASED RATES OF DEPOSITION[48]

(Reactor Diameter, 24 In.)

Process description:			
Coating	Carbon	Alumina	Beryllia
Rate, lb coating/hr/sq ft	30.0	10.0	7.5
Capacity, lb coating/year	678,000	226,000	169,000
Price of coating:			
Yearly operating expenses	$423,000	$352,000	$ 352,000
Materials expenses (90% yield)	17,850	287,000	4,450,000
Total yearly expenses (approximate)	$441,000	$639,000	$4,802,000
Price/lb coating	$0.65	$2.95	$28.40
Added price for 40-μ coatings on 127-μ fuel:			
Fuel material	UC_2	UO_2	UO_2
Weight coating/weight fuel	0.45	1.50	1.13
Plant capacity, kg fuel/year	681,000	68,400	68,000
Added price/kg fuel	$1	$9	$71

Carbide-Base Fuel. Additional information on the properties of carbon coatings deposited at General Atomic has been presented.[49,50] The crystal structure of the carbon coatings was found to depend on the temperature of deposition in the range from 1400 to 2400°C; the two-dimensional structure became more defined with increasing deposition temperatures. Subsequent annealing at a temperature of 2400°C of the coatings deposited at 1400°C and at 2200 to 2400°C produced graphitization, whereas coatings deposited at 1800 to 2000°C retained their two-dimensional character.[49] Preliminary evaluation of compacts heated at 1500°C for over 3000 hr revealed no apparent damage to the coating by solution of the PyC on the high-temperature side or by precipitation on the cooler side in a temperature gradient. Fission-product-retention testing of a compact that had been heated for 1450 hr in the temperature range (gradient) 1720 to 1615°C gave 0.44% Xe^{133} release in 5 hr at 1700°C, whereas a control compact showed 0.21% Xe^{133} release. Metallographic examination revealed carbide penetration of about 40% through the carbide coating. It appeared that the retentivity of the remaining coating was not seriously affected.[50] Fission-product-release studies at 1700°C on coatings deposited at temperatures between 1400 and 2200°C were also reported. The fractional Ba^{140} release varied from 0.4 to 0.8 for treatment times up to 1700 hr. A review paper on advanced fuels,[51] presented by General Atomic at the 1962 Nuclear Congress, included a summary of work on ceramic-coated nuclear fuel particles.

Oak Ridge has published specifications on a reference fuel element for their Pebble-Bed Reactor Experiment. The element is to be a molded, $1\frac{1}{2}$-in.-diameter sphere containing a uniform dispersion of PyC-coated uranium-thorium carbide particles, a $\frac{1}{16}$-in.-thick unfueled shell, and a 0.006- to 0.008-in.-thick coating of Si-SiC. The nominal diameter of the fuel particles is $180 \pm 20\ \mu$, and the coating thickness is $80 \pm 20\ \mu$. A maximum burnup of 130,000 Mwd/ton (U + Th) is expected with an average fuel temperature of 590°C and a maximum temperature of 1040°C. A maximum R/B for the element of $10^{-6} \times \sqrt{T_{\frac{1}{2}}}$, where $T_{\frac{1}{2}}$ is the half-life of the isotope in seconds, would be acceptable.[52]

Also reported are additional properties of carbon-coated uranium carbide particles received from General Atomic (GA), Minnesota Mining and Manufacturing Company (3M),[33] National Carbon Company (NCC), and High Temperature Materials, Inc. (HTM). HTM has supplied a columnar type of coating, presumably prepared at about 1650°C, 3M particles had

Table I-10 EFFECT OF PREACTIVATION HEAT-TREATMENT ON THE RELEASE OF Xe^{133} FROM FUELED-GRAPHITE SPECIMENS CONTAINING COATED PARTICLES[55]

Lot	Preactivation heat-treatment	Xe^{133}-release ratio, ppm									
		In vacuum						In He containing 0.6 vol.% H_2O at room temperature			
		1000°C		1600°C		2000°C					
		2 hr	24 hr	2 hr	24 hr	2 hr	24 hr	2 hr	24 hr	48 hr	96 hr
NC-6-96	None	13	18	65	121	*	*	†	†	†	†
NC-6-13	Acid leached‡ and thermally cycled§ three times to ~1500°C	18	40	150	250	*	*	†	2.5	*	*
	(Retested)	*	*	*	*	†	1520¶	2	1120	*	1500
NC-6-62	500 hr at 1000°C	82	136	540	690	*	*	42	71	*	*
NC-6-11	65 hr at 1600°C	24	41	180	380	*	*	†	†	*	*
NC-6-18	24 hr at 2000°C	80	200	1570	3400	*	*	†	†	*	>320**
NC-6-76	100 hr at 2000°C	170	300	2160	5500	*	*	39	2410	5440	5620

* Not determined.

† None detected; limit of detection was of the order of 0.1 ppm.

‡ Leached in 8*M* HNO_3 at 95°C for 8 hr and vacuum dried at approximately 200°C for 8 hr prior to thermally cycling.

§ Time at temperature during each thermal cycle was 1 hr.

¶ Bursts of Xe^{133} characteristic of coating rupture were observed during this test.

** An undetermined amount of Xe^{133} was lost during this part of the experiment.

laminar coatings, and NCC particles had a duplex coating structure that consists of an inner laminar layer and an outer columnar layer. All these manufacturers apparently had both good and bad samples, and there were no obvious indications that the material supplied by any specific manufacturer was any better than the others. Results of leaching studies on control samples of graphite-matrix specimens containing PyC-coated fuel particles showed that comparable but rather larger amounts of uranium were removed from fueled-graphite specimens prepared by both 3M and NCC. Many of the values were much larger than those usually observed in comparable tests of as-received coated particles. The implication was that the procedures used to fabricate the fueled-graphite bodies caused damage to some of the particles. Studies on chemical processing, particularly the electrolytic disintegration method, are being continued. Further work on the compatibility of PyC coatings with water vapor at temperatures between 800 and 1200°C is under way.[53]

More recent work has demonstrated the value of low-voltage radiography techniques.[54,55] Contact microradiographs were made on 31 lots of PyC-coated carbide particles, and 25 negatives were examined microscopically, using transmitted light and magnifications up to 500×. Evidence of fuel movement into the coating was found in 20 of the 25 lots. The migration as-

Table I-11 FRACTIONAL RELEASE OF Xe^{133} AND FRACTION OF URANIUM LEACHED FROM COATED-PARTICLE MATERIALS[47]

	Fuel core		Coating*					Fractional Xe^{133} release, ppm	Uranium removed in leach, %
Lot	Material	Dia., μ	Material	Thickness, μ	Matrix support	Irradiation temp., °C	U^{235} fission burnup, %		
715A	UO_2E3	127	Dense Al_2O_3	42	None	100	3.3	120	54
					None	100	4.7	140	39
					None	1070	1.7	0.10	0.86
					None	1070	3.2	0.02	0.22
					Graphite	100	3.5	2.2	33
					Graphite	100	5.0	0.83	43
					Graphite	1070	1.7		
					Graphite	1070	3.3	3.7	
4E	UO_2E0	127	Dense Al_2O_3	8					
			Porous Al_2O_3	6					
			Dense Al_2O_3	28	None	100	2.9	9.7	
721C	UO_2E3	127	Dense Al_2O_3	8					
			Porous Al_2O_3	18					
			Dense Al_2O_3	28	None	100	3.4	2.1	88
					None	100	4.6	17	4.7
					None	1070	1.7	4.3	3.2
					None	1070	3.2	51	0.45
					Carbon	100	3.0	2.0	33
					Carbon	100	4.9	3.9	43
					Carbon	1070	1.6	1.8	
					Carbon	1070	3.3	62	
					Graphite	100	3.4	18	44
					Graphite	100	4.8	2.1	30
					Graphite	1070	1.7	36	
					Graphite	1070	3.4	150	
921	UO_2E2	127	Dense Al_2O_3	48					
			Mixed PyC	32	None	100	3.1	56	46
					None	100	4.9	18	2.2
					None	1070	1.6	0.18	7.2
					None	1070	3.3	0.02	3.0
920	UO_2E3	127	Laminar PyC	45	None	100	3.4	290	
					None	1070	3.8	2100	

* In order of deposition on fuel particle.

sumed four forms: (1) limited, which had fuel remaining close to the fuel particles; (2) circumferential, which had the appearance of a series of rings of alternately high- and low-density material, often extending two-thirds of the way through the coating; (3) circumferential, which had slight density variations; and (4) projection into the coating, which had limited amounts in the circumferential direction. Particles that appeared to contain no fuel whatsoever were found in 6 of the 25 lots. The occurrence of multiple particles in a common coating (doublets) ranged from zero to 10% of the total. Particles of this type were found in 13 of the 25 lots. Average crushing strengths of the coated particles varied from 540 to 1253 g for seven different lots. Additional Xe^{133}-release information after neutron activation on seven new batches of coated particles from 3M, NCC, and GA was reported. Values were generally less than 1 ppm for carbide-base material, but release from the oxide-base fuel supplied by NCC was two to four orders of magnitude higher than that from the carbide-base fuel. Xe^{133}-release data on a number of neutron-activated graphite-matrix specimens containing PyC-coated UC_2 particles were reported as a function of heat-treatment of the sample before and after activation. These data are summarized in Table I-10. It is obvious that a 2000°C heat-treatment severely damages the particles. However, the effect of uranium diffusion at somewhat lower temperatures is not clear because of the uncertainty concerning the number of damaged particles present before testing.[55]

Irradiation and Evaluation of Coated-Particle Fuels

Oxide-Base Fuel. A complete summary of static capsule results on ceramic-coated UO_2 fuel particles, presented by Battelle,[47] is shown in Table I-11. Although there are considerable discrepancies between the postirradiation gas sampling and the leach data, it appears that very significant retention of fission products by Al_2O_3 coatings is possible at temperatures of about 1100°C. At low temperatures the Al_2O_3 coatings fail rather badly, and, apparently,

Table I-12 FISSION-GAS-RELEASE DATA[55] FOR COATED CARBIDE PARTICLES FROM BATCH HTM-1 IRRADIATED IN CAPSULE B9-7

Fission gas	Fission-gas release as ratio of release rate to birth rate, R/B				
	For irradiation at 820°C*		Average for irradiation at 740°C*	For irradiation at 900°C†	
	Average	Maximum		Average	Maximum
Kr^{85}	8.6×10^{-5}	1.1×10^{-3}	2.5×10^{-5}	2.9×10^{-4}	1.8×10^{-3}
Kr^{87}	2.4×10^{-5}	2.6×10^{-4}	6.3×10^{-6}	8.0×10^{-5}	4.7×10^{-4}
Kr^{88}	2.7×10^{-5}	3.5×10^{-4}	7.8×10^{-6}	1.0×10^{-4}	5.7×10^{-4}
Xe^{133}	3.3×10^{-4}	2.8×10^{-3}	7.8×10^{-5}	1.9×10^{-3}	1.3×10^{-2}
Xe^{135}	5.8×10^{-5}	4.5×10^{-4}	1.9×10^{-5}	2.3×10^{-4}	1.3×10^{-3}

* At a flux of 3.7×10^{13} neutrons/(cm²)(sec); estimated maximum burnup, 8 at.%.
† At a flux of 5.5×10^{13} neutrons/(cm²)(sec); estimated maximum burnup, 12 at.%.

Table I-13 AVERAGE FISSION-GAS-RELEASE DATA[55] ON PYROLYTIC CARBON-COATED CARBIDE PARTICLES COMPARED WITH BARE URANIUM CARBIDE PARTICLES AT APPROXIMATELY 820°C

Capsule	Burnup, at.% U	Batch	Type of coating	Fission-gas release as ratio of release rate to birth rate, R/B				
				Kr^{85m}	Kr^{87}	Kr^{88}	Xe^{133}	Xe^{135}
B9-7	8.0	HTM-1	Columnar	8.6×10^{-5}	2.4×10^{-5}	2.7×10^{-5}	3.3×10^{-4}	5.8×10^{-5}
C1-7	15.0	3M-SP-2	Laminar	4.0×10^{-4}	1.8×10^{-4}	1.8×10^{-4}	5.0×10^{-4}	2.0×10^{-4}
B9-8	14.7	NCC-AD	Duplex	2.3×10^{-5}	7.2×10^{-6}	9.2×10^{-6}	7.3×10^{-5}	1.8×10^{-5}
C1-8	4.3	3M-101-U	None	1.2×10^{-2}	3.1×10^{-3}	4.3×10^{-3}	6.7×10^{-2}	7.7×10^{-3}

they are essentially completely cracked, although a porous interlayer of Al_2O_3 appears to help in resistance to low-temperature failure. The effects of a graphite matrix on the behavior of the coated particles is less obvious, since considerable scatter in the data was obtained. In interpreting the data for lot 921, it should be borne in mind that the Al_2O_3 coatings were cracked during overcoating with PyC, and therefore the PyC is actually acting as the fission-gas seal. An interesting fact derived from these data is that, when PyC is protected from direct fission recoil at high temperatures, it apparently has excellent retention for Xe^{133}. In contrast, lot 920, which had no fission-recoil protection for the PyC, failed at high temperatures. Both of these materials were unsatisfactory at low temperatures.

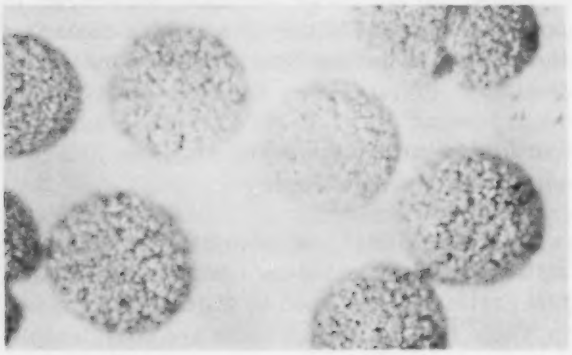

(*a*)

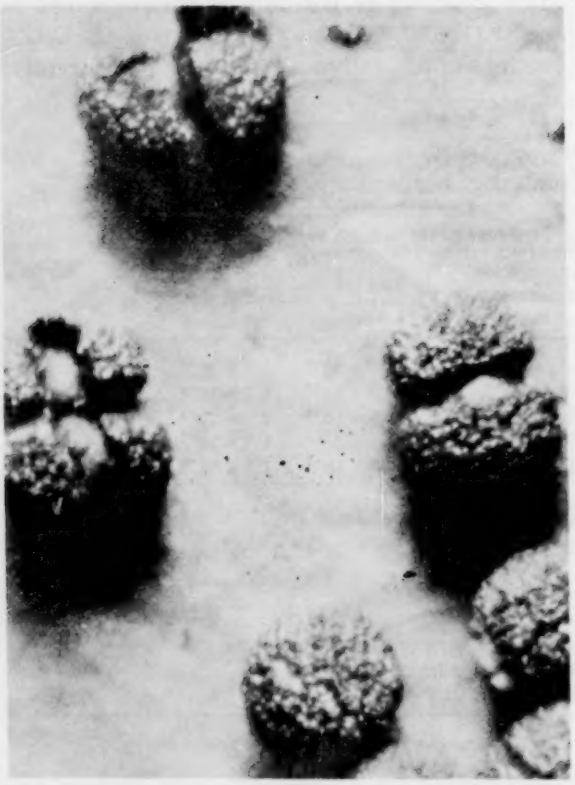

(*b*)

Fig. I-6 Macrophotographs of HTM-coated (82 μ) 3M carbide particles (200 μ). (*a*) Before irradiation. (*b*) After irradiation.[53]

Sweep data[25,46,47] from capsule CFP-S-8 have shown that, for 66 μ of 1600°C PyC on 127-μ UO_2 after 1400 hr at 1000°C and a burnup of about 5%, the R/B values had gradually increased to the 10^{-3} to 10^{-5} level after an initial jump from 10^{-8} to 10^{-6}, which occurred after about 200 hr. The initial breakdown of carbon coatings unprotected from fission recoils after about 200 hr has been shown to occur in other sweep-capsule work, i.e., the failure is strongly time dependent. Another sweep experiment, CFP-S-9, together with other sweep and static experiments, demonstrated that the failure of Al_2O_3 coatings is strongly temperature dependent and that operation at temperatures below about 500°C leads to rupture of the coatings.[25,47] It is pertinent to point out that the surface temperature of the fueled-graphite sphere in experiment SP-5, described in earlier reviews, was estimated to be 510°C at the end of the experiment, and the center temperature of the sphere was from 50 to 100°C higher as a result of heat generation. Thus the radial variation in coating failure could be explained by the radial variation in temperature, which approached, or perhaps overlapped, the independently determined failure temperature of about 500°C for Al_2O_3 coatings.

Carbide-Base Fuel. Carbon-coated uranium carbide particles[54,55] are being irradiated by Oak Ridge in four sweep capsules at temperatures of approximately 820°C. Materials supplied by NCC, HTM, and 3M are being compared with uncoated 3M carbide particles, all unsupported by matrix. The particles are approximately 200 μ in diameter, and the coating thicknesses are about 90 μ. The average and maximum release values for the HTM material are presented in Table I-12, and the average release behavior of all the materials is shown in Table I-13. The NCC material has release ratios that

are a factor of about 4 lower than those for the HTM sample, and the HTM sample has release values that are an order of magnitude better than those of the 3M sample. All carbon coatings exhibited at least one to two orders of magnitude of improvement over uncoated particles. It is not yet obvious which structural or processing condition leads to the superior performance. The NCC sample has so far performed more satisfactorily than any other all-carbon coating tested at any laboratory under comparable conditions.

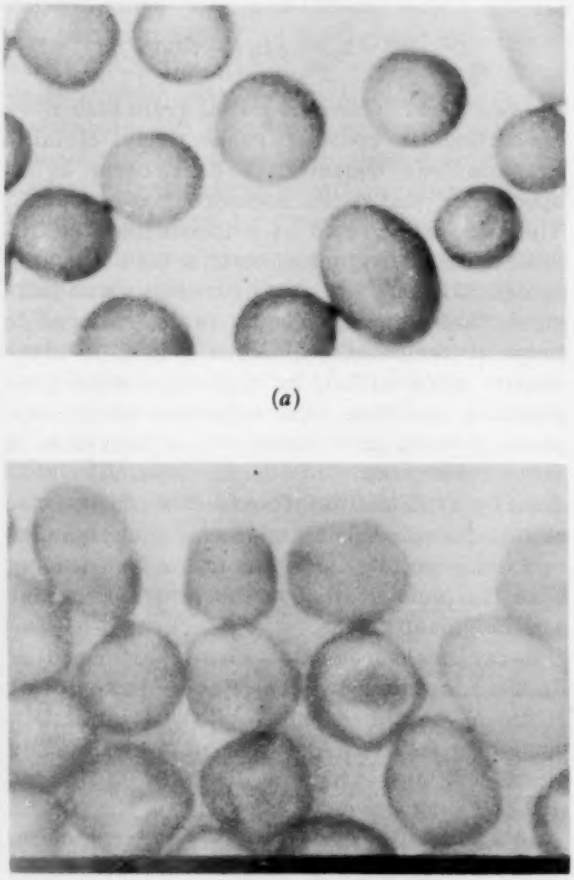

(*a*)

(*b*)

Fig. I-7 Macrophotographs of 3M-coated (82 μ) 3M carbide particles (200 μ). (*a*) Before irradiation. (*b*) After irradiation.[53]

Other irradiation programs now under way at the Oak Ridge Research Reactor (ORR) poolside facility or recently completed at the Materials Testing Reactor involve matrix specimens with carbon-coated carbide particles.[54,55] However, the results are not as promising as the results of the latest tests on unsupported particles. Postirradiation examination of matrix samples containing 3M PyC-coated particles from the MTR 48-5 experiment revealed that the coatings on all the particles had fractured after irradiation at temperatures up to 1300°C. In some instances fractures started at the inner surface of the coating and progressed outward. Similar examination of a control sample showed that less than 2% of the coatings were fractured prior to irradiation. Both matrix specimens were fabricated by NCC.

Recent postirradiation results from the Low-Intensity Test Reactor capsules with HTM PyC coatings on 3M particles and 3M PyC coatings on 3M particles have also been published.[53] The HTM coatings released between 100 and 1000 ppm Kr^{85} after 8% burnup at temperatures between 1070 and 1300°C. The 3M coatings released about 2000 ppm Kr^{85} and 500 to 900 ppm Xe^{133} under these same conditions. Both samples consisted of 82 μ of PyC on 200-μ fuel particles. Macrographs of these particles are shown in Figs. I-6 and I-7.

General Atomic has reported[56] that their PyC-coated $(U,Th)C_2$ particles that were separated from the GA-309-8 irradiation capsule and subsequently heated to 1900°C underwent a delamination of the "onion ring" or layered

Table I-14 POSTIRRADIATION GAS RELEASE OF TWO TYPES OF PyC-COATED URANIUM CARBIDE PARTICLES[25,46,47]

Lot	Fuel		Coating		Matrix support	Irradiation temp., °C	U^{235} burnup, %	Fractional Xe^{133} release, ppm
	Material	Dia., μ	Material	Thickness, μ				
918A	UC_2-E1	200	Columnar PyC	55	None	100	3.1	250
					None	1070	3.8	6200
919A	UC_2-E1	200	Laminar PyC	70	None	100	3.2	18
					None	1070	3.7	9000
					Graphite	440–1050	3.5	30

structure of the coating. Tests are being conducted to see if this phenomenon could have been caused by the nitric acid electrolysis used to separate the particles from the matrix. In addition, measurements were made of the release of fission products from particles recovered from the 309-8 specimen, as well as from the GAIL static capsules. Cesium release, particularly for the 309-8 particles, was high.

Additional data on postirradiation fission-gas release of PyC-coated carbide particles obtained by Battelle are summarized in Table I-14. On the basis of these data, it appears that a 70-μ laminar coating performs more satisfactorily than a 55-μ columnar coating at low and possibly intermediate temperatures, but that both types are unsatisfactory at 1070°C. The coatings were prepared at Battelle using acetylene decomposition at a temperature of 1400°C. The structure of the coating can be changed by varying the partial pressure of the hydrocarbon and hence the rate of deposition of carbon. (J. H. Oxley)

Refractory Fuel and Fertile Materials

Properties and Behavior of Uranium Oxides

In-pile studies of fission-gas release from UO_2 are continuing at Oak Ridge.[53] Measurements of Kr^{88} release from single-crystal UO_2 during irradiation at temperatures ranging from 600 to 1000°C followed an activation energy of about 30 kcal/gram mole. Diffusion coefficients for Kr^{88} in single-crystal UO_2 determined from the release data can be represented by the equation:

$$D = 5.8 \times 10^{-8} \exp(-30{,}000/RT) \text{ cm}^2/\text{sec}$$

Release of Kr^{85m}, Kr^{87}, Xe^{133}, and Xe^{135} was also observed to follow the same activation energy as the Kr^{88} over the same temperature range. In the case of the xenon isotopes, iodine-precursor diffusion was found to account for 40 to 50% of the Xe^{133} and about 80% of the Xe^{135} escaping from the UO_2.

A Hanford report[57] summarizes results of measurements of physical, chemical, and thermal properties of both irradiated and nonirradiated UO_2. This report includes studies of various factors that influence fuel relocating and measurements of fission-product and plutonium segregation during irradiation.

At Chalk River[58] grain growth was studied in 95% dense sintered UO_2 at temperatures ranging from 1555 to 2440°C. The mean grain size, D, after anneals of t hr at a temperature T°K can be expressed by the relation:

$$D^2 - D_0^2 = k_0 t^{0.8} \exp(-87{,}000/RT)$$

where D_0 and k_0 are the initial grain size and a proportionality constant, respectively. Metallic uranium was observed to be present in all specimens that were annealed above 2000°C. This was interpreted as evidence that the UO_2 lattice can be oxygen deficient at high temperatures. Evidence[59] is also presented which indicates that columnar grains can be induced to grow at temperatures above 1700°C in high-density sintered UO_2 by applying a steep temperature gradient. The columnar grains apparently form as a result of the migration of large transverse voids up a temperature gradient by a sublimation process. The consequence of this phenomenon in operating fuel elements containing solid UO_2 pellets is the formation of a central void surrounded by a region of oxide with columnar grains.

X-ray measurements were performed at Knolls[60] to determine the effect of isotopic enrichment on the density of UO_2. Natural UO_2 containing 0.7 wt.% U^{235} had an X-ray density of 10.96 g/cm^3, whereas UO_2 with 93.18 wt.% U^{235} had a density of 10.84 g/cm^3.

Compatibility tests of UO_2 with palladium, platinum, rhodium, and iridium in nonoxidizing atmospheres were performed at General Electric.[61] Small wires of these materials were heated in helium in contact with sintered UO_2 with a theoretical density of 93% at a temperature of 1400°C for 2 hr. Except for some bonding of the metals to the UO_2, visual examination of the rhodium and iridium wires revealed no adverse effects. The platinum and palladium wires in contact with the UO_2 melted, even though the temperature was well below the melting points of both these metals. Metallographic examination revealed extensive diffusion of both the platinum and the palladium into the UO_2. Further work with rhodium and iridium is planned at temperatures above 1500°C.

Studies of the sintering behavior of palladium-UO_2 compacts are in progress. Specimens were

cold pressed from a minus 325-mesh powder of 60 vol.% UO_2–palladium and sintered in both helium and vacuum for 2 hr at 1400°C. A density of 9.43 g/cm^3 was achieved for the material heated in vacuum, whereas sintering in helium yielded a density of 10.04 g/cm^3. Compacts of 45 vol.% UO_2–palladium with a theoretical density of 81% were sealed in palladium tubes with a 0.030-in. wall thickness and heated at 1400°C in flowing air. After 46 hr at 1400°C, the palladium cladding exhibited grain growth and evidence of cracking at grain boundaries. No significant weight changes occurred, and alpha counting showed no surface contamination indicative of uranium diffusion through the palladium cladding.

The Russians[62] have investigated solid-phase reactions between U_3O_8 and CaO, U_3O_8 and V_2O_5, and U_3O_8 and $Ca(VO_3)_2$. The results indicate that three parts U_3O_8 mixed with one part $Ca(VO_3)_2$ reacts to form $CaUO_2 \cdot V_2O_7$. A mixture of three parts CaV_2O_5 with one part U_3O_8 gave a reactant corresponding to $CaUO_4$, V_2O_5, and $CaUO_2V_2O_7$, along with other new products. In general, it was concluded that CaV_2O_7 reacts with U_3O_8 in air to form $CaUO_2V_2O_7$, which does not react with excess U_3O_8. Lattice parameters are also reported for $Ca(UO_3)_2$, $Ca_2V_2O_7$, and $CaUO_2V_2O_7$.

Another Russian article[13j] reports recent work on the UO_2-ZrO_2 system. UO_2 was found to form a continuous series of solid solutions with ZrO_2 which have the fluorite structure of UO_2 up to 51.3 mole % ZrO_2. Beyond this point the structure passes into a tetragonal one: that of the high-temperature modification of ZrO_2. Down to 1675°C these solid solutions do not change. At 1675°C and below, the solid solutions in the 13.5 to 86.0 mole % ZrO_2 range decompose into two solid solutions. One solution is based on UO_2 containing 13.5 mole % ZrO_2, and the second is based on ZrO_2 containing at least 14.0 mole % UO_2 at 140°C. The ZrO_2-base solid solutions undergo transformations at temperatures from 1040°C for pure ZrO_2 down to 140°C at a ZrO_2 content of 14 mole %.

The heat capacity for U_3O_8 up to 1000°C has been determined by Russian investigators.[63] It was found that U_3O_8 undergoes two phase changes: one at 770°C and the other at 940°C. From 368 to 769°C the specific heat of U_3O_8 increased from 0.079 to about 0.145 cal/(g)(°C). Above 790°C the specific heat increased from 0.072 to 0.259 cal/(g)(°C) at 938°C, whereas from 942 to 960°C the specific heat decreased from 0.266 to 0.097 cal/(g)(°C). The heats of phase transformation were 265 ± 5 cal/mole for the phase transition at 770°C and 1105 ± 15 cal/mole for the phase transition at 940°C.

(R. H. Barnes)

Properties of Uranium Carbides, Nitrides, and Sulfides

Two independent findings tend to strengthen the hypothesis that a pseudobinary exists between UC (probably containing some molybdenum) and molybdenum metal (probably containing some uranium). Atomics International reports[64] that, in low-carbon uranium-carbon alloys, an addition of molybdenum partitions to the metal alloy phase, whereas all compositions on the high-carbon side of the UC-molybdenum tie line contain $UMoC_2$.

Weinberg and Yang found[65] that essentially pure liquid uranium was formed by reaction of UC with niobium metal for 5 min at 1875°C and

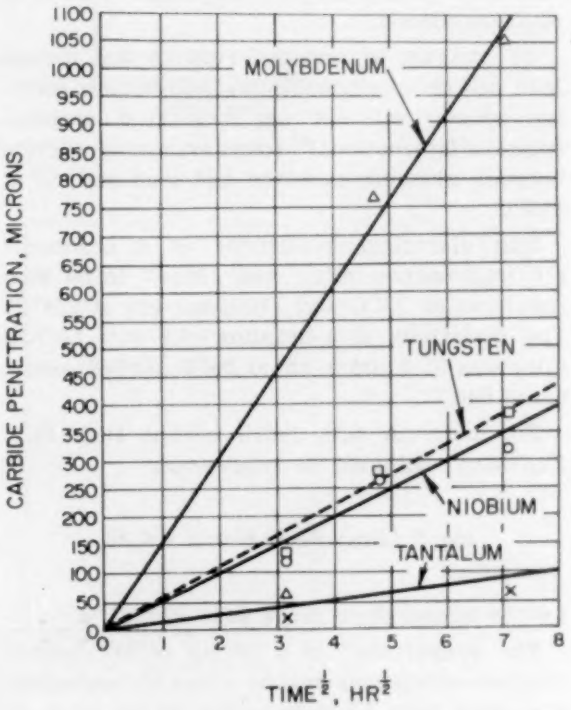

Fig. I-8 Penetration of reaction layers[65] after contact of UC_2 with refractory metals at 1800 ± 20°C. ○, niobium. ×, tantalum. □, tungsten. △, molybdenum.

with tantalum metal for 90 min at 1925°C. Liquid uranium, but no tungsten carbide, was observed between UC and tungsten after 30 hr at 2000°C. Molybdenum reacted with UC to form an intermediate layer in 10 hr at 1800°C. When the same metals were reacted with UC_2 at 1800°C, no liquid was formed, and the carbides Ta_2C, TaC, Nb_2C, NbC, W_2C, WC, and Mo_2C were identified in the intermediate diffusion layers to depths indicated in Fig. I-8. Analyses failed to show any uranium diffusion in these layers. The rate of carbide layer formation between niobium, tantalum, or molybdenum and a ZrC–10 mole % UC alloy at 1800°C was much slower than for the reactions of these metals with plain UC or UC_2. However, as can be seen in Fig. I-9, electron-microprobe analyses of the intermediate layers showed that appreciable uranium had diffused into the metal layer. No interdiffusion of the UZrC alloy with tungsten was observed.

Hanford noted[66] that $UC_{1.05}$ in contact with niobium for less than 3 min at 2250°C was decarburized to a depth of 0.010 in. The other reaction zones identified were as follows, starting from the niobium side: niobium interspersed with Nb_2C platelets, pure Nb_2C, and NbC with Nb_2C inclusions.

In contrast to previous reports that molten lead and tin (presumably just above their melting points) will not wet uranium carbide, Atomics International[64] found extensive reaction between uranium carbides and lead and tin at 870°C.

The electrical resistivity of a uranium–4.4 wt.% carbon alloy was found[64] to be 39.6 μohm-cm at 23°C and 110 μohm-cm at 524°C. The resistivity of a uranium–7.0 wt.% carbon alloy was 51.3 μohm-cm at 25°C and 137 μohm-cm at 648°C.

For uranium with more carbon than UC_2, Fujishiro[67] obtained the expression:

$$\log P_v(\text{atm}) = -30{,}600/T + 6.36$$

for the temperature range 2448 to 2731°K.

The properties[64] of a series of arc-melted uranium-zirconium-carbon alloys known to contain more than 50 at.% carbon in the form of UC_2 are presented in Table I-15.

A uranium–4.8 to 5.0 wt.% carbon alloy was irradiated at a peak surface temperature of 660°C in sodium to a burnup of 16,600 Mwd/metric ton of uranium. Atomics International noted[64] that the specimen came out in a severely cracked condition with a maximum measured diameter increase of about 2% and that it had released about 0.18% of the Kr^{85} produced during irradiation.

Table I-15 PROPERTIES OF SOME URANIUM-ZIRCONIUM-CARBON ALLOYS[64]

Nominal alloy, wt.%	Density, g/cm³	Hardness, R_A	Compressive strength at 20°C, psi
100 UC	13.4	79	88,700
95 UC + 5 ZrC		88	105,700
90 UC + 10 ZrC	11.5	84	114,800

Auskern and Schweitzer have determined[19] that, in the temperature range from 1000 to 1400°C, the diffusion of Xe^{133} from uranium carbide powders may be expressed by the relation:

$$D = 1 \times 10^{-6} \exp(-75{,}000/RT)$$

Keller[68] has irradiated 13 specimens of 96% dense UN and has concluded that any effects of the transmutation of nitrogen to hydrogen and carbon upon the dimensional stability of the UN are negligible. All effects of reactor irradiation noted on these samples could be attributed to growth as a consequence of fission. The irradiation conditions and the resulting density

Table I-16 URANIUM MONONITRIDE IRRADIATION RESULTS[68]

Uranium enrichment, %	Estimated uranium burnup, %	Cladding	Maximum estimated surface temp., °C	Density decrease, %
0.22	0.1	None	70	0.73
0.22	0.1	304 S.S.	70	1.6
0.22	0.1	None	65	1.6
0.22	0.1	304 S.S.	65	1.0
0.72	0.4	None	100	1.1
0.72	0.4	304 S.S.	100	1.7
0.72	0.4	None	105	2.1
0.72	0.4	304 S.S.	105	1.2
5	2.0	None	275	2.9
5	2.0	304 S.S.	275	2.3
5	3.5	None	580	
5	3.5	304 S.S.	580	6.4
5	3.5	304 S.S.	580	3.5

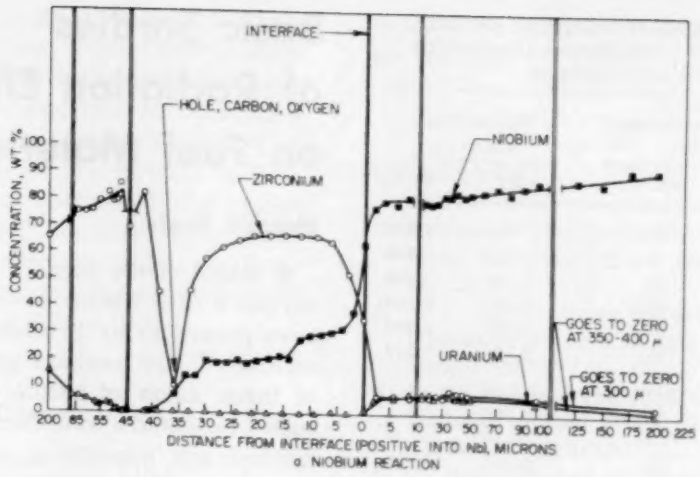

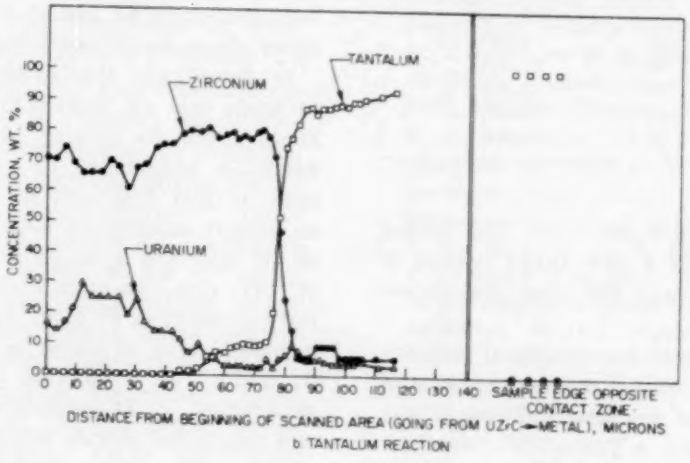

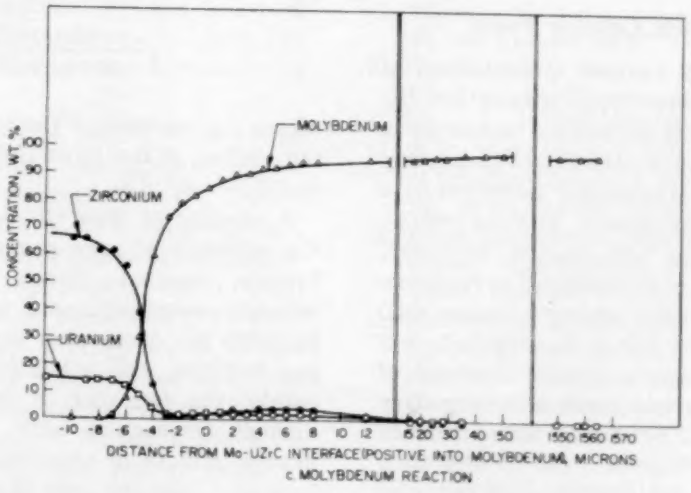

Fig. I-9 Electron-microprobe trace[65] showing niobium, tantalum, and molybdenum reactions with UZrC (6.0 mole % uranium–45.8 mole % zirconium–48.2 mole % carbon; 23.1 wt.% uranium–67.7 wt.% zirconium–9.2 wt.% carbon) at 1800 ± 20°C for 50 hr.

Table I-17 ELECTRICAL PROPERTIES[69] OF THE SULFUR, SELENIUM, AND TELLURIUM COMPOUNDS OF URANIUM AND THORIUM

Compound (nominal)	Seebeck coefficients, μv/°C		Resistivities, μohm-cm	
	200°C	800°C	*RT*	800°C
ThS	25	23	750	1,700
ThSe	25	15	210	400
ThTe	32	29	130	350
US	45	48	2,000	2,200
USe	40	30	2,200	2,000
UTe	11	45	4,100	5,200
ThS_2		410	2×10^6	
$ThSe_2$	12	15	6,000	
$ThTe_2$	45	8	2×10^4	
US_2	20	41	15,000	18,000
USe_2	38	19	24,000	
UTe_2	9	5	9,400	9,100
Th_2S_3			2.6×10^5	
Th_2Se_3		10	4,000	
Th_2Te_3	30	19	20,000	
U_2S_3	3	25	12,000	
U_2Se_3	20	10	2,000	
U_2Te_3		10	4,000	

changes are listed in Table I-16. The unclad specimens broke into a few large pieces in every instance, whereas the clad specimens remained intact.

Jordan[69] has surveyed the electrical properties of the thorium and uranium compounds of sulfur, selenium, and tellurium. Some of the data obtained are listed in Table I-17.

(W. Chubb)

Fabrication of Uranium Carbide Fuels

In the August 1962 review, a discussion of several liquid-phase-sintering studies for UC included one reportedly successful technique in which UAl_2 was added as the liquid-promoting agent. The reaction presumably occurred by a volatilization of the aluminum, with the resulting uranium combining with carbon. However, more recent results at Oak Ridge[53] have shown that starting UC carbon contents higher than stoichiometric (up to 5.3 wt.%) resulted in a lower sintered density, a greater amount of remaining aluminum, and more of a secondary constituent identified by X-ray diffraction as alpha uranium. Additions of 5 and 10 wt.% UAl_2 to UC of 4.8 wt.% carbon content were reported to result in only trace amounts of the secondary constituent after firing in the 1350 to 1450°C temperature range. (E. O. Speidel)

Basic Studies of Radiation Effects on Fuel Materials

Metallic Fuels

A model of the damage produced by the occurrence of a fission event within a metal has been presented by Brinkman of Atomics International.[70] The numbers and spatial distribution of three kinds of lattice defects produced by such an event are considered. The defects considered are interstitial atoms, vacant lattice sites, and displacement spikes. The role of each of these defects in producing swelling, radiation-induced phase transformations, and other physical-property changes is considered.

In developing this model the approximation is made that all fission fragments are of two kinds prior to coming to rest. Each fission event is considered to produce one of each kind: a light fragment with a mass of 96 amu, an atomic number of 39, and an initial energy of 95 Mev and a heavy fragment with a mass of 137 amu, an atomic number of 55, and an initial energy of 67 Mev. The interaction energy between pairs of atoms having atomic numbers Z_1 and Z_2 as a function of their internuclear separation, r, is considered to be given by a new empirical atomic interaction potential

$$V(r) = 1.9 \times 10^6 \, (Z_{\text{eff}})^{11/2} E_R \, \frac{\exp\left[-(Z_{\text{eff}})^{1/3} \, r/1.5 \, a_0\right]}{1 - \exp\left[-0.95 \times 10^{-6} \, (Z_{\text{eff}})^{7/3} \, r/a_0\right]}$$

where E_R represents the Rydberg energy, a_0 is the radius of the first Bohr orbit of hydrogen, and $Z_{\text{eff}} = Z_1^{1/2} \, Z_2^{1/2}$.

A number of theoretical subjects concerning the behavior of rare gases in solids have been brought together, based on simple thermodynamic considerations, by Blin[71] of France. Included for discussion are the equilibrium of gas bubbles, the solubility of rare gases in solids, the behavior of the fission gases including interaction with vacancies, agglomerates, effects of irradiation rate and of dislocations, and the role of grain boundaries and crystal perfection.

The diffusion coefficient and activation energy for diffusion of Xe^{133} in uranium metal has been

determined at Atomics International[72] for several physical conditions of the metal. High-purity and reactor-grade samples were studied in the annealed and cold-worked conditions. Thin foil samples were irradiated to 10^{14} to 10^{17} fissions/cm^3. Up to 14% release of Xe^{133} was observed. Diffusion coefficients in the range of 1×10^{-14} to 1×10^{-10} cm^2/sec were measured, and activation energies of 32 to 40 kcal/mole were obtained for various samples in the temperature interval of 600 to 1000°C.

(F. A. Rough)

Radiation Effects in Ceramic Fuels

New studies[73] indicate that the diffusion of Xe^{133} in almost stoichiometric UO_2 proceeds with an activation energy of about 50 kcal/mole.

Experiments have been conducted at Hanford[74] which show that UO_2 in the vicinity of a moving fission fragment does vaporize from the fission source film. The deposit, which condenses on collectors during vacuum irradiations, has been identified by electron diffraction as UO_2. Moreover, long fission-fragment tracks in the collector are produced by fragments originating from the deposit on the collector. A 200-A amorphous coating of carbon on the surface of UO_2 fission source films greatly reduces the vaporization. Three types of collectors (amorphous carbon, amorphous carbon with a thin coating of platinum, and large-grained aluminum) display holes and tracks after bombardment with fission fragments from carbon-coated UO_2 sources. Fission-fragment damage in these targets differs in track geometry and in the amount and uniformity of material ejected.

In studies of release of stored energy from irradiated oxides, Childs[75] has reported results for annealing in the range of 50 to 700°C after irradiations up to 1.1×10^{19} neutrons/cm^2. Little, if any, energy was released from single-phase UO_2 and U_4O_9 specimens, but a small release was observed at about 340°C for two-phase specimens of $UO_{2.08}$ composition. A major energy release was observed for U_3O_8. The temperature of the release varied from 150°C for 6×10^{15} neutrons/cm^2 to 380°C for 1.1×10^{19} neutrons/cm^2. The total energy released increased with exposure to a saturation value of 25.5 cal/g at 1.4×10^{17} neutrons/cm^2. In analyzing these data in terms of a homogeneous saturated disorder region for the passage of each fission fragment, a fission-fragment damage region of 2.7×10^{-16} cm^3 is obtained.

(F. A. Rough)

References

1. R. Resnick and L. Seigle, The Self-Diffusion of Alpha Uranium, *J. Nucl. Mater.*, 5: 5–11 (January 1962).
2. A. J. Jacobs, Grain Refinement of Uranium—A Literature Survey, Israeli Report IA-704, December 1961.
3. J. C. Rivière, The Structure of Uranium and Thorium in Thin Films, British Report AERE-R-3991, March 1962.
4. K. Pederson and G. Murphy, Effects of Temperature on Mechanical Properties of Normal Uranium Dingot, USAEC Report IS-400, Ames Laboratory, January 1962.
5. L. T. Lloyd and M. H. Mueller, Recrystallization in Rolled Uranium Sheet, USAEC Report ANL-6327, Argonne National Laboratory, March 1962.
6. D. G. Harrington and J. B. Newton, Capsule Irradiation of Unalloyed Uranium at High Temperatures, USAEC Report NAA-SR-7098, Atomics International, Apr. 15, 1962.
7. T. K. Bierlein, R. D. Leggett, B. Mastel, and J. W. Weber, Swelling in Uranium: A Comparison of the Effects of Irradiation and Postirradiation Annealing, USAEC Report HW-69393, Hanford Atomic Products Operation, April 1961.
8. J. Buddery and K. Scott, A Study of the Melting of Irradiated Uranium, *J. Nucl. Mater.*, 5: 81–93 (January 1962).
9. K. Scott and J. Buddery, The Release of Krypton 85 from Irradiated Uranium on Thermal Cycling Through the Phase Changes, *J. Nucl. Mater.*, 5: 94–100 (January 1962).
10. W. McDonell, Kinetics of Structural Changes During Beta Transformation of Uranium, *Nucl. Sci. Eng.*, 12: 325–336 (March 1962).
11. D. C. Minty and B. R. Butcher, Grain Refinement of Uranium-Chromium Alloys by Continuous Cooling, British Report AERE-R-3896, January 1962.
12. Ames Laboratory, Annual Summary Research Report in Metallurgy, July 1960–June 1961, USAEC Report IS-351, December 1961.
13. Academy of Sciences of the USSR, Institute of Metallurgy, *Structures of Alloys of Certain Systems With Thorium and Uranium* (in Russian), Gosatomizdat, Moscow, 1961.
    a. O. S. Ivanov and Yu. S. Virgil'ev, Transformation of the Gamma-Solid Solution in Binary Alloys of Uranium and Molybdenum, pp. 87–92.
    b. O. S. Ivanov and G. I. Terekhov, Transformations of the Gamma-Solid Solution During Quenching and Annealing in the Systems Ura-

nium-Niobium and Uranium-Niobium-Molybdenum, pp. 249–264.

c. O. S. Ivanov and G. N. Bagrov, Behavior of Gamma-Solid Solutions of the System Uranium-Molybdenum-Zirconium During Hardening and Annealing, pp. 191–198.

d. O. S. Ivanov and Yu. S. Virgil'ev, Investigating the Stability of Gamma-Solid Solutions Fixed by Quenching in Alloys of U-Zr-Nb-Mo After Prolonged Annealing in the 430–550°C Range, pp. 296–306.

e. T. A. Badayeva and R. I. Kuznetsova, Structure of the Alloys of the Thorium-Cerium System, pp. 381–386.

f. T. A. Badayeva and G. K. Alekseyenko, Phase Diagram of the Thorium-Zirconium System, pp. 369–380.

g. T. A. Badayeva and R. I. Kuznetsova, Determining Lead and Tin Solubility in Thorium in the Solid State, pp. 387–394.

h. T. A. Badayeva and R. I. Kuznetsova, Structure of Thorium-Beryllium Alloys, pp. 358–368.

i. T. A. Badayeva and G. K. Alekseyenko, Structure of Alloys of the System Thorium-Zirconium-Uranium, pp. 395–415.

j. N. M. Vororov et al., Phase Diagram of the System Uranium Dioxide-Zirconium Oxide, pp. 467–481.

14. G. Petzow and I. Kvernes, The Constitution of Uranium-Silicon-Aluminum Alloys, *Z. Metallk.*, 53(4): 248–256 (April 1962).
15. W. F. Murphy, A. C. Klank, and S. H. Paine, Examination of Uranium–2 wt.% Zirconium Experimental Fuel Slugs Irradiated in EBR-I, USAEC Report ANL-6114, Argonne National Laboratory, February 1962.
16. Atomic Energy of Canada Ltd. (Unpublished)
17. R. J. Beaver, J. H. Erwin, and R. S. Mateer, An Evaluation of the Uranium Contamination on the Surfaces of Alclad U-Al Alloy Research Reactor Fuel Plates, USAEC Report ORNL-3206, Oak Ridge National Laboratory, Mar. 19, 1962.
18. G. W. Gibson and O. K. Shupe, Annual Progress Report on Fuel Element Development for Fiscal Year 1961, USAEC Report IDO-16727, Phillips Petroleum Co., Mar. 9, 1962.
19. Brookhaven National Laboratory, Nuclear Engineering Department Progress Report, September 1–December 31, 1961, USAEC Report BNL-705, March 1962.
20. Ames Laboratory, Iowa State University, Newsletter for Division of Reactor Development Concerning Reactor Materials and Low Decontamination Separations for January 1962, Feb. 19, 1962.
21. Argonne National Laboratory, Reactor Development Program Progress Report, May 1962, USAEC Report ANL-6573, June 15, 1962.
22. Los Alamos Scientific Laboratory, Quarterly Status Report on LAMPRE Program for Period Ending February 20, 1962, USAEC Report LAMS-2681, March 1962.
23. I. I. Jones, The High Temperature Irradiation of Aluminum-Plutonium Alloys Clad in Stainless Steel, Canadian Report CRRM-1076, February 1962.
24. F. H. Ellinger et al., The Solubility Limits of Aluminum in Delta Plutonium and Some Revisions of the Plutonium-Aluminum Phase Diagram, *J. Nucl. Mater.*, 5(2): 165–172 (1962).
25. R. W. Dayton and R. F. Dickerson, Progress Relating to Civilian Applications During May 1962, USAEC Report BMI-1581, Battelle Memorial Institute, June 1, 1962. (Classified)
26. Los Alamos Scientific Laboratory, Quarterly Status Report on LAMPRE Program for Period Ending May 20, 1962, USAEC Report LAMS-2720, June 1962.
27. S. J. Paprocki, D. L. Keller, and W. M. Pardue, The Chemical Reactions of PuO_2 with Reactor Materials, USAEC Report BMI-1580, Battelle Memorial Institute, May 29, 1962.
28. Hanford Atomic Products Operation, US/UK Research Newsletter No. 13, March 1962.
29. T. D. Chikalla, A Note on the Structural Stability of Plutonium Dioxide, USAEC Report HW-71887, Hanford Atomic Products Operation, Nov. 30, 1961.
30. Hanford Atomic Products Operation, Reactor and Fuels Research and Development Operation Monthly Report, April 1962, USAEC Report HW-73514A, May 15, 1962. (Classified)
31. Hanford Atomic Products Operation, Plutonium Recycle Program Annual Report, Fiscal Year 1961, USAEC Report HW-70000, Aug. 11, 1961.
32. Hanford Atomic Products Operation, Plutonium Metallurgy Operation Quarterly Progress Report, July, August, September 1961, USAEC Report HW-70722, Oct. 16, 1961. (Classified)
33. T. D. Chikalla, The Liquidus for the System UO_2-PuO_2, USAEC Report HW-69832, Hanford Atomic Products Operation, June 1961.
34. S. Goldsmith (Ed.), Research and Development Programs Executed for the Division of Reactor Development, USAEC Report HW-73100, Hanford Atomic Products Operation, May 1, 1962.
35. Hanford Atomic Products Operation, Reactor and Fuels Research and Development Operation Monthly Report, March 1962, USAEC Report HW-73202A, Apr. 15, 1962. (Classified)
36. Hanford Atomic Products Operation, Unclassified Research and Development Programs Executed for the Division of Reactor Development and the Division of Research, USAEC Report HW-73541, Apr. 20, 1962.
37. P. G. Pallmer, Thermal Expansion of Plutonium Carbides, USAEC Report HW-72245, Hanford Atomic Products Operation, February 1962.

38. Argonne National Laboratory, Reactor Development Program Progress Report, March 1962, USAEC Report ANL-6544, Apr. 15, 1962.
39. Argonne National Laboratory, Reactor Development Program Progress Report, February 1962, USAEC Report ANL-6525, February 1962.
40. L. E. Russell, Improvements in or Relating to Plutonium Compounds, British Patent 887,953, Jan. 24, 1962.
41. J. Niemeic, X-ray Analysis of the Rhenium-Thorium System, *Bull. Acad. Polon. Sci., Ser. Sci. Chim.*, 9(8): 501–508 (1961).
42. Bureau of Mines, Metallurgical Progress Report No. 14 for the Period January 1, 1962, to March 31, 1962, USAEC Report USBM-U-921.
43. E. F. Stephan, P. D. Miller, and F. W. Fink, Corrosion of Thorium and Uranium During Long-Term Storage, USAEC Report BMI-1563, Battelle Memorial Institute, Jan. 24, 1962.
44. R. J. Burian, J. E. Gates, and R. F. Dickerson, Radiation Stability of Compacts of Aluminum and Fuel-Bearing Glass Fibers, USAEC Report BMI-1573, Battelle Memorial Institute, Mar. 30, 1962.
45. W. J. McDowell, Coating of UO_2 Particles with BeO by Solution Methods, USAEC Report ORNL-TM-220, Oak Ridge National Laboratory, May 9, 1962.
46. R. W. Dayton and R. F. Dickerson, Progress Relating to Civilian Applications During March 1962, USAEC Report BMI-1574, Battelle Memorial Institute, Apr. 1, 1962. (Classified)
47. R. W. Dayton and R. F. Dickerson, Progress Relating to Civilian Applications During April 1962, USAEC Report BMI-1577, Battelle Memorial Institute, May 1, 1962. (Classified)
48. J. H. Oxley et al., Coating Costs for Ceramic-Coated Nuclear Fuel Particles, paper presented at American Nuclear Society Symposium, New York City, Mar. 21, 1962.
49. G. B. Engle, C. S. Luby, and J. C. Bokros, Evaluation of (Th,U)C_2, Carbon-Coated (Th,U)C_2 Particles, and Carbon Coatings, USAEC Report GA-3067, General Atomic Div., General Dynamics Corp., Apr. 26, 1962.
50. W. V. Goeddel, Thermal Stability Testing of Graphite-Matrix Fuel Compacts Containing Pyrolytic-Carbon Coated Carbide Particles with Comments on the Amoeba Effect, USAEC Report GAMD-2675, General Atomic Div., General Dynamics Corp., Sept. 26, 1961.
51. J. F. Schumar and J. N. Siltanen, Fuels and Materials Development for Advanced Reactors, Preprint Paper No. 34, 1962 Nuclear Congress, June 4–7, 1962.
52. Oak Ridge National Laboratory, Conceptual Design of the Pebble Bed Reactor Experiment, USAEC Report ORNL-TM-201, May 17, 1962.
53. Oak Ridge National Laboratory, Gas-Cooled Reactor Program Quarterly Progress Report for Period Ending December 31, 1961, USAEC Report ORNL-3254, Apr. 6, 1962.
54. Oak Ridge National Laboratory, Coated Particle Fuel Element Development, USAEC Monthly Activity Letter for the Period February 15, 1962, to March 15, 1962, 2(3) (March 1962).
55. W. O. Harms, Coated Particle Fuel Element Development Activity Letter for the Period March 15 to May 15, 1962, USAEC Report ORNL-CF-62-6-75, Oak Ridge National Laboratory, June 29, 1962.
56. General Atomic Div., General Dynamics Corp., 40-MW(E) Prototype High-Temperature Gas-Cooled Reactor Research and Development Program. Quarterly Progress Report for Period Ending March 31, 1962, USAEC Report GA-3132.
57. W. E. Roake, Irradiation Alteration of Uranium Dioxide, USAEC Report HW-73072, Hanford Atomic Products Operation, March 1962.
58. J. R. MacEwan, Grain Growth in Sintered Uranium Dioxide. I. Equiaxed Grain Growth, *J. Am. Ceram. Soc.*, 45: 37–41 (January 1962).
59. J. R. MacEwan and U. B. Lawson, Grain Growth in Sintered UO_2. II. Columnar Grain Growth, *J. Am. Ceram. Soc.*, 45: 42–46 (January 1962).
60. Knolls Atomic Power Laboratory, Reactor Technology Report No. 20—Metallurgy, USAEC Report KAPL-2000-17, Mar. 22, 1962.
61. General Electric Co., Flight Propulsion Laboratory Dept., High-Temperature Materials Program Progress Report No. 11, Part A, USAEC Report GEMP-11A, May 15, 1962.
62. G. I. Khlebnikov et al., Investigating the Solid Phase Reactions Between CaO, V_2O_5, and U_3O_8, in *Issled. v Obl. Khim. Urania*, pp. 292–301, USSR Academy of Sciences, 1961.
63. K. G. Khomyakov et al., True Heat Capacity of U_3O_8, in *Issled. v Obl. Khim. Urania*, pp. 141–144, USSR Academy of Sciences, 1961.
64. Atomics International, Feb. 2, 1962. (Unpublished)
65. A. Weinberg and L. Yang, Interdiffusion Between Uranium-Bearing Reactor Fuels and Refractory-Metal Thermionic Emitters, USAEC Report GA-3124, General Atomic Div., General Dynamics Corp., May 4, 1962.
66. Hanford Atomic Products Operation, 1962. (Unpublished)
67. S. Fujishiro, The Dissociation Pressure of UC_2 at High Temperature and the Thermodynamic Properties, *Nippon Genshiryoku Gakkaishi*, 3(12): 913–917 (December 1961).
68. D. L. Keller, Development of Uranium Mononitride, Quarterly Progress Report for January-March 1962, USAEC Report BMI-X-197, Battelle Memorial Institute, Apr. 1, 1962.
69. C. B. Jordan, High Temperature Semiconducting Compounds for Thermoelectric Power Generation, Report EOS-1592-Final, Electro-Optical Systems, Inc., Dec. 15, 1961.
70. J. A. Brinkman, Fission Damage in Metals,

USAEC Report NAA-SR-6642, Atomics International, Mar. 1, 1962.

71. J. Blin, The Behavior of Rare Gases in Solids at High Temperatures, French Report CEA-1444, 1960.
72. J. W. Savage, Diffusion of Fission Product Xenon-133 in Uranium, *Bull. Am. Phys. Soc.*, Series II, 7: 27 (Jan. 24, 1962).
73. H. Matzke and R. Lindner, The Diffusion of Homogeneously Distributed Rare Gases from Solid Bodies (in German), *Z. Naturforsch.*, 16A: 845–849 (September 1961).
74. T. K. Bierlein and B. Mastel, Fission-Induced Vaporization of UO_2 from a Source and Subsequent Condensation on Collectors Exposed to Fission Fragment Bombardment, USAEC Report HW-72114, Hanford Atomic Products Operation, December 1961.
75. B. G. Childs, The Release of Stored Energy, *J. Nucl. Mater.*, 5: 128–139 (January 1962).

Section

II

Reactor Materials

Moderator Materials

Graphite

The possible catalytic effect of fission-product metals (barium, strontium, and cesium) on carbon transport or on the steam-graphite reaction has been explored.[1] Experiments conducted on graphite loaded with 0.013 wt.% barium indicated negligible effect on carbon transport reactions. However, barium and strontium were found to catalyze the steam-graphite reaction. Barium and strontium concentrations up to 0.7 wt.% of metal and at temperatures of 855 to 1050°C were investigated.

Electron microscopy has been used to observe microstructural changes and to study defect clusters in neutron-irradiated graphite. The technique of replica electron microscopy has been applied to the study of growth in neutron-irradiated graphite.[2] Thus the presence of cracks, which are parallel to the basal planes and which constitute about 5% of each grain volume in unirradiated pile graphite, has been confirmed. Such microstructure has been suggested by the acceleration that occurs in the rate of growth and the accompanying increase in coefficient of thermal expansion of specimens cut perpendicular to the extrusion at a certain dose, dependent on the temperature. For specimens irradiated at 200°C, this change is shown at approximately 3×10^{20} neutrons/cm^2. These microstructural cracks were observed to close as this point of change in growth and coefficient of thermal expansion was approached. Transmission electron microscopy[3] was used to study defect clusters formed in graphite by higher-flux neutron irradiation at temperatures up to 650°C. A linear relation was found to exist between cluster radius and irradiation temperature (see Fig. II-1), and the subsequent annealing behavior of the defects is consistent with the hypothesis that the visible defects are all of one kind, probably interstitial. A homogeneous nucleation theory has been shown to apply and to be consistent with some important microscopic properties. Some observations at the highest temperatures and doses suggest that vacancy clusters may also become identifiable.

Experimental carbon bodies have been developed which exhibit permeabilities as low as 10^{-12} cm^2/sec. Unlike conventional carbons and graphites, these new carbons are "monophase" materials prepared from a single raw material. Impermeable carbon,[4] a product of General Electric Co., Ltd., is prepared by the direct carbonization of a cellulose material. Exceptional tensile strength, on the order of 10,000 psi, is reported for this material, and preliminary tests indicated good stability toward neutron irradiation. An apparently similar material is reported to be prepared from different

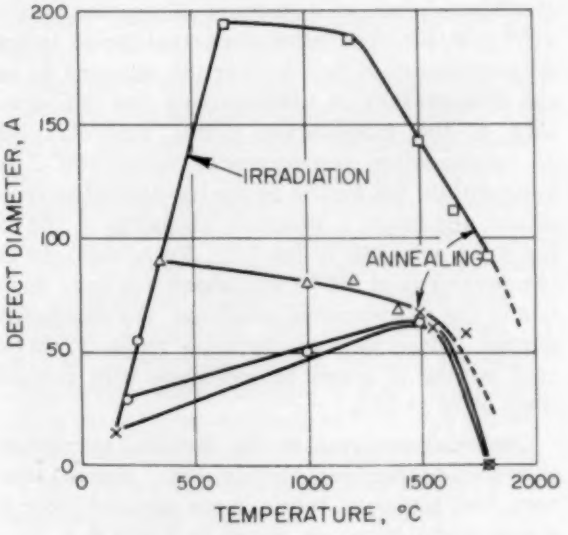

Fig. II-1 Mean defect diameter in graphite as a function of irradiation and annealing temperature.[3]

raw material and different processing by Japanese investigators.[5] (M. C. Brockway)

Beryllium Metal and Alloys

Casting, Vapor Deposition, and Refining

Russian authors[6] report some success in control of the cast grain size of beryllium melts by the application of ultrasound. The metal was melted by an electric arc under argon at a pressure of 400 mm Hg. Ultrasound, at a frequency of 19.7 kc/sec, applied during and after melting, was said to cause complete recrystallization of the metal to a grain size commensurate with that produced by powder metallurgy. The grains were slightly coarser near the surface than at the center of the ingot. Popov[7] also reported that the application of ultrasonic vibrations (15-μ amplitude at 17.2 kc/sec) to substrates on which beryllium or zinc films were being deposited brought about a considerable refinement of the grain structure and inhibited the development of preferred orientation.

Another report[8] from the same laboratory noted that vacuumtight, high-purity beryllium foil with a uniform thickness of 20 to 300 μ and satisfactory mechanical properties can be obtained by depositing beryllium vapors on a molybdenum plate in a vacuum of approximately 10^{-6} mm Hg. The most important factor in the determination of foil properties appears to be the temperature of condensation (the temperature of the molybdenum plate). Foil obtained at condensation temperatures below 300°C is vacuumtight but brittle in the as-deposited condition, and hence it requires annealing at 700°C for 6 hr or at 800°C for 3 hr. Foils obtained at temperatures of 850°C and above are very ductile in the as-deposited condition, but somewhat porous. These foils can be made vacuumtight by cold rolling at room temperature with reductions of 20 to 25%.

Chemical analysis of the distilled beryllium produced at Nuclear Metals, Inc.,[9] showed that very low impurity levels were attained after a single distillation, as shown in Table II-1. Redistillation reduced the iron content to between 1.0 and 2.5 ppm and the aluminum to less than 5 ppm. In spite of this extremely high purity, small black spherical particles, believed to be associated with the brittle fracture of beryllium, were observed on the fracture surfaces, and the metal showed a very limited bend ductility. Major metallic components of the spherical particles were iron and silicon. (Analysis cannot be made for oxygen or beryllium.)

Table II-1 ANALYSIS OF FEED AND DISTILLED BERYLLIUM[9]

	Analysis, ppm						
	Fe	Ni	Cr	Mn	Si	Al	Cu
Pechiney flake*	160	100	10	20	50	55	9
Distilled beryllium*	3	2	1	5	12	20	5

*Vacuum melted.

Table II-2 ANALYSIS OF ZONE-REFINED PECHINEY BERYLLIUM[11]

	Analysis, ppm					
	Fe	Ni	Cr	Mn	Al	Cu
Starting material	225	116	12	23	75	85
After five zone passes:						
Start end	49	215	3	<1	19	
Finish end	1290	28	112	230	965	13

Meanwhile work at the Franklin Institute[10] showed that purification (by zone refining) significantly increased the ratios of the critical resolved shear stress (CRSS) for prism to basal glide in single crystals.* This value, previously reported by Tuer and Kaufmann (*The Metal Beryllium*, p. 380) as 5:1, was found to be 25:1 in the purified crystals. However, it appears that this beryllium is actually less pure than the relatively brittle distilled beryllium. Chemical analysis on the start and finish ends of a 1¼-in.-diameter, five-pass zone-refined crystal gave the data shown in Table II-2. Iron, chromium, manganese, and aluminum move quite efficiently by zone refining to the last end of the bar to solidify, whereas copper and nickel have a tendency to concentrate at the purified starting end.[11]

*Treharne and Moore,[12] using 99.83% beryllium, found that the CRSS for (0001) slip remains constant at 750 psi in the temperature range 300 to 600°C and increases only by a factor of 5 in the range 300 to 196°C. They determined that the CRSS for $(10\bar{1}0)$ slip increased by a factor of 9 in the same temperature range. They concluded that increasing purity reduces the CRSS for both types of slip in beryllium.

Results of tensile testing of zone-refined single crystals produced at Nuclear Metals from both Pechiney and distilled beryllium are shown in Table II-3. Comparison of the start ends of the five-pass crystals adds additional evidence that the CRSS decreases and the overall elongation as well as the glide strain increases with (presumably) increased purity of the beryllium single crystal. The ratio[13–15] of the resistivity of beryllium at room temperature (RT) to that at the temperature of liquid hydrogen (4.2°K) increases with increasing purity (Table II-4). It seems probable that this ratio could be used to compare the overall purities of very pure metal.

Table II-3 TENSILE DATA ON ZONE-REFINED SINGLE CRYSTALS OF BERYLLIUM[14]

Starting material	No. of zone passes	Position in bar	Orientation, degrees χ_θ	Orientation, degrees λ_θ	CRSS, psi	Overall elongation, %	Glide strain, %	Remarks
Pechiney	1	Finish end	43	42	1940	27	50	
Pechiney	5	Finish end	55	55	2780	5	27	Nonuniform oxide
Pechiney	5	Start end	54	55	690	6	14	
Distilled	3	Finish end	50	55	1120	19	96	Nonuniform oxide
Distilled	5	Finish end	50	50	770	36	121	Nonuniform oxide
Distilled	5	Start end	49	48	410	61	100	

Fabrication of Beryllium

Brush Beryllium reported[16] that cross-rolled beryllium sheet can be brought to better than 1% out-of-flatness by roller leveling. The only effect that the process has on the properties is that some surface hardening can be removed readily by pickling. Annealing in the temperature range 1750 to 2020°F improved the third-dimensional ductility of the sheet, as shown in Fig. II-2. The lowest scatter in biaxial ductility data was found in specimens that were annealed 10 hr in this temperature range.

Beryllium sheet, 0.060-in. thick, produced in the laboratory of the Beryllium Corp. had 80,000 psi ultimate tensile strength, 61,000 psi yield strength, 44% tensile elongation, and 4% reduction in the thickness direction. Sheet material[17a] produced in the mill with careful processing control can show short transverse ductility ranging from 1 to 3%. The tensile- and yield-strength specifications to which beryllium sheet is commonly furnished apparently could be increased somewhat without hardship to the producers.

Table II-4 RESISTIVITY RATIO ($\rho_{RT}/\rho_{4.2°K}$) OF BERYLLIUM OF VARIOUS PURITY LEVELS[15]

Description	$\rho_{RT}/\rho_{4.2°K}$
Vacuum-melted Pechiney flake	7.2
Start end of three-pass single crystal (Pechiney)	18.7
Finish end of three-pass single crystal (Pechiney)	12.2
Start end of three-pass single crystal (distilled)	68.3
Finish end of three-pass single crystal (distilled)	50.3

Beryllium can be fabricated at elevated temperatures by methods commonly used for other metals. During fabrication the amounts of residual cold work, grain size, and grain orientation substantially influence the resulting mechanical properties. Tensile-strength variations from 20,000 to over 200,000 psi and ductilities from nil through some isotropic to considerable anisotropic elongation have been measured. The highest properties, nearly 200,000 psi with 3% elongation, were obtained in fine wire, apparently through the creation of very fine grains by strain recrystallization during cold working.[17b]

Beryllium sheets that were produced by three methods were compared by Giemza[18] from a structural viewpoint. Hot-cross-rolled sheet, although showing the highest nominal strength and ductility, underwent a marked embrittlement in bending, leading to fracture under low load in a box-beam test. Hot-pressed beryllium

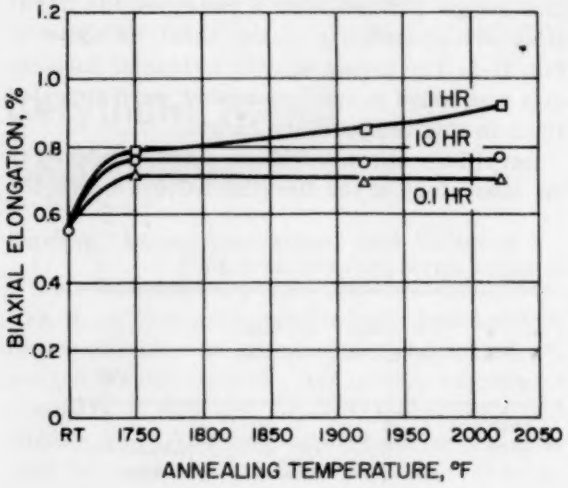

Fig. II-2 Percentage biaxial elongation at fracture vs. annealing temperature for cross-rolled beryllium sheet.[16]

sheet stood up slightly better in the box-beam test but was judged the least acceptable because of its low tensile, elongation, and notch strength. Hot-upset sheet gave markedly better results in the box-beam test than either of the other materials. However, it gave generally poorer values than the hot-pressed sheet on a constant-moment bend test of wide sheets.

Oak Ridge reported[19] that finned tubes produced by direct extrusion using the shaped-die technique[20] showed, at room temperature, burst stresses ranging from 3960 to 4820 psi, which correspond to hoop stresses of 45,400 to 65,400 psi. Burst tests on closed tubes with welded end caps showed: at 800°F, no rupture under 16,000-psi pressure; at 1150°F, rupture after 1.5 min at 1600-psi pressure; at 1150°F, rupture after 1.5 min at 1600-psi pressure; and at 1350°F, immediate fracture at 1350 psi.

A British paper[17c] comparing tube fabrication methods indicated that hot extrusion, followed by warm drawing while using electroplated silver as a lubricant, appeared the most successful.

Christensen[21] reported the successful development of a technique for extruding aircraft structural shapes from pure beryllium based on the aforementioned method of extruding finned beryllium tubes developed for the USAEC. The method requires encapsulation of the beryllium in mild steel finished both inside and outside to 32 μin. and then electroplating 0.030 in. of copper on the outside. During subsequent hot extrusion, the press container was lubricated with a mica-base material. Special die designs were developed for extrusion of a channel section.

Gas-pressure bonding of beryllium-clad UO_2 fuel elements was investigated at Battelle.[19,22] Beryllium-to-beryllium bonds were obtained after 2 to 4 hr at 1500 to 1650°F (815 to 900°C) at 10,000 psi. Chromium or pyrolytic carbon coatings on UO_2 cores prevented significant UO_2-beryllium reactions during bonding. Reaction products formed on the beryllium during compatibility experiments were easily removed by acid pickling. Joints at least as strong as the base metal were obtained on surfaces pickled with a 10 vol.% H_2SO_4 solution followed by a 4-hr bonding operation at 1650°F. Grains did not grow across the interface.

Whitson[23] described a method of brazing beryllium tubes to stainless steel to form leaktight joints. The stainless steel was first cleaned by electron bombardment at 1760°F at a pressure of 10^{-6} mm Hg and then cooled to 1290°F and coated with a thin film of silver-copper eutectic brazing alloy that was evaporated from a molybdenum boat. The steel tube was then cooled and fitted into a hole in a beryllium plate with a clearance of less than 0.001 in., and a ring of brazing alloy was placed around the tube at the joint. The jig with this assembly was placed in the vacuum furnace, heated to 1510°F for 5 min, and furnace cooled. Leak rates on all samples brazed in this manner were less than 5×10^{-9} standard atmosphere per cubic centimeter per second.

Beryllium also has been recommended[24] as a diffusion-bonding agent for joining various iron-base, nickel-base, and cobalt-base alloys. Diffusion bonding is a technique that, when successfully applied, can produce joints in the solid state which have properties approaching those of the base-metal members. Joints were readily formed when the faying surfaces were painted with a thermoplastic paint carrying beryllium powder or when one surface was vapor plated with beryllium, but the amount of beryllium added by these methods was difficult to control and tended to be excessive. Stronger joints could be made with a preplaced nickel-base brazing alloy containing 1.5 to 3% beryllium, with or without additions of chromium, iron, or manganese. These alloys, which contain beryllium in solid solution at the brazing tempera-

tures, produce diffusion-bonded joints in from ½ to 5 min at 1940 to 2100°F. Joints made on a complex nickel-base alloy containing 15% chromium had shear strengths of up to 72,900 psi at room temperature, and on a 12 wt.% chromium–10 wt.% cobalt–8 wt.% tungsten–4 wt.% titanium–4 wt.% aluminum (plus boron and zirconium) alloy had a shear strength of 53,000 psi at 1500°F.

Physical Metallurgy of Beryllium

Meyerhoff and Smith[25] measured the anisotropic thermal expansion of various metals, including beryllium, at low temperatures. Qualitative spectrographic analysis of the beryllium showed weak lines corresponding to iron and aluminum, and very weak lines from calcium, chromium, copper, nickel, manganese, and magnesium. The purity of the beryllium was believed to be over 99.5%. (Apparently, BeO was not determined.) Variations of the ratio $(c/a)_T$ to $(c/a)_{273.2°K}$ with temperature are listed:

Temp., °K	Ratio	Temp., °K	Ratio
273.2	1.000000	160	1.000221
260	1.000039	140	1.000247
240	1.000089	120	1.000269
220	1.000130	100	1.000284
200	1.000165	80	1.000294
180	1.000193		

Arzhanyi et al.[26] studied the solid-state diffusion of beryllium and aluminum in niobium at 900 to 1300°C. The diffusion of both occurs in several phases simultaneously. Beryllium forms four compounds: $NbBe_{12}$, NbBe, $NbBe_5$, and $NbBe_3$. Accordingly, four sharply defined zones were found in the diffusion layer. The outer $NbBe_{12}$ zone was the deepest. Beryllium diffuses into niobium at a much higher rate than aluminum.

Amonenko et al.[27] described the properties of beryllium films formed by vapor deposition on molybdenum plates preheated to 300 to 320°C (see also Refs. 7 and 8). The films, which were 170 to 300 μ thick, had a grain size of 8 to 15 μ and a density of 1.831 g/cm³. In addition to oxygen, they contained 0.013% impurities. Textures of the films depended on the conditions of deposition, texture, and surface treatment of the molybdenum plates. Tensile tests were made on three types of specimens: type I, which had the basal plane roughly corresponding with the specimen plane; type II, which had the basal plane forming a 45° angle with the specimen plane and the axis of the specimen coinciding with the (2 1 1) axis; and type III, which was the same as type II but which had the specimen axis corresponding with the (0 1 0) axis. Results of tensile tests on the films at room and at elevated temperatures are shown in Fig. II-3. The change in width and thickness of types II and III with the testing temperature is shown in Fig. II-4.

Amonenko et al.[28] measured the electrical conductivity of similar 300-μ-thick beryllium films vapor deposited on molybdenum sheet at

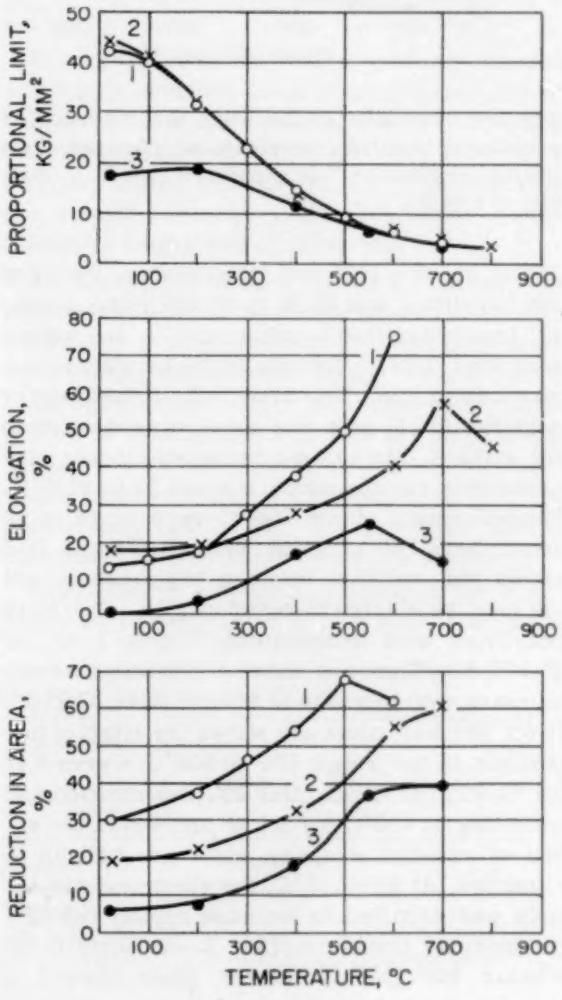

Fig. II-3 Tensile properties of texturized beryllium.[27] 1, texture of type I. 2, texture of type II. 3, texture of type III.

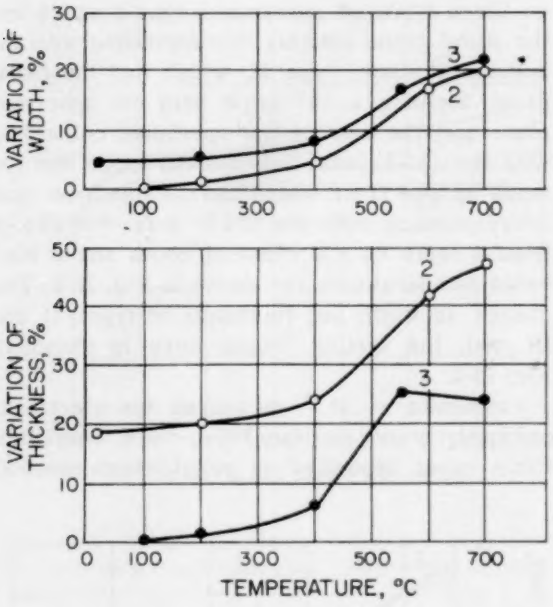

Fig. II-4 Variation of the width and thickness of samples of texturized beryllium as a function of the testing temperature.[27] 2, samples of type II. 3, samples of type III.

300°C and 2×10^{-6} mm Hg pressure. Purity of the beryllium was 99.96 to 99.97% (total metallic impurities 0.01%, oxygen 0.01%, and carbon less than 0.02%). Density of the beryllium film was 1.833 g/cm^3. The films had axial symmetry with the (0 0 1) axis that was perpendicular to the surface. The resistance measurements were made over the temperature range 18 to 1280°C. Measurements above 900°C were made in an atmosphere of purified helium. Figure II-5 shows the relation between temperature and the relative electrical resistance $(R_t - R_0)/R_0$ of beryllium with temperature. Curve 1 is for 99.97% beryllium and shows a continuous smooth increase with increase in temperature. Curve 2 is for 98% beryllium and shows the effect of impurities in the range 200 to 800°C. Curve 3 is for 99.97% beryllium after 10% deformation and annealing at 900°C for 1.5 hr and shows the effect of residual stresses, which are difficult to eliminate. At 1254 ± 5°C, the electrical resistance was reported to increase rapidly due to a polymorphic transformation. X-ray analysis on similar but slightly thicker films showed a transformation from the alpha-beryllium lattice to the body-centered cubic beta form at 1254 ± 5°C. The beta form had the lattice parameter $a = 2.5464$ kX.

Garber et al.[29] reported a study of the behavior of 99.98% pure beryllium single crystals under tensile stresses. Analysis of the results of mechanical tests, correlated with the examination of slip bands and microstructure of specimens after fracture, led to the following conclusions:

1. Plasticity of beryllium increases monotonically with rising temperature, showing no peak at 400°C, as does polycrystalline beryllium.

2. Deformation of beryllium single crystals with the basal plane at an acute angle to the tensile direction takes place mainly by slip along the basal planes (0 0 0 1) in the $[1\,1\bar{2}\,0]$ direction. At higher temperatures prismatic slip along the $(1\,0\,\bar{1}\,X)$ planes in the general $[1\,1\bar{2}\,0]$ direction and diffusion deformation play an increasingly important part.

3. Brittleness of beryllium single crystals at room temperature is caused by nonuniform plastic deformation along the basal plane, which causes the formation and growth of cracks along the main cleavage plane. At high temperatures slip becomes more uniform, and deformation takes place partly by prismatic slip.

Schultz[30] loaded specimens of Brush beryllium to failure in biaxial tests at temperatures ranging from room temperature to 1400°F. He found that the biaxial yield stresses for this beryllium in tests at 1000°F appear to be in agreement with the theory of Maximum Distor-

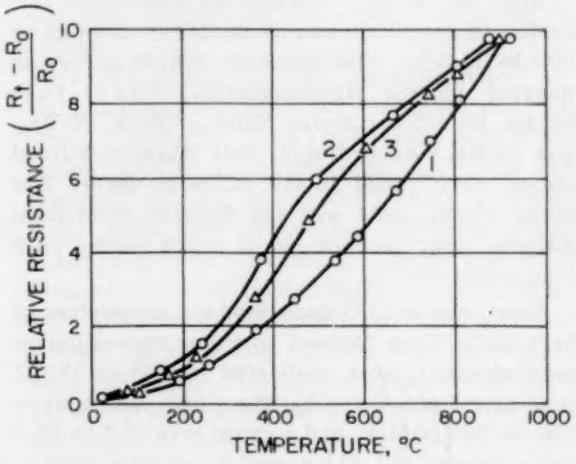

Fig. II-5 Variation in the relative electrical resistance of beryllium with temperature.[28] 1, 99.97% pure metal. 2, 98% pure metal. 3, 99.97% beryllium, cold-rolled 10% and annealed at 900°C for 1.5 hr.

tion Energy rather than the theory of Maximum Shear Stress.

A McDonnell report[31] noted that gold plating on beryllium appears to have no effect on notched or unnotched tensile strength, modulus of rupture, or fatigue strength at room temperature or at elevated temperature.

Nuclear and Corrosion Properties of Beryllium

Dienes and Damask[32] estimated the effect of radiation on the thermal conductivity of beryllium. From existing data on the effect of reactor irradiation on the electrical resistivity of beryllium, they predicted that a reactor exposure of 10^{19} nvt (fast) should decrease the thermal conductivity by approximately 0.04 watt/(cm)(°K) at temperatures of 20 to 30°K, an amount probably unimportant in practice. Warming to 250°K should cause rapid and complete annealing of the radiation-induced change in thermal conductivity.

Oak Ridge[19] found that the stress-rupture life at 520°C of machined beryllium tubes was not affected by fast-neutron (>1 Mev) exposures from 1 to 3.4×10^{20} neutrons/cm^2. Similarly, warm-extruded tubes exposed to 2×10^{20} neutrons/cm^2 showed no noticeable change in stress-rupture life.

Also reported[33] are the results of autoclave tests made to study the behavior of beryllium and beryllium oxide in heavy water at elevated temperatures. Sintered and hot-pressed QMV beryllium and Grade UOX beryllia were obtained from Brush Beryllium Company and were exposed from 60 to 120 days at 250 and 300°C in both degassed and oxygenated heavy water. There was no apparent difference in the corrosion behavior of beryllium in degassed water at either temperature. The results are summarized in Table II-5. Specimens in degassed water developed thin tenacious films that could not be removed by standard degassing techniques. Slightly thicker films developed in oxygenated water.

Recent work[34] on the reaction of beryllium metal with oxidizing gases reveals that, after an induction period of variable length, oxidation proceeds at an accelerating rate, accompanied by disintegration of the metal into small fragments. The earlier literature dealt only with the induction period and gave a picture of beryllium as one of the most oxidation resistant of metals. However, the present picture is that catastrophic oxidation may completely destroy specimens exposed to temperatures above 650°C for long periods.

During the induction period a network of pores and oxides develops along grain boundaries just below the oxidizing surface. The pores weaken the metal. Grain-boundary attack is affected by microstructure and purity; beryllium metal of exceptionally coarse grain size shows a significantly longer induction period.

An Australian report[35] noted that breakaway oxidation of beryllium did not occur on extruded specimens in commercially dry (<20 ppm moisture) carbon dioxide below 650°C. Even at 650°C breakaway oxidation was observed only in one series of specimens, and, in that case, the gas pressure was 280 psig. In all cases specimens with etched surfaces showed a weight gain approximately 25 to 30% greater than that of specimens with ground or polished surfaces.

Corrosion of beryllium in water at 100°C appears to be insensitive to flow rate. Specimens

Table II-5 EFFECT OF HEAVY WATER ON BERYLLIUM AND BERYLLIA[33]

Couple and exposure time	Heavy-water condition		
	Degassed	Oxygenated	
	250 and 300°C	250°C	300°C
Be to Be, 90 days	No adverse effects (shallow pitting)	0.2 mil/yr (shallow pitting)	0.5 mil/yr (shallow pitting)
Zircaloy-2 to Be, 120 days	Very shallow pitting	1.1 mils/yr, pits to 4.0 mils	0.5 mil/yr, pits to 6.4 mils
Be to type 347 stainless steel, 60 days	Little effect	Near catastrophic, pits 100 to 125 mils*	Severe, pits 100 to 125 mils*
BeO	1.0 mil/yr at 250° 1.2 mils/yr at 300°	1.5 mils/yr	1.5 mils/yr

*Surfaces covered with heavy tubercules of white corrosion product.

of QMV beryllium in 100°C water (pH = 5; 4 ppm oxygen) flowing at either 13 or 23 ft/sec corroded at rates varying from 2.1 to 2.8 mils/yr, regardless of velocity, in a 560-hr test. Other specimens under the same conditions, except for flow rates of 22 to 81 ft/sec, corroded at rates of 1.9 to 2.1 mils/yr in a 319-hr test, again showing no velocity effect.[36]

Beryllium Reviews

Hodge[37] prepared a wide-ranging but late-in-appearing review of unclassified government-sponsored research and selected literature on beryllium which covers the period 1958–1960. The report includes extensive tables of physical and mechanical properties of beryllium metal.

Cholak et al.[38] presented a comprehensive report on the health hazards of beryllium. The report is intended as a review and guide for use by individuals who have the responsibility for protecting the health of personnel engaged in operations involving beryllium. (W. Hodge)

Beryllium Oxide

Tobin of General Atomic[39] has reported the results of an irradiation experiment on unfueled BeO of several types. Specimens were fabricated by hot pressing and by either extrusion or cold pressing, followed by sintering. Additions of up to 1.5 wt.% Al_2O_3 or MgO and up to 2 wt.% bentonite were made to some specimens. Specimen densities ranged from 84 to 99% of theoretical, and average grain sizes ranged from 5 to 60 μ. The specimens were encapsulated and irradiated in the General Electric Testing Reactor at 550 to 1000°C to total exposures of 1 to 2×10^{21} nvt (fast).

The BeO specimens irradiated at 800 to 980°C showed no evidence of disintegration; however, those irradiated at 570 to 770°C seemed to be fragile. There appeared to be no clear advantage to high specimen density from the standpoint of radiation stability. Thermal diffusivities decreased 15 to 40% during irradiation. This tendency was depressed somewhat by the MgO and bentonite additions. Postirradiation compressive strengths were 50 to 67% lower than the initial values. Bentonite additions tended to lessen the magnitude of the decrease. Specimen dimensions were increased less than 1%, and densities were decreased less than 3%.

Investigators[40] at General Electric are continuing a comprehensive experiment on irradiation effects in BeO of various types, densities, and grain sizes. Preirradiation characterization has included measurements of crystallite orientation, Young's modulus, shear modulus, modulus of rupture, thermal expansion, compressive creep, density, grain size, and purity. A very large body of data is being accumulated.

Specimens for measurement of Young's modulus were irradiated at 100°C to total exposures in the ranges of 6.0 to 8.7×10^{18} nvt (fast) and 1.2 to 2.3×10^{20} nvt (fast). The modulus was substantially unchanged in specimens of all types, and compositions were irradiated to the lower exposures. In specimens irradiated to the higher exposures, Young's modulus was decreased to as little as 19% of the preirradiation values. The more typical decreases were in the range of 50%. Similar specimens irradiated at 1000°C to about 2×10^{20} nvt (fast) showed no change in Young's modulus.

Lattice-parameter measurements of irradiated BeO showed that, at 100°C, "*a*" increased linearly with exposure up to about 4×10^{20} nvt (fast). At that point the change in "*a*" saturated at an increase of about 0.15%.

Measurements of the refractive indices of BeO before and after irradiation have been made at Oak Ridge.[34] The specimens were irradiated at 120°C to 1.5×10^{21} nvt in the Engineering Test Reactor. Typical index values are shown below:

	n_ω	n_ϵ
Preirradiation	1.719	1.733
Postirradiation	1.700	1.712

The indices were returned to normal by annealing at temperatures as low as 650°C. The observers suggest petrographic measurement of refractive index as a rapid, quantitative, inexpensive, nondestructive method of measuring the extent of radiation effects in BeO.

Continued experiments on foamed BeO ceramics have been reported by General Electric.[41] Thermal conductivity was measured on a 3-cm thickness of foamed BeO that had a density of 0.77 g/cm³ (25.6% of theoretical). Pore size ranged from 0.01 to 0.025 cm. Hot- and cold-face temperatures were 1500 and 1300°C,

respectively, and the gradient was maintained for 260 hr. The thermal conductivity was stable in the range of 0.005 cal/(cm)(sec)(°C) during the entire test period. It was observed that BeO shapes that are foamed under restraint have somewhat higher density and smaller average pore size than similar shapes foamed in open molds. (A. K. Smalley)

Beryllides

Oak Ridge[19] is studying $ThBe_{13}$, UBe_{13}, $ZrBe_{13}$, $ThBe_{13}$ + 5 wt.% UBe_{13} and $ZrBe_{13}$ + 20 wt.% UBe_{13}. They found that freshly prepared, prealloyed powders pressed to higher green densities and sintered to higher densities, on the average, than commercial powders that were stored. In these studies, 3 wt.% camphor was used as a binder; it was removed after cold pressing by evaporation at 800°C. An argon atmosphere was found to reduce beryllium losses 2 to 3%. UBe_{13} and $ThBe_{13}$ were found to completely dissolve in boiling 4*M* HNO_3.

In studies of the thorium beryllide–uranium beryllide system,[42] the Russians have confirmed

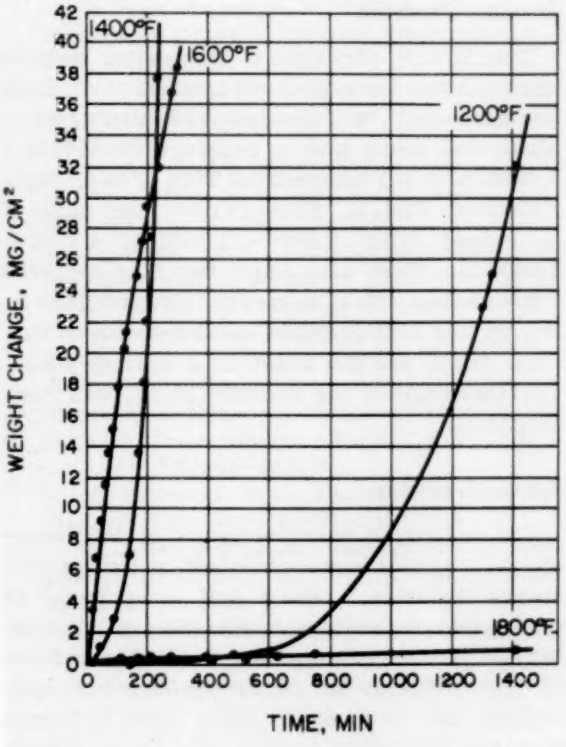

Fig. II-6 Oxidation[44] of $ZrBe_{13}$ in wet air at 1200, 1400, 1600, and 1800°F.

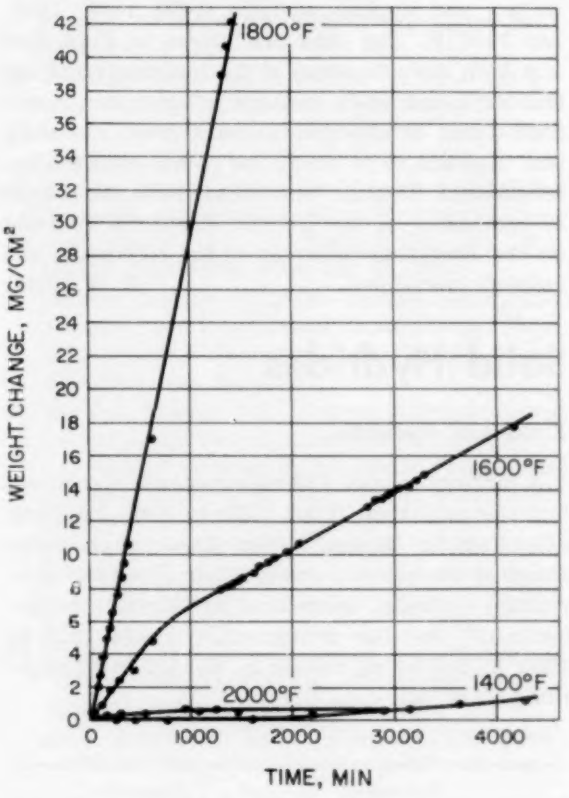

Fig. II-7 Oxidation[44] of Nb_2Be_{17} in wet air at 1400, 1600, 1800, and 2000°F.

that $ThBe_{13}$ and UBe_{13} are isomorphous. A series of alloys having 92.8 at.% beryllium was used, and a fair constancy in hardness and a linear change in lattice parameter were shown in varying from pure $ThBe_{13}$ to pure UBe_{13}. They report that the microstructures of these specimens were all the same.

Atomics International[43] measured the oxidation rates of $ZrBe_{13}$ and $NbBe_{12}$ in oxygen between 700 and 1500°C. Between 900 and 1500°C a BeO layer was found to have been produced on $ZrBe_{13}$, and the thickening of the BeO with time was parabolic. From 600 to 700°C $ZrBe_{13}$ was found to oxidize at an accelerating rate accompanied by disintegration of the metal phase. $NbBe_{12}$ did not show the disintegration oxidation, but it showed other complexities. They postulate a Be^{2+} vacancy-transport mechanism, with vacancies forming at the oxide-oxygen interface.

In oxidation studies of $ZrBe_{13}$, Zr_2Be_{17}, $NbBe_{12}$, and Nb_2Be_{17}, Denver Research Institute[44] has measured oxidation rates in wet air of

$ZrBe_{13}$ and Nb_2Be_{17} at 1200, 1400, 1600, 1800, and 2000°F. The data are shown in Figs. II-6 and II-7. Investigators at the Institute point out that ZrO_2 and Nb_2O_5 undergo polymorphic transformations at elevated temperatures, a concept that appears to be borne out by the Atomics International findings described above. Research is continuing at the Denver Research Institute on the oxidation behavior of the zirconium and niobium beryllides. (R. W. Getz)

Solid Hydrides

Zirconium Hydride

A bibliography of 114 references to zirconium hydride published from 1930 to 1960 has been compiled by Dirian.[45] The dissociation pressures of the various composition ranges of zirconium hydride, measured by Atomics International[46] for the temperature range 1200 to 1500°F, can be expressed by the following relations (T is °K):

Phases	Hydrogen/zirconium atom ratio	Equation
Beta + delta	0.9–1.4	$\log P$ (atm) = 10.10 − 11,630/T
Delta	1.40–1.60	$\log P$ (atm) = 6.50 H/Zr − 2.20 − 8640/T
Delta + epsilon	1.60–1.75	$\log P$ (atm) = 3.10 H/Zr + 3.15 − 8550/T
Epsilon	1.75–1.86	$\log P$ (atm) = 8.36 H/Zr − 6.23 − 8370/T

Nuclear-magnetic-resonance studies were made by Spalthoff[47] on zirconium hydride of the composition $ZrH_{1.40}$. The activation energy for hydrogen exchange was found to be 12.2 kcal/mole over the temperature range −190 to 300°C.

An evaluation of zirconium hydride as a moderator in integral, boiling-water superheat reactors was made by Atomics International,[48] and it was concluded that there appears to be no economic incentive for using zirconium hydride as a substitute for water as the moderator in this type of reactor.

Lithium Hydride

Extensive measurements of the effects of radiation on various compositions of lithium hydride containing combined tritium have been reported by Los Alamos.[49] Isothermal expansions of samples exposed to a flux of tritium beta radiation equal to 16.8 mr/hr have been observed at 12 temperatures between −196 and 400°C for up to seven years. The color-center model, which has been proposed to explain effects of radiation damage to the alkali halides, is shown also to be suitable to explain the radiation-induced optical and electron-spin paramagnetic-resonance absorption observed in the lithium hydrides. Calculations indicate that little dissociation and cavitation occur in samples stored below −7°C, whereas these effects are extensive and lead to disintegration of samples stored above 23°C.

Cerium Hydride

Studies of cerium hydride at the University of Southern California[50] have established that this compound has a face-centered cubic structure, with $a_0 = 5.539 \pm 0.001$ A for the composition $CeH_{2.97}$. The heat of dissociation was found to vary from 6.5 kcal/mole for $CeH_{2.80}$ to 6.8 kcal/mole for $CeH_{2.90}$.

Thorium Hydride

The lattice parameters of thorium hydride compositions have been determined at Atomics International.[51] A face-centered tetragonal phase was found with a_0 ranging from 5.7154 ± 0.0008 A at the composition $ThH_{1.73}$ to 5.7348 ± 0.0003 at $ThH_{1.93}$. Similarly, the value of c_0 ranged from 5.0096 ± 0.0010 to 4.9706 ± 0.0004 A. They also found two face-centered cubic phases with a_0 values of 5.080 and 5.489 A, the former cell constant corresponding to thorium metal and the latter to a hydride phase. The existence of the hydride Th_4H_{15} was confirmed.

Alloy Hydrides

The hydriding characteristics of 250 intermetallic phases were examined at Denver Research Institute.[52] About half were found to react exothermically and reversibly with hydrogen at elevated temperatures. Eighteen form ternary hydrides of relatively high hydrogen content. Six of these contain more hydrogen than the individual components could absorb alone: $ThCoH_{4.2}$, Hf_2CoH_5, $ZrCr_2H_{3.5}$, Hf_2MnH_5, $ZrNiH_3$, and ZrV_2H_4. However, none have hy-

driding characteristics as good as those of pure zirconium and yttrium.

The nickel-zirconium-hydrogen system was also studied at Atomics International.[53] Of the seven intermetallic compounds in the nickel-zirconium system, only ZrNi and possibly Zr_7Ni_{10} form new hydrides, $ZrNiH_3$ and $Zr_7Ni_{10}H_{17}$, respectively. The others either do not absorb significant amounts of hydrogen or decompose on hydriding.

Alloys of titanium and zirconium were hydrided at room temperature by McQuillan and Pessall,[54] who found both dihydrides to be tetragonal under these conditions. An extensive range of solid solution of TiH_2 in ZrH_2 was found, but not vice versa. (H. H. Krause)

References

1. General Atomic Div., General Dynamics Corp., 40-MW(E) Prototype High-Temperature Gas-Cooled Reactor Research and Development Program, USAEC Report GA-3132, Mar. 31, 1962.
2. P. A. Thrower and W. N. Reynolds, Microstructural Changes in Neutron-Irradiated Graphite, British Report AERE-R-4007, March 1962.
3. W. N. Reynolds and R. A. Thrower, Irradiation Damage in Graphite, British Report AERE-R-3979, March 1962.
4. H. W. Davidson, The Properties of G.E.C. Impermeable Carbon, *Nucl. Eng.*, 7(71): 159–161 (April 1962).
5. Shigenhiko Yamada and Hiroshi Sato, Some Physical Properties of Glassy Carbon, *Nature*, 193: 261–262 (Jan. 20, 1962).
6. B. E. Popov et al., Reduction of Grain Size in Beryllium and Chromium by Exposure to Ultrasound During Arc Melting (in Russian), *Fiz. Metal. i Metalloved.*, 10(6): 853–856 (December 1960).
7. B. E. Popov, The Influence of Ultrasonics on the Structure of Films and Beryllium and Zinc Obtained by Evaporation in a Vacuum, *Phys. Metals Metallog.*, 9(3): 41–43 (1960).
8. V. M. Amonenko et al., Beryllium Foil (in Russian), *Zavodsk. Lab.*, 5: 625–626 (1960).
9. S. H. Gelles, Beryllium Research and Development Program, Report NMI-9517, Nuclear Metals, Inc., Apr. 16, 1962.
10. G. E. Spangler, M. Herman, E. J. Arndt, D. B. Hoover, V. V. Damiano, and G. S. Tint, Preparation and Evaluation of High Purity Beryllium, Quarterly Progress Report, Oct. 2, 1961 to Apr. 2, 1962, Report NP-9819, Franklin Institute.
11. Nuclear Metals, Inc., Fundamental and Applied Research and Development in Metallurgy, Progress Report to United States Atomic Energy Commission for February 1962, USAEC Report NMI-2104, May 4, 1962.
12. P. I. Treharne and A. Moore, Tensile Deformation of Beryllium Single Crystals in Various Orientations Between 25°C and 600°C, *J. Less-Common Metals*, 4: 275–285 (June 1962).
13. Nuclear Metals, Inc., Fundamental and Applied Research and Development in Metallurgy, Progress Report, Oct. 1 Through Oct. 31, 1961, USAEC Report NMI-2100, Jan. 15, 1962.
14. Nuclear Metals, Inc., Fundamental and Applied Research and Development in Metallurgy, Progress Report, November 1961, USAEC Report NMI-2101, Jan. 25, 1962.
15. Nuclear Metals, Inc., Fundamental and Applied Research and Development in Metallurgy, Progress Report to United States Atomic Energy Commission for December 1961, USAEC Report NMI-2102, Feb. 26, 1962.
16. E. M. Grala, R. G. O'Rourke, G. L. Marsh, and L. S. Busch, Rolling Improved Beryllium Sheet, Report TR-269-234, Brush Beryllium Co., Oct. 5, 1961–Jan. 4, 1962.
17. Preprints of papers presented at the Institute of Metals Conference on the Metallurgy of Beryllium, London, Oct. 16–18, 1961.
    a. E. Weismantel and B. Kopelman, The Preparation, Properties, and Formability of Beryllium Sheet.
    b. W. W. Beaver, Wrought Fabrication of Beryllium Metal.
    c. D. B. Wright and G. C. Ellis, An Evaluation of Beryllium-Tube Fabrication Methods.
18. C. J. Giemza, Structural Response of Beryllium Sheet Produced by Three Fabrication Methods, Report ASD-TR-61-87, Martin Co., June 1961.
19. Oak Ridge National Laboratory, Gas-Cooled Reactor Program Quarterly Progress Report for Period Ending December 31, 1961, USAEC Report ORNL-3254, Apr. 6, 1962.
20. V. Nerses and J. Siergiej, Ribbed Tubing Extrusion Program, Final Report, Phase I, USAEC Report NMI-4950, Nuclear Metals, Inc., May 17, 1961.
21. L. M. Christensen, Program for the Development of Extruded Beryllium Shapes, Interim Engineering Report No. 13, June 1–Aug. 31, 1961, Report NOR-61-236, Northrop Corp.
22. S. J. Paprocki, E. S. Hodge, and J. S. Perrin, Preliminary Studies of Bonding of Beryllium-Clad UO_2 Fuel Elements, USAEC Report BMI-1545, Battelle Memorial Institute, Sept. 20, 1961.
23. E. M. Whitson, Vacuum Brazing of Stainless Steel to Beryllium, *Metal Progr.*, 82(1): 93–95 (July 1962).
24. W. Feduska and W. L. Horigan, Diffusion Bonding High Temperature Alloys with Beryllium, *Welding J. (N. Y.)*, 41(1): 28S–35S (January 1962).
25. R. W. Meyerhoff and J. F. Smith, Anisotropic Thermal Expansion of Single Crystals of Thal-

lium, Yttrium, Beryllium, and Zinc at Low Temperatures, *J. Appl. Phys.*, 33: 219–224 (January 1962).

26. P. M. Arzhanyi et al., Diffusion of Beryllium and Aluminum in Columbium (in Russian), *Izv. Akad. Nauk SSSR, Otd. Tekhn. Nauk, Met. i Toplivo*, (2): 119–121 (March–April 1961).
27. V. M. Amonenko et al., Texture and Properties of Vapor-Deposited Beryllium, *Fiz. Tverd. Tela*, 3(3): 760–802 (in Russian); also *Soviet Phys.-Solid State (English Transl.)*, 3(3): 580–584 (March 1961).
28. V. M. Amonenko et al., The High Temperature Polymorphism of Beryllium (in Russian), *Fiz. Metal. i Metalloved.*, 12(6): 865–872 (1961).
29. R. I. Garber et al., Tensile Tests on Beryllium Single Crystals in the 20–500°C Temperature Range (in Russian), *Fiz. Metal. i Metalloved.*, 12(3): 437–446 (1961).
30. E. W. Schultz, Stress and Strain Characteristics of Hot-Pressed Beryllium Loaded Biaxially at 1000°F and 1400°F Temperatures, Report LMSD-800937 (AD-270402), Lockheed Aircraft Corp., Oct. 2, 1961.
31. McDonnell Aircraft Corp., Strength Comparison of Coated Beryllium Specimens, Report 045-205-02 (AD-272735), June 21, 1961.
32. G. J. Dienes and A. C. Damask, An Estimate of the Effect of Radiation on the Thermal Conductivity of Beryllium, *J. Nucl. Mater.*, 3(1): 16–20 (1961).
33. Oak Ridge National Laboratory, Reactor Chemistry Division Annual Progress Report for Period Ending January 31, 1962, USAEC Report ORNL-3262, May 11, 1962.
34. J. R. Weeks (Ed.), Proceedings of the Eleventh Annual AEC Corrosion Symposium, May 23–25, 1962, USAEC Report BNL-728, Brookhaven National Laboratory.
35. A. Draycott, F. D. Nicholson, G. H. Price, and W. I. Stuart, Study of the Variables Affecting the Corrosion of Beryllium in Carbon Dioxide, Australian Report AAEC/E-83, December 1961.
36. Oak Ridge National Laboratory, June 12, 1962. (Unpublished)
37. W. Hodge, Beryllium for Structural Applications. A Review of the Unclassified Literature, Report DMIC-168, Battelle Memorial Institute, Defense Metals Information Center, May 18, 1962.
38. J. Cholak, R. A. Kehoe, L. H. Miller, F. Princi, and L. J. Schafer, Toxicity of Beryllium, Report ASD-TR-62-7-665, University of Cincinnati, April 1962.
39. J. M. Tobin, Some Effects of Neutron Irradiation on Selected Beryllia Materials, USAEC Report GA-2648, General Atomic Div., General Dynamics Corp., Apr. 30, 1962.
40. General Electric Co., Flight Propulsion Laboratory Dept., High-Temperature Materials Program Progress Report No. 12, Part A, USAEC Report GEMP-12A, June 15, 1962.
41. General Electric Co., Flight Propulsion Laboratory Dept., High-Temperature Materials Program Progress Report No. 11, Part A, USAEC Report GEMP-11A, May 15, 1962.
42. T. A. Badayeva and R. I. Kuznetsova, Structures of Alloys of Certain Systems with Thorium and Uranium (in Russian), Structure of $ThBe_{13}$ Alloys, pp. 358–368, Academy of Sciences of the USSR, Institute of Metallurgy, Gosatomizdat, Moscow, 1961.
43. G. Ervin, Jr., and M. M. Nakata, Oxidation Kinetics of $ZrBe_{13}$ and $NbBe_{12}$, USAEC Report NAA-SR-6493, Atomics International, Mar. 15, 1962.
44. F. C. Perkins, Intermediate-Temperature Oxidation of Beryllides, USAEC Report TID-16030, Mar. 8, 1962.
45. J. Dirian, Zirconium Hydride, French Report CEA-BIB-27, January 1962.
46. D. F. Atkins, Dissociation Pressures of Hydrided Zirconium-Uranium Alloys, USAEC Report NAA-SR-4245(Del.), Atomics International, Feb. 15, 1960.
47. W. Spalthoff, Nuclear Magnetic Resonance Studies on Metal Hydrides, *Z. Physik. Chem.*, 29: 258–276 (August 1961).
48. J. D. Gylfe, H. Hood, J. Greenleaf, K. Balkwill, L. Prem, and L. Goldfisher, Evaluation of Zirconium Hydride as Moderator in Integral, Boiling Water-Superheat Reactors, USAEC Report NAA-SR-5943, Atomics International, Mar. 1, 1962.
49. F. E. Pretzel, D. T. Vier, E. G. Szklarz, and W. B. Lewis, Radiation Effects on Lithium Hydride, USAEC Report LA-2463, Los Alamos Scientific Laboratory, Sept. 15, 1960.
50. J. C. Warf and K. Hardcastle, Studies of Rare-Earth Hydrogen Systems, Report NP-11180, University of Southern California, August 1961.
51. W. L. Korst, Observations on the Thorium-Hydrogen and Cobalt-Thorium-Hydrogen Systems, USAEC Report NAA-SR-6881, Atomics International, May 31, 1962.
52. R. L. Beck, Investigation of Hydriding Characteristics of Intermetallic Compounds, USAEC Report LAR-55, Denver Research Institute, Nov. 15, 1961.
53. I. R. Tannenbaum, W. L. Korst, J. S. Mohl, and G. G. Libowitz, Study of the Nickel-Zirconium-Hydrogen System, USAEC Report NAA-SR-7132, Atomics International, May 31, 1962.
54. A. D. McQuillan and N. Pessall, Lattice Parameter Changes in the Pseudo-Binary System of Titanium and Zirconium Dihydrides, *Acta Cryst.*, 14: 1287–1288 (December 1961).

Section

III

Reactor Materials

Nuclear Poisons

Metallic Poison Materials

In work at Los Alamos[1] on the vaporization behavior of hafnium diboride over the temperature range of 2175 to 2520°K, effusion-cell data were obtained from tests in both high- and ultrahigh-vacuum systems. Hafnium diboride was found to vaporize congruently at a nonstoichiometric composition of $HfB_{1.955 \pm 0.010}$. A value of 142 ± 7 kcal/mole was deduced for the heat of vaporization of hafnium metal.

The determination of hafnium-vanadium and hafnium-iridium phase diagrams is the objective of work at the Bureau of Mines.[2] Heat-treatment and metallography were used to establish a new eutectic composition (at 20 wt.% vanadium), the insolubility of HfV_2 in either hafnium or vanadium, the vanadium solidus, and the alpha, alpha + beta, and beta hafnium fields.

Corrosion studies were made at Rensselaer[3] on gadolinium, dysprosium, holmium, erbium, and yttrium in several moderately corrosive media. The studies indicated that these metals are very reactive to most acids at room temperature at concentrations below 1*N*. The metals, however, were fairly resistant to strong and dilute alkali solutions, hydrofluoric acid, and dilute phosphoric acid. The metals reacted slowly with water and moist air to form dark oxide coatings. (W. E. Murr)

Dispersion Control and Shielding Materials

A summary report on a B_4C-nickel dispersion that has been investigated as a control-rod material has been issued by General Electric.[4] The dispersion is produced in a unique manner to prevent reaction between the nickel and B_4C. Since nickel is electroplated on a base plate, B_4C particles that are in the plating bath are entrapped. One-sixteenth-in.-thick dispersions containing up to 30 vol.% B_4C have been prepared. A study of the chemical compatibility indicated extensive reaction at temperatures of 600°C or higher in short periods of time (25 hr or less), but no reaction phase was detected by X-ray studies after an 800-hr exposure at 375°C.

Both clad and unclad dispersions were tested for corrosion resistance in a steam-water mixture at 546°F and 1000 psi. After 300 hr, no significant weight change had occurred. No visual change was observed after 1000 hr in flowing water at 546°F.

Radiation stability was tested by irradiating 12 specimens in the General Electric Testing Reactor to burnups of 92 to 97% of the B^{10}. The specimens contained 26.7 vol.% B_4C in nickel, and were irradiated at a calculated average temperature of 170°C and a maximum temperature of 210°C. The helium release averaged 12% of the total helium produced. Changes in thickness ranged from 7.4 to 19.4%. During postirradiation anneals an additional 14% of the helium was released at 400°C, and there was a 7.4% change in thickness. Metallographic examination indicated that the only damage was the formation of blisters on three of the 12 samples. No change in microstructure was observed. Hardness increased during irradiation from about 340 to 461 Vickers hardness number.

At Bettis[5] the evolution of helium from slightly irradiated boron carbide and boron carbide–silicon carbide plates was measured as a function of temperature. Diffusion coefficients were calculated for the 500 to 1000°C temperature range. The data for boron carbide

were found to be represented by the equation $D = 1.4 \times 10^{-8} \exp(-29{,}000/RT)$. The activation energy was determined to be 29.0 ± 3.0 kcal/mole. The rate and amount of helium released from B_4C-SiC compacts was less than that for boron carbide alone.

Europium oxide dispersions for use as high-temperature control materials are also being investigated at General Electric.[6,7] Dispersions of 50 wt.% Eu_2O_3 in tungsten, tantalum, and niobium showed reaction after 2 hr at 1370°C in hydrogen. After 100 hr in hydrogen at 1650°C, dispersions of 50 wt.% Eu_2O_3 in rhenium and molybdenum had a red oxide coat and a zone near the surface where Eu_2O_3 was depleted. No change in structure was observed in the center of the specimens. Dispersions of Eu_2O_3 in the noble metals platinum, palladium, rhodium, and iridium are also being investigated. The Rh-Eu_2O_3 and Ir-Eu_2O_3 structures are not considered to be usable in air at 1200°C. In hydrogen, at 1200°C, Pd-Eu_2O_3 compacts had a liquid phase. Suboxides are also being studied. After heating Eu_2O_3 for 70 hr in hydrogen at 1430°C, a phase believed to have an oxygen-to-europium ratio of <1.13 was produced. EuO was prepared by reacting Eu_2O_3 and europium metal at 1275 to 1350°C in hydrogen or argon.

The most comprehensive review of neutron-absorber materials to date[8] has been published recently by the Naval Reactors Branch of the USAEC. The most extensive research on control materials in this country has been supported by Naval Reactor programs. This book, edited by W. K. Anderson and J. S. Theilacker, includes sections on applications, control material theory and calculations, effectiveness of control materials, nuclear properties, liquid-phase absorbers, hafnium, boron materials, silver and silver-base alloys, and the lanthanons. Fabrication, properties, and irradiation results of many alloys, ceramics, and dispersions are reported. (G. W. Cunningham)

References

1. M. C. Krupka, High Temperature Vaporization Behavior and Thermodynamic Properties of Hafnium Diboride, USAEC Report LA-2611, Los Alamos Scientific Laboratory, February 1962.
2. Bureau of Mines, Albany Metallurgy Research Center, Metallurgical Progress Report Number 14 for the Period January 1, 1962, to March 31, 1962, USAEC Report USBM-U-921.
3. N. D. Greene, the Electrochemical and Corrosion Characteristics of Rare Earth and Yttrium Metals, Annual Progress Report and Renewal Proposal, USAEC Report TID-14467, Rensselaer Polytechnic Institute, November 1961.
4. H. E. Williamson, D. L. Zimmerman, and K. C. Antony, Investigation of B_4N-Ni Electro Dispersions for Control Rod Applications, USAEC Report GEAP-3831, General Electric Co., Atomic Power Equipment Dept., Nov. 3, 1961.
5. J. C. Clayton, W. A. Bostrom, and F. C. Schrag, The Release of Helium from Slightly Irradiated Boron Carbide and Boron Carbide–Silicon Carbide Plates, USAEC Report WAPD-255, Westinghouse Electric Corp., Bettis Atomic Power Laboratory, January 1962.
6. General Electric Co., Flight Propulsion Laboratory Dept., High-Temperature Materials Program Progress Report No. 9, Part A, May 1961–December 1961, USAEC Report GEMP-9A, Mar. 30, 1962.
7. General Electric Co., Flight Propulsion Laboratory Dept., High-Temperature Materials Program Progress Report No. 11, Part A, USAEC Report GEMP-11A, May 15, 1962.
8. W. K. Anderson and J. S. Theilacker (Eds.), *Neutron Absorber Materials for Reactor Control*, Naval Reactors Branch, Division of Reactor Development, USAEC, 1962, U. S. Government Printing Office, $3.00.

Section

IV

Reactor Materials

Cladding and Structural Materials

Corrosion

Zirconium Corrosion

Oxidation. Several studies on oxidation of zirconium have been reported recently. Oak Ridge[1] has studied zirconium oxidation in pure oxygen at 1 atm partial pressure and 250°C with (1) reactor radiations including fission-fragment recoils, (2) reactor radiation in the absence of recoils, and (3) no radiation. Maximum thermal-neutron flux was 8.5×10^{11} neutrons/(cm^2)(sec), and the estimated average recoil intensity was 6×10^8 particles/(cm^2)(sec). It was concluded that the oxide film on surfaces exposed to fission fragments was thicker than that on surfaces exposed to reactor radiation alone. The corrosion was at least a factor of 10 less than that expected in a solution of uranyl sulfate producing an equivalent recoil intensity.

Norwegian workers have reported[2] on the oxidation of zirconium–0 to 18 at.% oxygen alloys at 800°C. Initial rates were found to be cubic for all alloys. A second and higher rate (breakaway) was also observed, which appeared at shorter times with increasing oxygen content. This rate increased with increasing oxygen content to 12 to 15 at.%, after which it did not increase. Two corrosion mechanisms were suggested by the authors, based on (1) simultaneous oxide formation and dissolution in the metal and (2) the zirconium-oxygen phase diagram. The former assumes that breakaway occurs when the oxygen content of the metal reaches a saturation value. This may occur at 12 to 15 at.% oxygen rather than at the solubility limit of 29 at.% because a structural change takes place which may affect the rate of oxygen dissolution. The second mechanism is related to the phase changes from homogeneous beta alloys at 0 to 4 at.% oxygen to homogeneous alpha alloys at greater than 12 at.% oxygen. The entire alpha phase at 12 at.% oxygen may give rise to an apparent "saturation" limit.

General Nuclear Engineering Corporation[3] has reported on continuing studies on the oxidation and diffusion of oxygen in unalloyed zirconium and in zirconium–0.5 wt.% copper–0.5 wt.% molybdenum alloy exposed to CO_2. Results obtained have indicated that hardening by oxygen diffusion has not occurred to any "important" depth (less than 0.1 mm) in the alloy or unalloyed zirconium after 2000-hr exposure to wet and dry CO_2 at 1150°F, in unalloyed zirconium exposed 6000 hr to dry CO_2 at 1050°F, or in the alloy exposed 15,000 hr to dry CO_2 at 1050°F.

Aqueous Corrosion. Knolls[4] has issued a detailed report on the corrosion of Zircaloy at crevices in *p*H 10.5 water under heat transfer of 500,000 Btu/(hr)(sq ft). They conclude that either Zircaloy-2 or Zircaloy-4 will corrode in crevices in closed vertical channels under boiling heat-transfer conditions at 587°F, and the attack is more drastic in lithiated than in ammoniated water. Zircaloy-4 appeared less resistant than Zircaloy-2. Crud (principally Fe_3O_4) did not increase the corrosion. Work at Battelle[5] has shown no corrosion of Zircaloy-4 in crevices under nonheat-transfer conditions.

Chalk River[6] has reported severe H_2 pickup by Zircaloy-2 in 300°C *p*H 10 (LiOH) water containing 10 ppm fluoride ion, but no accelerated attack when the fluoride-ion concentration was kept below 0.01 ppm. However, Battelle[5] has reported accelerated attack of Zircaloy-4 in 360°C *p*H 10 water containing about 190 ppm fluoride (0.01*M*), but no accelerated attack at about 19 ppm fluoride (0.001*M*). The Battelle

study has also shown that large quantities of Fe_3O_4 suspended in the water apparently adsorb the fluoride ion and thereby reduce attack of the Zircaloy-4.

Hydriding. Atomics International[7] has measured hydrogen permeation of oxide films (produced in oxygen) on crystal-bar zirconium and found the rates to be (1) inversely proportional to oxide film thickness (100 to 2500 A), (2) exponentially related to temperature (200 to 700°C), and (3) proportional to the hydrogen pressure (1 to 860 mm Hg). They believe that the rate of hydrogen permeation is controlled by interstitial diffusion of hydrogen molecules through the oxide film and that anion and cation vacancies must be present to allow passage from interstice to interstice. Supporting this view, work performed at Hanford[8] with Zircaloy-2 has suggested that hydrogen diffusion is related to oxygen vacancies in the oxide film. The Hanford workers found that hydriding occurred on preoxidized specimens heated in oxygen-free hydrogen atmospheres. Hydrogen pickup virtually ceased when an oxidant such as oxygen or water vapor was introduced. Oxygen vacancies were believed to have increased in number during the former operation and to have been filled during the latter.

Experiments on the hydriding of stressed Zircaloy-2 conducted at Savannah River[9] have shown that (1) hydride platelets precipitate perpendicular to the direction of tensile stresses and parallel to compressive stresses; (2) prior deformation by hammering, rolling, or extrusion causes hydride platelet precipitation to occur in the direction that the metal flowed during deformation; and (3) the Zircaloy-2 texture of preferred crystallographic orientation affects hydriding behavior.

Chalk River is studying zirconium alloys to determine whether the transfer of negative hydrogen ions through the oxide film is responsible for hydriding. A recent experiment,[10] involving the oxidation of oxide films after dissolving away the Zircaloy-2, indicated about 2 atoms per 100 were added to the oxide. It was concluded that no negative hydrogen ions were present in anion positions, otherwise the substoichiometry of the oxide would have been greater than that observed.

Hydrogen pickup in bare and clad Zircaloy-2 specimens exposed 76 days in an organic reactor loop has been investigated.[6] Water content of the organic varied between 113 and 157 ppm, the hydrogen partial pressure varied between 0.5 and 8.5 psia, and the temperature varied between 550 and 690°F. Hydrogen-pickup results exhibited considerable scatter and varied as indicated below:

Cladding material	H_2 pickup, ppm (range for several specimens)
1/32-in. stainless steel	58–278
1/16-in. stainless steel	107–207
1/32-in. aluminum	<1–166
1/16-in. aluminum	<1–47
Unclad Zircaloy-2	<1–1

Out-of-pile tests revealed the following hydrogen pickups: 371 ppm for 1/32-in. stainless-steel cladding, <1 ppm for 1/32-in. aluminum cladding, and 97 ppm for unclad Zircaloy-2. The anomalous behavior of Zircaloy-2 in pile and out of pile has not yet been explained.

(W. E. Berry)

Aluminum Corrosion

Hanford[11] is conducting loop tests in 600°F high-purity deionized water on two aluminum alloys under a heat flux of 228,000 Btu/(hr)(sq ft). After a 2500-hr exposure, the high-purity alloy A-288 (1 wt.% nickel, 0.5 wt.% iron, 0.1 wt.% titanium, 0.002 wt.% silicon maximum) continues to show better film retention (and presumably lower penetration rates) than X-8001 alloy (1 wt.% nickel, 0.5 wt.% iron, 0.17 wt.% silicon).

The Swiss[12] have studied the formation and corrosion resistance of boehmite films (gamma AlOOH or $Al_2O_3 \cdot 1H_2O$) formed by reaction between aluminum and water or steam at 98 to 155°C. It was concluded that a boiling solution containing 0.01*N* to 0.1*N* triethanolamine produced boehmite films with the best overall stability with respect to subsequent exposure to tap water and to light aggressive media, including foodstuffs. (W. E. Berry)

Stainless-Steel Corrosion

The corrosion of stainless steels in superheated steam has recently been reported by Argonne[8] and Hanford.[8] The Argonne results,

obtained in 600-psi steam at 650°C, indicated that types 309, 310, and 406 stainless steels had relatively low corrosion rates and adherent corrosion films, whereas the oxide films on types 304, 304L, 316, and 347 were subject to varying degrees of spalling. Types 304, 347, and 406 showed good resistance when exposed to 540°C steam. The Hanford results, obtained in 1000- and 3000-psi steam at 550°C, indicated average penetrations of 0.02 mil for type 446 stainless steel and 0.25 mil for types 304L, 406, and 430 after one-month exposure.

Hanford has reported on the stress-corrosion cracking behavior of Greek Ascoloy (13 wt.% chromium, 2 wt.% nickel, 3 wt.% tungsten) in flowing 300°C water at *p*H 10 adjusted[8] with LiOH. Specimens heat-treated to Rockwell C hardness number (R_C) 45 cracked within eight weeks of exposure when stressed to 140,000 psi, but no cracking occurred at 70,000 psi. Specimens heat-treated to 32 R_C did not crack at either of the aforementioned stress levels.

The effect of chloride ion in uranyl sulfate solutions on the stress-corrosion cracking of type 347 stainless steel is being investigated by Oak Ridge.[13] No cracking was detected below 10 ppm chloride, and cracking frequency appeared to be independent of chloride content in the range of 25 to 500 ppm. Removal of dissolved oxygen reduced but did not eliminate cracking. The addition of about 100 ppm sodium dichromate, or increasing the uranyl ion concentration beyond 0.4*M*, prevented cracking. Additions of antimony, arsenic, platinum, or zinc salts had no effect on cracking, whereas mercuric chloride additions or increasing the uranyl-ion concentration up to 0.4*M* increased cracking sensitivity.

Oak Ridge[13] reported no stress-corrosion cracking of stressed type 347 stainless steel and low corrosion rates for type 347, type 309SCb, and Croloy 16-1 after 3.5 years of exposure in the steam generators of HRE-2. The outstanding performance of these alloys was attributed to excellent boiler-water treatment which kept chloride and dissolved oxygen contents low.

Savannah River[14] has just issued a pertinent literature search on the stress-corrosion cracking of stainless steels. Literature was reviewed for the period 1955 to 1961, and abstracts are presented for each article.

(W. E. Berry)

Corrosion of Iron- and Nickel-Base Alloys

Aqueous. Inconel is reported to have excellent resistance to the primary coolant circuit of pressurized-water reactors. This was demonstrated in a Battelle[15] study simulating coolant conditions with (1) lithiated water (*p*H 10) at 300 and 550°F and (2) ammoniated water (*p*H 9.5) at 550°F. There was no acceleration of attack on Inconel as a result of dissimilar-metal couples, heat-treatment, cold reduction, tensile stresses, or nominal variations in alloy composition. Galvanic couples were made between the Inconel and iron-, cobalt-, nickel-, and zirconium-base alloys, respectively.

A comparison of low-carbon steel, Croloy 16-1, Inconel, and AISI-304 stainless steel for service in nuclear steam generators was conducted by the Martin Company.[16] The secondary-water environments were made severe to accelerate any damaging effects. A stainless-steel superheater showed chloride stress corrosion. Steel heat exchangers were satisfactory after 7.5 months of exposure when removed from test. Inconel and Croloy 16-1 also were satisfactory. There was some pitting on these metals, with the least amount on the Inconel. The heavy boiler scale, found on the Inconel tubes, flaked off after reaching a critical thickness. Corrosion underneath the scale was negligible. Inconel was recommended as the most resistant of the materials tested.

Chalk River,[6] in a study of crud formation, found that mild-steel turnings lose weight in ammoniated but not in lithiated water flowing at 1.2 m/sec. The hydrogen trapped is equivalent to 11 and 40 mg iron/dm^2 in ammoniated and lithiated water, respectively. For both types of water, the crud concentration, using a sintered stainless-steel filter, was 0.01 ppm. In the presence of hydrazine, the crud level remained below 0.01 ppm.

Candidate brazing alloys for the austenitic stainless-steel fuel elements in the SM-1 reactor (formerly APPR-1) were studied by Oak Ridge.[17] T-joints brazed with selected alloys were exposed to quiescent, degassed, and deionized autoclaved water at 565°F and 1200 psi. Five alloys showed satisfactory resistance to water containing (1) 1 cm^3 of oxygen per liter and (2) 1 cm^3 of oxygen plus 50 cm^3 of hydrogen per liter after 12 and 16 months, respectively. The designations and compositions (wt.%) of the alloys are

GE No. 81	66 Ni, 19 Cr, 10 Si, 4 Fe, 1 Mn
GE No. 75	75 Ni, 25 Fe
Coast Metals N.P.	50 Ni, 30 Fe, 12 Si, 4 P, 4 Mo
Low-melting Nicrobraz	80 Ni, 5 Cr, 5 Fe, 5 Si, 5 B*
Palladium-nickel-silicon	60 Pd, 37 Ni, 3 Si

Coast Metals N.P. was selected, since it was most amenable to the brazing method involved in the application. There is some localized corrosion of the matrix of the brazing alloy, but the authors do not consider it serious.

Alpha radiation at 2 watts/liter from added 20 g/liter of Am^{241} was used to cause radiolysis of water in chloride solutions at Oak Ridge.[18] One solution was boiling 6*M* HCl; the other was 10*M* LiCl + 0.5*M* HCl at 45 to 110°C. The H_2O_2 tended to increase the rate of attack for Hastelloys B and C and greatly decreased the attack on titanium. Tantalum, Zircaloy-2, and glass also were resistant. The ozone in the vapor phase inhibited the attack by the HCl on titanium.

Gaseous Corrosion. Work at General Electric[19] has led to alloys for nuclear fuel elements in oxidizing atmosphere above 1200°C. Iron-base alloys with (1) 24 wt.% chromium–4 wt.% aluminum–0.7 wt.% yttrium and (2) 25 wt.% chromium–4 wt.% aluminum–1 wt.% thorium show oxidation resistance after 200 hr at 1300°C. Alloy 2, a newer development, shows lower weight gain than alloy 1 and has a uniform and tenacious oxide protective film. Incipient melting of the second phase occurs at 1350°C (YFe_9) for alloy 1 and at 1375°C for alloy 2. This improvement, due to substitution of thorium for yttrium, is to be evaluated in longer time tests.

An electron probe was used by General Electric[20] to follow oxides that formed both internally and on the surface. The surface oxide on the yttrium alloy showed Al_2O_3 with particles of Y_2O_3. The latter are bright blue during exposure to the electron beam. At grain boundaries, Y_2O_3 is found and the amount of chromium is negligible. The YFe_9 phase is depleted after 600 hr at 1300°C.

At General Electric[21] chromium-base alloys with yttrium, iron-aluminum-yttrium, rhenium-aluminum-yttrium, and titanium-zirconium-carbon-yttrium were tested in high-temperature air. A chromium alloy with 15 wt.% rhenium–3 wt.% aluminum–0.75 wt.% yttrium showed a weight loss of 0.08 mg/(cm²)(hr) at 2500°F. This alloy type is competitive with or superior to any alloy capable of extended service in air at 2500°F.

Aerojet-General[8] has investigated long-term air corrosion of several nickel-base alloys for possible use in the ML-1 reactor. The depth of maximum oxide penetration for Hastelloy X and Inconel sheet exposed to 1750°F, 300-psi air is as follows:

Hr	Hastelloy X	Inconel
2,500	0.008	0.0025
5,000	0.0012	0.0024
10,000	0.0024	0.0060

Hastelloy X showed internal oxidation. Inconel, Nichrome V, and Inconel 702 showed intergranular oxidation.

Hastelloy X, Inconel X, and type 446 stainless steel showed the lowest corrosion rates, of a series of alloys under test in 550°C steam at 1000 and 3000 psi, at Hanford.[8]

(F. W. Fink)

Corrosion of Uncoated Refractory Metals

Norwegian research into low-temperature oxidation of tantalum[22] associated logarithmic and parabolic oxidation rates at temperatures less than 450°C with the formation of low-oxide forms (TaO_y, TaO_z). At temperatures greater than 450°C, initial parabolic rates yield to breakaway weight-gain behavior as nonprotective Ta_2O_5 forms. This behavior is similar to that observed in the oxidation of niobium. Morphological studies of the growth habits of TaO_z and NbO_z oxides[23] revealed that TaO_z grows parallel to the (3 2 0) planes of the parent metal, whereas NbO_z probably grows on the basal planes of the niobium lattice. The lower oxide forms (NbO_x and TaO_y) cannot be distinguished metallographically from the parent metals.

Investigations at Lawrence[24] provided interesting data concerning the reactions between tungsten and oxygen, nitrogen, and NO environments at low pressures (10^{-8} to 10^{-6} atm) and high temperatures (1680 to 2330°C). At constant oxygen pressure it was observed that the reaction rates decrease with increasing temperature. A further observation concerning the decrease in activation energy (assumed to define the formation of WO_3) from 14 to –20 kcal/mole

with decreasing oxygen pressure was attributed to competing processes for oxygen desorption at the reacting surface. In nitrogen environments, reaction rates were too low to permit measurement with the techniques employed. In NO environments, decomposition of NO increased with increasing pressure, and the rate of tungsten loss by reaction at constant NO pressures increased with increasing temperature. Atomic oxygen was evolved from reaction between tungsten and oxygen or NO environments at temperatures greater than 1730°C. An interesting side observation was that tungsten can be completely decarburized in oxygen at pressures of about 10^{-8} atm in 20 to 50 hr at high temperatures.

(E. S. Bartlett)

Corrosion of Coated Refractory Metals

Because of extensive activity in the field of protective coatings for refractory metals, this section will review the most significant recent developments that are not readily available in the open literature. A recent DMIC report[25] reviewed the status of coated vanadium, niobium, molybdenum, tantalum, and tungsten alloys as reported at the Fifth Refractory Composites Working Group Meeting.

Behavior of Coating Materials. Increasing recognition of the severity of rapid low-temperature oxidation failure that is generally characteristic of promising coating materials (primarily refractory-metal disilicide and trialuminide compounds) has stimulated direct examination of the behavior of the compounds themselves, isolated from the important mechanical effects of substrate interaction. The general failure pattern is characterized by rapid disintegration of the coating material at low or intermediate temperatures (generally 540 to 870°C for niobium or molybdenum compounds, 930 to 1260°C for tantalum or tungsten compounds).

Ames Laboratory[26] carried out X-ray analyses of oxides formed from $MoSi_2$. After oxidation at low temperatures, MoO_3 was identified as the major molybdenum-containing constituent in the oxide. However, in line with thermodynamic expectations, Mo_3Si_2 was identified as the principal molybdenum-containing ingredient of oxides resulting from high-temperature oxidation. The implications of this finding relative to the low-temperature-oxidation-failure problem have not been resolved.

Denver Research reported[27] the results of continued oxidation testing of several modifications of the compound $NbAl_3$ at 760°C. Seven modifications endured in excess of 100 hr at this temperature without failure, and tests are being continued for 1000 hr. Preliminary results are shown in Table IV-1. By comparison, unmodified $NbAl_3$ fails in 8 hr at 760°C in dry air.

Table IV-1 OXIDATION OF NIOBIUM-ALUMINUM ALLOYS[27]

Compound (balance niobium), wt.%	Condition after exposure for 1000 hr at 760°C in	
	Wet air	Dry air
3.15 Al–15 V	(Tests incomplete)	
53.25 Al–15 Ti	(Tests incomplete)	
41.5 Al–10 Sn	Test incomplete	Satisfactory
41.5 Al–5 Sn	Failed	Failed
45.25 Al–2.5 Sn	Failed	Satisfactory
45.5 Al–2 Sn	Failed	Failed
45.5 Al–2 Si	Test incomplete	Satisfactory

Investigations of Coated Systems. A program to develop protective coatings for vanadium alloys has been initiated at Armour.[28] A flame-sprayed nickel-rich coating was found to protect a vanadium–60 wt.% niobium–1 wt.% titanium substrate from oxidation for greater than 60 hr at 1090°C. Formation of a glassy oxide was observed. Pack-cementation silicide coatings were even more successful and protected this substrate for 500 hr at 1090°C or 283 hr at 1200°C. The silicide coating over a vanadium–20 wt.% niobium–5 wt.% titanium substrate has been protective for more than 30 hr at 1090 or 1200°C.

The tin-aluminum coating protects tungsten and molybdenum for times in excess[29] of 8 hr at 1370°C. The addition of $TaAl_3$ compound to the coating mix prior to the diffusion treatment improves coating uniformity and general control of coating quality.

In a presentation at the Sixth Refractory Composites Working Group Meeting,[30] Lockheed described anomalously rapid high-temperature low-pressure failures that appear to characterize behavior of disilicide coatings. The observed behavior appears to result from volatilization of SiO (the thermodynamically stable oxidation product under low-pressure condi-

tions). The effects observed for a specific $MoSi_2$ coating under appropriate conditions are described by the following tabulation:

Max. temp., °C, at which substrate is protected for 30 min	Pressure of environment, mm Hg	
	Static oxygen	Dynamic air
1760	760	
1730	5	
1700	4	
1650	2	20
1590	0.8	10
1540	0.25	3
1480	0.07	0.6

Temperatures such as these in dynamic-air environments may be anticipated during reentry conditions. Additional items of particular significance brought out at the Sixth Refractory Composites Working Group Meeting were:

1. The Chromalloy W-3 coating, 1 to 1½ mils thick, will protect molybdenum for about 800 hr at 1370°C or 250 hr at 1480°C.

2. Preliminary results for the TAPCO coating (titanium-chromium-silicon) on tantalum and tantalum–10 wt.% tungsten alloy are very encouraging. (E. S. Bartlett)

Corrosion by Liquid Metals and Fused Salts

The many and varied research reports presented at the NASA-AEC Liquid Metals Corrosion Meeting, December 14–15, 1961, at Brookhaven National Laboratory, have been compiled into a single document.[31] The meeting was devoted primarily to investigations of corrosion by mercury and alkali metals and to allied thermodynamic and physical-properties research. Attention was also given to liquid-metal purity and problems of analysis. A résumé of some of the corrosion results follows; other corrosion results presented at the meeting have been touched on in prior issues of this Review and consequently are not repeated.

Mercury. TAPCO (a division of Thompson Ramo Wooldridge, Inc.) conducted a broad screening test series[31,32] to evaluate containment materials. At 900°F, several materials, including type 410 stainless steel, PH 15-7 molybdenum, 1010 Sicromo, and Haynes 25, exhibited satisfactory corrosion behavior. Generally, high manganese, nickel, and chromium contents lowered corrosion resistance. In two-phase natural-circulation loop tests, Haynes 25 suffered about 2-mil penetration in 1000 hr in a 1000°F zone, and niobium appeared to be inert to attack at 1180°F. Titanium and magnesium were utilized in several systems for corrosion inhibition, but their effect did not appear to be significant.

One of a series of long-time boiling loop experiments at Brookhaven (after 6015 hr at 1000°F boiling at 1150°F superheat, with titanium inhibitor present) exhibited overall attack of less than 1 mil in depth. Mass-transfer type deposits were not found. The construction material in this particular case was carbon steel.

Potassium. Results of a 50-hr boiling potassium loop (fabricated of Haynes 25 and type 321 stainless steel) test at Rocketdyne were essentially as follows: Samples of molybdenum, niobium–1 wt.% zirconium, and wrought niobium located at the boiler exit (1800°F, 100 ft/sec fluid) lost 7, 66, and 77 mg/(cm²)(day), respectively, whereas a similarly located tantalum sample disappeared. Niobium samples placed downstream from a nozzle (Mach 2.5 vapor) were not found. In general, however, the loop construction materials did not show any visible signs of attack. In a shorter, less severe exposure (1700 to 1750°F at much lower velocities), the specimen attack was considerably less, with molybdenum again showing the least change.

Capsule experiments at AiResearch Manufacturing Company of Arizona showed:

1. Good corrosion resistance for niobium–1 wt.% zirconium, molybdenum–½ wt.% titanium, and Hastelloy X in the 1350 to 1800°F range

2. Minor weight changes for bearing materials and ceramics including tungsten and Kennametal 94 at 1000°F and for Al_2O_3 and BeO at 500°F

3. Complete disintegration at 500°F of a variety of potting compounds such as Allen PBX and two Sauereisens

A Hastelloy X loop test was also operated. After 530 hr during which potassium was circulated at a peak temperature of 1800°F, intergranular attack to 4 mils, heavy surface roughening, and cold-zone deposition were observed.

Thermal convection and capsule tests at General Electric Company, Flight Propulsion Laboratory Department, devoted almost entirely to

investigations with Haynes 25, demonstrated its high resistance to surface and intergranular attack by potassium up to 1850°F. However, certain aging embrittlement effects were noted.

Cesium. Investigators at Rocketdyne obtained the following data from 100-hr static capsule exposures: molybdenum, nickel, and tungsten—virtually unaffected at 1290 and 1830°F; type 321 stainless steel—virtually unaffected at 1290°F but noticeably attacked at 1830°F.

Sodium. Experiments at Atomics International to investigate behavior in the sodium-carbon type 304 stainless-steel system showed that equilibrium at the steel surface was reached in less than 1 hr. Equilibrium carbon contents of the steel with carbon-saturated sodium varied from 2.68 wt.% at 1000°F to 4.35 wt.% at 1600°F. Sodium containing 15 to 18 ppm carbon was found to be in equilibrium with uncarburized type 304 stainless steel, at low oxygen content. Diffusion coefficients (4.6×10^{-12} cm^2/sec at 1200°F and 1.21×10^{-9} cm^2/sec at 1600°F) were independent of the carbon content in the steel.

Mass transfer in polythermal sodium flow systems fabricated of selected steels is the subject of comprehensive study at the Vallecitos Atomic Laboratory.[8] Experimental conditions are as follows:

Temperature, °F:	
Maximum	1300
Minimum	600
ΔT, °F	200 to 500
Pressure, psig	100
Velocity, ft/sec	Up to 30
Purity, ppm oxygen	50
Flow, gal/min	1

This research is in its early stages, but data from initial loop systems are available. These systems were constructed of three alloys (type 316 stainless steel, Croloy 2½, and Croloy–5Ti) used singly and in bimetallic combinations. After runs of up to 2800 hr, it was found that:

1. Croloy 2½ decarburized at 1000 and 1200°F in both monometallic and bimetallic systems.
2. Croloy–5Ti exhibited intergranular penetration to 1 mil in 1000 to 1200°F zones but was neutral to carbon transport.
3. Type 316 stainless steel exhibited significant carburization when Croloy 2½ was present in the low-temperature section. In monometallic systems, type 310 stainless steel did not carburize significantly.

In experiments at Brookhaven, nine refluxing niobium–1 wt.% zirconium capsules were operated with 2200°F boiling sodium under a vacuum of approximately 1×10^{-5} torr for periods[33] of 2039 and 3043 hr. There was no evidence of corrosion in any system. In three cases, inserts of niobium, molybdenum, or tantalum were present.

Investigation of lithium corrosion problems continued at Oak Ridge, with a broad conclusion that niobium, tantalum, vanadium, titanium, and zirconium are resistant to dissolution type attack even at temperatures in excess[34] of 1800°F. However, in the case of niobium and particularly in the case of tantalum, small quantities of oxygen impurity (in these metals) can result in rapid penetration by lithium over a wide temperature range. This relation between oxygen content and penetration is not observed in the cases of vanadium, titanium, and zirconium. In all systems a thermodynamically predictable redistribution of oxygen occurs from the test metal to the liquid metal. This fact would indicate that this oxygen migration is not a direct factor contributing to the lithium penetration.

Defense Metals Information Center (DMIC) has issued a summary report[35] that presents in some detail liquid-metal corrosion data accumulated from a broad spectrum of laboratory research. Also included is a review of the state of the art of sliding and bearing properties of metals in sodium and NaK. This reference document may be obtained by directing a request to DMIC. (J. H. Stang)

Radiation Effects in Nonfuel Materials

Defects: Structure and Properties

Metals. New data have been reported in the electron-microscope studies of fission tracks in thin evaporated metal films. Kelsch et al.[36] show tracks in micrographs of very thin (10 to 20 A) aluminum and platinum films. The degree of damage increases with increasing atomic number Z. They conclude that the formation of the track is due to a thermal-spike phenomenon. Bierlein and Mastel[37] have shown tracks

in aluminum films between 300 and 1000 A thick. The tracks they observe are broad on one end and taper to very narrow regions on the other. They also observe discontinuities in track-length distributions and state that thicker films show no tracks. Noggle and Stiegler,[38] in studying tracks in platinum and palladium, conclude that the observed track regions are formed through the thermal processes of melting and vaporization. They develop a model in which free electrons disperse the energy over the volume of the track in a time so short that little heat is conducted away from the tracks. They support this hypothesis in another experiment[39] where they bombard typical platinum films (<25 A thick) with 24-Mev nitrogen ions and fission fragments. The energy loss rate is decreased by about a factor of 10 in the nitrogen-damaged films, and the observed track widths are also smaller by an order of magnitude. The tracks are essentially different and are explained in terms of charge interaction as opposed to the thermal processes that are considered to produce the observed fission tracks.

Sherman[40] has suggested that the studies of fission tracks in thin metal films be used to develop a heavy-particle nuclear detector. His concept for a detector is a thin film held in the superconducting state. As the heavy particle passes through the film, it will produce a region of elevated temperatures; in fact, in some regions this temperature might reach 10^5°K. As the temperature of a region exceeds the transition temperature of the material, that portion of the film will begin to conduct normally. Sherman's calculations show that, for the traversal of a 1000 A thick tin film which is 10 μ wide, the resistance will increase from zero in the superconducting state to 1 ohm from the damage produced by a fission fragment and to 0.2 ohm for an alpha particle. Films of the proper thickness should not be affected permanently, he states. The dead time for this detector, or time required between recordable counts, is of the order of 1 μsec.

The electron microscope revealed no damage produced by fission fragments or heavy recoil atoms bombarding the surface of bulk metal specimens.[41] Alpha bombardment, however, did cause a smoothing of the metal surface. Cold (room temperature) sintering of pressed powder was also observed after irradiation. Sputtering effects were determined to increase with an increase in mass of the high-energy particle; for example, a recoil from ThC sputters about 100 atoms from gold, whereas a fission fragment sputters about 1000 gold atoms.

Nickel crystals bombarded with 3-Mev electrons have been studied by means of Kossel line techniques.[42] The use of an electron-microbeam probe to obtain the Kossel patterns resulted in absolute precision of lattice-parameter measurements of ±0.00003 A. Changes of 0.9×10^{-4} in $\Delta a/a$ were observed after irradiations of 10^{18} electrons/cm^2. Annealing studies showed that interstitials were immobile at 30°C, most probably because they were trapped at impurities or other sinks. The irradiation damage was completely annealed by 400°C.

Fission-fragment (3×10^{13}/cm^2) irradiation of 0.001-in.-thick zone-refined (better than 99.999%) aluminum at 60°C in vacuum produced dislocation loops[43] with an average diameter of 450 A. Some of the loops are in (1 1 1) planes, whereas the larger loops are frequently on (1 1 0) planes. Both vacancy loops and interstitial loops have been observed. Point-defect clusters appearing as spots and dislocation loops were also observed in foils of molybdenum which had been bombarded with 38-Mev He^{2+} and 85-kev H^+ ions.[44] Doses to 1.5×10^{17} He^{2+}/cm^2 and 6×10^{18} H^+/cm^2 were used. The observed clusters were larger in foils where the He^{2+} ions came to rest than in foils through which the ions passed. This is concluded to be evidence that the defects are preserved in the regions of localized concentration of helium gas.

In measuring resistivity as a function of neutron dose, Blewitt et al.[45] found that the resistivity of sodium increased about five times more than the corresponding increase observed in copper. They suggest that a lower value of the displacement threshold in sodium could explain these results. The data indicate that the damaged zone is larger in sodium than in copper, since a low-neutron-dose effect is observed in sodium and explained in terms of overlapping damaged regions. Up to this time, only pyrolytic graphite showed a similar overlap effect. Martin's studies[46] of the influence of impurities on the annealing kinetics of neutron-irradiated copper, which have been reported,[47] are now published.

The ranges of nitrogen, neon, argon, krypton, and xenon ions in beryllium, boron, carbon, and aluminum have been measured[48] to ±10% for

incident-ion energy of 50 to 500 kev. A monoenergetic ion beam from an electrostatic accelerator strikes a thick target of the absorber, and the penetration depth is determined by a momentum analysis of monoenergetic protons elastically scattered from the target and the embedded atoms. An expression relating the penetration depth to the actual path length is derived. Linear range-energy behavior is found for argon, krypton, and xenon ions; for nitrogen and neon ions, dE/dx increases with ion energy. The experimental ranges are 20% shorter than theoretical values based on energy loss by elastic nuclear collisions. By including electronic contributions to the stopping process, good agreement with experiment is achieved.

Order-disorder changes were observed in gold films[49] (~200 to 400 A thick) after doses of 10^{18} neutrons/cm^2 (gamma dose = 2×10^8 r). Colloidal gold was formed from polycrystalline gold. Electron diffraction, electron microscopy, and metallographic examinations were used. Differences were noted between effects observed in specimens irradiated in vacuum and in air or oxygen. Only fcc structures were detected, and no diffraction diagrams corresponding to gold oxides were observed.

Nelson[50] has found that an increase in temperature will broaden the distribution of collisions focused in the ⟨1 1 0⟩ plane of gold. He observed the distribution of gold sputtered from a {1 1 1} surface due to preferential ejection of atoms in the ⟨1 1 0⟩ close-packed directions resulting from the intersection of the ⟨1 1 0⟩ focused collision sequences with the surface. The irradiation used was 43.5-kev argon ions for about 15 min, with a beam current of 50 μa. The temperatures were varied up to just below the melting point (1063°C).

It has been observed that energetic ions, such as those of oxygen and nitrogen, mark with color the region of their impingement on certain metals.[51] This was first observed when, under the same conditions of bombardment, different multicharged ions of the same gas marked their impact areas with different colors. In the energy region of this investigation (approximately 5 to 50 kev), these colors ranged through the visible spectrum from violet to red. The colors seem sensitive to the type and energy of the ion as well as to the metal bombarded. It is possible that the colors are the result of reflections from thin films formed by reactions with the ion at the target. Since the colors indicate that thicker films are produced as the ion energy is increased, a comparison can be made between the depth of ion penetration as predicted by range-energy theory and the depth indicated by the colors observed. Metals were bombarded with helium ions with somewhat similar results. Applications for this effect are discussed.

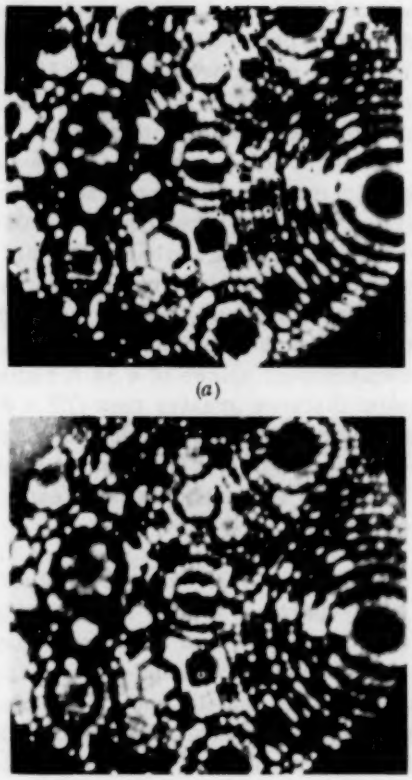

(*a*)

(*b*)

Fig. IV-1 Tungsten irradiated with 5-Mev alpha particles: (*a*) before an impact and (*b*) after an impact.[52] Atoms subsequently sputtered are dotted in (*a*), and two additional atoms are similarly marked in (*b*).

Brandon and Wald[52] have shown the feasibility of using the field-ion microscope to study damage produced by a single high-energy impact. Individual atoms are visible, and vacancies produced by alpha bombardment of tungsten are shown, as illustrated in Fig. IV-1. The figure shows the point of tungsten before and after bombardment; the white dots are the individual atoms. (Atoms that are removed by the damage are marked with tiny black dots in Fig. IV-1*a*). The arrangement of the atoms is produced by the geometry of the surface atoms.

Defects in Metal Alloys. Piercy[53] has concluded that he is observing displacement spikes

in irradiated copper–2 wt.% cobalt. The alloy is aged to form precipitates up to 50 A in radius and irradiated with doses of 3.4×10^{19} fission neutrons/cm^2 at 50°C. Precipitate size is measured by the superparamagnetic effect due to the presence of a magnetic material in a nonmagnetic matrix. The irradiation dissolved precipitates that are less than 12.4 A in radius (the average size dissolved had a radius of 11 A). The analysis shows that thermal considerations alone are not sufficient to give the amount of diffusion that such dissolution involves. However, displacement spikes of a 34 A radius with a diffusion distance greater than $\sqrt{Dt} = 8$ A can explain the results. The author also gives a very detailed analysis of the present knowledge in the attempts to verify the existence of irradiation spikes.

Defects in Other Materials. Two other studies of heavy-particle tracks in materials have been reported. Knorr and Schwartz[54] have observed self-decorated fission-recoil tracks in AgCl crystals. A one-to-one correspondence between expected and observed results indicates that each fragment that enters the crystal produces a decorated region. These regions range in diameter from 2000 to 5000 A. Tracks were followed for 11 μ, which is about the range of fission recoils in AgCl. Surface events produced in LiF surfaces were also reported. The diameters of these events ranged in size from about 500 A to 1 μ, with a distribution that could be described by a negative exponential. Layer et al.,[55] in reporting on various studies in silver halides, state that heavy primary cosmic-ray tracks can be decorated but only in crystals in which dislocations can be easily decorated. This appears in a discussion of the decorability of the silver halides as a function of impurity content and refers to a report that is to be published soon.

Some of the papers reprinted from the Prague Conference on Semiconductor Physics are of interest;[56] for example, the displacement threshold energy for diamond[56a] was reported to be 80 ev.

Ionization in the inner shells of material stopping fission recoils as well as in the fission fragments has been detected.[57] The measured X-ray quanta have energies from 2 kev up to 11.5 kev. The data give evidence of the ionization cross section and its dependence on the velocity of the fission fragments. The cross section varies appreciably with the ionization energy. It has a value ranging from 10^{-17} to 10^{-23} cm^2. Formvar, used as stopping material, shows an ionization cross section that increases with the tenth power of the relative velocity of the colliding particles.

(T. G. Knorr)

Theories of Radiation Effects

General Electric has developed computer programs for studying the lattice damage produced by ion collisions.[58] Use is made of a two-dimensional lattice with a 50-50 at.% binary material. Two-body collisions with the hard-sphere type of screened coulomb potential interaction are considered. Results are reported for iodine and krypton (1 to 50 kev) bombardment of BeO at various angles of incidence, in the form of maps of the displaced atoms. A typical cascade is shown in Fig. IV-2. The I^{127} terminates at a point 64 lattice distances from the point of incidence and is surrounded by undefected material. Most of the displacements occur in the first half of the path. About an equal number of atoms were displaced, but they returned quickly to their original positions. In a series of runs, 33% of all vacancies were alone, 10% in pairs, 5% in groups of three, and 52% in groups of four or more. Similar results were observed for 5-kev Kr^{85} bombardments. A discussion of ion penetration is also included.

Goland[59] suggests that a mechanism other than displacement spikes is important in the creation of defect clusters in neutron-irradiated metals. He discusses the results of a number of other investigators. His argument is based on the fact that there is no difference, fundamentally, in the clusters produced in copper and gold (thus not requiring two explanations as has been suggested) but that the difference is related to the impurity trapping in the two metals. Hesketh[60] discusses a new interpretation for the data of Makin[61] et al. on loop formation in copper during neutron irradiation. Hesketh's theory indicates a better fit to the data. His conclusions are that heterogeneous nucleation is in agreement with long-range defect-dislocation loop elastic interaction, that it is possible that all the loops formed are of the same species (either all vacancy loops or all interstitial loops), and that the diameter of the nuclei on which the

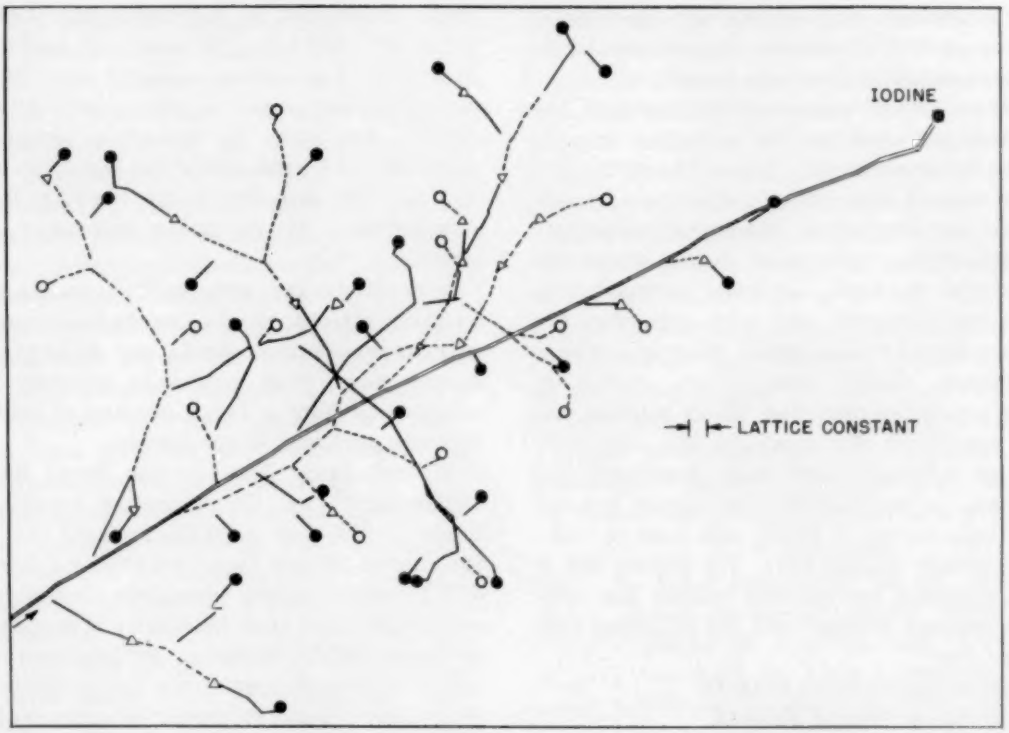

Fig. IV-2 Schematic of trajectories of beryllium and oxygen knock-on atoms (in a square planar lattice) making up the cascade created by bombardment of BeO with a 5-kev I^{127} ion.[58] ═══, iodine path. ——, beryllium path. - - -, oxygen path. ○, oxygen absorption point. ●, beryllium absorption point. △, replacement collisions.[58]

loops form is probably 6 A and certainly less than 10 A.

Calculations for the averages of certain physically interesting quantities concerned with the slowing down of an energetic particle in a solid material have been reported.[62] Hard-core distributions are used, and the quantities determined are the averages of the total distance traveled and the vector distance to the final position. Further calculations using the Yukawa potential to describe the interacting forces in the crystal are in progress. (T. G. Knorr)

Surveys on Radiation-Induced Defects

Course 18 of the Enrico Fermi International School of Physics (1960) is entitled *Radiation Damage in Solids*.[63] The contents are lectures given by various participants and are included in the following sections:

Crystalline Defects and Their Detection
Radiation Damage Theory
Radiation Damage in Semiconductors
Radiation Damage in Ionic and Covalent Crystals
Radiation Damage in Metals
Radiation Damage in Uranium and Special Seminars

The titles of the papers indicate that they are generally interesting.

Simmons et al.[64] have prepared a report on the present knowledge of point defects produced by irradiation in fcc metals. Their discussion includes theory and experiments concerned with equilibrium of thermally produced defects, quenching, annealing, and plastic deformation. References are made to 159 other reports. Houtman[65] has written an introductory review for a number of papers concerned with the effects produced by ionization radiation in matter. Atomic effects are distinguished from microscopic effects which are discussed in the later papers. A review of the studies of noble-gas-ion (0 to 10 kev) bombardment of metal surfaces has appeared.[66] The particular emphasis is on sputtering, penetration, and sorp-

tion. Theoretical expressions are developed, and these predict reasonable experimental values. There are 97 references quoted.

A 579-reference annotated bibliography has been prepared covering the property changes produced by irradiation.[67] Consideration is given to optical absorption, reflectance, transmittance and emittance, electrical resistivity and conductivity, refractive index, dielectric constant and strength, magnetic permeability, thermal conductivity, and heat capacity. Six major headings are employed: general and surface studies, metals and alloys, ceramics, plastics and other organics, alkali halides, and azides. Volume 10, No. 4, of *Acta Metallurgica*[68] is devoted to papers that were presented at a *Conference on Internal Friction Due to Crystal Lattice Imperfections*, which was held at Cornell University in July 1961. The papers are of general interest and include invited and contributed reports divided into the following four sections:

1. Effects Due to Point Defects
2. Dislocation Pinning Effects
3. Relaxation Peaks Produced by Deformation
4. High-Frequency Techniques

Simmons[69] has presented a review on the stored energy in irradiated graphite. Clarke[70] has gathered information on the radiation-produced damage in BeO. The report covers material available to the end of 1961 and includes 36 references. Clarke et al.[71,72] have also reviewed the British work on the effects produced by irradiation of BeO.

Thompson[73] has written a short review of the papers presented at the Symposium on Ion Bombardment held at Bellevue, Paris, in December 1961. The papers are grouped as follows: (a) Sputtering, (b) Internal Damage, (c) Impurity Injection, (d) Erosion as a Phenomenon, (e) Erosion as a Technique, (f) Secondary Emission, (g) Chemical Effects, and (h) Apparatus. (T. G. Knorr)

Effects of Radiation on Mechanical Properties

One of the most important irradiation effects on mechanical properties of pressure-vessel steels is radiation-induced embrittlement. Workers at Oak Ridge[74] have investigated the effects of neutron irradiation on the ductility transition temperature of type A-212B steel. Standard Charpy V-notch impact specimens were irradiated at approximately 0.44×10^{19}, 1.1×10^{19}, and 2.6×10^{19} neutrons/cm^2 (>1 Mev) at 475°F. The control samples were heated for an equivalent time, approximately 23 days at 500°F. Increases in transition temperatures were 90, 115, and 190°F for the 20 ft-lb range and 95, 140, and 200°F for the 30 ft-lb range, respectively, for the three exposures investigated.

Several review articles[75–77] in the area of neutron effects on the mechanical properties of pressure-vessel steels and other structural steels have been published recently. These articles present a large number of references that are pertinent to the subject.

Studies being done at the Naval Research Laboratory[78] on the pressure-vessel steels types A-302 and A-212B indicate that steels irradiated at low temperatures (less than 300°F) show nearly complete recovery after relatively short heat-treatment at temperatures as low as 600°F. However, irradiations carried out at higher temperatures on the same steels show less recovery under similar annealing conditions. Some irradiated samples have exhibited a reembrittlement phenomenon, following the first stages of recovery by annealing. The degree of reembrittlement appears to be a function of the irradiation temperature, of total neutron exposure, and of the time and temperature of the postirradiation heat-treatment. In all cases, annealing temperatures of 750°F or greater are necessary to prevent reembrittlement effects.

Researchers at Brookhaven[79] have investigated the change in electrical resistivity of unalloyed iron as a function of neutron exposures. They have found that pure iron irradiated to 2×10^{18} and 1×10^{19} neutrons/cm^2 shows resistivity increases of 12 and 22%, respectively. Measurements were made at −196°C.

Stainless steels have been investigated for uses in neutron environments and were found to be less susceptible to embrittlement than the carbon and low-alloy steels. Hanford[80] investigators have compared the tensile properties of two stainless steels and one Fecral alloy after irradiation to 2.5×10^{20} neutrons/cm^2 (thermal) at 650°F, with unirradiated control samples heat-treated in helium at 650°C for 500 hr. Heat-treatment time was comparable to irradiation time. This comparison was made on the basis of room-temperature tensile prop-

erties. The greatest change occurred in the modified Fecral alloy containing iron, 7.6 wt.% aluminum, 5 wt.% chromium, 2 wt.% niobium, and 0.72 wt.% zirconium. It showed a 26% reduction in strength and an 80% reduction in ductility. The stainless steels AISI types 316 and 347 reflected only minor effects of irradiation.

Oak Ridge[81] workers examined the influence of neutron irradiation (about 2×10^{20} neutrons/cm^2 on the elevated-temperature stress-rupture properties of AISI type 304 stainless steel. They found that, except for one sample which had the same rupture strength, all specimens tested in-reactor showed a decrease in rupture strength. This decrease was from 15 to 20% in the 1200 to 1500°F temperature range.

Additional work done by the Canadians[82] on annealed type 410 stainless steel irradiated at 265°C to 7×10^{19} neutrons/cm^2 (fast) has shown an increase in brittle-ductile transition temperature from −48 to −34°C. Tensile samples of type 410 stainless steel irradiated in contact with water showed a yield point after irradiation, whereas those which received a similar neutron exposure in air did not. The irradiation hardening was found to anneal out in the range of 200 to 400°C, having an activation energy of 2.4 ev.

Still another stainless steel, a semiprecipitation-hardenable A-286, has been tested after irradiation by the General Electric Company.[19,20] They investigated the creep and tensile properties at 540, 650, and 870°C after irradiation at approximately the same temperatures. In most cases the stainless steel showed a reduction in rupture strength at elevated temperatures after neutron exposures of approximately 7×10^{19} neutrons/cm^2 (>1 Mev). Electron-microscopy studies of A-286 indicated some slight change in the microstructure after irradiation. The phase that usually occurs as isolated colonies of platelets at grain boundaries on normally heat-treated A-286 seems to be present in smaller quantities after irradiation. Additional studies were carried out on the effect of aging prior to irradiation on the postirradiation ductility of A-286 steel. Underaged samples exhibited the largest ductility, and overaged samples the least.

The elevated-temperature stress-rupture properties of Hastelloy and René 41, a precipitation-hardenable alloy, were found[19,20] to be reduced slightly as the result of irradiation at elevated temperatures. The ductility of the Hastelloy X did not show any large degree of degradation as a result of irradiation.

Knolls workers[83] found that Inconel suffers about the same irradiation effects as the austenitic nickel-chromium steels. These are a large increase in yield strength, a somewhat smaller increase in tensile strength, and a slight reduction in ductility. The changes in properties of Inconel after irradiation are shown[83] in Table IV-2.

Oak Ridge[81] has investigated the effect of small B^{10} concentrations in Inconel on its in-reactor creep-rupture strength. The data for six specimens varying in B^{10} content from 1 to 190 ppm do not show a trend with respect to B^{10} content.

Zircaloy-2, used extensively as cladding and structural components in reactors, has received much attention with regard to the effects of irradiation on its mechanical and corrosion properties. In work conducted by the Canadians,[82] Zircaloy specimens in the annealed and cold-worked condition were irradiated at tempera-

Table IV-2 EFFECT OF IRRADIATION ON THE MECHANICAL PROPERTIES OF NICKEL-CHROMIUM-IRON ALLOY AT ROOM TEMPERATURE[83]

Integrated flux (fast), neutrons/cm^2	Irradiation temp., °F	Yield strength, 1000 psi	Ultimate tensile strength, 1000 psi	Reduction in area, %	Elongation in 1 in., %	Rockwell hardness	Yield strength/tensile strength
0		35.2 (0.02)	89.2		49	77−30 T	0.39
1×10^{20}	100 to 500	88.8 (0.02)	109.0		59.5		0.90
0			106		31	88 B	
4×10^{19}	110		116		29	100 B	
0			108.5		33	90 B	
4×10^{19}	540		113.0		29	93−102 B	
0		30.2 (0.2)	89.0	66	32		
2.6×10^{20}	550	78 (0.2)	104	58	44		

tures up to 280°C to 10^{19} and 10^{20} neutrons/cm^2 (>500 ev). The usual changes in properties were noted, including increases in proportional limit, yield strength, ultimate strength, and a reduction in ductility. Irradiations of both the annealed and cold-worked material at 380°C showed that damage occurs at a greater rate than does recovery at this temperature. The impact properties of the annealed and cold-worked Zircaloy were also investigated and found to be unaltered by neutron irradiation. Postirradiation annealing of the Zircaloy-2 produced some measure of recovery at temperatures of 250 and 400°C.

Studies of the effect of an instantaneous flux on the creep properties of Zircaloy-2 have been continued at two sites, namely, Chalk River and Hanford.[37,84] The data are somewhat inconclusive, but in most instances it would appear that creep rates in the reactor during reactor operation are usually less than in bench type tests at the same temperatures.

Workers at Savannah River[85] have investigated the effects of irradiation on the mechanical properties of zirconium and Zircaloy-2. These materials were irradiated to a maximum of 7×10^{20} neutrons/cm^2 fast (>1 Mev). The results of the zirconium irradiations are shown in Table IV-3, which tabulates the room-temperature properties before and after irradiation.

Materials of lesser interest in the field of radiation effects include beryllium, magnesium, and aluminum. Work on beryllium at Oak Ridge[81] is concerned with the stress-rupture properties during irradiation. Tubes are statically loaded with gas pressure, which is maintained throughout the test or until rupture occurs. Test temperatures are as high as 1500°F. The results indicate that exposures to fast fluxes well over 10^{20} neutrons/cm^2 (>1 Mev) have no significant effect on the rupture time of either machined or warm-extruded tubes. The results are shown in Figs. IV-3 and IV-4.

Samples of aluminum alloy 2024-T3,[86] which had been irradiated in the age-hardened condition in the MTR to doses up to 8.5×10^{19} fast neutrons/cm^2, showed definite signs of overaging as a result of the exposures. To determine whether the overaging was, in fact, radiation

Table IV-3 ROOM-TEMPERATURE MECHANICAL PROPERTIES OF ANNEALED ZIRCONIUM[85]

Calculated exposure to fast neutrons, nvt	Strength, psi		Elongation, % (by extensometer)		Reduction in area, %	Elastic modulus, psi	Hardness (Rockwell A)	
	Ultimate	Yield (0.2% offset)	Total	Uniform			Pre-irradiation	Post-irradiation
0	58,900		19.3	9.0	54.7		45.8	
0	59,100		20.4	10.5	53.2		45.7	
0	57,900	29,300			51.3	12.7×10^6	45.8	
8.5×10^{19}	66,200	52,200			47.0	13.7×10^6	45.2	48 7
1.3×10^{20}	66,200		14.3	4.4	43.8		45.2	49.1
1.6×10^{20}	67,700	56,000			44.7	12.7×10^6	45.2	50.1
1.7×10^{20}	66,700		13.3	3.9	41.6		45.7	49.5
1.9×10^{20}	67,000	57,300			45.7	13.8×10^6	45.2	50.2
2.1×10^{20}	71,300	59,800			44.1	13.0×10^6	45.5	48.6
2.5×10^{20}							45.7	50.6
2.7×10^{20}	69,800		12.4	1.1	49.6		45.0	54.8
3.2×10^{20}	66,200	58,600			46.2		45.7	50.8
3.8×10^{20}	69,000		13.4	3.5	48.3		46.2	52.2
4.0×10^{20}	68,500			3.6	49.5		45.5	55.6
4.2×10^{20}	69,500		11.8	3.6	41.6		45.2	50.4
5.2×10^{20}	71,800	64,100			40.6	12.1×10^6	45.3	53.8
6.3×10^{20}	72,600		10.7	2.0	39.2		45.3	55.8
7.0×10^{20}	74,600		10.1	2.0	46.0		45.7	55.0
Averages:								
Preirradiation	58,600	29,300	19.8	9.8	53.1	12.7×10^6	45.4*	
Postirradiation	69,100	58,000	12.4	3.0	44.8	13.1×10^6	51.7	

*Average preirradiation hardness measured on specimens 1 to 15.

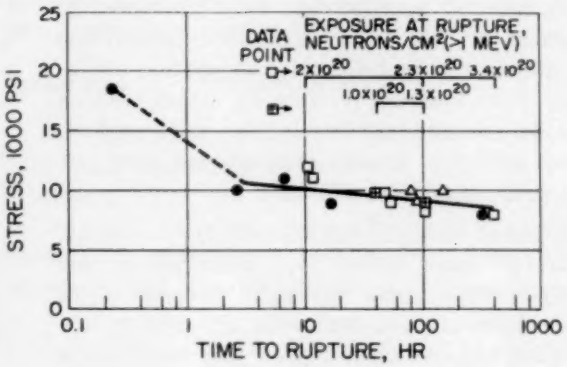

Fig. IV-3 Effect of irradiation on the stress-rupture properties at 520°C of beryllium tubing manufactured by machining from hot-pressed block.[81] ●, unirradiated. △, unirradiated control (equivalent thermal history). □, irradiated.[81]

induced, the specimens were annealed and examined by various techniques. The irradiated material appeared to have experienced temperatures in excess of the irradiation temperature by at least 150°F, thus indicating that the exposure had provided the energy equivalent of at least 1500°F increase in the ambient temperature of the sample during irradiation and was responsible for the overaging.

As part of an investigation on structural materials, Hanford[37,87] personnel have studied the properties of irradiated magnesium alloys. It is shown that the 3 wt.% thorium alloy HK-31A-H24 is not subject to great changes in yield or ultimate strength as the dosage increases from 5.4×10^{19} to 10^{20} nvt (>1 Mev). Elongation experiences the greatest change, decreasing about 20% for this factor of 2 increase in exposure. In contrast, the 3 wt.% aluminum alloy A-3XA-O demonstrates progressive changes in mechanical properties as exposure level increases. Over the exposure range experienced (0 to 10^{20} nvt), the yield strength was nearly doubled, the ultimate strength increased by 40%, and the elongation dropped from 10 to 5.4%. (F. R. Shober)

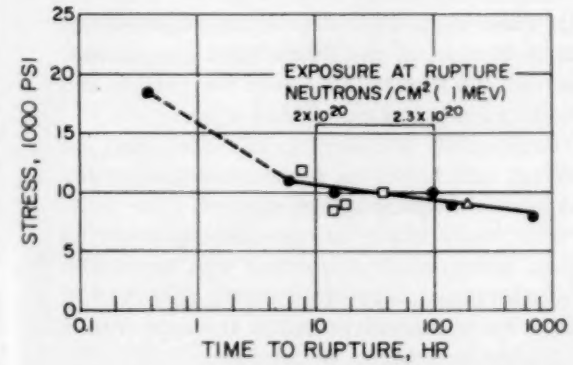

Fig. IV-4 Effect of irradiation on the stress-rupture properties at 520°C of beryllium tubing manufactured by warm extrusion.[81] ●, unirradiated. △, unirradiated control (equivalent thermal history). □, irradiated.[81]

Selected Mechanical Properties of Cladding and Structural Materials

Stainless Steel

The Defense Metals Information Center has published a report[88] that reviews the properties of the semiaustenitic precipitation-hardenable stainless steels. This report contains a rather complete compilation of information.

The effect of cold working on cladding strength is being studied at Combustion Engineering, Inc.[89] The stainless-steel tubing is being evacuated by cold and hot (550°F) hydrostatic collapse tests on empty tubes. The collapse pressure of tubing with a thickness-to-radius (T/R) ratio of 0.06 or less was shown to be independent of yield strength and is a function of the dimensions and modulus of elasticity only. With increased tube thickness (T/R of 0.08), the collapse pressure varies with yield strength. Therefore, for cladding with T/R of 0.06 or less, collapse pressure cannot be increased by the use of cold-worked tube rather than annealed, whereas with a T/R of 0.10 or greater, collapse pressure can be increased significantly by greater degrees of cold work.

Strength of René 41

Investigators at the University of Michigan[90] have shown that thermally induced structural changes reduce both room-temperature strength and ductility of René 41 when the exposure temperature is 1500°F or higher. These structural changes are accelerated by creep. Strain hardening, possibly in combination with strain-induced precipitation hardening, raised the tensile strength for exposures below 1500°F. The losses in strength from thermally induced structural changes appear to be due to overaging of the

gamma-prime precipitate. The loss in ductility was associated with the agglomeration of carbides and gamma prime in the grain boundaries.

Additional work on René 41 (at the University of Michigan[91]) has shown that the damage effects, except for surface reaction, were not permanent. Strength can be restored by redissolving and reprecipitating gamma prime. Resolution of carbides, particularly M_6C, by heating to 2150°F was necessary to completely restore ultimate strength and ductility; creep strength was also restored. The absence of creep damage is believed to be due to the complete absence of microcracking during creep.

Strength of Refractory Metals

Chromium-base alloys are under development at General Electric.[21] A chromium–1 wt.% yttrium alloy is reported to have a tensile strength of 6000 psi at 2200°F, whereas a chromium-TZC alloy has a 15,000-psi yield strength at 2000°F and a chromium–15 wt.% rhenium–3 wt.% aluminum–0.75 wt.% yttrium alloy has a 7500-psi yield strength at 2500°F.

Miscellaneous Properties Reviews

An excellent compilation[92] of the tensile properties of a number of high-strength alloys has been published by the Defense Metals Information Center.

A bibliography on the brittle fracture of steel has been compiled by General Electric.[93] It covers the unclassified literature for the period January 1950 through Nov. 15, 1961. Reviews and bibliographies that are listed furnish references to historical reviews and earlier studies on brittle fracture. Author and subject indexes are included. (J. A. DeMastry)

Selected Metallurgical Aspects of Cladding and Structural Materials

Refractory Metals

General Atomic[94] is conducting a program designed to determine basic information on the mechanical properties of reactor materials. As part of the general program to investigate the rate-controlling mechanisms for plastic flow in bcc metals, detailed data were presented on the effect of cold work on the internal friction (of niobium) due to dislocation relaxation oscillation. This internal friction is manifested as peaks in the internal friction vs. temperature curve, with the lowest temperature peak, or alpha peak, seen near 175°K.

Studies of vanadium-niobium alloys at Armour Research[95] have shown that fabricability and elevated-temperature strength properties of these materials are markedly affected by interstitial impurities. Samples that were found to be brittle after testing (dynamic helium atmosphere) contained at least 0.15 wt.% each of oxygen and nitrogen. Good elevated-temperature strength with room-temperature bend ductility was noted when nitrogen and oxygen were in the 0.07 and 0.13 wt.% range.

Tensile data obtained under vacuum at 2000°F show that the addition of 0.05 wt.% oxygen to vanadium–5 wt.% titanium–20 wt.% niobium produced an ultimate tensile strength of 37,000 psi, whereas a 0.03 wt.% carbon addition to the same base resulted in an ultimate strength of 30,600 psi. The composition vanadium–1 wt.% titanium–60 wt.% niobium–0.05 wt.% oxygen had an ultimate tensile strength of 48,000 psi under vacuum at 2000°F.

Ductility of Iron-Aluminum Alloys

Observations based on a study by Denver Research Institute[96] of factors influencing the ductility of iron-aluminum alloys are as follows:

1. The heat-treatment schedule conducive to optimum ductilities was a recovery anneal in the temperature range 600 to 650°C, followed by oil quenching. This treatment relieved the residual strains of the fabrication operations, preserved the fibrous shapes of the grains, and tended to minimize $Fe_3Al/FeAl$ order.

2. Rare-earth scavenging additions had no beneficial effects on the mechanical properties of the iron-aluminum alloys studied.

3. The desirability of minimizing order to enhance mechanical properties was suggested by the elevation of yield strengths observed in highly ordered materials and by the appearance of slip lines in ordered structures.

4. The deformation by slip was observed to be limited to planes of the type (110), except at very advanced stages of deformation. Specimens that exhibited over 10% tensile elongation

frequently manifested a curved, wavy type of slip superimposed over the (1 1 0) traces.

Properties of Zirconium Alloys

The electrical resistivity for a zirconium–1.25 wt.% aluminum–1 wt.% tin–1 wt.% molybdenum alloy was measured by Atomics International.[97] The thermal conductivity was then calculated from these values by using the Ewing equation. The results are given in Table IV-4.

Table IV-4 ELECTRICAL RESISTIVITY AND THERMAL CONDUCTIVITY OF ZIRCONIUM–1.25 WT.% ALUMINUM–1 WT.% TIN–1 WT.% MOLYBDENUM ALLOY[96]

Temp., °F	Electrical resistivity, μohm-cm	Thermal conductivity, Btu/(ft)(hr)(°F)
200	128.2	4.84
400	134.0	5.80
600	137.8	6.79
800	140.3	7.80
1000	141.8	8.86
1200	141.8	9.97
1400	139.8	11.33
1600	133.0	13.04

Activation energies determined at Hanford[98] for the creep of Zircaloy-2 are presented as a function of temperature in Figs. IV-5 and IV-6. The curves are separated into two regions which show two distinct activation-energy behaviors.

The activation energy in region 1 decreases with increasing strain rate at constant temperature and stress. In these tests strain rates decrease with increasing creep strain; thus activation energy U can also be considered to increase with creep strain. The strain-rate or creep-strain dependence decreases as region 1

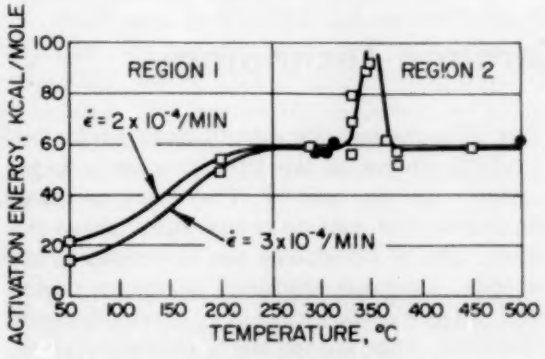

Fig. IV-5 Activation energies for Zircaloy-2 creep at 20,000 psi.[98] ●, cold worked. □, annealed.

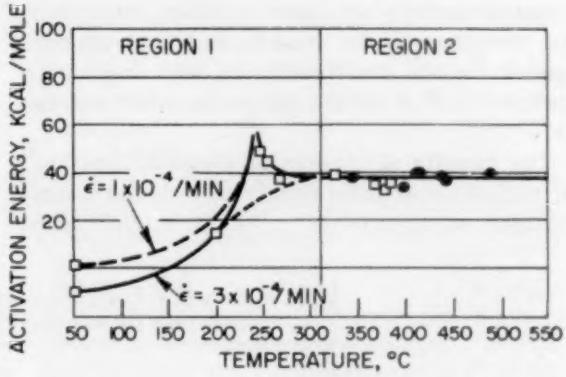

Fig. IV-6 Activation energies for Zircaloy-2 creep at 30,000 psi.[98] ●, cold worked. □, annealed.

values approach those of region 2. In contrast to region 1 behavior, the activation energies of region 2 are independent of stress, strain, strain rate, cold work, and temperature. The upper temperature limit of region 2 behavior was not determined but is in excess of 500°C.

A third activation-energy behavior, seen as an abrupt rise followed by an abrupt fall in the U vs. T curve, is superimposed on regions 1 and 2. The temperature of occurrence of the peak in the U vs. T curves is stress dependent, being 345°C at 20,000 psi and 235°C at 30,000 psi. The peak was not observed in tests conducted at 25,000 psi; however, temperatures at which a peak would be expected, 250 to 300°C, were not investigated.

The temperature of transition from region 1 to region 2 increases with increasing stress, being 250°C at 20,000 psi, 280°C at 25,000 psi, and probably near 310°C at 30,000 psi. The transition temperature at 30,000 psi is obscured by the activation-energy peak and therefore can be estimated only. The dotted line in Fig. IV-6 represents the form of the curve expected in the absence of the peak.

Miscellaneous Alloys

The following boundaries of the alpha and beta regions in scandium-yttrium alloys were determined at Ames.[99]

At.% yttrium in scandium	Lower boundary, °C	Upper boundary, °C
41.1	1183	1191
46.3	1186	1194
54.1	1195	1204
62.9	1238	1246

From these data and those reported previously, the minimum in the transformation from hexagonal to bcc solid solution was tentatively placed at 43.0 at.% yttrium in scandium and 1175°C.

The results of studies at General Electric[19] on palladium-iridium binary systems are summarized in Table IV-5. (J. A. DeMastry)

Table IV-5 METALLOGRAPHIC STRUCTURE AND X-RAY DIFFRACTION ANALYSES OF PALLADIUM-IRIDIUM BINARY SYSTEM[19]

Iridium content, at.%	Metallographic structure	X-ray diffraction analysis*
10	2 phases, homogeneous, dendritic	Major phase Pd, a = 3.88 A; also unknown phase
20	3 phases, dendritic	Major phase Pd, a = 3.88 A; also unknown phase
30	3 phases, dendritic	Small range of solid solutions, fcc, a = 3.876 A
40	3 phases, major—Ir, minor—Pd	Major fcc, a = 3.85 A Ir; minor fcc, = 3.88 A Pd
50	3 phases, major—Ir, minor—Pd	Major fcc, a = 3.85 A Ir; minor fcc, a = 3.88 A Pd
60	3 phases, possibly fourth phase	Major fcc, a = 3.85 A Ir; minor fcc, a = 3.88 A Pd
70	2 phases	Small range of solid solutions, fcc, a = 3.88 A Pd
80	Single phase; trace of unidentified material in grain boundaries	Fcc, a = 3.84 A Ir
90	Single phase, large grains	Diffraction results masked by large grain size, only Pd lines detected

*Lattice parameter of iridium is a = 3.84 A and that of palladium is a = 3.89 A.

Diffusion Studies

The rate of diffusion of oxygen in alpha zirconium has been determined in the temperature range 622 to 840°C by a method based on the linear relation between hardness and oxygen content of zirconium.[100] In this study, investigators at Bettis obtained hardness vs. distance curves from the diffusion zones in conventional couples composed of zirconium containing two levels of dissolved oxygen. The diffusivity was found to be independent of oxygen concentration in the range studied and to fit the Arrhenius equation

$$D\ (\mathrm{cm^2/sec}) = 3.3 \exp(-49{,}500/RT)$$

Agreement of these results with three other sets of published data is generally good, and the combined results follow the equation

$$D\ (\mathrm{cm^2/sec}) = 5.4 \exp(-50{,}800/RT)$$

A literature survey has been issued by the Germans[101] on experimental methods and equipment used for the measurement of release of radioactive rare gases in solids. The advantages and disadvantages of the various techniques are discussed. Included in the survey are continuous methods with sweep gas or circulation and various discontinuous methods. Apparatus used for Hahn emanation, DAD, or PAD experiments is described, and references are given on such subjects as sampling, purifying, and measuring of these gases. (D. C. Carmichael)

Ceramic Technology

Los Alamos investigators[102] have performed a critical review of the literature on carbides of groups 4a, 5a, and 6a. They have compiled information and data on preparation, phase relations, lattice structures and parameters, appearance, chemical stability, hardness, resistivity, superconductivity, thermodynamic properties, and vaporization characteristics. Particular attention was given to methods by which the materials can be made oxygen- and

nitrogen-free. An extensive bibliography is included.

A recently issued U. S. patent[103] describes a method for joining refractory carbides such as UC or ZrC to refractory metals such as tantalum or niobium. The method involves carburizing the metal and then sintering the two components together at 2000°C in a nonoxidizing atmosphere. The pieces are held together during heat-treatment. The disclosure states that sintering aids such as iron, nickel, or cobalt may be used in amounts up to 5 wt.% to reduce sintering time and temperature.

Interesting experiments are in progress at Ames Laboratory[26] on self-diffusion and sintering of Y_2O_3 and on the emissivity of refractory oxides. No data have yet been reported. The oxidation of $MoSi_2$ is also being studied. It is reported that the oxidation rate decreases at high temperature, although no temperatures are given. The oxidation mechanism probably is one of diffusion at all temperatures. At low temperatures, MoO_3 probably is the principal molybdenum-containing product; the product is probably Mo_3Si_2 at high temperatures. Apparently, MoO_3 formation is disruptive to the silica coating and causes high oxidation rates.

Alfred[104] workers have measured Young's modulus and internal friction of hot-pressed MgO at room temperature and have correlated these properties with specimen densities. Young's modulus increased linearly with specimen density, but internal friction decreased with increasing density. Internal friction appeared to be inversely proportional to the square of the grain diameter. MgO specimens having the same density did not always have the same Young's modulus or internal friction. These differences were attributed to differences in grain size and impurity content.

A literature survey for the period 1940 to 1960 has been made at Battelle[105] on emittance, reflectance, and transmittance of graphites and ceramics. The materials included carbides, cemented carbides, nitrides, oxides, silicides, graphites, and the microcrystalline material Pyroceram. (A. K. Smalley)

References

1. W. C. Yee et al., Fission Fragment Recoil Effects on Zirconium Oxidation, *J. Electrochem. Soc.*, 109(3): 198–204 (March 1962).
2. K. Osthagen and P. Kofstad, Oxidation of Zirconium and Zirconium-Oxygen Alloys at 800°C, *J. Electrochem. Soc.*, 109(3): 204–207 (March 1962).
3. General Nuclear Engineering Corp., Ninth Monthly Progress Report Covering Work for the Month of March 1962, USAEC Report GNEC-225, Apr. 2, 1962.
4. W. K. Anderson and M. J. McGoff, Corrosion of Zircaloy in Crevices Under Nucleate Boiling Conditions, USAEC Report KAPL-2203, Knolls Atomic Power Laboratory, Apr. 13, 1962.
5. W. E. Berry, E. L. White, and F. W. Fink, Zircaloy-4 Corrosion in Halide Solutions and at Crevices in High-Temperature Work, USAEC Report BMI-1571, Battelle Memorial Institute, Mar. 19, 1962.
6. Atomic Energy of Canada, Ltd., 1962. (Unpublished)
7. T. Smith, Hydrogen Permeation of Oxide Films on Zirconium, USAEC Report NAA-SR-6267, Atomics International, May 15, 1962.
8. J. R. Weeks (Ed.), Proceedings of the Eleventh Annual AEC Corrosion Symposium, May 23–25, 1962, USAEC Report BNL-728, Brookhaven National Laboratory.
9. R. R. Hood (Comp.), Heavy Water Moderated Power Reactors, Progress Report, March 1962, USAEC Report DP-725, E. I. du Pont de Nemours & Co., April 1962.
10. H. R. Longfield, Atomic Energy of Canada, Ltd., 1961. (Unpublished)
11. Hanford Atomic Products Operation, Mar. 30, 1962. (Unpublished)
12. D. G. Altenpohl, Use of Boehmite Films for Corrosion Protection of Aluminum, *Corrosion*, 18 (4): 143t–153t (April 1962).
13. Oak Ridge National Laboratory, Reactor Chemistry Division Annual Progress Report for Period Ending January 31, 1962, USAEC Report ORNL-3262, May 11, 1962.
14. M. S. Feldman, Stress-Corrosion Cracking of Stainless Steel. A Literature Search, USAEC Report DP-683, Savannah River Laboratory, February 1962.
15. H. R. Copson and W. E. Berry, Corrosion of Inconel Nickel-Chromium Alloy in Primary Coolants of Pressurized-Water Reactors, *Corrosion*, 18(1) 21t–26t (January 1962).
16. J. W. McGrew, Testing Steam Generator Materials for Pressurized Water Reactor Plants, *Corrosion*, 18(1): 27t–32t (January 1962).
17. R. J. Beaver, C. F. Leitten, Jr., and J. L. English, An Investigation of the Corrosion Resistance of Brazing Alloys for Austenitic Stainless-Steel Fuel Elements for Service in 565°F Pressurized Water, USAEC Report ORNL-2834, Oak Ridge National Laboratory, Apr. 12, 1962.
18. R. D. Baybarz, Effect of High Alpha Radiation on the Corrosion of Metals Exposed to Chloride Solutions, USAEC Report ORNL-3265, Oak Ridge National Laboratory, Apr. 10, 1962.

19. General Electric Co., Flight Propulsion Laboratory Dept., High-Temperature Materials Program, Progress Report No. 11, Part A, USAEC Report GEMP-11A, May 15, 1962.
20. General Electric Co., Flight Propulsion Laboratory Dept., High Temperature Materials Program, Progress Report No. 9, Part A, USAEC Report GEMP-9A, Mar. 30, 1962.
21. J. E. Fox, Chromium-Base Alloy Development, USAEC Report APEX-680, General Electric Co., Flight Propulsion Laboratory Dept., April 1962.
22. P. Kofstad, Oxidation of Tantalum at 300–550°C, Norwegian Report ARL-240, November 1961.
23. N. Nornam, P. Kofstad, and O. J. Krudtaa, Metallic Oxide Phases of Niobium and Tantalum. II. Metallurgical Studies, Norwegian Report ARL-239(Pt. II), October 1961.
24. H. U. Anderson, Kinetic Studies of the Reactions Occurring Between Tungsten and Gases at Low Pressures and High Temperatures, USAEC Report UCRL-10135, University of California Lawrence Radiation Laboratory, April 1962.
25. W. D. Klopp, Summary of the Fifth Meeting of Refractory Composites Working Group, Report DMIC-167, Battelle Memorial Institute, Defense Metals Information Center, Mar. 12, 1962.
26. Ames Laboratory, Iowa State University, Newsletter for the Division of Reactor Development Concerning Reactor Materials and Low Decontamination Separations for January 1962, Feb. 19, 1962.
27. D. T. Klodt, R. L. Wells, and C. E. Lundin, An Investigation of the Effect of Metallic Additions upon the Oxidation Resistance of $NbAl_3$, USAEC Report TID-14956, Denver Research Institute, Feb. 8, 1962.
28. F. C. Holtz, High-Temperature Oxidation Protective Coatings for Vanadium-Base Alloys, Report ARF-2227-3, Armour Research Foundation, Illinois Institute of Technology, Jan. 8, 1962.
29. Sylvania Electric Products, Inc., High-Temperature Oxidation-Resistant Coatings for Tantalum-base Alloys, Report SCNC-336, Apr. 24, 1962.
30. Sixth Meeting of Refractory Composites Working Group, June 16–19, 1962, Dayton, Ohio. Proceedings to be summarized as DMIC report.
31. NASA-AEC Liquid Metals Corrosion Meeting, December 14–15, 1961, USAEC Report TID-7626(Pt. I), April 1962.
32. J. F. Nejedlik, The SNAP-II Power Conversion System, Topical Report No. 14, Mercury Materials Evaluation and Selection, USAEC Report NAA-SR-6306, Atomics International, Apr. 15, 1962.
33. D. H. Gurinsky, High-Temperature Corrosion by Liquid Metals Group, April 1962, Monthly Progress Report. Apr. 30, 1962.
34. Oak Ridge National Laboratory, June 12, 1962. (Unpublished)
35. M. F. Amateau, The Effect of Molten Alkali Metals on Containment Metals and Alloys at High Temperatures, Report DMIC-169, Battelle Memorial Institute, Defense Metals Information Center, May 28, 1962.
36. J. J. Kelsch et al., Observation of Fission Fragment Damage in Thin Films of Metals, *J. Appl. Phys.*, 33: 1475–1482 (April 1962).
37. Hanford Atomic Products Operation, Quarterly Progress Report, Fuels Development Operation, October, November, December 1961, USAEC Report HW-72346, Jan. 15, 1962. (Classified)
38. T. S. Noggle and J. O. Stiegler, Fission Fragment Tracks in Metal Films, *J. Appl. Phys.*, 33: 1726–1730 (May 1962).
39. J. O. Stiegler and T. S. Noggle, Nitrogen Ion Bombardment of Thin Platinum Films, *J. Appl. Phys.*, 33: 1894–1895 (May 1962).
40. N. K. Sherman, Superconducting Nuclear Particle Detector, *Phys. Rev. Letters*, 8(11): 438–439 (June 1, 1962).
41. N. Riechl, Effect of High Energy Radiation on the Surface of Solid Bodies, *Kerntechnik*, 3: 518–521 (December 1961).
42. R. E. Hanneman et al., Kossel Line Studies of Irradiated Nickel Crystals, *J. Appl. Phys.*, 33: 1429–1435 (April 1962).
43. K. H. Westmacott, A. C. Roberts, and R. S. Barnes, Vacancy and Interstitial Clusters in Zone-Refined Aluminum Bombarded with Fission Fragments, British Report AERE-R-3946, February 1962.
44. C. J. Beevers and D. J. Mazey, Irradiation Damage in Molybdenum After Energetic H^+ and He^{++} Ion Bombardment, British Report AERE-M-991, March 1962.
45. T. H. Blewitt et al., Low-Temperature Resistivity of Sodium and the Effects of Nuclear Irradiation, *J. Appl. Phys.*, 33: 1612–1613 (April 1962).
46. D. G. Martin, The Influence of Impurity Atoms on the Annealing Kinetics of Neutron Irradiated Copper, *Phil. Mag.*, 7: 803–826 (May 1962).
47. D. G. Martin, The Influence of Impurity Atoms on the Annealing Kinetics of Neutron Irradiated Copper, *Reactor Materials*, 5(2): 49 (May 1962).
48. D. Powers and W. Whaling, Range of Heavy Ions in Solids, *Phys. Rev.*, 128: 61–69 (April 1962).
49. C. Motoc and I. Teodorescu, Study of the Structure of Thin Gold Films Irradiated in a Reactor, *Rev. Phys.*, 6: 397–401 (1961); also *Acad. Rep. Populare Romine, Studii Cercetari Fiz.*, 12: 335–340 (1961).
50. R. S. Nelson, The Effect of Temperature on the Propagation of Focused Collisions Sequences in Gold, *Phil. Mag.*, 7: 515 (March 1962).
51. K. W. Ehlers, Color Production from Energetic Ions Impinging on Metals, USAEC Report UCRL-9845, University of California Lawrence Radiation Laboratory, September 1961.

52. D. G. Brandon and M. Wald, The Direct Observation of Lattice Defects by Field Ion Microscopy, *Phil. Mag.*, 6(8): 1035–1044 (August 1961).
53. G. R. Piercy, The Detection of Displacement Spikes by Measuring the Effect of Particle Size on the Dissolution of Precipitate Particles by Fast-Neutron Irradiation, *J. Phys. Chem. Solids*, 23: 463–477 (May 1962).
54. R. W. Dayton and R. F. Dickerson, Progress Relating to Civilian Applications During April 1962, USAEC Report BMI-1577, Battelle Memorial Institute, May 1, 1962. (Classified)
55. H. Layer et al., Effects of Quenching and Annealing on Ionic Conductivity and on Dislocation Decorability in Silver Chloride, Report AFOSR-TN-1432 (AD-263713), University of North Carolina, 1962.
56. *Proceedings of the International Conference on Semiconductor Physics, Prague (1960)*, Academic Press, New York, and Publishing House of the Czechoslovak Academy of Sciences, Prague, 1961.
    a. C. D. Clark et al., The Threshold Energy for Production of Irradiation Damage Effects in Diamond, pp. 316–319.
57. P. Armbruster, Ionization of Internal Electron Shells in the Stopping of Fission Products, *Z. Physik*, 166: 341–354 (1962).
58. J. R. Beeler, Jr., and D. G. Besco, Knock-On Cascades and Point Defect Configurations in Binary Materials, USAEC Report ORO-547, General Electric Co., Flight Propulsion Laboratory Dept., May 1962.
59. A. N. Goland, Comparison of Electron-Microscope Observations in Neutron-Irradiated Copper and Gold, USAEC Report BNL-5925, Brookhaven National Laboratory, March 1962.
60. R. V. Hesketh, The Formation of Dislocation Loops in Copper During Neutron Irradiation, *Phil Mag.*, 7: 519 (March 1962).
61. M. J. Makin et al., The Formation of Dislocation Loops in Copper During Neutron Irradiation, *Phil Mag.*, 7(74): 285 (February 1962).
62. G. Leibfried, Calculation of Averages for Primary Recoil Distributions, *J. Appl. Phys.*, 33: 1933–1943 (June 1962).
63. D. S. Billington (Director), *Physics of Solids (Radiation Damage in Solids), Course 18 (1960)*, Academic Press, New York, 1962.
64. R. O. Simmons, J. S. Koehler, and R. W. Balluffi, Present Knowledge of Point Defects in Irradiated FCC Metals, USAEC Report TID-15929, University of Illinois, March 1962.
65. J. P. W. Houtman, The Effects of Ionizing Radiation on Matter, *Atoomenergie Haar Toepassingen*, 3: 219–225 (November 1961).
66. J. S. Colligon, Ion Bombardment of Metal Surfaces, *Vacuum*, 11: 272–281 (1961).
67. R. C. Gex (Comp.), Effects of Nuclear Radiation on the Optical, Electrical, and Thermophysical Properties of Solids: An Annotated Bibliography, Report NP-10969, Lockheed Aircraft Corp., August 1961.
68. Conference on Internal Friction Due to Crystal Lattice Imperfections, *Acta Met.*, 10(4): (April 1962).
69. J. H. W. Simmons, Stored Energy in Irradiated Graphite, *Progr. Nucl. Energy, Ser. IV*, 3: 324–347 (1960).
70. F. J. P. Clarke, Irradiation Damage in BeO, British Report AERE-R-3971, February 1962.
71. F. J. P. Clarke and J. Williams, Aspects of Irradiation Damage in BeO, *J. Nucl. Mater.*, 4: 121–124 (July 1961).
72. F. J. P. Clarke et al., Some Irradiation Induced Property Changes in BeO, *J. Nucl. Mater.*, 4: 125–132 (July 1961).
73. M. W. Thompson, Symposium on Ion Bombardment, Bellevue, Paris, December 1961, *Brit. J. Appl. Phys.*, 13: 194–196 (1962).
74. V. O. Haynes and W. C. Thurber, Determination of the Effect of Neutron Irradiation on the Nil-Ductility-Transition Temperature for Type A-212, Grade B Steel Used in the N. S. *Savannah* Pressure Vessel, USAEC Report ORNL-TM-132, Oak Ridge National Laboratory, Mar. 21, 1962.
75. Fast Neutron Change Metals, *Iron Age*, 189(12): 80–82 (Mar. 22, 1962).
76. W. S. Pellini et al., Analysis of Engineering and Basic Research Aspects of Neutron Embrittlement of Steels, Report NRL-5780, Naval Research Laboratory, Apr. 17, 1962.
77. P. H. J. Simonis, The Effect of Nuclear Radiation on the Properties of Construction Steel: III, The Effects on the Design and Manufacture of Reactor Pressure Vessels, *Atoomenergie Haar Toepassingen*, 3: 211–218 (October 1961).
78. J. R. Hawthorne, L. E. Steele, and W. S. Pellini, Effects of Nuclear Radiation on the Properties of Reactor Structural Materials, Report NRL-5731, Naval Research Laboratory, Jan. 22, 1962.
79. J. H. Reynolds (Ed.), Nuclear Engineering Department Progress Report, USAEC Report BNL-705, Brookhaven National Laboratory, March 1962.
80. S. Goldsmith (Ed.), Plutonium Recycle Program Annual Report, Fiscal Year 1961, USAEC Report HW-70000, Hanford Atomic Products Operation, Aug. 11, 1961.
81. Oak Ridge National Laboratory, Gas-Cooled Reactor Program Quarterly Progress Report, USAEC Report ORNL-3254, Apr. 6, 1962.
82. L. M. Howe, Radiation Damage in Zirconium, Zircaloy-2, and 410 Stainless Steel, Canadian Report AECL-1484, April 1962.
83. Knolls Atomic Power Laboratory, Metallurgy, Reactor Technology Report No. 20, USAEC Report KAPL-2000-17, March 1962.

84. L. G. Bell, The Mark I In-Pile Creep Test, Canadian Report CRGM-1047 (AECL-1468), March 1962.
85. R. R. Hood (Comp.), Heavy Water Moderated Power Reactors, Progress Report, February 1962, USAEC Report DP-715, E. I. du Pont de Nemours & Co., March 1962.
86. A. M. Adair, R. E. Hook, and H. J. Garrett, Radiation Induced Overaging of a 2024-T3 Aluminum Alloy, Report ARL-132, Wright Air Development Center, Aeronautical Research Laboratory, September 1961.
87. F. W. Albaugh, Reactor and Fuels Research and Development Operation Monthly Report, March 1962, USAEC Report HW-73202A, Hanford Atomic Products Operation, Apr. 15, 1962. (Classified)
88. D. C. Ludwigson, Semiaustenitic Precipitation-Hardenable Stainless Steels, Report DMIC-164, Battelle Memorial Institute, Defense Metals Information Center, Dec. 6, 1961.
89. Hanford Atomic Products Operation, US/UK Research Newsletter No. 13, March 1962.
90. J. V. Gluck and J. W. Freeman, Effect of Creep Exposure on Mechanical Properties of René 41, Report ASD-TR-61-73, University of Michigan, August 1961.
91. J. V. Gluck and J. W. Freeman, Effect of Creep Exposure on Mechanical Properties of René 41, Part II; Structural Studies, Surface Effects, and Re-Heat Treatment, Report ASD-TR-61-73(Pt. II), University of Michigan, November 1961.
92. J. E. Campbell, Compilation of Tensile Properties of High-Strength Alloys, Report DMIC-Memo-150, Battelle Memorial Institute, Defense Metals Information Center, Apr. 23, 1962.
93. E. R. Appleby (Comp.), Brittle Fracture of Steel, 1950–1961, USAEC Report HW-71794, Hanford Atomic Products Operation, Dec. 6, 1961.
94. T. A. Trozera, R. H. Chambers, and J. L. White, A Program of Basic Research on Mechanical Properties of Reactor Materials, USAEC Report GA-3076, General Atomic Div., General Dynamics Corp., May 1, 1962.
95. B. R. Rajala and F. C. Holtz, Pilot Evaluation of Vanadium Alloys, Report ARF-2231-2, Armour Research Foundation, Illinois Institute of Technology, Apr. 13, 1962.
96. J. F. Nachman, G. P. Rauscher, Jr., and F. C. Perkins, Study of Factors Influencing Ductility of Iron-Aluminum Alloys, USAEC Report DRI-2040, Denver Research Institute, Dec. 29, 1961.
97. Atomics International, Quarterly Technical Progress Report, AEC Unclassified Programs, October–December 1961, USAEC Report NAA-SR-6999, Feb. 2, 1962.
98. J. J. Holmes, The Activation Energies for Creep of Zircaloy-2, USAEC Report HW-70151, Hanford Atomic Products Operation, March 1962.
99. Ames Laboratory, Iowa State University, Newsletter for Division of Reactor Development Concerning Reactor Materials and Low Decontamination Separations for February 1962, Mar. 19, 1962.
100. J. J. Kearns and J. N. Chirigos, The Use of Microhardness in the Determination of the Diffusivity of Oxygen in Alpha Zirconium, USAEC Report WAPD-TM-306, Westinghouse Electric Corp., Bettis Atomic Power Laboratory, February 1962.
101. P. Schmeling and F. Felix, Experimental Methods and Equipment for Diffusion Measurements of Radioactive Rare Gases in Solids, German Report HMI-B-19, November 1961.
102. E. K. Storms, A Critical Review of Refractories, Part I: Selected Properties of Group 4a, 5a, and 6a Carbides, USAEC Report LAMS-2674, Los Alamos Scientific Laboratory, Feb. 1, 1962.
103. N. H. Koikorian et al., Method of Joining Carbides to Base Metals, U. S. Patent 3,020,632 (to USAEC), Feb. 13, 1962.
104. R. Hanna and W. B. Crandall, The Young's Modulus and Internal Friction of Polycrystalline MgO at Room Temperature, Report AROD-2891.1, Alfred University, Sept. 1, 1961.
105. W. D. Wood, H. W. Deem, and C. F. Lucks, The Emittance of Ceramics and Graphites, Report DMIC-Memo-148, Battelle Memorial Institute, Defense Metals Information Center, Mar. 28, 1962.

Section V

Reactor Materials

Special Fabrication Techniques

Melting, Hot and Cold Working

Continuing work at the Bureau of Mines on the thermodynamics of the cold-mold consumable-electrode arc-melting process[1] led to the following observations:

1. Varying the external cooling-water flow from Reynolds numbers of 4000 to 40,000 had no significant effect on the arc-current value at which damage to the anode wall occurred.
2. The effectiveness of flow rate increased with a decrease in wall thickness (between 1 and $\frac{1}{2}$ in.).
3. The ability of the anode to sustain higher amperages without surface damage increased with decreasing wall thickness.
4. At a wall thickness of 1 in., a current of 450 amp was sufficient to damage the wall regardless of coolant flow rate.

Studies on the electron-beam melting of hafnium revealed that oxygen is removed mainly as hafnium monoxide (HfO) and carbon as carbon monoxide, but the latter reaction is of minor significance. During melting, temperatures on the order of 2600 to 2900°K were obtained. Metallic impurities and hydrogen were removed during the first few minutes the molten alloy was held at low pressure. The carbon, nitrogen, and oxygen, in that order, were removed at slower rates. Comparisons of the rates of evaporation indicated that aluminum, magnesium, titanium, and zirconium evaporated as monoxides, whereas copper, chromium, and iron evaporated as suboxides or as the metal.

Ames Laboratory has been performing similar purification studies[2] on thorium sponge in which the sponge is consolidated by arc melting and then exposed to the electron beam. A hardness decrease of Rockwell hardness numbers 90 to 58 resulted from electron-beam melting with analyses indicating that, most significantly, losses of carbon, chromium, and iron had occurred.

National Lead Company of Ohio[3] reported on the removal of impurities from ingot and dingot uranium as a consequence of consumable-electrode vacuum arc-melting processing. In the melting operations conducted at Battelle, 2-in.-diameter electrodes were melted into 4-in.-diameter crucibles using various melting parameters (arc voltage, arc currents, and magnetic stirring) and single and double melting. On the basis of the products of these tests, it was concluded that magnetic stirring increased both melting rate and degassing of metal. Hydrogen content decreased with each melt. For single-melted dingot material, the hydrogen content dropped from 4 to about 1.2 ppm, and, for single-melted ingot stock, it dropped from 2.6 to about 0.7 ppm. Both aluminum and manganese levels decreased significantly after a single vacuum arc melt. Additional values for this type of processing were estimated high yields (99%, core to good fuel core) for production operation because of the fine and uniform dispersion of remaining impurities.

Indicative of the increasing interest in chromium as a high-temperature material are reports (1) from Ames on the preparation of single crystals $\frac{1}{4}$ by $\frac{1}{4}$ by $1\frac{1}{4}$ in. long,[4] (2) from Ames on attempts to purify it by electron-beam zone refining,[2] and (3) from Battelle on the successful preparation of chromium–1 wt.% yttrium alloy in 1-in.-diameter bar by arc melting and extrusion and by high-temperature, isostatic pressure compaction of prealloyed powder.[5]

Continuing efforts to develop efficient and acceptable techniques (in terms of metal quality)

for the fabrication of uranium tubes for fuel elements are being exerted by National Lead.[6] Feasibility was demonstrated in work conducted at the Ithaca Gun Company on a GFM (from the builder's initials) rotary forging machine, normally used to make shotgun barrels. Tolerances of the rotary-forged uranium were better than those of extruded stock, and analyses of grain size and texture revealed a structure equivalent to that of normally produced tube material.

Pratt & Whitney has been active in the fabrication of niobium tubing by spinning methods.[7] Tubes from $1\frac{1}{8}$ to $4\frac{1}{4}$ in. in diameter have been successfully spun; no difference in formability of niobium or niobium–1 wt.% zirconium was discerned. Starting shapes made from welded steel required more stress relieving (after every pass) than did forged and ingot stock. Initial wall thicknesses greater than 0.350 in. could not be reduced due to layering. The mechanical properties of the spun tube material were between those of as-extruded and 20% cold-reduced material.

Additional publications in the general area of the progress and status of refractory-metals fabrication are: the report of the National Research Council's subpanel on Consolidation and Fabrication of Refractory Metals,[8] and reports from Du Pont on niobium,[9] from Allegheny Ludlum on molybdenum,[10] and from Wah Chang on tantalum.[11] (E. L. Foster)

Cladding

Cladding by Rolling and Swaging

British investigators have developed a prototype planetary-swaging machine for tube drawing.[12] Preliminary runs yielded accurately dimensioned tubing with excellent surface finish as compared to products made by more conventional swaging techniques. As judged from trial runs, planetary swaging has potential as a means to (1) provide close fittings between cans and fuel, (2) consolidate various types of powder fuels within cans, and (3) aid in bonding between fuels and cans.

In addition to much work on the swaging of UO_2, investigators at Allis-Chalmers have tried "draw bonding" and "stretch bonding" as a means of cladding UO_2 with stainless steel.[13] In both of these experiments, pelletized UO_2 was clad with type 316L stainless steel. The draw-bonding experiments consisted of drawing canned UO_2 pellets to reductions in area of 2.0 to 6.5%. Partial cladding contact was obtained in the low-reduction ranges, but the higher ranges yielded severe pellet damage. The best bonding in the experiment was obtained at 3.5% reduction in area. Stretch bonding utilizes the stresses generated by stretching a can of stacked pellets. Twenty-nine-inch-long rods were stretched $\frac{3}{4}$, $\frac{7}{8}$, and 1 in. Stretching $\frac{3}{4}$ in. resulted in contact between the cladding and the fuel pellets, and higher amounts of stretching separated the pellets. The major problem in this experiment was devising a method for gripping the rods without tearing the cladding.

The roll cladding of delta-phase plutonium alloys is being investigated at Hanford.[14,15] The particular fuel material currently of interest is a plutonium–15 wt.% zirconium alloy clad with Zircaloy-2. The core prior to bonding was wrapped in aluminum foil. The entire composite was then rolled at 840°C to a total reduction of 93% in a mild-steel container. Less than 90% reductions gave no bonding. Metallographic examination of the bonded composite revealed that there was a brittle intermetallic compound present in the bond interface. This compound was thought to be $PuAl_2$.

Smith and coworkers at Battelle[16] are currently investigating the roll-form bonding of Zircaloy-2 pressure tubes to type 410 stainless-steel pressure fittings. Gold and silver inlays are included in the bond interfaces to promote a cold joint. A postbonding heat-treatment in the range of 600 to 700°C is being investigated. Metallographic examination of the heat-treated bonds revealed that times of less than 8 hr at 700°C produced a diffusion bond between these joints, but the joints were brittle.

Emonds in Germany studied mechanical processes that take place during roll cladding of aluminum-alloy sheet.[17] A plating diagram was presented to show the dependence of adhesion on temperature and rate of rolling. He concluded that above 300°C welding occurred by three almost-simultaneous processes: deformation, recrystallization, and renewed deformation. During recrystallization, grains grew across the plating plane aiding bonding, as confirmed by electron microscopy. Bonding was improved by having the cladding plates in a fine-grained, annealed condition and was even

better if the plates had been milled in the direction of rolling. (H. D. Hanes)

Pressure Bonding

A series of 50 stainless-steel-clad uranium dioxide fuel elements were vibrationally compacted at Hanford[18] and bonded at Battelle[19] as part of the effort to develop the gas-pressure-bonding process for the simultaneous cladding and densification of the vibratory-compacted uranium dioxide. Examination of the bonded fuel elements revealed that densities of 98% or greater were achieved with a mixture of 70 wt.% fused and 30 wt.% micronized uranium dioxide. To prevent excessive distortion of the cladding during the densification of the oxide, it was determined that an initial vibratory-compacted density of 75% or greater was required. In addition, the fused uranium dioxide contained in the fuel elements must be less than 20 mesh in rods having cladding less than 15 mils thick.

Swaged elements were also subjected to gas-pressure bonding and evaluated. It was observed that fuel materials having high surface area and small particle size were more amenable to precompaction by swaging than to vibrational compaction. Swaged elements containing PWR and micronized grades of uranium dioxide powder could be hot isostatically compacted to high densities. Gas-pressure-bonding parameters normally employed in this study[19] were 3 hr at 10,000 psi at 2100 to 2300°F.

(E. S. Hodge)

Diffusion Bonding

An investigation at Westinghouse[20] showed that beryllium is a useful primary diffuser element for diffusion bonding of iron-, nickel-, and cobalt-base high-temperature alloys. Beryllium-transport alloys, which contain beryllium in solid solution at bonding temperatures, were also developed, and these facilitate preplacement of beryllium at the interfaces between the base metals to be joined. These alloys can be rolled into strip stock and formed into complex shapes to facilitate preplacement in joints, and they produce diffusion-bonded joints rapidly in ½ to 5 min at bonding temperatures of 1940 to 2100°F. It is reported that the shear strengths of the diffusion bonds qualitatively correlate with the base-metal ultimate and yield strengths at 1500°F.

A comprehensive study of the structure of aluminum-nickel-uranium diffusion bonds showed that the limiting factor in the quality of the bonds is the presence of oxide contamination in the diffusion zone. At Du Pont,[21] reactor fuel elements fabricated by bonding aluminum to nickel-plated uranium were investigated by optical and electron metallography and by X-ray diffraction in order to study their diffusion zones and the relation between the microstructure of the bonds and their strength and corrosion resistance. Two aluminum-nickel zones in bonded fuel elements were identified as Al_3Ni and Al_3Ni_2, and two nickel-uranium zones were identified as U_6Ni and UNi_5. An oxide, believed by the investigators to be either UO_2 or a uranium-nickel-oxygen ternary compound, was observed either as a dispersed phase within the UNi_5 zone or as a continuous layer between the U_6Ni and UNi_5 zones. The dispersed form of the oxide was observed to coalesce into a continuous layer and finally to dissolve during prolonged annealing. The proposed limiting factor in the quality of the bonds was the presence of this oxide within the nickel-uranium portion of the bond. When the oxide occurred as a continuous layer, the strength of the bond averaged less than 10,000 psi, and the bond was rapidly undercut during a pinhole corrosion test. When the oxide occurred as dispersed particles, the strength averaged greater than 15,000 psi and the bond confined corrosion. (D. C. Carmichael)

Coextrusion

The coextrusion process was used by Nuclear Metals to fabricate 56 driver-tube elements, consisting of a thin Zircaloy cladding over a core of zirconium–9.3 wt.% uranium of 93% enrichment, for use in the Heavy-Water Components Test Reactor (HWCTR) at the Savannah River Plant.[22] The driver elements are approximately 2.3 in. in outside diameter, 2 in. in inside diameter, and 9.5 ft in length; the core thickness is 0.137 in.; and the cladding thickness is 0.015 in. The assembled billets were extruded in a 2400-ton press at 1250°F. The hot tubes were immediately rotated on a power-driven set of rollers to provide uniform cooling and assure straightness. Fifty-three of the tubes produced were satisfactory in all respects, giving a 95% yield. A very high degree of uniformity was maintained among these tubes. It

appears that other experienced fabricators should, by strict adherence to the established process sequence and a rigid quality control, be able to fabricate driver-tube elements to present specifications with similarly high yields.

Extrusion characteristics have been determined at Hanford[23] for a series of uranium-zirconium and uranium-carbon alloys in the range of 0 to 2 wt.% zirconium and 40 to 1600 ppm carbon. Zirconium additions to uranium in excess of 1 wt.% zirconium will produce a uniform coextruded Zircaloy jacket from either heat-treated or cast billets. Prior heat-treatment of cores with as low as 0.25 wt.% zirconium will also produce a uniform coextruded jacket. Small zirconium additions to the uranium rapidly increased the extrusion coefficient, whereas carbon additions only resulted in a gradual increase. The carbon additions to the uranium had little effect on the fabrication properties; however, in excess of 800 ppm, carbon tends to nullify the beneficial effects of the zirconium addition. Excessive carbon in the zirconium-uranium alloy caused formation of a zirconium carbide in preference to the formation of a zirconium-uranium compound. When the carbide formed, the metal behaved differently than either the uranium-carbon or the uranium-zirconium alloys.

Workers at Hanford[18,24,25] have experienced cladding-thickness variations or "Wanderlust" in Zircaloy components due to different extrusion characteristics. If one area extrudes more easily than another, then thick and thin cladding could result. It has been demonstrated that metals have a memory of the previous working, such as preferred orientations impacted by forging. In analyzing the manufacture of components, asymmetrical or uneven working was present in the forging operation employed by all vendors. Tests are being made to study the memory mechanism between components made with and without a preforging operation. Hanford workers are also conducting a study where several metals will be extruded along with uranium in a composite billet assembly, to determine the effects of both grain size and extrusion coefficient on interface roughness. A direct comparison will be made at the same time between the interface roughness of alpha-extruded and beta-heat-treated alpha-extruded uranium.

Experiments conducted at Savannah River have shown that, for the same flow and expenditure of pumping power, the burnout heat flux of a rough surface is as much as 80% greater than that of a smooth surface. If the reactor power is limited by the heat flux from the surfaces of the fuel elements, higher power or a greater margin of safety from heat-transfer burnout can be obtained from fuel elements with rough surfaces. This gain can only be realized, however, if the rough surfaces can be produced uniformly over all the critical heat-transfer surfaces. The inner and outer surfaces of coextruded fuel tubes that had an aluminum-uranium core and type 1100 aluminum cladding were knurled with a diamond pattern for this study. A standard knurling tool was satisfactory for producing the specified uniform pattern of roughness on the outside surface of these tubes. A special tool and process involving a hydraulically actuated mechanism was developed,[26] however, to produce the same pattern on the inner surface of the long coextruded fuel tubes. Dimensions for the coarse diamond knurl were specified as approximately 14 diamonds/in. of circumference and 11 diamonds/in. of length, or 154 diamonds/sq in. The height of the knurl was specified as 25 ± 4 mils.

(C. B. Boyer)

Canning

Recent studies[27] at Hanford have been concerned with the vibratory compaction of sintered and crushed UO_2 powders. A density of 88% of the theoretical density was achieved, corresponding to a 92.5% compaction efficiency. AISI 406 stainless-steel tubes (0.563 in. in outside diameter by 12 in. long by 0.009 in. in wall thickness) were bonded with fuel material prepared from sintered pellets (95% of theoretical density) by crushing and vibrational milling. The tubes were coupled to a 9-ft-long beam supported horizontally between a fixed fulcrum and a 5000-lb-thrust vibrator.

A comprehensive review[28] of all vibratory-compaction work was made at Combustion Engineering, Inc. It was pointed out that the use of inexpensive, small pneumatic vibrators was potentially favorable, although the densities attainable during compaction decreased for increasing fuel-column length. A total of 105 multitube fuel elements were produced as a result of experience gained during this research.

Several observations regarding pneumatic vibratory compaction were made based on the

studies to date. Densities of 93 to 94% of the theoretical density can be produced using irregularly shaped fused UO_2 particles in tubes of short length. A specific particle-size distribution, limited to a narrow range, was necessary to achieve the high densities. This distribution can be obtained either by direct blending of the specific formulation, or indirectly, by comminution of the coarse particles during compaction.

A variety of starting formulations can be used for the indirect method, and approximately the same final particle-size distribution is obtained. However, a sufficient number of coarse particles must be initially present to permit the production of the necessary medium particles. It is reported that approximately one-half of the coarse particles break down to produce medium-size particles. The amount of fines must be optimum at the start, since they are not generated in appreciable quantities during the compaction process. An excess or deficiency of fines has been found to lower the density obtainable. The compaction time for distributions obtained in the direct method was 9 min, which compared to 21 to 24 min for particle-size formulations obtained by the indirect method.

A study was made to investigate the effect on density of the tube variables (length, cross section, and nature of material) and compaction parameters (frequency and time). Also determined was the effect on density of a lateral vibration component. The results of this study were:

1. The percentage of theoretical density is a function of the logarithm of the compaction time.
2. The slopes of the density-log time curves for tubes 2 and 3 ft long are greater than those for tubes 4.5 and 6 ft in length, indicating more effective densification for the shorter tubes.
3. The ultimate density attained for a 60-min compaction time is inversely proportional to the tube length.
4. The slopes of the density-log time curves are radically increased during the initial stages of precompaction when a lateral vibration component is used with the normal vertical motion.

Further studies of vibratory compaction at Combustion Engineering[29] have led to a modification of the loading process to bring the fuel length and density to a fixed level prior to final high-impact compaction to 89 to 90% of theoretical density. Hand blending and mechanical V-cone blending were compared to determine the difference in densities attainable with both techniques. The hand-blended specimens yielded slightly higher final densities than the mechanically blended specimens.

The results of vibrational compaction of six Mark I type fuel elements have recently been reported.[30] The UO_2 fuel densities obtained varied from 87 to 88.5% of the theoretical density. The rods were compacted by vibrational energy transmitted through a steel beam. The efficiency of compaction or the density of the fuel rods varied along the length of the beam, both with respect to position and to the number of rods being processed.

A recent Argonne progress report[31] describes a technique for jacketing small plutonium-aluminum fuel slugs in aluminum cans. This process involves both a shrinking and a coining operation to form the assembly to the final size and shape. Sealing of the cans is accomplished by capacitor-discharge welding. Also discussed in the report were two methods to can 0.150-in.-diameter plutonium-disk specimens of 0.005-in. thickness. The first method attempted was gas-shielded tungsten-arc welding of a zirconium-clad sandwich. This was accomplished successfully for cladding thicknesses down to 0.005 in. To circumvent the possibility of contamination of the weld and cladding, a cold-pressure-welding technique was considered. Plutonium disks were positioned between aluminum foils, and the entire assembly was placed in a punch and die assembly. The aluminum foils were forced together around the periphery of assembly to effect a seal in a single application of load. Careful alignment of the plutonium disks with respect to the punch and die was required to prevent cutting into the disks.

A recent article[32] describes the processing of EBR-II fuel rods. This involves sodium loading, welding, weld inspection, bonding, and bond-inspection techniques. These techniques were developed from the experience gained from the manufacture of the first core loading.

(E. G. Smith, Jr.)

Nonelectrolytic Chemical-Plating Techniques

A review article on chemical vapor deposition[33] suggests the possibility of opening new areas of ceramic technology by use of this

potentially valuable process. Current applications include the coating of extended surfaces and the production of high-purity ceramics and coated powders.

Experiments were conducted[34] to determine the feasibility of coating uranium–10 wt.% molybdenum alloy with a dense layer of niobium by hydrogen reduction of $NbCl_5$ at 600°C. A 1-mil layer of electrodeposited copper was used on the alloy in an attempt to prevent side reactions between the HCl by-product and the alloy. Blistering at the copper-uranium alloy interface was minimized by hot outgassing and ultrasonic cleaning. Vacuum deposition of copper, followed by diffusion annealing at 1600°F, is being attempted to improve the copper-uranium bond.

Chemical vapor deposition can be used as a means of preventing the degradation of hot metal surfaces by evaporation or sublimation.[35] Active gaseous materials, such as chlorine, react with subliming metal and transport it back to the hot surface in the form of a vapor. A similar principle has been used commercially in the lamp industry. Iodine vapor combines with evaporating tungsten and returns it to the filament. Hypothetical systems considered include tungsten-chlorine, molybdenum-chlorine, tungsten-molybdenum-chlorine, and tungsten-oxygen.

Nickel coatings, applied to uranium by pyrolysis of $Ni(CO)_4$, have shown a wide margin of superiority over certain electrodeposited coatings when exposed to air at 150°C for more than 140 days and to boiling water for more than 170 days.[36] Coatings 1, 3, or 5 mils thick were used.

High-temperature pyrolysis of $W(CO)_6$ in a simple bell-jar system was used to coat manifolds and ionizers with tungsten.[37] Chemical-vapor-deposition techniques were used in an investigation of the formation of oriented or epitaxial tungsten films on single-crystal tungsten substrates.[38] The reaction employed was the hydrogen reduction of WF_6.

Silicide coatings for molybdenum and tungsten were applied at 1050°C, using SiF_4 vapor transport.[39] Performance of coatings formed by this siliciding system appears to be at least as good at 1800°C under oxidizing conditions as is that of coatings formed by other siliciding systems.

Chemical vapor deposition is being investigated as one of the processes having considerable potential as a means of fabricating components of refractory materials difficult to form by conventional techniques.[40]

Chromium, copper, iron, gold, and nickel whiskers were grown on substrates placed in the supersaturated metal vapors.[41] To prevent interference by a metal-oxidation reaction during growth, the partial pressure of oxygen was maintained below the dissociation pressure of the oxide of the metal from which the whiskers were grown.

An attempt was made to prepare pure beryllium by thermal decomposition of the iodide by passing BeI_2 vapor over a tungsten filament, heated from 800 to 1800°C, in an all-glass de Boer bulb.[42] At wire temperatures in the range 1400 to 1800°C, the surface of the tungsten wire became spongy. It was postulated that the wire had been attacked by BeI_2 to form beryllium metal, which volatilized. Hydrogen reduction of the iodide likewise did not meet with success.

Layers of deposited tungsten, prepared by hydrogen reduction of WF_6 at temperatures of 600 to 850°C and at slightly less than atmospheric pressure, are of high quality.[43] The material maintains its original grain size and other characteristics at temperatures up to 2000°C. The bond between vapor-deposited tungsten and a graphite substrate is very strong, and the interface is free of carbides.

Refractory metals, having virtually equiaxed crystals with almost complete disruption of columnar grain growth, can be deposited by chemical vapor deposition.[44] A description was given of the formation of refractory-metal structures by placing high-strength refractory filaments on a mandrel in the desired position using regular winding techniques. Refractory-metal matrix material then is vapor deposited to fill the voids between the filaments and thereby to restrain them. Better results are obtained by using a matrix material of lower elastic modulus than that of the filaments.

Whiskers were grown by vapor deposition of alumina, produced by the oxidation of aluminum vapor in a H_2-H_2O atmosphere.[45] Some of the larger whiskers were as long as 2 in., whereas the very fine ones grew in a woolly deposit. Beryllium oxide single crystals of both simple and complex form were grown using a reversible reaction between BeO and H_2O vapor at high temperatures.[46] Beryllium hydroxide was

formed at temperatures of 1300 to 1650°C and then was allowed to decompose to BeO and H_2O at a temperature several hundred degrees lower. Crystals could nucleate on any substrate tried, provided it was situated at the proper location in the furnace. Single crystals of stannic oxide 30 by 4 by 2 mm were prepared by a high-temperature vapor-deposition technique.[47] Using high-purity SnO_2 powder, crystallization and growth were studied under both neutral and oxidizing conditions. Three different SnO_2 growth habits were observed, apparently dependent on the temperature at which growth occurred.

The preparation and evaluation of refractory-metal (molybdenum, tungsten, and boron) alloys of pyrolytic graphite[48] were investigated. Variables studied included source-gas concentration, flow rate, and deposition temperature. In each system analogous reaction conditions are found to be operative, and microstructural and other physical aspects similar to those of pyrolytic graphite are observed. Development of pyrolytic graphite containing 0.5 to 3% boron was described.[49] Preliminary property measurements on flat-plate samples show an improvement in strength and other properties over pyrolytic graphite. Pyrolytic graphite deposits from propane and methane were formed on tubular substrates of three grades of graphite[50] at 1340°C. The deposit on a relatively non-graphitic substrate had a finer microstructure than that on a "standard" graphite surface. On high-purity coarse-grained graphite, the deposit was relatively more coarse. Steam pretreatment of the substrate produced an increase in the cone size of pyrolytic graphite. This phenomenon is thought to be the result of increased activity of local sites on the substrate surface. The flexural strength of a laminar composite structure, consisting of alternate layers of pyrolytic zirconium carbide and pyrolytic graphite, was equivalent to that of the stronger component.[51] A carbon-rich alloy of pyrolytic zirconium carbide was four times as strong as pyrolytic graphite.

(E. M. Sherwood)

Ceramic Coatings

A patent[52] has been issued on a method for coating carbon with molybdenum carbide to reduce permeability and improve corrosion and erosion resistance. The technique consists of condensing MoO_3 vapor on the carbon surface and then carbonizing the oxide *in situ* by continued heating in an inert atmosphere.

(B. W. King)

Welding and Brazing

Joining of sintered aluminum products (SAP) tube-to-cap closures is being investigated by

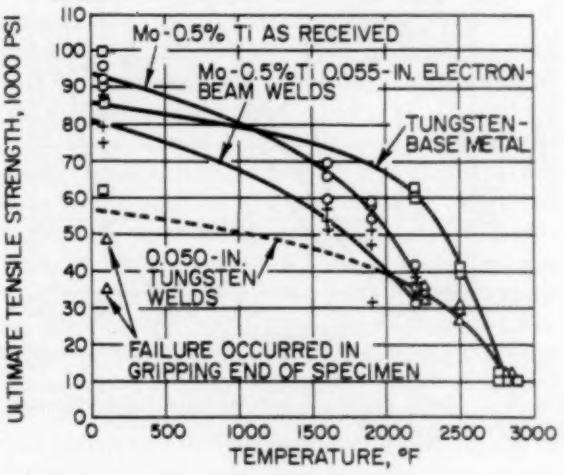

Fig. V-1 Ultimate tensile strength vs. temperature.[55]

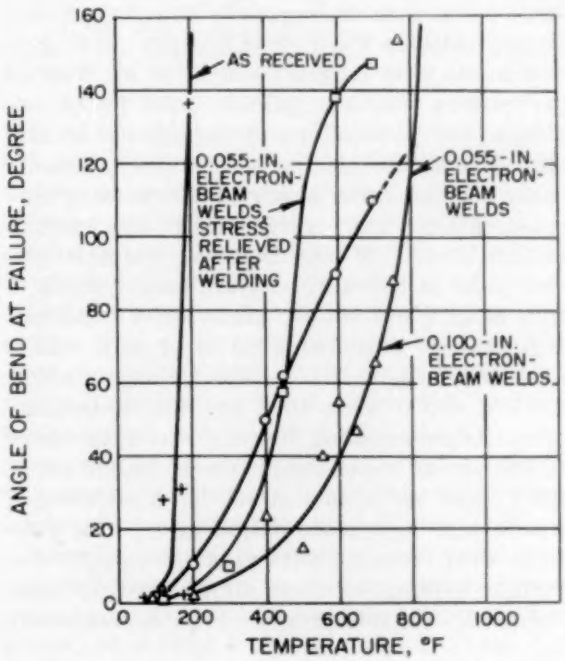

Fig. V-2 Bend angle vs. temperature for 0.005- and 0.100-in. molybdenum–0.5% titanium.[55]

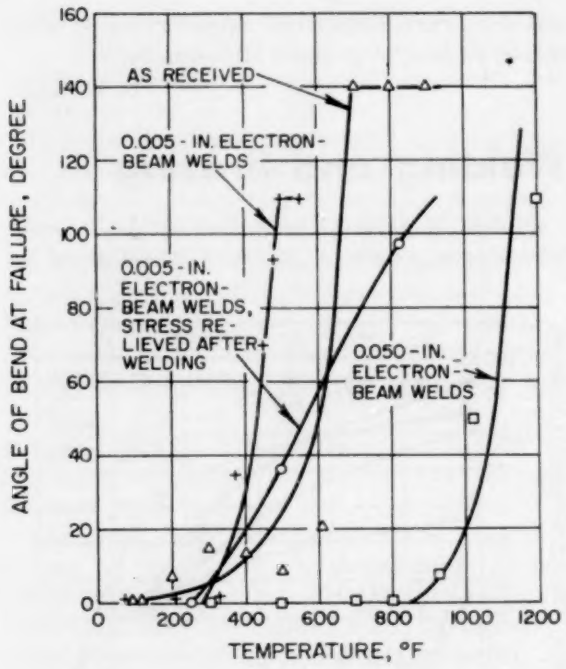

Fig. V-3 Bend angle vs. temperature for 0.005- and 0.050-in. tungsten.[55]

Hanford and Battelle.[16,53] The most successful technique for making such joints has involved the use of magnetic-force butt welding. Welds were made with this process in material containing between 7 and 10 wt.% oxide. So long as continuous and careful control of all welding parameters was maintained, good joints resulted. The parameters of importance include part tolerances, electrode tolerances, cleanliness, and the input power to the welding machine. Alloys that were welded successfully include M-257, M-583, SAP-930, and SAP-895. The room-temperature failure load of joints in alloy M-257, in 0.551-in.-diameter by 0.022-in.-wall tubing, averaged 1430 lb of pull, with a total deviation of 135 lb. The average loads at 200 and 400°C were 1070 and 465 lb, respectively. Corresponding tensile strengths were 38,200 psi at room temperature, 29,200 psi at 200°C, and 12,700 psi at 400°C. A majority of tensile-test specimens failed in the tube material away from the weld area. Attempts to use friction welding on these alloys have not been promising, and this program is being concluded.

The development of joining procedures for Zircaloy components is continuing to provide better methods of fabricating reactor components. Many of these procedures were tested and developed at Hanford specifically for use on some of their newer reactor designs. Thus the information obtained in much of this work applies to Hanford configurations. However, the general techniques being used should be of interest to anyone encountering similar fabrication problems. Techniques used in fabrication of nested tubular fuel elements[54] are conventional, utilizing the tungsten inert-gas process and resistance seam welding to produce the fuel-element closure joints. Assembly of the nested-fuel-element design also required extensive use of tungsten inert-gas-shielded welding.

The general area of refractory-metal joining is of particular interest to many AEC facilities at present. In addition to those programs being supported directly by the AEC, there also are many programs on refractory-metal joining being conducted for other agencies such as the Air Force and the National Aeronautics and Space Administration (NASA). The joining techniques being investigated are quite often restricted in nature because of the specific design requirements of the group supporting or conducting the research.

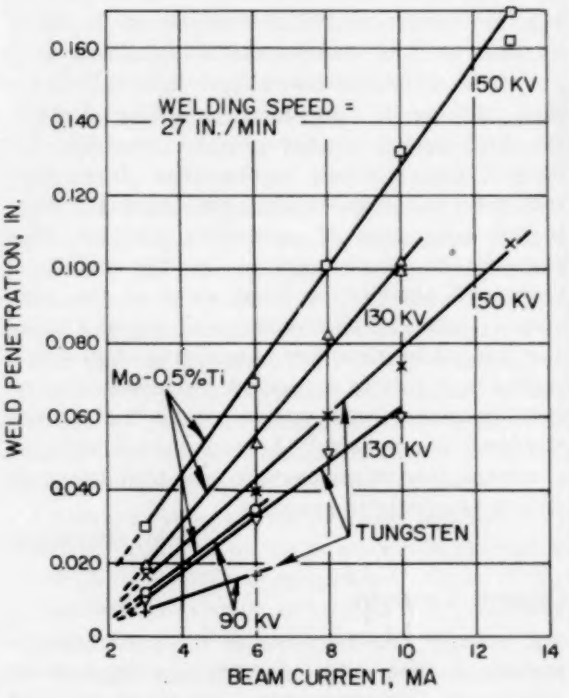

Fig. V-4 Weld penetration vs. current and voltage for electron-beam welds.[55]

Table V-1 BRAZING ALLOYS FOR NIOBIUM AND TUNGSTEN[56]

Base alloy	Braze alloy, wt.%	Brazing temp., °F	Service temp., °F
Nb–1.0 wt.% Zr	Zr–28 V–16 Ti	2250	1800
Nb–1.0 wt.% Zr	Ti–6 Fe–4 Cr	2850	2200
F-48	Ti–30 V	3000	2500
F-48	V–35 Nb	3400	2500
Unalloyed W	Nb–2.2 B	4000	3500
Unalloyed W	Nb–20 Ti	4100	3500

An extensive investigation of high-voltage electron-beam welding techniques for tungsten and molybdenum was recently completed for the Air Force.[55] Emphasis in this program was placed on producing welds of maximum strength and ductility. The effects of welding conditions on welding characteristics also were investigated. Pertinent information on this program is presented in Figs. V-1 to V-4.

A fairly broad investigation of alloy systems for the brazing of niobium and tungsten was completed recently for the Air Force.[58] The alloy systems based on niobium, tantalum, vanadium, titanium, and zirconium were evaluated for melting range, wettability, flow, and metallurgical compatibility with the selected base metal. Brazing alloys identified in this program for various service conditions are shown in Table V-1. (R. E. Monroe)

Explosive Forming

A program is being conducted by Propellex Division of Chromalloy Corporation[57] on the investigation of the explosive-forming characteristics of molybdenum–0.5 wt.% titanium and tungsten, with major emphasis being placed on obtaining strain-rate data. The determination of the effects of explosive forming at 1000°F and the investigation and development of the most suitable transfer medium for obtaining maximum formability are also being studied.

The technique used by Propellex to obtain strain-rate data consists of moving a high-coercive-force permanent magnet concentrically through a shielded inductance coil. The d-c voltage generated is directly proportional to linear velocity. One prime advantage of this device is that, since the permanent-magnet core does not contact the coil, the friction is essentially zero.

During this program, strain-rate data were obtained by attaching the magnetic core to the bottom side of the metal blank by means of a connecting rod that passes through a hole in the die. When the charge is detonated, the blank is forced into the die and the connecting rod pushes the core through the inductance coil. The output voltage from the coil is monitored by means of an oscilloscope, from which a voltage-time trace is recorded photographically. Since the voltage produced is directly proportional to velocity, it is possible to convert the voltage-time trace to a velocity-time trace of the metal blank.

A 4-in.-diameter cup die, 6-in.-diameter metal blanks, and a 6000-lb draw-ring pressure were used during this testing. When the explosive was RDX, the equilibrium strain rate of molybdenum–0.5 wt.% titanium was approximately 60 sec^{-1}, and the maximum velocity of the metal blank through space was approximately 160 ft/sec. Substituting a lower-detonation-velocity explosive (40% dynamite) for the RDX produced improved ductility.

A program to determine the feasibility of achieving mechanical and metallurgical bonding between Zircaloy-2 and type 410 stainless steel by explosive techniques is being conducted at Battelle.[16] Explosive techniques are being employed to bond 6-in.-OD by 3.400-in.-ID by 3-in.-long type 410 stainless-steel tubes to Zircaloy-2 tubes measuring 3.390 to 3.240 in. in outside diameter by 3 in. long, with varying wall thicknesses. Charge configurations and joint designs have been varied during this testing in an effort to produce sound bonds. However, during the initial phases of this program, no bonding of the tubular-component specimens was obtained. This was attributed to the lack of movement in the Zircaloy-2 member of the joint. Clearances between the type 410 stainless steel and Zircaloy-2 and a reduction in the thickness of the Zircaloy-2 were then incorporated into the design. A marked improvement in the integrity of the joint produced was noted, particularly in specimens that were impacted in an evacuated sock of Gooch tubing.

Bend tests and thermal-cycling tests have been conducted on sections of explosively joined straight-joint tubular-component specimens that possessed 0.020- to 0.030-in.-thick Zircaloy-2 members and 0.030- to 0.050-in. clearances between the Zircaloy-2 and type 410 stainless steel. In all cases the specimens could be

bent with the Zircaloy-2 in tension and the type 410 stainless steel in compression to a $\frac{1}{8}$-in. radius without separation of the weld or rupturing of the Zircaloy-2. At a $\frac{1}{16}$-in. radius, however, the Zircaloy-2 ruptured, causing some slight separation in the joint at the point of rupture. The thermal-cycling tests consisted of subjecting sections of the specimens to a total of 1070 heating and cooling cycles ($9\frac{1}{4}$ min/cycle) between 150 and 590°F. A visual examination of the joints of these sections after thermal cycling revealed that no separation had occurred. (C. C. Simons)

Nondestructive Testing

Ultrasonic Techniques

Aeroprojects has been investigating acoustic means of measuring the concentration and relative sizes of particles in gaseous dispersions.[58,59] The particular need arises from current interest in the use of such dispersions as heat-exchange media. Acoustic-propagation characteristics of the gas vary with the loading due to the particles. These changes are detected as variations in the resonant frequency of a column of the particle-laden gas.

It has been shown empirically during investigations of Lamb wave propagation in thin-walled Zircaloy tubing that a 20° entry angle results in the best response. Investigators at Hanford[27] explain this by the theory which says the particle motion in thin specimens is entirely in the direction parallel to the surface for Lamb wave modes with a phase velocity equal to the longitudinal-mode velocity. The angle of entry from water for a Lamb wave with phase velocity equal to the longitudinal velocity in Zircaloy is about 20°. Such a wave experiences less attenuation in the tubing than would other modes, with the result that more energy is available for reflection from defects. Thus the reflected signals from defects can be sufficiently separated (in time) from the confusion of noise signals which exist at the entry point of the ultrasonic beam.

Hanford[15] also reports that ultrasonic attenuation is higher in hydrided than in non-hydrided regions of Zircaloy-2 pipes containing small, highly hydrided spots but that they found no detectable difference between the attenuation in a small Zircaloy-2 plate containing 7000 ppm hydrogen uniformly distributed and one containing no appreciable hydride. They attribute this to large local stresses about the hydrided spot in the pipe, which are not present in the uniformly hydrided plate.

Hanford[30] has been using schlieren techniques and continuous sine-wave ultrasound to study Lamb wave propagation in zirconium and Zircaloy, particularly to obtain V vs. fD curves. Lamb modes are generated in the specimen immersed in water, and their existence is verified by leakage energy in the water which can be observed by schlieren techniques. The optimum entry angle for a particular mode is associated with indications of maximum leakage energy. By this technique Hanford has shown that experimental curves of phase velocity in Zircaloy-2 plate and tubing specimens were consistently higher than the theoretical curves for zirconium, probably because of slight differences in longitudinal and shear velocities in the two materials.

Silicone rubber appears promising as a solid-state material for dry coupling of ultrasonic energy into test materials, according to Oak Ridge.[60] Air pockets are eliminated by pressure or by very small amounts of liquid — various of which are being evaluated.

Oak Ridge has developed a digital-display thickness-measuring apparatus employing immersion pulse-echo techniques.[61] This unit was developed primarily for detecting possible corrosion or erosion of the wall of the vessel comprising the heart of a 5-Mw test reactor. The travel time t between selected pulses and the number of trips k the pulse makes across the wall thickness during the measured interval are determined electronically. With the longitudinal velocity V determined in advance, thickness D is determined electronically by the following relation:

$$D = \frac{tV}{k}$$

The multiplication is performed very rapidly by accumulating a number of measurements equal to V/k. The cumulative measurements are made at the pulse-repetition rate of the generating device, i.e., about 600 pulses/sec. (D. Ensminger)

References

1. Bureau of Mines, Albany Metallurgy Research Center, Metallurgical Progress Report Number

14 for the Period January 1, 1962, to March 31, 1962, USAEC Report USBM-U-921.

2. Ames Laboratory, Iowa State University, Newsletter for Division of Reactor Development, Reactor Materials and Low Decontamination Separations for January 1962, Feb. 19, 1962.
3. H. M. Eickenberry and T. D. Nixon, Consumable-Electrode Arc-Melting of Uranium, USAEC Report NLCO-849, National Lead Co. of Ohio, June 15, 1962.
4. Ames Laboratory, Iowa State University, Newsletter for Division of Reactor Development, Reactor Materials and Low Decontamination Separations for February 1962, Mar. 19, 1962.
5. E. L. Foster, Preparation of Chromium Alloy Specimen by Arc-Melting and Fabrication Techniques, USAEC Report BMI-X-203, Battelle Memorial Institute, June 6, 1962.
6. R. J. Jansen, Hot Rotary Forging of Uranium Tubing, USAEC Report NLCO-842, National Lead Co. of Ohio, May 31, 1962.
7. W. R. Barker, Spinning of Columbium and Columbium–1% Zirconium Tubing, Interim Report, USAEC Report CNLM-3342, Pratt & Whitney Aircraft Div., Jan. 19, 1961.
8. National Research Council, Report of the Subpanel on Consolidation and Fabrication. Refractory Metals Sheet Rolling Panel, Report MAB-179-M, Dec. 1, 1961.
9. J. S. Clark, Columbium and Columbium Alloy Extrusion Program. Phase IV: Development of the Extrusion Operation and Post-Extrusion Conditioning, Report AMC-TR-7-775(V), E. I. du Pont de Nemours & Co., Jan. 16, 1962.
10. P. A. Santoli, Molybdenum Alloy Extrusion Development Program. Fourth Interim Technical Engineering Report, August 15–December 15, 1961, Report ASD-TR-7-785(IV), Allegheny-Ludlum Steel Corp., January 1962.
11. Wah Chang Corp., Tantalum Extrusion Program. Second Interim Report, April 10–August 24, 1961, Report NP-11284.
12. A. McLean-Elrick and H. Lloyd, Planetary Swaging, British Report AERE-R-3907, January 1962.
13. Allis-Chalmers Mfg. Co., Pathfinder Atomic Power Plant, Technical Progress Report, October to December 1961, USAEC Report ACNP-62005, Apr. 20, 1962.
14. S. Goldsmith (Ed.), Plutonium Recycle Program Annual Report, Fiscal Year 1961, USAEC Report HW-70000, Hanford Atomic Products Operation, Aug. 11, 1961.
15. Hanford Atomic Products Operation, Mar. 30, 1962. (Unpublished)
16. R. W. Dayton and R. F. Dickerson, Progress Relating to Civilian Applications During May 1962, USAEC Report BMI-1581, Battelle Memorial Institute, June 1, 1962. (Classified)
17. F. Emonds, The Mechanical and Bonding Processes in the Roll Coating of Aluminum and Its Alloys (in German), *Z. Metallk.*, 52: 615–625 (October 1961).
18. F. W. Albaugh, Reactor and Fuels Research and Development Operation Monthly Report, March 1962, USAEC Report HW-73202A, Hanford Atomic Products Operation, Apr. 15, 1962. (Classified)
19. Hanford Atomic Products Operation, US/UK Research Newsletter No. 13, March 1962.
20. W. Feduska and W. L. Horigan, Diffusion Bonding High-Temperature Alloys with Beryllium, *Welding J. (N. Y.)*, 41: 28s–35s (January 1962).
21. C. L. Angerman, Metallographic Studies of Al-Ni-U Bonds in Nuclear Fuel Elements, *Am. Soc. Metals, Trans. Quart.*, 54: 260–275 (September 1961).
22. R. C. Pugh, Fabrication Quality of HWCTR Driver Tubes, USAEC Report DP-691, E. I. du Pont de Nemours & Co., March 1962.
23. J. C. Tverberg and J. J. Holmes, Extrusion Characteristics of Uranium-Zirconium and Uranium-Carbon Alloys, USAEC Report HW-62347, Hanford Atomic Products Operation, June 1961.
24. F. W. Albaugh, Reactor and Fuels Research and Development Operation Monthly Report, January 1962, USAEC Report HW-72590A, Hanford Atomic Products Operation, Feb. 15, 1962. (Classified)
25. F. W. Albaugh, Reactor and Fuels Research and Development Operation Monthly Report, April 1962, USAEC Report HW-73514A, Hanford Atomic Products Operation, May 15, 1962. (Classified)
26. D. Baker, Jr., Knurling Fuel Tube Surfaces, USAEC Report DP-679, Savannah River Laboratory, February 1962.
27. Hanford Atomic Products Operation, January 1962. (Unpublished)
28. B. E. Murtha and W. P. Chernock, The Development and Testing of UO_2 Fuel Systems for Water Reactor Applications, USAEC Report CEND-152, Combustion Engineering, Inc., Nuclear Div., January 1962.
29. B. E. Murtha and W. P. Chernock, Combustion Engineering, Inc., Nuclear Div., April 1962. (Unpublished)
30. Hanford Atomic Products Operation, Apr. 20, 1962. (Unpublished)
31. Argonne National Laboratory, Reactor Development Program Progress Report, USAEC Report ANL-6525, February 1962.
32. T. C. Cameron and N. F. Hessler, Assembling, Sodium Bonding, and Bond Testing of EBR-II Fuel Rods, *Nucl. Sci. Eng.*, 12(3): 424–431 (March 1962).
33. J. M. Blocher, Jr., and J. H. Oxley, Chemical Vapor Deposition Opens New Horizons in Ceramic Technology, *Am. Ceram. Soc. Bull.*, 41(2): 81–84 (Feb. 15, 1962).
34. Atomics International, Quarterly Technical Progress Report, AEC Unclassified Programs, Octo-

ber–December 1961, USAEC Report NAA-SR-6999, Feb. 2, 1962.

35. L. K. Tower, An Analytical Study of the Continuous Chemical Regeneration of Surfaces, Report NASA-TN-D-1194, National Aeronautics and Space Administration, February 1962.
36. L. W. Owen, Protective Coatings for Uranium, *J. Less-Common Metals*, 4(4): 35–39 (May 1962).
37. E. M. Gold, Simplified Vapor Plating of Tungsten, *Am. Rocket Soc. J.*, 32: 437–438 (March 1962).
38. G. D. Barnett and A. Miller, Oriented Tungsten Deposition, *J. Appl. Phys.*, 33(4): 1505–1508 (April 1962).
39. L. Sama et al., High-Temperature Protective Coatings for Refractory Metals, Parts I and II, paper presented at 6th Meeting of the Refractory Composites Working Group, Dayton, Ohio, June 16–19, 1962, Report TR-62-475.3, June 1962.
40. M. E. Browning, Interim Progress Report No. 2, November 1, 1961, Through February 1, 1962, Deposition for the Production of Structure, American Machine and Foundry Co., Feb. 1, 1962.
41. C. R. Morelock, Sub-Micron Whiskers by Vapor Deposition, *Acta Met.*, 10(2): 161–167 (February 1962).
42. W. J. Metcalfe et al., Attempts To Prepare Pure Beryllium by Thermal Decomposition of the Iodide, British Report O-21/62, February 1962.
43. High Temperature Materials, Inc., Design, Development, and Fabrication of Pyrolytic Tungsten Components, Summary Progress Report, May 26, 1961–Mar. 15, 1962.
44. R. A. Holzl, Physical Properties Obtainable from Thermochemically Formed Refractory Metal Shapes, paper presented at American Rocket Society Conference, Phoenix, Airzona, April 1962.
45. A. Talento, The Growth of Alpha Alumina Whiskers, paper presented at American Ceramic Society, Basic Science Div., Fall Meeting, October 8–10, Schenectady, N. Y., October 1961.
46. S. B. Austerman and A. R. Hopkins, Beryllium Oxide Single Crystal Growth. II. Water Vapor Transport Method, USAEC Report NAA-SR-6420, Atomics International, Nov. 15, 1961.
47. J. A. Marley and T. C. MacAvay, Growth of Stannic Oxide Crystals from the Vapor Phase, *J. Appl. Phys.*, 32(12): 2504–2505 (December 1961).
48. R. Francis, Development of Pyrolytic Refractory Materials for Solid-Fuel Rocket Motor Applications, Report WAL-766.41/3, Arthur D. Little, Inc., Jan. 10, 1962.
49. High Temperature Materials, Inc., Development of Boron Pyralloy for Rocket Motor Hardware, Monthly Progress Report for February 1962, Feb. 28, 1962.
50. J. D. Batchelor et al., Improvement of the Usefulness of Pyrolytic Graphite in Rocket Motor Applications, Quarterly Progress Report, December 1961 Through February 1962, Atlantic Research Corp., Mar. 20, 1962.
51. Raytheon Co., High Temperature Materials Dept., Progress Report, May 1962, High-Temperature Materials Development, June 15, 1962.
52. M. T. Simnad, Method for Forming a Coating of Molybdenum Carbide on a Carbon Body, U. S. Patent 3,028,256 (to USAEC), Apr. 3, 1962.
53. L. E. Mills, Magnetic Force Welding Sintered Aluminum Powder Materials, USAEC Report HW-72379, Hanford Atomic Products Operation, March 1962.
54. M. K. Millhollen, Specifications for Vibrationally Compacted UO_2 Nested Tubular Fuel Element (PRTR Mark II-C), USAEC Report HW-70999, Hanford Atomic Products Operation, December 1961.
55. H. A. Kokanson and W. I. Kern, Electron Beam Welding of Tungsten and Molybdenum, Report ASD-TR-61-461, Hamilton Standard Div., United Aircraft Corp., December 1961.
56. W. R. Young, Alloy Systems for Brazing of Columbium and Tungsten, Report ASD-TR-61-592, General Electric Co., Flight Propulsion Laboratory Dept., January 1962.
57. Chromalloy Corp., A Study of Explosive Forming Selected Refractory Metals, Progress Report No. 4, November 1 Through December 31, 1961, Report NP-11351, Jan. 30, 1962.
58. Aeroprojects, Inc., Applications of Ultrasonic Energy. Task 2: Ultrasonic Metal and Ceramic Powder Processing. Task 3: Ultrasonic Instrumentation, USAEC Report NYO-9584, August 1961.
59. Aeroprojects, Inc., Applications of Ultrasonic Energy. Ultrasonic Instrumentation for Nuclear Applications, USAEC Report NYO-9585, October 1961.
60. Oak Ridge National Laboratory, Apr. 11, 1962. (Unpublished)
61. R. W. McClung and K. V. Cook, Development of Ultrasonic Techniques for the Remote Measurement of the HRT Core Vessel Wall Thickness, USAEC Report ORNL-TM-103, Oak Ridge National Laboratory, Mar. 15, 1962.

Index

Reactor Materials

Volume 5

Included in this issue is the index for Volume 5 of *Reactor Materials*. An index for this quarterly is prepared annually and appears in the final (Number 4) issue. A cumulative index for Volumes 4 to 6 will appear in the November 1963 issue. Here the bold numbers denote issues, and the other numbers denote pages.

A

Adhesive bonds, nondestructive testing, **2**: 75–6
Allen PBX, corrosion by K, **4**: 62
Alloys, alkali-metal corrosion, **4**: 63
Alloys (high-strength), tensile properties, **4**: 72
Alloys (irradiated), property changes, **4**: 68
Alloys (refractory), forging, **3**: 65
Alloys (superlattice) (irradiated), phase transformation, **4**: 6–7
Alloys (supersaturated) (irradiated), phase transformation, **4**: 7
Aluminides, protective coatings for Nb alloys and Ta, **1**: 38
Aluminum, bonding, **1**: 71
  corrosion, **1**: 39, 41; **2**: 43; **4**: 58
  diffusion bonding, **1**: 67
  diffusion in Nb, **4**: 47
  explosive extrusion, **1**: 70
  explosive joining to mild steel, **1**: 71
  extrusion, **1**: 64
  Mn diffusion in, **1**: 58–9
  plating, **3**: 68
  self-diffusion, **1**: 58–9
  slip, **1**: 56
  solubility in Pu, **4**: 23
  U diffusion into, **4**: 21
  U solubility in, **4**: 21
Aluminum (irradiated), annealing, **1**: 44
  damage, **1**: 44; **2**: 49
  dislocations, **2**: 48; **4**: 64
  fission tracks, **3**: 45; **4**: 63–4
  ion range, **2**: 48; **4**: 64–5
  mechanical properties, **1**: 49
Aluminum (molten), reaction, with steam, **2**: 47
  with water, **3**: 43–4
  with water vapor, **1**: 44
Aluminum (sintered), friction welding, **2**: 70
  magnetic-force welding, **4**: 85–6
  technology, **2**: 65–6
Aluminum alloys, corrosion, **2**: 43
  diffusion bonding, **2**: 67–8
  explosive forming, **2**: 71
  grain refinement, **3**: 56
  roll cladding, **4**: 80–1
Aluminum alloys (irradiated), vacancy trapping, **1**: 46
Aluminum alloys (1100), corrosion, **1**: 39; **2**: 43
Aluminum alloys (1100) (irradiated), mechanical properties, **1**: 49
Aluminum alloys (1100)–uranium oxide-fueled glass dispersions (irradiated), stability, **4**: 26–7
Aluminum alloys (2024-T3), overaging, **4**: 70–1
Aluminum alloys (5154), corrosion, **1**: 39
Aluminum alloys (6061), corrosion, **1**: 39; **2**: 43
Aluminum alloys (6063) (irradiated), mechanical properties, **1**: 49
Aluminum alloys (6068), corrosion, **3**: 38
Aluminum alloys (X2219) (irradiated), mechanical properties, **1**: 49
Aluminum alloys (X8001), corrosion, **1**: 39; **2**: 43
  welding, **1**: 72
Aluminum alloys (X8001) (irradiated), mechanical properties, **1**: 49
Aluminum–aluminum oxide dispersions, tensile properties, **2**: 52
Aluminum-calcium-plutonium alloys, aqueous corrosion, **4**: 23
Aluminum-chromium-iron alloys, corrosion, **1**: 40
  explosive forming, **2**: 72
Aluminum-chromium-iron-thorium alloys, oxidation, **4**: 60
Aluminum-chromium-iron-yttrium alloys, corrosion, **1**: 40; **4**: 60
  oxidation, **2**: 44; **4**: 60
  rupture, **1**: 53
  stress oxidation, **1**: 53
  tensile strength, **1**: 53
Aluminum-chromium-niobium-titanium alloys, oxidation, **3**: 40
Aluminum-chromium-rhenium-yttrium alloys, corrosion, **4**: 60
  yield strength, **4**: 72
Aluminum-chromium-silicon mixtures, diffusion coating with, **3**: 70
Aluminum-copper-plutonium alloys, aqueous corrosion, **4**: 23
Aluminum-iron alloys, ductility, **4**: 72–3
Aluminum-iron-nickel alloys, corrosion, **2**: 43
Aluminum-iron-nitrogen systems, cubic nitrides, **3**: 57
Aluminum-magnesium alloys (A-3XA-0) (irradiated), mechanical properties, **4**: 71
Aluminum-magnesium-oxygen system (irradiated), damage bibliography, **1**: 48
Aluminum-magnesium-plutonium alloys, aqueous corrosion, **4**: 23
Aluminum-molybdenum-silicon-uranium system, creep and tensile properties, **1**: 3
Aluminum-molybdenum-tin-zirconium alloys, corrosion, **2**: 46
  electrical resistivity, **4**: 73
  fabrication, **3**: 65
  mechanical properties, **3**: 65
  thermal conductivity, **4**: 73
  welding, **3**: 65, 70–1
Aluminum-molybdenum-uranium alloys, casting, **2**: 65
  creep properties, **1**: 3
  tensile properties, **1**: 3
Aluminum-molybdenum-zirconium alloys, aging and properties, **2**: 53
Aluminum-nickel alloys, aqueous corrosion, **4**: 58
Aluminum-nickel-nitrogen system, cubic nitrides, **3**: 56
Aluminum-nickel-plutonium alloys, aqueous corrosion, **4**: 23
Aluminum-nickel-plutonium alloys (Zircaloy-2-clad) (irradiated), effects, **2**: 8
Aluminum-nickel-titanium alloys, corrosion, **1**: 39–40
Aluminum-nickel-uranium bonds, metallography and quality, **4**: 81
Aluminum-niobium-tin-zirconium alloys, creep properties, **2**: 53
Aluminum-niobium-titanium alloys, oxidation, **1**: 38; **3**: 40
Aluminum-niobium-vanadium alloys, compatibility with UC, **1**: 17
Aluminum-niobium-zirconium alloys, creep properties, **2**: 53
Aluminum oxide, chemical plating with, **1**: 69
  coating with fissionable oxide, **1**: 11
  corrosion, **1**: 41; **4**: 62
  forming with ultrasonic energy, **2**: 74
  fracture analysis, **3**: 59–60
  hot pressing, **2**: 74
  vapor coating with, **3**: 69
Aluminum oxide (irradiated), annealing, **1**: 48
  catalytic activity, **4**: 9
  effects, **4**: 3, 5, 7
  gas absorption, **4**: 9
  gas diffusion, **4**: 10
Aluminum oxide coatings, compatibility with gaseous coolants, **1**: 10
  crushing strength, **1**: 10

Aluminum oxide coatings (Continued)
overcoating with C, 1: 11
oxidation, 1: 10
reaction with C overcoating, 1: 10–11
thermal expansion, 1: 10
Aluminum oxide crucibles, reaction with Mn-Pu-U alloys, 3: 5
Aluminum oxide–magnesium oxide crystals (irradiated), thermal conductivity, 4: 7
Aluminum oxide powder, explosive compaction, 2: 72
Aluminum oxide–rhenium couples, reactions, 3: 59
Aluminum oxide whiskers, vapor deposition, 4: 84
Aluminum-oxygen-uranium system (molten), reaction with water, 4: 21–2
Aluminum-plutonium alloys, corrosion, 1: 5–6
deformation, 1: 6
hardness, 2: 7–8, 10
heat-treatment effects, 1: 6; 2: 8, 10
load-carrying capacity, 1: 6
recrystallization, 2: 7
Aluminum-plutonium alloys (Al-canned), preparation, 4: 83
Aluminum-plutonium alloys (irradiated), deformation, 3: 4
spheroidization, 1: 6
Aluminum-plutonium alloys (S.S.-clad) (irradiated), effects, 4: 23
Aluminum-plutonium-silicon system, aqueous corrosion, 4: 23
Aluminum-plutonium-silicon system (irradiated), deformation, 3: 4
Aluminum-plutonium-uranium alloys, aqueous corrosion, 4: 23
Aluminum-plutonium-zirconium alloys, aqueous corrosion, 4: 23
Aluminum powder (sintered) (irradiated), mechanical and stress-rupture properties, 3: 54
Aluminum powder alloys (M-583) (sintered), friction bonding, 3: 71
Aluminum-silicon system, corrosion, 2: 43
Aluminum-silicon-uranium system, corrosion, 1: 5–6
phase studies, 4: 18
Aluminum-tantalum alloys, corrosion, 2: 47
Aluminum-thorium-uranium alloys (molten), containment, 4: 21
Aluminum-tin-zirconium alloys, aging and tensile properties, 2: 53
Aluminum-titanium-vanadium alloys, explosive extrusion, 1: 71
Aluminum-uranium alloys, corrosion, 1: 5–6
fabrication, 1: 5
phase studies, 4: 20–1
preparation, 3: 3
thermal conductivity, 4: 20
work hardening, 4: 20
Aluminum-uranium alloys (Al-clad), fabrication, 2: 67
U^{235} contamination, 4: 20–1
Aluminum-uranium alloys (Al alloy-clad), coextrusion, 4: 82
Aluminum-uranium alloys (Al alloy-clad) (irradiated), effects, 4: 21
Aluminum-uranium alloys (irradiated), swelling, 3: 3
Aluminum-uranium alloys (molten), reactions with water, 2: 47
Aluminum-uranium compounds, Al diffusion, 2: 4
Aluminum-uranium diffusion couples, annealing and phase-boundary behavior, 3: 3
Aluminum–uranium dioxide dispersions (irradiated), effects, 4: 26
Aluminum–uranium oxide (U_3O_8) dispersions, (irradiated), effects, 3: 3; 4: 26
Aluminum (X8001)–uranium oxide dispersions, welding to Al (X8001), 1: 72
Aluminum-uranium-zirconium alloys, phase studies, 2: 4
Aluminum-zirconium alloys, creep properties, 2: 53
mechanical properties, 2: 53
oxidation, 3: 41
Aluminum-zirconium compounds, corrosion, 2: 42
Arc-melting process, development, 4: 79
Atoms, focusing collisions in chains, 2: 49–50
Azides (irradiated), property changes, 4: 68

B

Barium, diffusion in graphite, 1: 21
Barium-oxygen-uranium system, phase studies, 1: 15; 3: 14
Barium titanate (irradiated), phase transformation, 4: 7
Beryllium, aging, 1: 28–9; 2: 30
annealing, 1: 28; 2: 29
bibliographies, 1: 26; 2: 33–4
brazing, 1: 27; 4: 46
brittleness, 2: 29
casting, 3: 22–3; 4: 44
compatibility with metals and refractories, 3: 25
corrosion, 1: 29; 2: 32, 46; 3: 25–6; 4: 49–50
creep rupture, 3: 25
crystal properties, 1: 28–9
deformation, 1: 26
deoxidation, 1: 64
D_2O effects, 4: 49
diffusion bonding with, 4: 46–7, 81
diffusion in Nb, 4: 47
dislocations, 2: 31
drawing, 1: 27
ductile-brittle transition, 2: 30; 3: 24
ductility, 1: 28–9; 2: 30; 3: 24
dynamic properties, 1: 28
electrical resistivity, 1: 28–9; 2: 31; 4: 45
electrolytic polarization, 3: 25–6
electroplating with, 1: 68
elongation, 1: 28
enthalpy, 3: 24
extrusion, 1: 27; 3: 23; 4: 46
fabrication, 1: 26–7; 2: 28–9; 3: 22–4; 4: 45
fastener properties, 1: 28
fatigue properties, 1: 28
forging, 3: 23
fracture, 1: 26
glide elements, 3: 24
grain size, 4: 44
hardness, 1: 29
heat of fusion, 3: 24
heat-treatment, 1: 28–9
high-temperature stability of beta phase, 3: 24
hot working, 1: 26–7
H behavior in, 2: 31–2
isostatic forming, 3: 23
joining, 1: 27–8
Lorentz ratio, 1: 28; 2: 31
low-temperature properties, 1: 28
lug properties, 1: 28
machining, 1: 27
magnetic properties, 1: 28
mechanical properties, 1: 28–9; 2: 29; 4: 50
melting, 1: 63–4; 3: 24
metallurgy, 1: 27–8
microscopy, 2: 33
notch sensitivity, 1: 28
oxidation, 1: 29
phase transformation, 2: 30–1
physical metallurgy, 2: 29–31; 3: 24; 4: 47–9
physical properties, 1: 28–9; 4: 50
plastic deformation, 2: 33
powder metallurgy, 1: 26
precipitation reaction, 2: 29
pressure welding, 2: 70
production, 3: 22
protective coatings, 2: 33
purity, 1: 26; 3: 22; 4: 44
reaction, 1: 29; 2: 31–2
with CO_2, 1: 29; 2: 31–2
with CO, 1: 29
with UC, 1: 59
with water vapor, 1: 29
rupture, 1: 28
slip casting, 3: 23
specific heat, 3: 24
stress rupture, 3: 25
tensile properties, 1: 26; 2: 29–31; 4: 48–9
tensile strength, 1: 28
thermal conductivity, 1: 28; 2: 31
thermal expansion, 2: 31; 4: 47
thermoelectric power, 1: 28; 2: 31
toxicity, 1: 26; 2: 33; 4: 50
twinning, 1: 28
U diffusion into, 2: 21
vapor deposition, 4: 84
vapor pressure, 3: 28
welding, 1: 27; 2: 29; 3: 23–4
yield, 1: 28
Beryllium (Au-plated), strength, 4: 49
Beryllium (coated), corrosion, 3: 25
Beryllium (irradiated), annealing, 1: 45
bubble formation, 1: 45
damage, 1: 44–5
heavy-ion range, 4: 64–5
H agglomeration, 1: 49
mechanical properties, 2: 31
strength, 3: 27
swelling, 1: 29; 3: 26
thermal conductivity, 4: 49
Beryllium alloys, high-temperature stability of beta phase, 3: 24
production, 3: 22
Beryllium borides, carburization and oxidation, 1: 31
Beryllium-boron system, electrical resistivity, 1: 28
phase studies, 1: 28; 2: 35
Beryllium-calcium-titanium alloys, phase studies, 1: 27
Beryllium chips, processing, 2: 33
Beryllium compounds, with Si and Ta, 1: 30
Beryllium-copper alloys, tensile and yield strength, 1: 28
Beryllium-copper alloys (irradiated), annealing, 1: 45–6; 2: 49
electrical resistivity, 2: 49
Beryllium crystals, tensile properties, 4: 45, 48
Beryllium disease, 2: 33
Beryllium films, properties, 4: 47–8
Beryllium foil, preparation and properties, 4: 44
Beryllium-hafnium alloys, properties, 3: 34
Beryllium hydroxide, purification, 2: 34–5
Beryllium ingots, properties, 2: 30
Beryllium-molybdenum-nickel alloys, phase studies, 1: 28
Beryllium-molybdenum-uranium alloys, tensile properties, 1: 3
Beryllium-nickel alloys, high-temperature stability of beta phase, 3: 24
phase studies, 1: 28
Beryllium-nickel-tungsten alloys, phase studies, 1: 28
Beryllium oxide, bibliography, 1: 26, 30
chemical plating with, 1: 69
chemical plating with W, 1: 68
coating with fissionable oxide, 1: 11
compatibility with Mo, Nb, and W, 3: 40

Beryllium oxide (Continued)
compatibility with W crucibles, 3: 28
corrosion by K, 4: 62
creep, 2: 34
crystal properties, 1: 30
crystallization, 3: 27
decrepitation, 2: 34
D_2O effects, 4: 49
diffusion in graphite, 1: 21
elasticity, 1: 30
foamed ceramics, 2: 35
hot pressing, 2: 74
lattice parameters, 1: 30
O diffusion, 1: 30
phase transformation, 3: 27
Poisson's ratio, 1: 30
refractive index, 4: 50
strength, 1: 30
synthesis, 3: 27
thermal properties, 1: 30
Beryllium oxide (irradiated), annealing, 4: 8
effects, 2: 35; 3: 28, 46; 4: 3–8, 50, 66, 68
Beryllium oxide (translucent), fabrication and properties, 2: 34
Beryllium oxide crucibles, reaction with Mn-Pu-U alloys, 3: 5
Beryllium oxide crystals, growth, 2: 34
vapor deposition, 4: 84–5
Beryllium oxide-foamed ceramics, development, 3: 60
thermal conductivity, 4: 50–1
Beryllium oxide–molybdenum couples, reactions, 3: 59
Beryllium oxide–niobium couples, reactions, 3: 59
Beryllium oxide powder, explosive compaction, 2: 73
production, 3: 27
Beryllium oxide–rhenium couples, reactions, 3: 59
Beryllium oxide–tungsten composite, chemical plating with W, 2: 69
Beryllium oxide–tungsten couples, reactions, 3: 59
Beryllium oxide–uranium dioxide ceramics, dissolution, 3: 27–8
Beryllium oxide–uranium dioxide compacts (irradiated), effects, 4: 5–6
Beryllium oxide–uranium dioxide pellets (irradiated), effects, 1: 15
Beryllium oxide–uranium fuels (irradiated), thermal conductivity, 4: 8
Beryllium-oxygen-thorium-uranium system, phase studies, 2: 19
sintering, 3: 28
Beryllium-oxygen-tungsten system, chemical plating with W, 1: 68
coating with W, 3: 69
Beryllium-plutonium alloys, preparation, 3: 5
Beryllium powder, explosive compaction, 2: 73
metallurgy, 1: 26
Beryllium sheet, grain refinement, 3: 24
mechanical properties, 4: 45–6
tensile properties, 3: 24; 4: 45
Beryllium-silicon-tantalum system, phase studies, 1: 30
Beryllium-thorium alloys, phase studies, 4: 25
Beryllium-thorium-uranium alloys, structure, 4: 51
Beryllium tubing, ductility, 2: 31
fabrication, 4: 46
heat-treatment, 2: 31
rupture, 4: 46
texture, 3: 24
Beryllium tubing (irradiated), stress-rupture properties, 4: 49, 70
Beryllium wire, drawing, 3: 23
Beryllium-zirconium alloys, braze corrosion, 2: 70
brazing with, 2: 70; 3: 71
Beryllium-zirconium compounds, corrosion, 2: 42
Biotite (irradiated), fission tracks, 1: 46
Bismuth (molten), corrosive effects, 2: 47
Bismuth-lead alloys, corrosion of steel, 2: 46
Bismuth-thorium-uranium alloys, dissolution mass transfer, 3: 7–8
Boron, chemical plating with, 1: 69
melting, 1: 64
Boron (irradiated), heavy-ion range, 4: 64–5
Boron carbide (irradiated), effects, 3: 34
He release, 3: 34; 4: 55–6
Boron carbide (sintered) (Zr-clad), radiographic testing, 2: 76
Boron carbide burnable-poison plates (irradiated), dimensional changes, 1: 36
Boron carbide dispersions [S.S.(347)-clad] (irradiated), effects, 1: 10
Boron carbide–graphite compacts (irradiated), dimensional changes and strength, 3: 36
Boron carbide–nickel dispersions, properties, 4: 55
Boron carbide–nickel dispersions (irradiated), stability, 4: 55
Boron carbide–silicon carbide compacts (irradiated), He release, 4: 55–6
Boron carbide–silicon carbide plates (irradiated), dimensional changes, 1: 36
He release, 3: 34
Boron-carbon-lithium system, 3: 35
Boron-carbon-niobium-titanium-vanadium system, tensile properties, 2: 53
Boron-carbon system, melting, 1: 64
phase studies, 2: 40
Boron-chromium-silicon mixtures, diffusion coating with, 3: 70
Boron-copper system (irradiated), dimensional changes and stored energy, 2: 50
Boron-graphite system, chemical deposition, 4: 85
Boron-iron absorber sections (irradiated), swelling, 1: 36
Boron-iron system (irradiated), effects, 3: 34–5
Boron-lithium-oxygen system, glass formation, 2: 19
Boron-niobium-titanium-vanadium system, stress-rupture and tensile properties, 2: 53
Boron nitride, applications, 3: 69
chemical deposition, 2: 69
Boron oxide–stainless steel–uranium dioxide dispersions, poison-containing fuel-plate applications, 3: 36
Boron-oxygen-uranium system, glass formation, 2: 19
Boron silicide, properties, 2: 40
Boron-silicon system, melting, 1: 64
Boron–stainless steel alloys (irradiated), dimensional changes, 1: 36
effects, 3: 34–5
Boron–stainless steel dispersions, B loss, 1: 36
Boron-tungsten coatings, preparation, 3: 70
Brass, diffusion bonding, 1: 66–7
Brass (70/30), extrusion, 1: 64
Brass (alpha) (irradiated), diffusion, 4: 9
Brazing, 2: 69–70

C

Cadmium-copper alloys (irradiated), annealing, 1: 45–6; 2: 49
electrical resistivity, 2: 49
Cadmium-europium-silver alloys, reactor-control properties, 2: 40
Cadmium-plutonium alloys, density and stabilization, 2: 6–7
Cadmium-uranium alloys, phase diagram, 2: 3
Calcium fluorides, densification, 2: 75
sintering, 3: 59
Calcium fluorides (irradiated), effects bibliography, 1: 48
Calcium hydride, creep, 2: 36
density, 2: 36
H content, 3: 28
Calcium oxide, reaction, with Mn-Pu-U alloy, 3: 5
with U_3O_8, 4: 35
Calcium oxide–uranium dioxide–zirconium dioxide dispersions (irradiated), dimensional changes, 4: 5
Calcium-oxygen-uranium-zirconium system, phase studies, 1: 15–16
preparation, 1: 15
thermal properties, 1: 15–16
Calcium vanadate, reaction with U_3O_8, 4: 35
Carbides, emittance, 4: 75
review, 4: 74–5
Carbides (cemented), emittance, 4: 75
Carbides (refractory), joining to refractory metals, 4: 75
Carbon
See also Graphite
chemical plating graphite with, 1: 68
deposition kinetics, 2: 15
diffusion into S.S.(304), 2: 20–1
permeability, 4: 43
physical properties, 4: 43–4
tensile strength, 4: 43
Carbon (irradiated), heavy-ion range, 4: 64–5
Carbon (Mo carbide-coated), protective properties, 4: 85
Carbon (pyrolytic)
See also Graphite (pyrolytic)
chemical deposition, 2: 69; 3: 69
Carbon-chromium-titanium-yttrium-zirconium system, corrosion, 4: 60
Carbon-chromium-uranium system, behavior, 3: 17
phase studies, 2: 20
Carbon coatings, on Al_2O_3, 1: 10–11
density, 1: 12
Carbon (pyrolytic) coatings, density, 2: 15
Carbon-cobalt-uranium system, phase studies, 2: 20
Carbon-copper-uranium system, behavior, 3: 17
phase studies, 2: 20
Carbon dioxide, compatibility with reactor materials, 2: 46
Carbon-hafnium system, phase studies, 2: 40
Carbon-hafnium-uranium system, phase studies, 2: 20
Carbon-iron-uranium system, behavior, 3: 17
eutectic, 3: 17
phase studies, 2: 20
Carbon-metal-uranium systems, properties, 3: 17
Carbon-metal (transition)-uranium systems, phase studies, 2: 20
Carbon-molybdenum-niobium-titanium-zirconium system, strength, 3: 56
Carbon-molybdenum-titanium-zirconium system, strength, 3: 56
Carbon-molybdenum-tungsten-zirconium system, forgeability and recrystallization, 3: 65
strength, 3: 56
Carbon-molybdenum-uranium system, phase studies, 4: 35
Carbon-nickel-uranium system, phase studies, 2: 20
Carbon-niobium-titanium-vanadium system, stress-rupture and tensile properties, 2: 53
Carbon-niobium-uranium system, melting-point curve, 1: 17
phase studies, 2: 20
Carbon-plutonium system, phase studies, 4: 24–5

Carbon-plutonium-uranium system, phase studies, 2: 20
Carbon (pyrolytic)-silicon coatings, strength, 2: 15
Carbon-tantalum system, corrosion, 2: 47
Carbon-tantalum-tungsten system, tensile properties, 2: 53
Carbon-tantalum-uranium system, phase studies, 2: 20
Carbon-thorium-uranium system, oxidation, 2: 11
Carbon-uranium system, C diffusion into S.S.(304), 2: 20–1
electrical resistivity, 4: 36
extrusion, 4: 82
high-temperature properties, 2: 21
oxidation, 3: 16
phase studies, 2: 21
thermal expansion, 2: 21
U diffusion into metals and alloys, 2: 21
vapor pressure, 2: 21
Carbon-uranium system (irradiated), cracking and Kr^{85} release, 4: 36
Carbon-uranium-zirconium system, casting, 1: 19
electrical resistivity, 3: 16
lattice parameters, 1: 17
melting-point curve, 1: 17
phase studies, 2: 20
physical properties, 4: 36
reaction with metals, 4: 36
thermionic emission, 3: 16
Carpenter 20Nb, corrosion, 1: 41
Ceramic coatings, physical properties of flame-sprayed, 3: 70
Ceramic oxides, hot-pressing, 2: 74
Ceramics, bonding to metals, 2: 75
chemical plating with, 4: 83–4
chemical plating with Ti and Zr, 1: 68
coating applications, 2: 75
coating Y with, 1: 69–70
corrosion by molten Mn-Pu-U alloys, 4: 23
emittance, 4: 75
sealing to metals, 3: 70
vapor coating with Al_2O_3, 3: 69
Ceramics (irradiated), annealing, 4: 10
effects, 2: 50; 4: 1–10, 68
H_2 diffusion, 1: 58
Cerium, diffusion in graphite, 1: 21
Cerium-cobalt-plutonium alloys (molten), corrosion of Ta, 4: 22–3
reactions with crucibles, 3: 4–5
viscosity, 3: 5
Cerium dioxide, densification, 2: 75
Cerium hydride, H content, 3: 28
heat of dissociation, 4: 52
structure, 4: 52
Cerium-oxygen-uranium system, thermal shock, 1: 16
Cerium-thorium alloys, phase studies, 4: 25
Cermets, electroplating with, 1: 67–8
Cesium, diffusion in graphite, 1: 21
Cesium (molten), corrosion by, 4: 63
Chromalloy W-2, analysis, 2: 45
Chromium, annealing, 2: 52
chemical plating with, 1: 69
chemical plating with oxides and silicides, 2: 69
corrosion, 1: 41
diffusion in Ni alloys, 1: 59
electron-beam zone refining, 4: 79
electroplating with, 1: 67
self-diffusion, 1: 59
solubility in Li, 1: 42
tensile properties, 2: 52
vapor deposition, 3: 9
Chromium borides, deposition, 2: 69
Chromium cermets, deposition, 2: 68–9
Chromium crystals, preparation, 4: 79
Chromium-hydrogen-yttrium system (Al-Cr-Fe alloy clad), H loss in air, 3: 30
thermal-mechanical stability, 3: 30–1
Chromium-iridium-molybdenum combinations, interdiffusion, 2: 61
Chromium-iron alloys, stress-corrosion cracking, 2: 43
Chromium-iron-molybdenum alloys, oxidation, 3: 38
Chromium-iron-molybdenum-nickel alloys, mechanical properties, 3: 54–5
stress corrosion, 2: 43; 3: 41
Chromium-iron-nickel alloys, electroplating, with Cr, 1: 67
oxidation, 3: 38
stress-corrosion cracking, 2: 43
Chromium-iron-plutonium alloys, hardness and heat-treatment, 3: 5
Chromium-molybdenum-nickel alloys, oxidation, 3: 38
Chromium-molybdenum-niobium alloys, phase studies, 1: 56
Chromium-molybdenum-rhenium combinations, interdiffusion, 2: 61
Chromium-molybdenum-uranium alloys, grain size, 2: 3
phase studies, 4: 18
Chromium-nickel alloys, stress-corrosion cracking, 2: 43
Chromium-niobium alloys, creep properties, 1: 53, 55
Chromium-niobium-titanium alloys, oxidation, 3: 40
Chromium-rhenium couples, interdiffusion, 2: 61
Chromium-rhenium-yttrium alloys, oxidation, 2: 46
Chromium-ruthenium alloys, phase studies, 3: 57
Chromium silicides, deposition, 2: 69
Chromium-silicon-titanium mixtures, diffusion coating with, 3: 70
Chromium systems, diffusion, 1: 58
Chromium-TZC alloy, yield strength, 4: 72
Chromium-uranium alloys, grain size, 2: 3; 4: 17–18
heat-treatment, 2: 3; 3: 2
substructure, 3: 2
Chromium-uranium-zirconium alloys, grain size, 2: 3
Chromium whiskers, vapor deposition, 4: 84
Chromium-yttrium alloys, corrosion, 4: 60
preparation, 4: 79
tensile strength, 4: 72
Chromium-zirconium alloys, H absorption, 2: 42
Chromium-zirconium intermetallic compounds, corrosion, 2: 42; 4: 52–3
Cobalt, deoxidation, 1: 64
melting, 1: 64
Cobalt alloys, corrosion, 1: 40
diffusion bonding, 4: 46–7, 81
Cobalt-copper alloys (irradiated), displacement spike detection, 4: 65–6
Cobalt-hafnium intermetallic compounds, hydriding, 4: 52–3
Cobalt-nitrogen-zinc system, cubic nitrides, 3: 56
Cobalt-thorium intermetallic compounds, hydriding, 4: 52–3
Copper, diffusion bonding to Au, 1: 67
electroplating U oxide with, 1: 68
extrusion, 1: 64
plating, 3: 68
pressure bonding, 1: 66
stable equilibrium configuration, 2: 49
thermal diffusion, 2: 60
Copper (irradiated), annealing, 1: 45–6; 2: 49; 4: 64
characteristic temperature, 2: 48
damage, 2: 49
defect clusters, 4: 66–7
diffusion, 4: 9
dislocation loops, 2: 48, 50; 3: 45
electrical resistivity, 2: 48–9; 4: 64
etching, 3: 45
focusing collisions in atom chains, 2: 50
hardness, 2: 48
multiple thermal points, 2: 50
quenching, 2: 50
threshold energy, 2: 48
vacancy formation energy, 3: 47
Copper (sputtered), reactor-radiation-damage monitor, 1: 48
Copper-molybdenum-zirconium alloys, oxidation and O diffusion in, 4: 57
Copper-silver alloys, brazing with, 2: 75
Copper-silver alloys (irradiated), annealing, 1: 45–6; 2: 49
electrical resistivity, 2: 49
Copper tubing, ultrasonic drawing, 3: 65
Copper-tungsten-zirconium alloys, H absorption, 2: 42
Copper-uranium alloys, oxidation, 2: 3
Copper whiskers, vapor deposition, 4: 84
Copper-zinc alloys (irradiated), irradiated Zn diffusion in, 1: 46
Copper-zirconium alloys, H absorption, 2: 42
Copper-zirconium compounds, corrosion, 2: 42
Core vessel, ultrasonic testing, 4: 88
Croloy, corrosion, 4: 59, 63
Croloy-titanium alloys, corrosion, 4: 63
Crucibles, coating for graphite, 2: 65
Crud deposition, 2: 43
Crystals (irradiated), defect study, 1: 48
effects, 4: 67–8
Crystals (ionic) (irradiated), effects, 1: 48
vacancy-pair mobility, 3: 47
Crystals (nonmetallic) (irradiated), chemical physics, 3: 47

D

Diamond (irradiated), displacement threshold energy, 4: 66
Disilicide coatings, corrosion, 4: 61–2
Dispersions (irradiated), effects, 2: 12
Dysprosium, corrosion, 4: 55
fabrication, 1: 64

E

Eddy-current testing, development, 1: 73–4
thickness of materials, 2: 76
Electromagnetic testing, development, 1: 73
Electron microscope, ion damage to metal films inside, 2: 49
Enrico Fermi Atomic Power Plant, fuel development, 1: 4
Erbium, corrosion, 4: 55
fabrication, 1: 64
Europium, fabrication, 1: 64
reactor-control properties, 2: 40
Europium alloys, reactor-control properties, 2: 40
Europium monoxide, preparation, 4: 56
Europium oxide dispersions, development, 3: 35
Europium oxide–iridium dispersions, development, 4: 56
Europium oxide–molybdenum dispersions, hydriding, 4: 56
Europium oxide–niobium dispersions, hydriding, 4: 56
Europium oxide–palladium dispersions, development, 4: 56
Europium oxide–platinum dispersions, development, 4: 56
Europium oxide–rhenium dispersions, hydriding, 4: 56

Europium oxide–rhodium dispersions, development, **4**: 56
Europium oxide–stainless steel dispersions, corrosion, **3**: 36
poison applications, **3**: 35
Europium oxide–stainless steel dispersions (irradiated), effects, **1**: 36
Europium oxide–tantalum dispersions, hydriding, **4**: 56
Europium oxide–tungsten dispersions, hydriding, **4**: 56
Europium titanate–stainless steel dispersions, fabrication, **2**: 40
Experimental Breeder Reactor II, fuel-element Na bonding, **2**: 68; **4**: 83

F

Fecral (irradiated), tensile properties, **4**: 68–9
Fiberglas (U_3O_8-bearing), development for fuel elements, **2**: 11–12
Fissium-uranium alloys, phase studies and thermal properties, **1**: 2
Fluorophlogopite (irradiated), fission tracks, **1**: 46
Formvar (irradiated), ionization, **4**: 66
Forsterite (irradiated), mechanical properties, **4**: 5
Fuel elements, metal spraying, **2**: 70
nondestructive testing, **2**: 75; **3**: 75
welding, **2**: 70
Fuel particles (C-coated), properties, **4**: 29
Fuel particles (ceramic-coated), costs, **4**: 28
Fuel powders, magnetic testing of Fe contamination, **3**: 75
Fuel wafers, C-coating thickness gauge, **3**: 75
Fuels, pelletizing, **2**: 15
pressure bonding, **1**: 65
Fuels (Al_2O_3-coated), preparation, **3**: 9–10
Fuels (BeO-coated), preparation, **3**: 9
Fuels (ceramic-coated), **2**: 13
Fuels (clad), ultrasonic welding, **2**: 67
Fuels (coated-particle), preparation, **3**: 8–14
Fuels (metal-coated), **2**: 13
Fuels (MgO-coated), preparation, **3**: 9
Fuels [S.S.(304)-clad], Na bonding, **2**: 68

G

Gadolinium, corrosion, **4**: 55
fabrication, **1**: 64
Gadolinium oxide–niobium dispersions, production, **2**: 40
Gadolinium–stainless steel (304) alloys, phase studies, **1**: 35
Gaseous dispersions, ultrasonic particle measurement, **4**: 88
Germanium (irradiated), effects, **3**: 46
Glass (borated), preparation and strength, **1**: 36
Glass (borosilicate), poison applications, **1**: 35–6
Glass (inorganic) (irradiated), effects bibliography, **1**: 48
Glass (irradiated), corrosion by chlorides, **4**: 60
Glass (poisoned), fabrication, **2**: 40
Glass (Pu-bearing), strength, **2**: 10
Glass (rare-earth oxide), devitrification, **1**: 36
Glass (Si) (irradiated), damage, **1**: 47
Glass–plutonium dioxide fibers, **1**: 7
Gold, diffusion bonding to Cu, **1**: 67
electroplating U oxide with, **1**: 68
thermal diffusion, **2**: 60
Gold (irradiated), effects, **1**: 44; **2**: 49; **3**: 45; **4**: 64–6
Gold films (irradiated), damage, **2**: 49; **3**: 45
structure, **4**: 65
Gold-plutonium alloys, phase studies, **1**: 6; **2**: 8
Gold whiskers, vapor deposition, **4**: 84
Graphite
See also Carbon
C transport, **4**: 43
chemical plating of, **1**: 68; **2**: 69
chemical plating with, **1**: 68–9
coating for, **3**: 70
corrosion, **1**: 41
diffusion studies, **1**: 21
electroplating with Cr cermets, **2**: 68–9
emittance, **4**: 75
fission-product release, **1**: 21
impregnation, **2**: 37
with Si and Ti, **1**: 25
oxidation, **3**: 31
oxidation inhibition by Cl, **1**: 25
reaction with steam, **4**: 43
strength, **3**: 31
Graphite (irradiated), annealing, **1**: 47; **2**: 50; **4**: 8, 10
cavities, **1**: 48
chemical reactivity, **4**: 8–9
damage, **2**: 36–7; **3**: 46
dimensional changes, **1**: 25–6; **2**: 36–7; **3**: 45–6; **4**: 3–4
electrical resistivity, **1**: 47
electron microscopy, **4**: 43
He permeability, **2**: 36
internal energy, **1**: 48
lattice constants, **1**: 48
lattice defects, **1**: 47; **3**: 45
mechanical properties, **4**: 5–6
microstructure, **4**: 43
oxidation inhibition by Cl, **1**: 25
spin resonance, **1**: 47
stored energy, **1**: 47; **2**: 37; **3**: 45–6; **4**: 68
thermal conductivity, **4**: 8
Graphite (PuO_2-impregnated) (irradiated), effects, **3**: 6
Graphite (pyrolytic)
See also Carbon (pyrolytic)
annealing, **1**: 25
deposition, **3**: 69; **4**: 85
properties, **3**: 69
rocket-nozzle component fabrication, **3**: 69
strength, **4**: 85
structure, **1**: 25
Graphite (pyrolytic)–metal (refractory) "alloys," chemical plating and preparation, **3**: 69
Graphite (pyrolytic)–zirconium carbide (pyrolytic) laminates, flexural strength, **4**: 85
Graphite (Si-impregnated), permeability, **1**: 25
Graphite (Si-SiC coated) (irradiated), oxidation, **1**: 25
Graphite (Ti-impregnated), permeability, **1**: 25
Graphite-molybdenum couples, reactions, **3**: 59
Graphite-molybdenum system, chemical deposition, **4**: 85
Graphite powder, explosive compaction, **2**: 73
Graphite–stainless steel (304L) couples, interdiffusion, **3**: 58
Graphite-tantalum couples, reactions, **3**: 59
Graphite-tungsten system, chemical deposition, **4**: 85
Graphite-uranium mixtures, cold-compacting and sintering, **3**: 17

H

Hafnium, corrosion, **2**: 40
hardness, **2**: 65
heat of vaporization, **4**: 55
melting, **1**: 64; **2**: 65; **3**: 64; **4**: 79
production, **1**: 63
purification, **2**: 65; **4**: 79
scaling, **2**: 40–1
Hafnium alloys, corrosion, **3**: 34
Hafnium carbide, compatibility, with H_2, **1**: 58
with Mo, **3**: 40
with Nb, **3**: 40
with W, **1**: 58; **3**: 40
pyrolytic deposition, **3**: 69
UC behavior with, **1**: 17
Hafnium diboride, compatibility with H_2 and W, **1**: 58
vaporization, **4**: 55
Hafnium-iridium alloys, phase studies, **4**: 55
Hafnium-iron-tantalum alloys, corrosion, **3**: 34
Hafnium-lutetium alloys, corrosion, **3**: 34
Hafnium-manganese intermetallic compounds, hydriding, **4**: 52–3
Hafnium monocarbide, preparation, **3**: 64
reaction with Ce-Co-Pu alloy, **3**: 4–5
Hafnium monocarbide–molybdenum couples, reactions, **3**: 59
Hafnium-niobium-tungsten alloys, weld strength, **2**: 70
Hafnium-niobium-vanadium alloys, tensile properties, **2**: 53
Hafnium-niobium-zirconium alloys, weld strength, **2**: 70
Hafnium nitride, compatibility with H_2 and W, **1**: 58
Hafnium-oxygen-tungsten system, tensile properties, **2**: 53
Hafnium-plutonium alloys, density and stabilization, **2**: 6–7
Hafnium systems, diffusion, **1**: 58
Hafnium-tantalum alloys, corrosion, **2**: 47; **3**: 34
Hafnium-tungsten alloys, corrosion, **3**: 34
Hafnium-vanadium alloys, phase studies, **4**: 55
Halides, chemical plating with, **1**: 69
Halides (alkali) (irradiated), effects, **1**: 48; **4**: 68
Halides (metal), chemical plating with, **1**: 69
Hastelloy (irradiated), stress-rupture properties, **4**: 69
Hastelloy B (irradiated), corrosion, **4**: 60
Hastelloy C, corrosion, **1**: 40
Hastelloy C (irradiated), corrosion, **4**: 60
Hastelloy X, corrosion, **1**: 40; **3**: 39; **4**: 60, 62
mechanical properties, **3**: 54–5
oxidation, **4**: 60
stress-rupture properties, **3**: 55
Hastelloy X (irradiated), ductility, **4**: 69
Haynes 25, corrosion, **1**: 41–2; **3**: 41; **4**: 62–3
Haynes Stellite powders, explosive compaction, **2**: 73
Holmium, corrosion, **4**: 55
Holmium-thorium alloys, phase studies, **4**: 26
properties, **3**: 7
Hydrogen-niobium-vanadium system, tensile properties, **2**: 53
Hydrogen-zirconium system, phase studies, **2**: 35–6

I

Inconel, brazing, **3**: 71
carburization, **1**: 40
compatibility, with fluoride salts, **3**: 41
with LiH, **2**: 36
corrosion, **1**: 40–3; **4**: 59
Cr self-diffusion in, **1**: 59
ductility, **1**: 53
elasticity, **1**: 53

Inconel (Continued)
electroplating with Cr, 1: 67
oxidation, 4: 60
stress-corrosion, 3: 39
tensile properties, 1: 53
thermal cycling, 1: 52–3
Inconel (irradiated), properties, 1: 49; 2: 50–1; 3: 50; 4: 69
Inconel 702, oxidation, 4: 60
Inconel X, corrosion, 4: 60
mechanical properties, 3: 54–5
U diffusion into, 2: 21
Inconel X (irradiated), stress-rupture and tensile properties, 3: 49–50
Indium-thorium alloys, fabrication, 1: 9
hardness, 1: 8
INOR-8, carburization, 1: 40
compatibility with fluoride salts, 3: 41
Cr self-diffusion in, 1: 59
specific heat, 3: 57
strain-fatigue properties, 3: 55
Intermetallic compounds, hydriding, 1: 32; 2: 36; 4: 52–3
Invar (irradiated), dimensional changes, 1: 49
Iodine, diffusion, 1: 21; 3: 18
Ion bombardment, symposium, 4: 68
Iridium, compatibility with UO_2, 4: 34
corrosion, 3: 39
dimensional changes, 1: 40
oxidation, 1: 40; 2: 46
Iridium-palladium alloys, structure and X-ray diffraction analysis, 4: 74
Iridium-tungsten base-barrier combination, properties, 3: 58
Iron, corrosion, 1: 39–40, 42–3
self-diffusion in Fe-Ni alloys, 1: 59
solubility in Li, 1: 42
vapor deposition, 2: 69
Iron (irradiated), annealing, 1: 46; 2: 48
characteristic temperature, 2: 48
coercive force, 1: 46
damage, 1: 46; 2: 49
electrical resistivity, 2: 48; 4: 68
hardness, 2: 48
magnetic properties, 1: 46
mechanical properties, 2: 48
threshold energy, 2: 48
Iron alloys, cracking, 1: 53
diffusion bonding, 4: 46–7, 81
Iron-molybdenum alloys, phase studies, 1: 56
Iron-molybdenum-nickel-ruthenium-tungsten alloys, mechanical properties, 3: 56
oxidation, 2: 45
Iron-molybdenum-plutonium alloys, hardness and heat-treatment, 3: 5
Iron-nickel alloys, Fe self-diffusion in, 1: 59
Iron-nickel alloys (irradiated), annealing, coercive force, and ordering, 1: 46
Iron-nickel-tungsten alloys, creep-rupture strength, 2: 52
mechanical properties, 3: 56
Iron-niobium alloys, phase studies, 1: 56
Iron-nitrogen-zinc system, cubic nitrides, 3: 57
Iron oxides (Fe_3O_4), deposition, 2: 43
Iron oxides (Fe_2O_3) (irradiated), dissolution, 4: 9
Iron-oxygen-plutonium system, phase studies, 2: 10
Iron-plutonium alloys, corrosion of Ta, 2: 46–7
hardness, 2: 6; 3: 5
heat-treatment, 2: 6; 3: 5
impact properties, 2: 5–6
microcracking, 2: 6
microstructure, 2: 6
rolling, 4: 23
tensile properties, 2: 6
Iron-silicon-uranium system, grain size, 2: 3
Iron whiskers, vapor deposition, 4: 84
Iron-zirconium alloys, H absorption, 2: 42
Iron-zirconium compounds, corrosion, 2: 42

K

Kennametal 94, corrosion by K, 4: 62
Kovar, corrosion, 1: 41
Krypton-85, diffusion, 3: 18

L

Lanthanum, diffusion in graphite, 1: 21
Lead, extrusion, 1: 64
reaction with UC, 4: 36
Lead (irradiated), annealing, 2: 50
Lead-thorium alloys, phase studies, 4: 25
Lithium, solubility of metals in, 1: 42
Lithium (molten), corrosion by, 4: 63
Lithium fluoride (irradiated), annealing, 2: 49
dislocations, 2: 49
surface effects, 4: 66
Lithium hydride, compatibility with Inconel, 2: 36
corrosion of S.S., 1: 31–2
thermal conductivity, 1: 32
viscosity, 1: 31
Lithium hydride (irradiated), effects, 4: 52
Lithium-niobium-oxygen system, reactions, 3: 41, 43

M

M257
See Aluminum–aluminum oxide dispersions
Magnesium, corrosion by, 4: 62
Magnesium (irradiated), annealing, 1: 49
Magnesium oxide, coating with fissionable oxide, 1: 11
compatibility with Mo, Nb, and W, 3: 40
internal friction, 4: 75
slip casting, 2: 74
Young's modulus, 4: 75
Magnesium oxide (irradiated), dimensional changes, 4: 3
Magnesium oxide crucibles, reaction with Mn-Pu-U alloy, 3: 5
Magnesium oxide–molybdenum couples, reactions, 3: 59
Magnesium oxide–molybdenum-tungsten couples, reactions, 3: 59
Magnesium oxide–niobium couples, reactions, 3: 59
Magnesium oxide–silicon oxide crystals (irradiated), thermal conductivity, 4: 7
Magnesium-plutonium alloys, density and stabilization, 2: 6–7
Magnesium-thorium alloys (HK-31A-H24) (irradiated), mechanical properties, 4: 71
Magnesium-zinc melt, ultrasonic activation, 3: 60
Magnetic testing, methods, 1: 74
Manganese, corrosion, 1: 41
diffusion in Al, 1: 58–9
Manganese-plutonium-uranium alloys (molten), reactions with containers, 3: 5; 4: 23
Materials, 1: 77
mechanical properties, 4: 72
ultrasonic energy dry coupling, 4: 88
Materials (binary)(irradiated), lattice damage, 4: 66
Materials (cladding), bonding, 1: 66
compatibility with UO_2, 1: 15
Materials (cladding)(irradiated), damage, 2: 50
Materials (high-temperature), 1: 77
Materials (irradiated), ion bombardment, 4: 68
recoil distributions, 4: 67
Materials (refractory), literature search, 2: 55
Materials (shielding), 1: 77
Matter (irradiated), effects, 4: 67
Mercury, corrosion by, 1: 41
Mercury-tantalum-tungsten alloys, tensile properties, 1: 55
Metal (alkali)-oxygen-uranium systems, X-ray diffraction, 1: 15
Metal (refractory) coatings, oxidation, 4: 61
Metal (refractory) compounds, chemical plating, 1: 68
Metal films (irradiated), damage in electron microscope, 2: 49
Metal halides, chemical plating with, 1: 69
Metals, bearing properties in Na and NaK, 4: 63
bonding to ceramics, 2: 75
chemical plating, 1: 68–9; 4: 84
corrosion, 4: 63
diffusion bonding, 1: 66
extrusion, 2: 66; 3: 65
fabrication, 1: 64
H_2 diffusion, 1: 58
reaction with water, 1: 44
sealing to ceramics, 2: 70
self-diffusion, 2: 59
surface-degradation prevention, 4: 84
Metals (alkali) (canned), thermal bonding, 2: 68
Metals (alkali) (molten), corrosion by, 4: 63
Metals (ceramic-coated), H_2 diffusion, 1: 58
Metals (fissile), atomic displacement and impurity effects, 3: 45
Metals (fissile) (irradiated), effects, 3: 17–18
Metals (irradiated), annealing, 1: 48
color production, 4: 65
damage, 2: 49; 3: 46; 4: 38, 67–8
interstitial atom clusters, 3: 46
surface effects, 4: 64, 67–8
vacancies, 3: 46–7
Metals (molten), corrosion by, 4: 62–3
reactions with water, 2: 47
Metals (noble) (alumina-coated), oxidation, 2: 46
Metals (noble) (irradiated), complexes and vacancies, 3: 46
Metals (nonmagnetic), ultrasonic testing, 1: 73
Metals (refractory), chemical plating of, 1: 69
consolidation, 4: 80
corrosion, 4: 60–1
diffusion, 1: 58
diffusion barriers, 2: 61; 3: 58–9
explosive forming, 1: 70
fabrication, 4: 80
joining, 4: 75, 86
review, 2: 59
silicide diffusion coating of, 3: 69
vapor deposition, 4: 84
Metals (refractory) (coated), corrosion, 3: 40–1; 4: 61–2
ignition, 3: 40–1
Metals (structural) (irradiated), effects, 2: 50; 3: 54
Mica (irradiated), fission tracks, 3: 45
mechanical properties, 4: 5
Minerals (irradiated), mechanical properties, 4: 5
Molybdenite (irradiated), fission tracks, 1: 47
Molybdenum, annealing, 1: 52
boriding, 3: 69
chemical plating of, 1: 69; 2: 69
chemical plating with, 1: 68
coating of, 1: 38; 2: 75; 3: 69–70
compatibility with carbides, 3: 40; 4: 36
with oxides, 3: 40
corrosion, 1: 41; 2: 45; 4: 62–3
deoxidation, 1: 64
electrical resistivity, 2: 31

Molybdenum (Continued)
electroplating, with cermets, 1: 67; 2: 68–9
explosive forming, 1: 70
extrusion, 2: 66
forging, 2: 66
Lorentz ratios, 2: 31
melting, 1: 63
notch sensitivity, 1: 55
powder-rolling, 2: 65
production, 3: 68–9
solubility in Li, 1: 42
tensile properties, 1: 55
thermal conductivity, 2: 31
thermoelectric power, 2: 31
welding, 4: 87
Molybdenum (Al-Sn coated), oxidation, 4: 61
Molybdenum (Chromalloy W-3 coated), corrosion, 4: 62
Molybdenum (Cr-Ni, Al_2O_3-coated), oxidation, 2: 45
Molybdenum (Cr-Ni coated), oxidation, 2: 45
Molybdenum (irradiated), annealing, 1: 52; 2: 50
electrical resistivity, 1: 52; 2: 48
hardness, 1: 52; 2: 48
lattice constants, 1: 45
vacancy diffusion, 1: 52
Molybdenum (silicide-coated), chemical plating, 4: 84
corrosion, 2: 45
Molybdenum alloys, extrusion, 3: 55–6; 4: 80
fabrication, 3: 65
heat-treatment, 3: 65
mechanical properties, 3: 55–6
melting, 3: 64
protective coatings for, 3: 69–70
Molybdenum alloys (coated), corrosion, 4: 61
Molybdenum alloys (PH 15-7), corrosion, 4: 62
Molybdenum alloys (TZM), extrusion and microstructure, 3: 65
Molybdenum carbide, compatibility with H_2 and W, 1: 58
Molybdenum disilicide, corrosion, 4: 62
oxidation, 2: 45; 4: 75
Molybdenum disilicide powder, explosive compaction, 2: 73
Molybdenum disilicide–zirconium diboride powder, explosive compaction, 2: 73
Molybdenum foils (irradiated), point-defect clusters, 4: 64
Molybdenum-niobium alloys, ignition, 3: 40
Molybdenum–niobium monocarbide couples, reactions, 3: 59
Molybdenum-niobium-tantalum alloys, creep properties and tensile strength, 2: 53
Molybdenum-niobium-tantalum-tungsten alloys, creep properties, 2: 53
Molybdenum-niobium-titanium-tungsten-zirconium alloys, phase studies and precipitation hardening, 1: 56–7
Molybdenum-niobium-titanium-vanadium alloys, stress-rupture and tensile properties, 2: 53
Molybdenum-niobium-tungsten alloys, creep properties. 2: 53
tensile properties, 1: 55
Molybdenum-niobium-tungsten-zirconium alloys, phase studies, 1: 56–7
precipitation hardening, 1: 56–7
weld strength, 2: 70
Molybdenum-niobium-tungsten-zirconium alloys (F-48), extrusion, 3: 65
ignition, 3: 40
Molybdenum-niobium-uranium alloys, phase transformation, 4: 20
Molybdenum-niobium-uranium-zirconium alloys, phase studies, 4: 18, 20
Molybdenum–plutonium dioxide cermets, fabrication, 3: 6
Molybdenum-rhenium base-barrier combination, properties, 3: 58
Molybdenum-rhenium couples, interdiffusion, 2: 61
Molybdenum-ruthenium-uranium alloys, phase studies, 1: 2
Molybdenum silicides, oxidation, 4: 61
Molybdenum-silicon-uranium system, creep and tensile properties, 1: 3
Molybdenum systems, diffusion, 1: 58
Molybdenum-tantalum alloys, creep properties, 2: 53
tensile properties, 1: 55; 2: 53
Molybdenum–tantalum monocarbide couples, reactions, 3: 59
Molybdenum-tantalum-tungsten alloys, creep properties and tensile strength, 2: 53
Molybdenum-tin-uranium alloys, tensile properties, 1: 3
Molybdenum-titanium alloy–rhenium couples, interdiffusion, 2: 61
Molybdenum-titanium alloys, corrosion, 4: 62
dispersion strengthening, 1: 55
explosive forming, 1: 70; 2: 70–1; 4: 87
explosive welding, 3: 71, 73
notch sensitivity, 1: 55
tensile properties, 1: 55
Molybdenum-tungsten alloys, creep properties, 2: 53
explosive forming, 4: 87
melting, 3: 64
tensile properties, 2: 53; 3: 56
Molybdenum-tungsten base-barrier combination, properties, 3: 58
Molybdenum–uranium alloy–uranium carbide dispersions, cladding of, 1: 9
Molybdenum–uranium alloy–uranium dioxide dispersions, cladding of, 1: 9
Molybdenum-uranium alloys, casting, 1: 4; 2: 65; 3: 2
chemical plating with Nb, 1: 68
corrosion, 3: 2
creep properties, 1: 3–4
development, 1: 4
oxidation, 2: 3; 3: 2
phase studies, 2: 4; 4: 18
phase transformation, 1: 4–5; 2: 4; 3: 2; 4: 20
rolling, 3: 2
tensile properties, 1: 3
thermal cycling, 3: 2
U self-diffusion, 3: 2
Molybdenum-uranium alloys (irradiated), dimensional changes, 1: 4; 2: 4
Molybdenum-uranium alloys (Nb-clad), roll bonding, 1: 65
Molybdenum-uranium alloys (Nb-coated), development, 4: 84
Molybdenum–uranium dicarbide diffusion couples, reactions, 3: 16
Molybdenum–uranium dioxide dispersions, densification, 1: 9
Molybdenum-uranium-zirconium alloys, phase studies, 4: 18, 20
Molybdenum-vanadium base-barrier combination, properties, 3: 58
Molybdenum-zirconium alloys, oxidation, 3: 41
Molybdenum-zirconium compounds, corrosion, 2: 42
Molybdenum-zirconium couples, reactions, 3: 59
Molybdenum-zirconium dioxide (CaO) couples, reactions, 3: 59
Molybdenum–zirconium monocarbide couples, reactions, 3: 59
Monel, stress-corrosion, 3: 39
Muscovite (irradiated), fission tracks, 1: 46

N

NaK
See Potassium-sodium alloys
Neodymium-thorium alloys, phase studies, 4: 26
properties, 3: 7
Neptunium-239, electroplating with, 1: 68
Neutron absorbers, review, 4: 56
Nichrome V, oxidation, 4: 60
Nickel, annealing, 1: 52
boriding, 3: 69
chemical plating of, 1: 69; 2: 69
chemical plating with, 1: 68
corrosion, 1: 41; 4: 63
deposition, 2: 69
diffusion bonding to Al and U, 1: 67
electroplating with, 1: 67–8; 3: 68
melting, 1: 63
oxidation, 2: 44
solubility in Li, 1: 42
stress corrosion, 3: 39
Nickel (irradiated), annealing, 1: 52; 2: 50
damage, 2: 49
electrical resistivity, 1: 52; 2: 48
hardness, 1: 52
threshold energy, 2: 48
vacancy diffusion, 1: 52
Nickel alloys, corrosion, 1: 40
Cr diffusion in, 1: 59
diffusion bonding, 4: 46–7, 81
Nickel crystals (irradiated), Kossel line studies, 4: 64
Nickel-nitrogen-zinc system, cubic nitrides, 3: 56–7
Nickel oxide (irradiated), reduction, 4: 9
Nickel-plutonium alloys (Zircaloy-4-clad) (irradiated), fission-product release, 3: 4
Nickel-plutonium couples, interdiffusion, 3: 58–9
Nickel-tungsten alloys, diffusion, 1: 59
Nickel whiskers, vapor deposition, 4: 84
Nickel-zirconium alloys, H absorption, 2: 42
Nickel-zirconium intermetallic compounds, hydriding, 2: 42; 4: 52–3
Niobium, Al diffusion in, 4: 47
Be diffusion in, 4: 47
boriding, 3: 69
brazing alloys, 1: 72; 4: 87
chemical plating of, 2: 69
chemical plating with, 1: 68
cold-work effects, 4: 72
compatibility, with carbides, 3: 40; 4: 35–6
with oxides, 3: 40
containment of molten Al-Th-U alloys, 4: 21
corrosion, 1: 41; 2: 44–5; 3: 57; 4: 62–3
diffusion bonding, 3: 66
diffusion coating of, 3: 70
diffusion in, 2: 59
diffusion of, 1: 58; 2: 61
extrusion, 2: 66; 4: 80
fabrication, 3: 57
forging, 2: 66
ignition, 3: 40
internal friction, 4: 72
manual, 1: 56
mechanical properties, 3: 55, 57
metallurgy, 3: 57
notch sensitivity, 1: 55
oxidation, 1: 38; 2: 44; 3: 39, 57; 4: 60
reaction with US, 2: 22
self-diffusion, 2: 59
surface tension, 1: 56
tensile properties, 1: 55
U diffusion into, 2: 21
vapor deposition, 3: 9
weld bend ductility, 1: 72
welding, 2: 70

Niobium (Al-Ni-Zn alloy-coated), oxidation, **2**: 44
Niobium (silicide-coated), corrosion, **2**: 45
Niobium (zinc-coated), oxidation, **2**: 44
Niobium alloy–rhenium couples, interdiffusion, **2**: 61
Niobium alloys, coating of, **1**: 38; **3**: 70
  extrusion, **2**: 66; **4**: 80
  fabrication, **3**: 65
  forging, **2**: 66
  heat-treatment, **3**: 65
  hot hardness, **3**: 55
  melting, **3**: 64
  oxidation, **3**: 55
Niobium alloys (Cb-74), explosive forming, **1**: 70
Niobium alloys (coated), corrosion, **4**: 61
Niobium alloys (CT-2WZ), explosive forming, **1**: 70; **2**: 70–1
Niobium alloys (F-48), melting, **3**: 64
Niobium alloys (Nb-74), explosive forming, **2**: 70–1
Niobium aluminides, oxidation, **2**: 45; **3**: 41; **4**: 61
Niobium beryllides, **1**: 30; **4**: 51–2
Niobium carbide, chemical plating with, **1**: 69
  coating graphite with, **3**: 70
  compatibility, with H_2, **1**: 58
    with Mo, **3**: 40
    with Nb, **3**: 40
    with W, **1**: 58; **3**: 40
  pyrolytic deposition, **3**: 69
  UC behavior with, **1**: 17
Niobium diboride, compatibility with H_2 and W, **1**: 58
Niobium diboride dispersions [S.S.(347)-clad] (irradiated), effects, **1**: 10
Niobium monocarbide, lattice parameters, **3**: 59
Niobium nitride, compatibility with H_2 and W, **1**: 58
Niobium-nitrogen-titanium-tungsten alloys, stress-rupture properties, **2**: 53
Niobium-nitrogen-titanium-vanadium alloys, tensile properties, **2**: 53
Niobium-osmium base-barrier combination, properties, **3**: 58
Niobium oxide (Nb_2O_5), O diffusion, **2**: 44
Niobium-oxygen-potassium system, reactions, **3**: 41
Niobium-oxygen-potassium-zirconium system, reactions, **3**: 41
Niobium-oxygen-titanium system, tensile properties, **1**: 55
Niobium-oxygen-titanium-vanadium alloys, stress-rupture and tensile properties, **2**: 53
Niobium-oxygen-uranium system, composition limits, **1**: 6
  X-ray diffraction, **1**: 15
Niobium-oxygen-zirconium system, tensile properties, **1**: 55
Niobium-plutonium-silicon system, phase studies, **1**: 6; **2**: 8
Niobium-plutonium-uranium alloys, hardness, **1**: 7; **4**: 23
  structure, **4**: 23
Niobium-plutonium-uranium-zirconium alloys, hardness, **1**: 7
Niobium-plutonium-zirconium alloys, Pu-Zr coalescence, **1**: 6–7
Niobium-rhenium base-barrier combination, properties, **3**: 58
Niobium-rhenium couples, interdiffusion, **2**: 61
Niobium-silicon system, diffusion, **3**: 58
Niobium-sodium–stainless steel (316) alloys, mass transfer, **1**: 42
Niobium systems, diffusion, **1**: 58
Niobium-tantalum alloys, tensile strength, **2**: 53
Niobium-tantalum-tungsten alloys, creep properties, **2**: 53
  hot hardness, **3**: 55
  oxidation, **3**: 55
  tensile properties, **1**: 55; **2**: 53
Niobium-tantalum-vanadium alloys, protective coatings for, **1**: 38–9
Niobium-tin alloys, compounds, **2**: 55, 58
Niobium-tin-zirconium alloys, H uptake, **1**: 39
  tensile properties, **2**: 53
Niobium-titanium alloys, oxidation, **3**: 40
Niobium-titanium-tungsten-vanadium alloys, stress-rupture and tensile properties, **2**: 53
Niobium-titanium-vanadium alloys, chemical plating with silicide, **1**: 69
  stress-rupture properties, **2**: 53
  tensile properties, **2**: 53; **4**: 72
Niobium-titanium-vanadium alloys (coated), oxidation, **2**: 45; **4**: 61
Niobium tubing, spinning, **4**: 80
  ultrasonic drawing, **3**: 65
Niobium-tungsten alloys, creep and tensile properties, **2**: 53
Niobium-tungsten base-barrier combination, properties, **3**: 58
Niobium-uranium alloys, corrosion, **1**: 6
  development, **1**: 6
  fabrication, **1**: 6
  oxidation, **2**: 3
  phase studies, **4**: 18, 20
  preparation, **1**: 6
  properties, **1**: 4, 6; **3**: 2
  U self-diffusion, **3**: 2
Niobium–uranium dicarbide diffusion couples, reactions, **3**: 16
Niobium–uranium dioxide couples, Nb diffusion, **3**: 58
Niobium–uranium monocarbide diffusion couples, reactions, **3**: 16
Niobium-uranium-zirconium alloys, creep properties, **1**: 4
  phase studies, **4**: 18
Niobium-vanadium alloys, creep properties, **1**: 53, 55
  fabricability, **4**: 72
  oxidation, **3**: 40
  strength, **4**: 72
Niobium-vanadium alloys (coated), oxidation, **2**: 44–5
Niobium-vanadium-zirconium alloys, hardening, **1**: 57–8
  tensile properties, **2**: 53
Niobium-zinc compounds ($NbZn_2$), crystal structure, **3**: 57
Niobium-zirconium alloy tubing, spinning, **4**: 80
Niobium-zirconium alloys, aging, **2**: 53
  compatibility with UC, **1**: 17
  corrosion, **1**: 42; **3**: 37, 41; **4**: 62–3
  creep properties, **1**: 53, 55; **2**: 53
  heat-treatment effects, **3**: 37
  mechanical properties, **2**: 53
  oxidation, **3**: 40
  physical properties, **2**: 58
  tensile properties, **1**: 55; **2**: 53; **3**: 55
  weld strength, **2**: 70
Niobium-zirconium alloys (Al-Cr-Si coated), corrosion, **2**: 45
Niobium-zirconium alloys (irradiated), creep properties, **2**: 50
  stress-rupture properties, **2**: 50–1
Niobium-zirconium base-barrier combination, properties, **3**: 58
Niobium–zirconium dioxide (CaO) couples, reactions, **3**: 59
Nitrides, emittance, **4**: 75
  in ternary systems, **3**: 56–7
Nonmetals, chemical plating, **1**: 68
Nuclear particle detector development, **4**: 64
Nuclei (heavy)(irradiated), excitation by fast nucleons, **1**: 48

O

Organic-Moderated Reactor Experiment, fuel-element cladding, **1**: 65
Organics (irradiated), property changes, **4**: 68
Osmium-tantalum base-barrier combination, properties, **3**: 58
Oxides, chemical deposition, **2**: 69
  emittance, **4**: 75
Oxygen-phosphorus-sodium-uranium system, glass formation, **2**: 19
Oxygen-plutonium system, phase studies, **3**: 5–6
Oxygen-plutonium-uranium system, phase studies, **4**: 24
Oxygen-plutonium-zirconium system, phase studies, **3**: 6
Oxygen-strontium-uranium system, phase studies, **1**: 15
Oxygen-thorium-uranium system, tensile properties, **2**: 53
Oxygen-tungsten-uranium system, chemical interactions, **3**: 14
Oxygen-uranium system, properties, **2**: 19
Oxygen-uranium-zirconium system, phase studies, **4**: 35
Oxygen-uranium-zirconium system (irradiated), phase transition, **2**: 49
Oxygen-zirconium solid solutions, X-ray studies, **3**: 58
Oxygen-zirconium system, electrical resistivity, **2**: 58–9
  phase studies, **2**: 59

P

Palladium, compatibility with UO_2, **4**: 34
  corrosion, **3**: 39
  dimensional changes, **1**: 40
  oxidation, **1**: 40; **2**: 46
Palladium films (irradiated), fission tracks, **4**: 64
Palladium–uranium dioxide compacts, sintering, **4**: 34–5
Palladium-zirconium compounds, corrosion, **2**: 42
Plastics (irradiated), property changes, **4**: 68
Platinum, compatibility with UO_2, **4**: 34
  corrosion, **1**: 41; **3**: 39
  dimensional changes, **1**: 40
  oxidation, **1**: 40; **2**: 46
Platinum (irradiated), fission tracks, **1**: 45; **2**: 50; **4**: 63–4
Platinum phthalocyanine (irradiated), fission tracks, **1**: 46–7
Platinum-rhodium alloys, corrosion, **3**: 39
  dimensional changes, **1**: 40
  oxidation, **1**: 40; **2**: 46
Platinum systems, diffusion, **1**: 58
Platinum-zirconium compounds, corrosion, **2**: 42
Plutonium, Al solubility in, **4**: 23
  book, **2**: 5
  compression properties, **2**: 7, 9
  cooling-rate effects, **1**: 6
  creep properties, **1**: 6
  Hall effect, **3**: 4
  hardness, **1**: 6; **2**: 6
  heat-treatment effects, **2**: 6
  impact properties, **2**: 5
  mechanical properties, **3**: 4
  melting, **3**: 64–5
  microstructure, **1**: 6; **2**: 6
  oxidation, **2**: 6
  phase transformation, **1**: 6; **3**: 3–4
  tensile properties, **2**: 7, 9
Plutonium (molten), oxidation, **2**: 6
Plutonium (Zircaloy-2-clad), rolling, **2**: 66
Plutonium alloys (jacketed), pulsed-field reflection bond testing, **3**: 75

Plutonium aluminides, polymorphic transformation, 4: 23
Plutonium beryllide, 2: 8
Plutonium carbide, casting, 1: 7; 4: 25
hydriding, 4: 25
phase studies, 1: 7
thermal expansion, 4: 25
Plutonium carbide–uranium carbide solid solutions, sintering, 1: 7; 4: 25
Plutonium compounds, literature survey, 2: 8
physical properties, 2: 8
preparation, 4: 25
Plutonium dioxide, etching, 1: 7
lattice expansion, 4: 24
moisture pickup, 3: 6
production, 1: 7
reactions, 4: 24
reduction, 1: 8; 4: 24
sintering, 1: 7; 2: 11; 4: 24
stability, 3: 5
thermal expansion, 1: 7
vapor pressure, 2: 10; 3: 6
Plutonium dioxide (Cu- and Ni-coated), preparation, 3: 9
Plutonium dioxide (Zircaloy-clad), rolling, 2: 66
Plutonium dioxide particles (Ni-coated), preparation, 2: 12–13
Plutonium dioxide–thorium dioxide solid solutions, sintering, 3: 6
Plutonium dioxide–uranium dioxide dispersions, hot rolling, 3: 6
Plutonium dioxide–uranium dioxide mixtures, fabrication, 4: 24
vibratory compaction, 3: 67
Plutonium dioxide–uranium dioxide particles (Ni-coated), preparation, 2: 12–13
Plutonium dioxide–uranium dioxide paste, viscous flow, 4: 23–4
Plutonium dioxide–uranium dioxide pellets, sintered density, 1: 7
Plutonium dioxide–uranium dioxide solid solutions, liquidus, 4: 24
Plutonium dioxide–uranium dioxide solid solutions (irradiated), effects, 4: 24
Plutonium dioxide–uranium dioxide system, preparation, 2: 10
Plutonium monocarbide, phase studies, 3: 6
production, 2: 10
sintering, 2: 10
Plutonium nitrides, arc melting, 4: 25
preparation, 3: 6
Plutonium-ruthenium alloys, phase diagram, 2: 8, 11
Plutonium silicide, density, 4: 25
melting point, 4: 25
preparation, 1: 7–8; 2: 10–11; 3: 6; 4: 25
Plutonium-silicon alloys, density and stabilization, 2: 6–7
Plutonium-silicon-titanium alloys, density and stabilization, 2: 6–7
Plutonium-tellurium alloys, density and stabilization, 2: 6–7
Plutonium-thorium alloys, recrystallization, 2: 8
Plutonium-tin alloys, density and stabilization, 2: 6–7
Plutonium-titanium alloys, phase transformation temperatures, 2: 7, 10
Plutonium-titanium-uranium alloys, density and stabilization, 2: 6–7
Plutonium-zirconium alloys, aging effects, 2: 6–7
heat-treatment effects, 2: 6–9
mechanical properties, 1: 6; 3: 4
phase transformation, 3: 4
physical properties, 1: 6
tensile properties, 2: 6–8
thermal expansion and contraction, 3: 4
Plutonium-zirconium alloys (Zircaloy-2-clad), roll bonding, 4: 80
Polonium, electroplating with, 1: 68
Potassium (molten), corrosion by, 1: 41–2; 4: 62–3
Potassium-sodium alloys, compatibility with UC_2, U_2C_3, and US, 2: 22
Praseodymium-thorium alloys, phase studies, 4: 26
properties, 3: 7
Pressure-vessel reinforcing bands, air-gap magnetic testing, 3: 75
Pyroceram, corrosion, 1: 41
emittance, 4: 75
Pyrolytic carbon coatings
See Carbon (pyrolytic) coatings

R

Radiation, effects, 2: 50
sputtered Cu as reactor-damage monitor, 1: 48
Radiographic testing, development, 1: 74
Reactors, sputtered Cu as radiation-damage monitor, 1: 48
René 41, corrosion, 1: 41
creep exposure effects, 4: 71–2
mechanical properties, 4: 71–2
René 41 (irradiated), stress-rupture properties, 4: 69
Rhenium, boriding, 3: 69
fabrication, 2: 65
Rhenium-tantalum base-barrier combination, properties, 3: 58
Rhenium-thorium alloys, phase studies, 4: 26
Rhenium–thorium dioxide couples, reactions, 3: 59
Rhenium-tungsten base-barrier combination, properties, 3: 58
Rhenium-uranium alloys, phase studies, 4: 18
Rhenium–uranium dioxide couples, reactions, 3: 59
Rhodium, compatibility with UO_2, 4: 34
corrosion, 3: 39
dimensional changes, 1: 40
oxidation, 1: 40; 2: 46
Rhodium-tungsten base-barrier combination, properties, 3: 58
Rubidium (molten), corrosion by, 1: 42
Ruthenium-tantalum base-barrier combination, properties, 3: 58
Ruthenium-tungsten alloys, oxidation, 2: 45
Ruthenium-tungsten base-barrier combination, properties, 3: 58
Ruthenium-zirconium compounds, corrosion, 2: 42

S

Samarium, fabrication, 1: 64
Sauereisens, corrosion by K, 4: 62
Scandium-yttrium alloys, phase studies, 4: 73–4
Selenium, melting, 1: 63
Semiconductors (irradiated), damage, 4: 67
Silicides, chemical plating with, 1: 69; 2: 69
corrosion, 4: 61–2
diffusion coating with, 3: 70
emittance, 4: 75
protective coatings of, 1: 38–9
Silicon, chemical plating steel with, 1: 69
coatings containing, 3: 70
melting, 1: 63
vapor deposition, 3: 9
Silicon (irradiated), length changes, 3: 46
range-energy relation, 2: 49
Silicon carbide, compatibility with H_2 and W, 1: 58
Silicon carbide (irradiated), dimensional changes, 4: 3–4
oxidation, 4: 9
Silicon dioxide (irradiated), catalytic activity, 4: 9
dimensional changes, 4: 3–5
phase transformation, 4: 7
thermal conductivity, 4: 7
Silicon dioxide gel (irradiated), catalytic activity, 4: 9
Silicon-tantalum system, corrosion, 2: 47
Silicon-thorium system, phase studies, 1: 8
Silicon-uranium system, grain size, 2: 3
oxidation, 2: 3
specific heat, 1: 17–18
Silicon-uranium-zirconium system, phase studies, 3: 2
Silicon-yttrium-zirconium coatings, preparation, 3: 70
Silicon-zirconium compounds, corrosion, 2: 42
Silver, electroplating U oxide with, 1: 68
Silver (irradiated), damage, 2: 49
electrical resistivity, 2: 48
threshold energy, 2: 48
vacancy-formation energy, 1: 45
Silver alloys (Consil 995), corrosion, 1: 40
Silver chloride crystals (irradiated), fission-recoil tracks, 4: 66
Silver cyanamide (irradiated), fission tracks, 1: 47
Silver halide crystals (irradiated), cosmic-ray tracks, 4: 66
Silver-zirconium alloys, H absorption, 2: 42
Silver-zirconium compounds, corrosion, 2: 42
Slugs, canning, 3: 66
Sodium, reaction with steam, 1: 44
Sodium (irradiated), annealing, 2: 50
electrical resistivity, 4: 64
Sodium (molten), corrosion by, 2: 46; 4: 63
Sodium chloride (irradiated), Cl activation energy, 2: 50
Sodium polyphosphate (molten), corrosion by, 1: 42–3
Solids, rare-gas diffusion in, 4: 74
Solids (inorganic) (irradiated), effects, 1: 47–8; 3: 47
Solids (irradiated), effects, 4: 67–8
range-energy relations, 2: 50
rare-gas behavior in, 4: 38
reactivity, 3: 47; 4: 9
Spinel (irradiated), mechanical properties, 4: 5
Stainless steel, brazing, 3: 71; 4: 46
brazing-alloy corrosion, 4: 59–60
canning applications, 3: 22
corrosion, 4: 58–9
diffusion bonding to Zircaloy-2, 2: 68
plasma-jet spraying with UO_2, 3: 70
reaction with US, 2: 22
stress-corrosion cracking, 2: 43; 4: 59
welding to Zr, 2: 70
Stainless steel (17-4 PH), stress-corrosion cracking, 3: 38
Stainless steel (17-7 PH), stress-corrosion cracking, 3: 38
Stainless steel (300), corrosion, 1: 41
Stainless steel (304), C diffusion into, 2: 20–1
compatibility with U_2Si_2, 1: 18
corrosion, 2: 46; 3: 38; 4: 59, 63
explosive extrusion, 1: 71
oxidation, 3: 40
U diffusion into, 2: 21
Stainless steel (304) (irradiated), creep properties, 2: 50
ductility, 1: 49
rupture, 1: 49
stress-rupture properties, 2: 50–1; 4: 69
Stainless steel (304) (molten), reaction with water, 3: 43–5
Stainless steel (310), corrosion, 1: 41
explosive welding, 3: 71, 73

Stainless steel (316), corrosion, **1**: 41–2; **3**: 38; **4**: 63
physical properties, **2**: 58
stress-corrosion cracking, **2**: 43–4
Stainless steel (316) (Inconel-clad), stress-corrosion cracking, **2**: 44
Stainless steel (316) (irradiated), tensile properties, **4**: 68–9
Stainless steel (316) (Ni-plated), stress-corrosion cracking, **2**: 43–4
Stainless steel (317), corrosion, **3**: 38
Stainless steel (321), corrosion, **4**: 62–3
Stainless steel (347), stress-corrosion cracking, **4**: 59
Stainless steel (347) (irradiated), tensile properties, **4**: 68–9
Stainless steel (410), corrosion, **1**: 41; **4**: 62
explosive bonding to Zircaloy-2, **1**: 71; **3**: 74; **4**: 87–8
roll bonding to Zircaloy-2, **4**: 80
Stainless steel (410) (irradiated), effects, **1**: 49
tensile properties, **4**: 69
Stainless steel (446), corrosion, **4**: 60
Stainless steel (A286), corrosion, **1**: 41
stress-corrosion cracking, **3**: 38
Stainless steel (A286) (irradiated), creep properties, **4**: 69
stress-rupture properties, **3**: 49–50
tensile properties, **3**: 49–50; **4**: 69
Stainless steel (AF 1753), corrosion, **1**: 41
Stainless steel (AISI 4340), explosive extrusion, **1**: 71
Stainless steel (AM-350), stress-corrosion cracking, **3**: 38
Stainless steel (austenitic), corrosion, **1**: 31–2, 40
Stainless steel (ferritic), corrosion, **1**: 40
Stainless steel (Greek Ascoloy), stress-corrosion cracking, **4**: 59
Stainless steel (irradiated), effects, **1**: 45; **3**: 54
mechanical properties, **3**: 47
Stainless steel (Ag-plated), corrosion, **1**: 40
Stainless steel (semiaustenitic), mechanical properties and cladding strength, **4**: 71
Stainless steel (UO_2-coated), preparation, **3**: 15
Stainless steel–uranium dioxide dispersions, development, **2**: 11–12
thermal expansion, **1**: 9
Stainless steel–uranium dioxide dispersions (irradiated), effects, **2**: 12
Stainless steel (318)–uranium dioxide dispersions (irradiated), stability, **1**: 9–10
Stainless steel–uranium dioxide dispersions (S.S.-clad), roll bonding, **1**: 65
Stainless steel–uranium dioxide powder, explosive compaction, **2**: 73
Stainless steel–uranium dioxide–zirconium diboride dispersions, B loss and preparation, **1**: 36
Steel, brittle fracture, **4**: 72
chemical plating with Si, **1**: 69
corrosion, **2**: 43; **4**: 59
explosive extrusion, **1**: 70
explosive forming, **2**: 71
Steel (17-4 PH), corrosion, **1**: 41
Steel (A-212 B) (irradiated), annealing, **4**: 68
ductility transition temperature, **4**: 68
mechanical properties, **3**: 47–8
Steel (A-302) (irradiated), annealing, **4**: 68
Steel (AISI 406), explosive forming, **2**: 72
Steel (AISI 1020), explosive extrusion, **1**: 71
Steel (AISI 4340), explosive welding, **3**: 71–3
Steel (carbon), corrosion, **1**: 40–1; **2**: 43, 46; **3**: 38–9, 41; **4**: 62
Steel (carbon) (Inconel-clad), corrosion, **3**: 41
Steel (carbon) (irradiated), effects, **3**: 54
Steel (Conlo I) (irradiated), ductile-brittle transition temperature, **3**: 49
Steel (Cr), corrosion, **2**: 47
Steel (Cr) (irradiated), phase transformation, **1**: 46
Steel (Cr-Mo) corrosion, **2**: 46; **3**: 41
oxidation, **3**: 39
U diffusion into, **2**: 21
Steel ($2\frac{1}{4}$ Croloy), corrosion, **1**: 41
Steel (irradiated), mechanical properties, **1**: 48; **4**: 68
Steel (low-alloy), corrosion, **1**: 40; **3**: 39
oxidation, **1**: 40
Steel (low-alloy) (irradiated), effects, **3**: 54
Steel (low-carbon), aqueous corrosion, **4**: 59
Steel (mild), explosive joining to Al, **1**: 71
welding to Zr, **2**: 70
Steel (Neatro Tool), corrosion, **1**: 41
Steel (PH 15-7 Mo), corrosion, **1**: 41
Steel (SA-212B) (irradiated), coercive force, hardness, and magnetic properties, **1**: 48–9
Steel (Sicromo), corrosion, **1**: 41; **4**: 62
Strontium, diffusion of, **1**: 21, 58
Strontium oxide, diffusion in graphite, **1**: 21
Sulfur-thorium-uranium system, hardness, **2**: 22
Sylvania No. 4, corrosion, **1**: 41

T

Tantalum, boriding, **3**: 69
chemical plating of, **2**: 69
containment of molten Al-Th-U alloys, **4**: 21
corrosion, **1**: 41; **2**: 45–7; **3**: 41; **4**: 22–3, 63
diffusion bonding, **3**: 66
electroplating with Cr cermets, **2**: 68–9
extrusion, **2**: 66; **4**: 80
fabrication, **3**: 65
forging, **2**: 66
notch sensitivity, **1**: 55
oxidation, **3**: 39–40; **4**: 60
protective coatings for, **1**: 38–9
reaction with carbides, **4**: 35–6
tensile properties, **1**: 55; **2**: 53
vapor deposition, **3**: 9
weld bend ductility, **1**: 72
welding, **2**: 70
Tantalum (coated), corrosion, **2**: 45; **4**: 62
Tantalum (irradiated), corrosion, **4**: 60
Tantalum alloys, extrusion, **1**: 64
hot hardness, **3**: 55
fabrication, **3**: 65
heat-treatment, **3**: 65
oxidation, **3**: 55
protective coatings for, **1**: 38–9
Tantalum alloys (coated), corrosion, **4**: 61
Tantalum beryllides, heating effects, **1**: 30
oxidation, **3**: 28
properties, **2**: 35
vapor pressure, **3**: 28
Tantalum carbide, chemical plating with, **1**: 69
compatibility, with H_2, **1**: 58
with Mo, **3**: 40
with Nb, **3**: 40
with W, **1**: 58; **3**: 40
corrosion, **1**: 41
melting, **1**: 64
pyrolytic deposition, **3**: 69
UC behavior with, **1**: 17
Tantalum crucibles, reaction with Ce-Co-Pu alloy, **3**: 4
Tantalum diboride, compatibility with H_2 and W, **1**: 58
Tantalum monocarbide crucibles, reaction with Ce-Co-Pu alloy, **3**: 4–5
Tantalum nitride, compatibility with H_2 and W, **1**: 58
Tantalum systems, diffusion, **1**: 58
Tantalum-thorium alloys, corrosion, **2**: 47
phase studies, **1**: 8
Tantalum–thorium dioxide powder, explosive compaction, **2**: 73
Tantalum-tungsten alloys, annealing, **1**: 57
chemical plating with silicide, **1**: 69
corrosion, **2**: 47
creep properties, **2**: 53
melting, **1**: 64
recrystallization, **1**: 57
tensile properties, **1**: 55; **2**: 53
welding, **1**: 72
Tantalum-tungsten alloys (Al-Sn coated), oxidation, **2**: 45
Tantalum-tungsten alloys (Cr-Si-Ti coated), corrosion, **4**: 62
Tantalum-tungsten base-barrier combination, properties, **3**: 58
Tantalum–uranium dicarbide diffusion couples, reactions, **3**: 16
Tantalum–uranium dioxide couples, reactions, **3**: 59
Tantalum–uranium monocarbide diffusion couples, reactions, **3**: 16
Tantalum-yttrium alloys, corrosion, **2**: 47
Tellurium, diffusion in graphite, **1**: 21
Thorium, bibliography, **1**: 8
C diffusion in, **3**: 7
corrosion protection, **4**: 26
electroplating, with Cr, **1**: 67
with Ni, **1**: 67; **2**: 69
production, **1**: 8
properties, **1**: 8–9
Thorium (irradiated), effects, **1**: 8
mechanical properties, **3**: 7
spallation, **1**: 45
tensile properties, **1**: 9
Thorium (molten), ThO_2 solubility in, **3**: 7
Thorium (Zr-clad), rolling, **3**: 66
Thorium aluminide, casting, **1**: 19–20
Thorium beryllide, preparation, **1**: 20
sintering, **4**: 51
Thorium beryllide–thorium–uranium oxide system, sintering, **3**: 28
Thorium boride, preparation, **1**: 20
Thorium carbide–uranium carbide particles (PyC-coated), specifications, **4**: 29
Thorium dicarbide, casting, **1**: 19–20
oxidation, **1**: 16
Thorium dicarbide–uranium dicarbide particles (PyC-coated), development, **2**: 14
Thorium dicarbide–uranium dicarbide particles (PyC-coated) (irradiated), delamination, **4**: 33–4
fission-gas release, **2**: 17
Thorium dicarbide–uranium dicarbide system, oxidation, **2**: 11
Thorium dioxide, densification, **2**: 74–5
production, **1**: 20
solubility in molten Th, **3**: 7
vapor pressure, **3**: 7
Thorium dioxide powder, explosive compaction, **2**: 72
Thorium dioxide–uranium dioxide ceramics, solution in HNO_3 and ultrasonic activation, **3**: 60
Thorium dioxide–uranium dioxide mixtures, vibratory compaction, **3**: 67
Thorium hydride, lattice parameters, **4**: 52
Thorium monocarbide, casting, **1**: 19–20
Thorium monosulfide, hardness and oxidation, **2**: 22
Thorium oxide–uranium dispersions, particle preparation, **2**: 22–3
Thorium selenides, electrical properties, **4**: 38
Thorium silicides, casting, **1**: 19–20
Thorium sponge, melting and purification, **4**: 79
Thorium sulfide, phase studies, **1**: 17
properties, **1**: 17; **4**: 38
rupture, **1**: 17

Thorium tellurides, electrical properties, 4: 38
Thorium-tin alloys, phase studies, 4: 25
Thorium-uranium alloys, casting and melting, 2: 65
Thorium-uranium alloys (irradiated), mechanical properties, 3: 7
Thorium-uranium beryllides, oxidation, 3: 8
Thorium-uranium borides, compressive strength, oxidation, and thermal expansion, 3: 8
Thorium-uranium carbides, compressive strength, oxidation, and thermal expansion, 3: 8
Thorium-uranium compounds, casting, 1: 19
Thorium-uranium dicarbide (C-coated), fuel migration, 1: 11
preparation, 3: 10–11
thermal cycling, 1: 11
Thorium–uranium dicarbide (C-coated) (irradiated), effects, 3: 12, 14
fission-gas release, 1: 11, 13–14
Thorium-uranium-zirconium alloys, phase studies, 4: 25
Thorium-ytterbium alloys, phase studies, 1: 8
Thorium-zirconium alloys, aging effects, 2: 11
hardness, 1: 8–9; 2: 11
heat-treatment effects, 2: 11
phase studies, 1: 8; 2: 11; 4: 25
Tin, reaction with UC, 4: 36
self-diffusion, 2: 59
Tin (irradiated), annealing, 2: 50
phase transformation, 4: 6
Tin oxide crystals, vapor deposition, 4: 85
Tin-zirconium alloys, H absorption, 2: 42
oxidation, 3: 41
Tin-zirconium compounds, corrosion, 2: 42
Titanium, chemical plating ceramics with, 1: 68
corrosion, 1: 41; 2: 46; 4: 63
explosive extrusion, 1: 70
melting, 1: 63
solubility in Li, 1: 42
Titanium (irradiated), corrosion, 4: 60
isochronal annealing, 2: 48
Titanium alloys, explosive forming, 2: 71
hydriding, 4: 53
Titanium alloys (6A1-4V), explosive welding, 3: 71–3
Titanium alloys (B120VCA), explosive welding, 3: 71, 73
Titanium carbide, compatibility with H_2 and W, 1: 58
melting, 1: 64
Titanium coatings, preparation, 3: 70
Titanium diboride, compatibility with H_2 and W, 1: 58
Titanium diboride crucibles, reaction with Ce-Co-Pu alloy, 3: 4–5
Titanium monocarbide crucibles, reaction with Ce-Co-Pu alloy, 3: 4–5
Titanium nitride, compatibility with H_2 and W, 1: 58
Titanium systems, diffusion, 1: 58
Titanium-tungsten alloys, ceramic coatings for, 3: 70
Titanium-uranium alloys, oxidation, 2: 3
strength, 3: 2
Titanium-uranium-zirconium alloys, phase studies, 4: 18
Transducers, ultrasonic testing, 1: 73
Tubing, planetary swaging, 4: 80
ultrasonic testing, 2: 75–6
Tungsten, boriding, 3: 69
brazing alloys, 4: 87
chemical plating of, 1: 69; 2: 69; 3: 69
chemical plating with, 1: 68; 3: 69; 4: 84
compatibility, with borides, 1: 58
with carbides, 1: 58; 3: 40
with nitrides, 1: 58
with oxides, 1: 58; 3: 40
corrosion, 1: 41; 2: 45; 4: 60–3
creep properties, 2: 53
deposition, 2: 69; 3: 9, 69; 4: 84
electrical resistivity, 2: 31
electroplating with Cr cermets, 2: 68–9
explosive forming, 1: 70; 2: 70–1
extrusion, 2: 66
forging, 2: 66
Lorentz ratios, 2: 31
mechanical properties, 3: 55
melting, 1: 63–4
notch sensitivity, 1: 55
oxidation, 1: 39; 2: 45
production, 3: 69
protective coatings, 1: 39; 3: 70
reaction with carbides, 4: 36
tensile properties, 1: 55; 2: 53
thermal conductivity, 2: 31
thermoelectric power, 2: 31
welding, 4: 87
Tungsten (Al-Sn coated), oxidation, 4: 61
Tungsten (irradiated), annealing, 2: 50
field-ion microscopy, 4: 65
lattice defects, 4: 65
Tungsten (silicide-coated), chemical plating, 4: 84
oxidation, 2: 45
Tungsten alloys, development, 1: 63–4
extrusion, 3: 55–6
fabrication, 3: 65
heat-treatment, 3: 65
hot hardness, 3: 55
mechanical properties, 3: 55–6
melting, 3: 64
oxidation, 3: 55
sintering, 2: 58
strength, 2: 53, 58
Tungsten alloys (coated), corrosion, 4: 61
Tungsten boride, compatibility with H_2 and W, 1: 58
Tungsten carbide, compatibility with H_2 and W, 1: 58
corrosion, 1: 41
Tungsten crucibles, compatibility with BeO and machining, 3: 28
Tungsten disilicide, oxidation, 2: 45
Tungsten powder, explosive compaction, 2: 72–3
rolling, 2: 65
Tungsten systems, diffusion, 1: 58
Tungsten–uranium dicarbide diffusion couples, reactions, 3: 16
Tungsten–uranium dioxide powder, explosive compaction, 2: 73
Tungsten-zirconium alloys, H absorption, 2: 42
Tungsten-zirconium compounds, corrosion, 2: 42
Tungsten–zirconium dioxide (CaO) couples, reactions, 3: 59

U

Ultrasonic testing, symposia, 1: 72–3
techniques, 3: 75
transducers, 1: 73
Uranium, atomic position parameter, 1: 1
cell dimensions, 1: 1
chemical plating with Ni, 2: 69
corrosion, 2: 5; 3: 1–2
data compilation, 2: 3
diffusion, 1: 58; 2: 3, 21; 3: 1; 4: 21
diffusion bonding to Al and Ni, 1: 67
dimensional stability, 1: 1
electroplating of, 1: 67–8; 2: 69; 3: 68
electroplating with, 1: 68–9
extrusion, 1: 64–5
formability, 1: 64
grain refinement, 4: 16
heat-treatment, 2: 1, 3, 66
H_2 diffusion, 1: 58; 2: 3
ingot production, 1: 63
interatomic distances, 1: 1
mechanical properties, 2: 1; 4: 16
melting, 4: 79
outgassing, 2: 66
oxidation, 3: 3; 4: 21
phase transformation, 3: 1; 4: 17
preferred orientation, 1: 1
purification, 4: 79
rare-gas diffusion, 1: 58
reaction with steam, 4: 21
reaction with water, 1: 43–4
recrystallization, 3: 1–2
rolling effects, 2: 1
self-diffusion, 2: 59; 3: 1; 4: 16
solubility in Al, 4: 21
solubility in UC, 3: 15–16
structure, 4: 17
substructure, 3: 2
thermal conductivity, 1: 2
thermal-cycling effects, 1: 1
Uranium (Al-clad), diffusion bonding, 2: 68
Uranium (Al-Si coated), fabrication, 2: 68
Uranium (C-coated), U diffusion, 1: 11–12
Uranium (C-coated) (irradiated), fission-gas release, 1: 11
Uranium (irradiated), behavior as function of fabrication, 1: 1
bubble formation, 2: 24
creep, 1: 20
dimensional changes, 1: 20–1; 2: 1, 3, 23–4; 3: 18; 4: 17
dislocation loops, 2: 23
effects, 3: 18; 4: 67
ejection by fission fragments, 3: 45
gas bubbles, 1: 21
Kr^{85} release, 4: 17
mechanical properties, 1: 1–2
melting, 4: 17
oxidation, 3: 3
stability, 2: 1–3
thermal-cycling effects, 1: 20
Xe^{133} diffusion, 4: 38–9
Uranium (molten), density, 3: 1
reaction with water, 3: 43–4
Uranium (Ni-coated), chemical plating, 4: 84
Uranium (Zircaloy-2-clad) (irradiated), swelling, 3: 18; 4: 17
Uranium alloys, corrosion, 2: 5
diffusion studies, 1: 58; 2: 3
extrusion, 1: 64–5
phase studies, 2: 4
Uranium alloys (irradiated), dimensional changes, 2: 24
Uranium beryllides, sintering, 4: 51
Uranium carbide particles (C-coated) (irradiated), fission-gas release, 4: 32–3
fracture, 4: 33
Uranium carbide particles (PyC-coated), properties, 4: 29–31
Uranium carbide particles (PyC-coated) (irradiated), fission-gas release, 4: 33
Uranium carbide powders (irradiated), Xe^{133} diffusion, 4: 36
Uranium carbides, bibliography, 2: 20
casting, 1: 18
compatibility with H_2 and W, 1: 58
reactions with Pb and Sn, 4: 36
sintering, 4: 38
technology, 1: 16
Uranium carbides (irradiated), effects, 1: 17; 2: 21
Uranium compacts, extrusion, 1: 64–5
Uranium compounds, diffusion studies, 1: 58; 2: 3
Uranium dibismuthide (irradiated), Xe^{133} diffusion from, 3: 18

Uranium dicarbide, dissociation pressure, 4: 36
oxidation, 1: 16
phase transformation, 2: 20
reaction with metals, 4: 36
reaction with water, 1: 16–17
Uranium dicarbide (C-coated), coating rupture, 1: 12
Uranium dicarbide (C-coated) (irradiated), effects, 1: 13; 3: 12, 14
fission-gas release, 1: 12, 14; 3: 11–12
Uranium dicarbide (irradiated), compatibility with NaK, 2: 22
Uranium dicarbide particles (PyC-coated), compatibility with HNO_3, 2: 15
fuel-element fabrication, 2: 14–15
Uranium dicarbide particles (PyC-coated) (irradiated), fission-gas release, 2: 16–17; 4: 34
Uranium dioxide, applications, 1: 14
compatibility, with cladding materials, 1: 15
with metals, 4: 34
diffusion studies, 1: 58; 2: 3
electrical conductivity, 2: 18
explosive compaction, 1: 71; 3: 73–4
fabrication of porous, 1: 16
flame spraying, 3: 15
F removal, 1: 16
gas evolution on heating, 1: 16
Nb diffusion in, 1: 58
outgassing, 3: 15
oxidation, 2: 18
phase studies, 1: 14
plasma-jet spraying with, 3: 70
power-generation simulation, 3: 15
pressure bonding, 2: 67
properties, 1: 14; 4: 34
rare-gas diffusion, 1: 58
self-diffusion, 1: 58
solid solutions, 1: 14
Sr diffusion in, 1: 58
thermal conductivity, 1: 15; 2: 18
vaporization, 2: 18
vibratory compaction, 3: 66–8
Zr diffusion in, 1: 58
Uranium dioxide (Al-clad), diffusion bonding, 2: 67–8
Uranium dioxide (Al_2O_3-coated), preparation, 1: 10–11; 3: 10
Xe release, 1: 11
Uranium dioxide (Al_2O_3-coated) (irradiated), fission-gas release, 1: 13; 3: 12
Uranium dioxide (Be-clad), bonding, 1: 65; 2: 67; 4: 46
Uranium dioxide (C-coated), preparation, 3: 10
Uranium dioxide (C-coated) (irradiated), Xe^{133} release, 3: 12
Uranium dioxide (clad), swaging, 1: 65; 3: 65–6
Uranium dioxide (Cr-coated), preparation, 3: 8–9
Uranium dioxide (enriched), density, 4: 34
Uranium dioxide (Inconel X-clad), pressure bonding, 2: 67
Uranium dioxide (Fe-coated), preparation, 3: 8–9
Uranium dioxide (irradiated), crystal growth, 1: 15
effects, 1: 14
electrical conductivity, 2: 18
fission-product release, 1: 21; 2: 23; 3: 18; 4: 34
I^{133} and I^{135} diffusion in, 3: 18
Kr^{85} diffusion in, 3: 18
melting point, 2: 17–18; 3: 14–15
properties, 4: 34
stored-energy release, 4: 39
thermal conductivity, 1: 16; 2: 18
vaporization, 2: 18; 4: 39
Xe^{133} diffusion in, 1: 15; 2: 23; 3: 18; 4: 39
Xe^{135} diffusion in, 3: 18
Uranium dioxide (Mo-coated), preparation, 3: 8–9
Uranium dioxide (Ni-coated), preparation, 3: 8–9
Uranium dioxide (PuO_2-enriched), irradiation testing, 3: 6
Uranium dioxide (sintered), grain growth, 4: 34
microscopy, 2: 18
Uranium dioxide (S.S.-clad), coextrusion, 3: 66
pressure bonding, 1: 66; 2: 67; 4: 81
tandem rolling, 3: 66
Uranium dioxide [S.S.(304)-clad], stress-corrosion cracking, 3: 38
Uranium dioxide [S.S.(304L)-clad], pressure bonding, 2: 67
Uranium dioxide [S.S.(316L)-clad], bonding, 4: 80
Uranium dioxide [S.S.(406)-clad], pressure bonding, 2: 67
Uranium dioxide (Zircaloy-clad), hydriding, 3: 37
Uranium dioxide (Zircaloy-2-clad), pressure bonding, 2: 67
welding, 3: 71
Uranium dioxide (Zircaloy-4-clad), pressure bonding, 2: 67
Uranium dioxide dispersions [S.S.(347)-clad] (irradiated), effects, 1: 10
Uranium dioxide particles (Al_2O_3-coated), corrosion, 2: 14
development, 2: 13
graphite-matrix grain orientation, 4: 27–8
oxidation, 2: 14
preparation, 4: 27
Uranium dioxide particles (Al_2O_3-coated) (irradiated), fission-gas release, 2: 15–16
Uranium dioxide particles (BeO-coated), development, 2: 13–14
oxidation, 2: 14
preparation, 4: 27
Uranium dioxide particles (C-coated), preparation, 2: 13
Uranium dioxide particles (ceramic-coated) (irradiated), leached U, 4: 31–2
Xe^{133} retention, 4: 31–2
Uranium dioxide particles (MgO-coated), corrosion, 2: 14
development, 2: 13–14
preparation, 4: 27
properties, 4: 27
Uranium dioxide particles (Ni-coated), preparation, 2: 12
Uranium dioxide particles (PyC-coated) (irradiated), fission-gas release, 2: 16–17
Uranium dioxide powders, compaction, 2: 72; 4: 82–3
sintering, 1: 16
Uranium dioxide powders [S.S.(AISI-406)-canned], vibratory compaction, 4: 82
Uranium dioxide–zirconium dioxide mixture, coating with pyrolytic C, 3: 69
Uranium dioxide–zirconium dioxide systems, phase studies, 1: 16
reduction of ZrO_2, 2: 19
solid-solution studies, 2: 19
thermodynamic properties, 2: 19
Uranium dioxide–zirconium dioxide systems (irradiated), dimensional changes, 4: 5
phase studies, 1: 16
thermal conductivity, 1: 16
Uranium disilicide, preparation, 3: 64
Uranium films, surface structure, 4: 16
Uranium monocarbide, annealing, 1: 19
C self-diffusion, 2: 21
casting, 1: 18
compatibility, with Al-Nb-V and Nb-Zr alloys, 1: 17
with Co, 3: 17
explosive compaction, 1: 71
grain growth, 3: 16
oxidation, 1: 16; 3: 16
plastic deformation, 2: 21
preparation, 2: 22; 3: 64
pressing, 1: 19
production, 1: 19
reaction, with Be, 1: 59
with metallic carbides, 1: 17
with metals, 1: 59; 4: 35–6
with water, 1: 16–17
solubility in carbides, 1: 17
storage, 1: 19
U self-diffusion, 2: 21
U solubility in, 3: 15–16
Xe^{133} diffusion from, 3: 16
Uranium monocarbide (irradiated), annealing, 2: 22
damage, 2: 23
density, 1: 17
lattice strain, 2: 22
resistivity, 2: 22
Uranium monocarbide [S.S.(304)-clad] (irradiated), damage, 2: 21
Uranium monocarbide compacts, failure, 3: 17
Uranium monocarbide particles (PyC-coated) fission-product retention, 2: 14
Uranium monocarbide powder, explosive compaction, 2: 72
metallurgy, 1: 18–19
production, 2: 22
sintering, 1: 18–19; 3: 17
Uranium mononitride, compatibility with Ni, 3: 17
Uranium mononitride (irradiated), damage, 2: 23
density, 4: 36, 38
Uranium monosulfide, hardness, 2: 22
oxidation, 2: 22
physical properties, 3: 16
reaction with metals and alloys, 2: 22
Uranium nitride dispersions [S.S.(347)-clad] (irradiated), effects, 1: 10
Uranium oxides, electroplating, 1: 68
lattice parameters, 3: 15
Uranium oxides (U_2O_7), phase studies, 2: 18–19
Uranium oxides (U_3O_8), dissociation, 2: 18
heat capacity, 4: 35
reduction by H, 3: 14
solid-phase reactions, 4: 35
Uranium oxides (U_3O_8) (Al-clad), coextrusion, 2: 68
Uranium oxides (U_3O_8) (irradiated), stored-energy release, 4: 39
Uranium oxides (U_4O_9), oxidation, 2: 19
Uranium oxides (U_4O_9) (irradiated), stored-energy release, 4: 39
Uranium selenides, electrical properties, 4: 38
Uranium sesquicarbide (irradiated), compatibility with NaK, dimensional changes, and electrical resistivity, 2: 22
Uranium sheet, recrystallization, 4: 16–17
Uranium silicides, compatibility with S.S.(304) 1: 18
dynamic modulus, 1: 18
electrical resistivity, 1: 5, 17
thermal properties, 1: 5, 17
Uranium silicides (U_3Si_2), preparation, 3: 64
Uranium sulfides, oxidation, 1: 17
phase studies, 1: 17
powder production, 1: 19
properties, 1: 17; 4: 38
rupture, 1: 17
Uranium systems, intermediate layer growth, 2: 59

Uranium tellurides, electrical properties, 4: 38
Uranium trioxide, dissociation, 2: 18
reduction, 3: 14
Uranium tubing, production, 1: 63; 4: 79–80
Uranium–uranium dioxide dispersions, oxide effects, thermal cycling, and transverse bend strength, 1: 2–3
Uranium–uranium monocarbide cermets, grain growth, 3: 16
Uranium-vanadium alloys, oxidation, 2: 3
Uranium-yttrium alloys (irradiated), swelling, 2: 5
Uranium-zinc alloys, preparation, 1: 6
Uranium-zirconium alloys, corrosion, 2: 4
electrical resistivity, 2: 4
extrusion, 4: 82
heat-treatment, 1: 3; 4: 18
magnetic susceptibility, 2: 4
metallography, 1: 3
oxidation, 2: 3
phase studies, 4: 18
U self-diffusion, 3: 2
Uranium-zirconium alloys (irradiated), bubble formation, 1: 4
dimensional changes, 4: 18–20
metallography, 1: 3
point defects, 3: 18
Uranium-zirconium alloys (molten), reaction with water, 4: 21
Uranium-zirconium alloys (Zircaloy-clad), coextrusion, 4: 81–2
Uranium-zirconium beryllides, 1: 30
Uranyl sulfate solutions, corrosive effects, 2: 46

V

Vanadium, chemical plating of, 2: 69
corrosion, 4: 63
deoxidation, 1: 64
melting, 1: 64
reaction with US, 2: 22
Vanadium alloys, protective coatings for, 3: 70
Vanadium alloys (coated), corrosion, 4: 61
Vanadium oxide (V_2O_5), solid-phase reaction, 4: 35
Vanadium systems, diffusion, 1: 58
Vanadium-zirconium intermetallic compounds, hydriding, 4: 52–3
Vycor, coating with PyC, 3: 69

W

Waspalloy, corrosion, 1: 41
Welding, joint evaluation, 3: 71
ultrasonic, 2: 69–70
ultrasonic testing, 3: 74–5
Wigner energy, 2: 37
Windscale Advanced Gas-Cooled Reactor, stainless steel for canning, 3: 22

X

Xenon isotopes, diffusion, 1: 21; 3: 18

Y

Yttrium, coating with ceramics, 1: 69–70; 2: 75
corrosion, 4: 55
elasticity, 3: 29
fabrication, 2: 65
Yttrium coatings, preparation, 3: 70
Yttrium hydride, H content, 3: 28
pressure-composition isotherms, 3: 29
properties, 2: 36; 3: 29
solubility relations, 3: 29
Yttrium oxide, diffusion in graphite, 1: 21
self-diffusion, 4: 75
sintering, 4: 75
Yttrium oxide crucibles, reaction with Mn-Pu-U alloy, 3: 5

Z

Zinc, plating, 3: 68
Zinc (irradiated), diffusion in irradiated Cu-Zn alloy, 1: 46
Zircaloy, brazing, 2: 70
creep properties, 2: 53
extrusion, 4: 82
joining, 4: 86
ultrasonic testing, 2: 75–6; 4: 88
Zircaloy-2, annealing, 2: 58
bonding to S.S., 1: 71; 2: 68; 3: 74; 4: 80, 87–8
brazing, 3: 71
corrosion, 2: 42–3; 3: 37; 4: 57
creep activation energy, 4: 73
deformation twinning, 3: 57–8
F pickup, 4: 57
fracture properties, 2: 54–5
hydriding, 1: 39; 2: 42; 3: 37; 4: 58
oxidation, 3: 41
plasma-jet spraying with UO_2, 3: 70
stress effects, 2: 54–5
U diffusion into, 2: 21
ultrasonic testing, 1: 73; 4: 88
welding, 1: 71; 3: 71
X-ray diffraction, 1: 57
yield properties, 2: 54–5
Zircaloy-2 (Al-clad), hydriding, 4: 58
Zircaloy-2 (irradiated), corrosion, 4: 60, 69
creep properties, 1: 50; 2: 51
fatigue properties, 2: 51–2
mechanical properties, 3: 50, 54; 4: 69–70
rupture, 1: 50
stress-rupture properties, 2: 51
tensile properties, 1: 49–50; 2: 51
Zircaloy-2 (molten), reaction with water, 3: 43
Zircaloy-2 (S.S.-clad), hydriding, 4: 58
pressure bonding, 1: 65
rolling, 2: 67
Zircaloy-2 (UO_2-coated), preparation, 3: 15
Zircaloy-2 powder, explosive compaction, 2: 73
Zircaloy-2 tubing, fabrication and ultrasonic drawing, 3: 65
Zircaloy-3, corrosion, 2: 42
Zircaloy-3 (molten), reaction with water, 2: 47
Zircaloy-4, aqueous corrosion, 4: 57
F pickup, 4: 57–8
Zirconium, adiabatic elastic moduli, 2: 58
annealing, 1: 52
chemical plating ceramics with, 1: 68
corrosion, 1: 41; 2: 42–3, 46; 4: 57–8, 63
deformation, 1: 57
diffusion in, 1: 58; 2: 59–61; 4: 57, 74
electroplating with, 1: 68
hydriding, 1: 39; 2: 42; 4: 58
melting, 1: 63
oxidation, 3: 41; 4: 57
production, 1: 63
reaction, with CO_2, 3: 37–8
with US, 2: 22
with water, 1: 43
recovery, 2: 66
recrystallization, 2: 66
scaling, 2: 41
ultrasonic testing, 4: 88
welding, 2: 70
X-ray diffraction, 1: 57
Zirconium (irradiated), annealing, 1: 52; 2: 48
electrical resistivity, 1: 52
hardness, 1: 52
mechanical properties, 4: 70
oxidation, 4: 57
vacancy diffusion, 1: 52
Zirconium (molten), reaction with water, 3: 43
Zirconium alloys, corrosion, 1: 39; 2: 42
hardness, 1: 56
hydriding, 2: 42; 4: 53
recovery, 2: 66
recrystallization, 2: 66
strength, 1: 39
Zirconium beryllides, C and O effects, 1: 30
heating effects, 1: 30
oxidation, 1: 30; 4: 51–2
preparation, 1: 30
rupture, 1: 30
sintering, 4: 51
spalling, 1: 30
strength, 1: 30
thermal-stress resistance, 1: 30
vapor pressure, 3: 28
Zirconium carbides, compatibility, with H_2, 1: 58
with Mo, 3: 40
with Nb, 3: 40
with W, 1: 58; 3: 40
pyrolytic deposition, 3: 69
strength, 4: 85
UC behavior with, 1: 17
Zirconium coatings, preparation, 3: 70
Zirconium deuteride, electrical resistivity, 2: 36
Zirconium diboride, compatibility with H_2 and W, 1: 58
melting, 1: 64
Zirconium diboride crucibles, reaction with Ce-Co-Pu alloy, 3: 4–5
Zirconium diboride dispersions [S.S.(347)-clad] (irradiated), effects, 1: 10
Zirconium dioxide, chemical plating with, 1: 69
compatibility with H_2 and W, 1: 58
diffusion in graphite, 1: 21
PuO_2 effects on thermal-shock properties, 1: 8
Zirconium dioxide (irradiated), dimensional changes, 4: 3
mechanical properties, 4: 5
phase transformation, 4: 7
Zirconium hydride, bibliography, 4: 52
cladding, 2: 35–6
dissociation pressures, 1: 31; 4: 52
H content, 3: 28
mechanical properties, 2: 35
moderator evaluation, 4: 52
nuclear magnetic resonance, 4: 52
phase studies, 1: 31; 3: 29
rupture, 1: 31
Zirconium hydride (S.S.-clad), pressure bonding, 2: 67
Zirconium monocarbide crucibles, reaction with Ce-Co-Pu alloy, 3: 4–5
Zirconium monoxide, diffusion in graphite, 1: 21
Zirconium nitride, compatibility with H_2 and W, 1: 58
Zirconium oxide, compatibility with Mo, Nb, and W, 3: 40
oxidation, 4: 57
Zirconium oxide coatings, cohesive strength, 3: 70
Zirconium systems, diffusion, 1: 58
Zirconium–uranium hydride, thermal expansion, 1: 32

LEGAL NOTICE

This document was prepared under the sponsorship of the U. S. Atomic Energy Commission. Neither the United States, nor the Commission, nor any person acting on behalf of the Commission:

A. Makes any warranty or representation, expressed or implied, with respect to the accuracy, completeness, or usefulness of the information contained in this report, or that the use of any information, apparatus, method, or process disclosed in this report may not infringe privately owned rights; or

B. Assumes any liabilities with respect to the use of, or for damages resulting from the use of any information, apparatus, method, or process disclosed in this report.

As used in the above, "person acting on behalf of the Commission" includes any employee or contractor of the Commission, or employee of such contractor, to the extent that such employee or contractor of the Commission, or employee of such contractor prepares, disseminates, or provides access to, any information pursuant to his employment or contract with the Commission, or his employment with such contractor.

NUCLEAR SCIENCE ABSTRACTS

The U. S. Atomic Energy Commission, Division of Technical Information, publishes *Nuclear Science Abstracts (NSA)*, a semimonthly journal containing abstracts of the literature of nuclear science and engineering.

NSA covers (1) research reports of the U. S. Atomic Energy Commission and its contractors; (2) research reports of government agencies, universities, and industrial research organizations on a world-wide basis; and (3) translations, patents, books, and articles appearing in technical and scientific journals.

Complete indexes covering subject, author, source, and report number are included in each issue. These are cumulated quarterly, semiannually, and annually providing a detailed and convenient key to the literature.

Availability of *NSA*

SALE *NSA* is available on subscription from the Superintendent of Documents, U. S. Government Printing Office, Washington 25, D. C., at $22.00 per year for the semimonthly abstract issues and $15.00 per year for the four cumulated-index issues. Subscriptions are postpaid within the United States, Canada, Mexico, and all Central and South American countries, except Argentina, Brazil, British and French Guiana, Surinam, and British Honduras. Subscribers in these Central and South American countries, and in all other countries throughout the world, should remit $27.50 per year for subscriptions to semimonthly abstract issues and $17.50 per year for the four cumulated-index issues.

EXCHANGE *NSA* is also available on an exchange basis to universities, research institutions, industrial firms, and publishers of scientific information. Inquiries should be directed to the Division of Technical Information Extension, U. S. Atomic Energy Commission, P. O. Box 62, Oak Ridge, Tennessee.

TECHNICAL PROGRESS REVIEWS may be purchased from Superintendent of Documents, U. S. Government Printing Office, Washington 25, D. C. for $2.00 per year for each subscription or for $0.55 per issue. The use of the coupon below will facilitate the handling of your order.

POSTAGE AND REMITTANCE: Postpaid within the United States, Canada, Mexico, and all Central and South American countries except as hereinafter noted. Add $0.50 per year, or $0.15 per single issue, for postage to all other countries, including Argentina, Brazil, British and French Guiana, Surinam, and British Honduras. Payment should be by check, money order, or document coupons, and MUST accompany order. Remittances from foreign countries should be made by international money order, or draft on an American bank, payable to the Superintendent of Documents, or by UNESCO book coupons.

order form

SUPERINTENDENT OF DOCUMENTS
U. S. GOVERNMENT PRINTING OFFICE
WASHINGTON 25, D. C.

Enclosed:
document coupons ☐ check ☐ money order ☐

Charge to Superintendent of Documents No. _____

Please send a one-year subscription to

☐ REACTOR MATERIALS
☐ POWER REACTOR TECHNOLOGY
☐ NUCLEAR SAFETY
☐ REACTOR FUEL PROCESSING

(Each subscription $2.00 a year; $0.55 per issue.)

SUPERINTENDENT OF DOCUMENTS
U. S. GOVERNMENT PRINTING OFFICE
WASHINGTON 25, D. C.

(Print clearly)

Name _____

Street _____

City _____ Zone ____ State _____